STRUCTURAL PROPERTIES OF RICOBENDAZOLE AND CEFRADINE USING VIBRATIONAL SPECTROSCOPY AND QUANTUM CHEMICAL METHODS

A THESIS SUBMITTED TO THE

CENTRAL DEPARTMENT OF PHYSICS

INSTITUTE OF SCIENCE AND TECHNOLOGY

TRIBHUVAN UNIVERSITY

NEPAL

FOR THE AWARD OF

DOCTOR OF PHILOSOPHY

IN PHYSICS

BY

MANOJ KUMAR CHAUDHARY

AUGUST 2021

STRUCTURAL PROPERTIES OF RICOBENDAZOLE AND CEFRADINE USING VIBRATIONAL SPECTROSCOPY AND QUANTUM CHEMICAL METHODS

A THESIS SUBMITTED TO THE

CENTRAL DEPARTMENT OF PHYSICS

INSTITUTE OF SCIENCE AND TECHNOLOGY

TRIBHUVAN UNIVERSITY

NEPAL

FOR THE AWARD OF

DOCTOR OF PHILOSOPHY

IN PHYSICS

BY

MANOJ KUMAR CHAUDHARY

AUGUST 2021

DECLARATION

Thesis entitled **"STRUCTURAL PROPERTIES OF RICOBENDAZOLE AND CEFRADINE USING VIBRATIONAL SPECTROSCOPY AND QUANTUM CHEMICAL METHODS"** which is being submitted to the Central Department of Physics, Institute of Science and Technology (IOST), Tribhuvan University, Nepal for the award of the degree of Doctor of Philosophy (Ph.D.), is a research work carried out by me under the supervision of Prof. Dr. Bhawani Datt Joshi, Department of Physics, Siddhanath Science Campus, Tribhuvan University, Mahendranagar, Nepal and co-supervised by Prof. Dr. Poonam Tandon, Department of Physics, University of Lucknow, Lucknow, India.

This research is original and has not been submitted earlier in part or full in this or any other form to any university or institute, here or elsewhere, for the award of any degree.

Manoj Kumar Chaudhary

RECOMMENDATION

This is to recommend that **Mr. Manoj Kumar Chaudhary** has carried out research entitled **"STRUCTURAL PROPERTIES OF RICOBENDAZOLE AND CEFRADINE USING VIBRATIONAL SPECTROSCOPY AND QUANTUM CHEMICAL METHODS"** for the award of Doctor of Philosophy (Ph.D.) in **Physics** under our supervision. To our knowledge, this work has not been submitted for any other degree.

He has fulfilled all the requirements laid down by the Institute of Science and Technology (IOST), Tribhuvan University, Kirtipur for the submission of the thesis for the award of Ph.D. degree.

. . . . . .

Dr. Bhawani Datt Joshi
Supervisor
(Professor)
Department of Physics
Siddhanath Science Campus
Tribhuvan University
Mahendranagar, Nepal

. . . . . .

Dr. Poonam Tandon
Co-supervisor
(Professor and Head)
Department of Physics
Lucknow University
Lucknow, India

AUGUST 2021

TRIBHUVAN UNIVERSITY
CENTRAL DEPARTMENT OF PHYSICS
Kirtipur, Kathmandu, Nepal
☎ 4331054

Ref. No.: (F.No .....) CDP ..... Date .....

LETTER OF APPROVAL

[Date: 16/08/2021]

On the recommendation of Prof. Dr. **Bhawani Datt Joshi**, Department of Physics, Siddhanath Science Campus, Tribhuvan University, Mahendranagar, Nepal and Prof. Dr. **Poonam Tandon**, Department of Physics, University of Lucknow, Lucknow, India, this Ph.D. thesis submitted by **Manoj Kumar Chaudhary**, entitled **"STRUCTURAL PROPERTIES OF RICOBENDAZOLE AND CEFRADINE USING VIBRATIONAL SPECTROSCOPY AND QUANTUM CHEMICAL METHODS"** is forwarded by Central Department Research Committee (CDRC) to the Dean, IOST, T.U.

.....

Dr. Om Prakash Niraula
Professor
Head
Central Department of Physics
Tribhuvan University
Kirtipur, Kathmandu
Nepal

ACKNOWLEDGMENTS

First of all, I would like to express my profound gratitude to my supervisors Prof. Dr. Bhawani Datt Joshi and Prof. Dr. Poonam Tandon for their prominent and valuable guidance for this research work. I also heartily express my acknowledgment to Prof. Dr. Binil Aryal, Dean, IOST (TU), Prof. Dr. Om Prakash Niraula, Head of the Central Department of Physics (CDP), Prof. Dr. Ishwar Koirala, Dr. Bal Ram Ghimire, Prof. Dr. Raju Khanal, Prof. Dr. Narayan Prasad Adhikari, Dr. Gopi Chandra Kaphle, Dr. Rajendra Prasad Koirala and Mr. Shyam Prakash Khanal and all the CDP family who encouraged and supported me in this work.

I would also like to express my cordial thanks to the Lab members of the Macromolecular Laboratory: Dr. Karthick Thangavel, Mr. Keshav Kumar Singh, Dr. Rajesh Kumar, Dr. Karnica Srivastava, Dr. Swapnil Singh, Dr. Preeti Prajapati, Dr. Jaya Pandey, Dr. Anuradha Shukla, Dr. Anubha Srivastava, Dr. Sweta Singh, Dr. Eram Khan, Dr. Pravat Singh, Dr. Neetu Singh, Ms. Rajani Chaudhary, Ms. Aarati Yadav, Dr. Sanjeev, Dr. Debraj Gangopadhyay, Mr. Jay Deep Singh, Mr. Krishna and the staff members of the Physics Department, University of Lucknow for their valuable cooperation in my research during my stay in India.

Similarly, I would like to thank Prof. Dr. Rajendra Parajuli, Dr. Ghanshyam Thakur, Mr. Vijaya Kumar Jha, Mr. Birendra Prasad Yadav, Mr. Dinesh Chaudhary, Dr. Manoj Kumar Thakur, Dr. Saran Lamichhane, Mr. Hari Krishna Neupane, Mr. Tarun Chaudhary and all the well-wishers, faculty and the staff members of the Physics Department, Amrit Campus for their significant support and cooperation. I am grateful to Mr. Rajesh Kumar Bachchan and Mr. Abhinav Thakur for their endless support to arrange the required format of the present thesis.

I am thankful to the Centre for Co-operation in Science and Technology among Developing Societies (CCSTDS), India for the partial financial support under the Indian Science and Research Fellowship (ISRF-2019).

Finally, I must express my deep appreciation to my parents and all my family members especially, Mrs. Binu Jha, Mr. Satyandra Jha, Ms. Anuskha Chaudhary and Mr. Aaditya Chaudhary for their support and encouragement during my research works.

Manoj Kumar Chaudhary
August, 2021

ABSTRACT

This research aims to analyse the structural, electronic and the vibrational features of ricobendazole (RBZ) and cefradine based on spectroscopic and quantum chemical approach. The basic structural properties of RBZ and cefradine have been examined based on optimized geometry, spectroscopic activity, intermolecular interaction, chemical reactivity, intramolecular hydrogen bonding and molecular docking analysis. The infra-red (IR) spectra of the RBZ and the cefradine have been recorded in the solid form of sample in which the pellet was prepared by mixing the KBr and white crystalline powder of the sample (RBZ and cefradine). The Fourier transform infrared (FT-IR) spectra has been listed in the order of (400 to 4000) cm^{-1} with a resolution of 4 cm^{-1}, whereas the Raman spectra of the RBZ and the cefradine sample have been listed in the order (100 to 3500) cm^{-1}. The 96 normal modes of vibration of the RBZ and 123 normal modes of vibration of the cefradine were calculated by using the Gar2Ped program from Pulay's recommendations along with their potential energy distribution (PED) by using the density functional theory (DFT) from the B3LYP/6-311++G(d,p) level of calculation. The comparison of simulated spectra with the observed spectra was carried out, which identifies the inter molecular hydrogen bonding in compact (solid) form in terms of red and blue shift. The minimum energy conformers of these molecules were identified by performing one-dimensional potential energy surface (PES) scan along the flexible bonds at B3LYP/6-311++G(d,p) level of calculation. The vibrational features of the molecules along with the potential energy distribution across the various modes of vibrations have been calculated. The chemical reactivity and stability of all the favorable conformers of RBZ and cefradine were predicted on the basis of energy gap between the highest occupied molecular orbital (HOMO) and the lowest unoccupied molecular orbital (LUMO) (i.e., HOMO-LUMO energy gap) and the natural bond orbital (NBO) procedure. The distribution of charges on the particular atoms of the molecule were calculated by molecular electrostatic potential (MEP) surface map which identifies the nucleophilic and the electrophilic regions. The quantitative investigation of the electrophilicity and the nucleophilicity indices was done by Hirshfeld charge analysis. The non-linear optical (NLO) activity of these molecules has been analyzed which motivates about the potential use of the molecules as NLO material. The variation of the thermodynamic parameters like: entropy, enthalpy and specific heat capacity with temperature have been explored. The Quantum theory of atoms in molecule (QTAIM) study is used to analyze the quality and the strength of the hydrogen bonding interactions. Furthermore, the molecular docking analysis were performed to investigate the active binding

sites of the drug molecules with the predicted protein targets.

Similarly, the structural stability and the fundamental chemical reactive sites of the frovatriptan molecule has been examined from the structural evaluation and the quantum chemical calculation technique. The conformational analysis was performed across the flexible bonds to indicate the most stable conformers from the DFT at B3LYP/6-311++G(d,p) level of calculation. The chemical reactivity has been demonstrated in terms of the frontier molecular orbitals (HOMO-LUMO) energy gap, the MEP surface and the global reactivity. The local reactivity descriptors give an explanation about the donor, the acceptor and the free radical reactive sites present in the frovatriptan molecule. Furthermore, the NBO analysis was performed to study the interactions between the bonding and the anti-bonding orbitals. The expected use of the frovatriptan as NLO substance and the variation of the thermodynamic parameters like: entropy, enthalpy and specific heat capacity with temperature have been calculated. The drug-likeness properties of frovatriptan have also been studied. Furthermore, the molecular docking with the expected targets has been performed to analyse the protein-ligand interaction as well as to predict the active sites of the drug molecule.

LIST OF ACRONYMS AND ABBREVIATIONS

ABL	Antibiotics do Brazil Ltd.
ABZ	Albendazole
AIM	Atoms in molecule
ADT	Auto dock tools
API	Active pharmaceutical ingredient
AM1	Austim model 1
ATP	Adenosine triphosphate
BCP	Bond critical point
BCS	Biopharmaceutical classification systems
BLYP	Becke-Lee-Yang-Parr
BOA	Born-Oppenheimer approximation
BP	Becke-Perdew
CC	Coupled cluster
CGRP	Calcitonin gene-related peptide
CGTO	Contracted Gaussian Type Orbital
CI	Configuration interaction
COX-2	Cyclooxygenase-2
DFT	Density functional theory
DFT-D	Dispersion-corrected density functional theory
DNA	Deoxyribonucleic acid
DPP	Dipeptidyl peptidase
ECT	Electrophilicity based charge transfer
ED	Electron density
FF	Fukai function
FT-IR	Fourier transform infrared
FT-Raman	Fourier transform Raman
FTase	Farnesyltransferase
FWHM	Full width at half maximum
GGA	Generalized gradient approximation
GTO	Gaussian-type orbital
HEG	Homogeneous electron gas
H-F	Hartree-Fock
H-K	Hohenberg-Kohn
HOMO	Highest occupied molecular orbital
HT	Hydroxytryptamine
IR	Infrared

IUPAC	International Union of Pure and Applied Chemistry
K-S	Kohan–Sham
K. E.	Kinetic energy
KBr	Potassium Bromide
LCAO	Linear combination of atomic orbitals
LDA	Local density approximation
LGA	Lamarckian Genetic Algorithm
LP	Lone pair
LUMO	Lowest unoccupied molecular orbital
MAPK	MAP kinase p38 alpha
MEP	Molecular electrostatic potential
MMA	Menstrually associated migraine
MO	Molecular orbital
MP	Molar-Plesset
MR	Molar refractivity
MW	Molecular weight
NBO	Natural bond orbital
NLO	Non-linear optical
NMR	Nuclear magnetic resonance
PARP	Poly [ADP-ribose] polymerase-1
PDB	Protein data bank
PED	Potential energy distribution
PES	Potential energy surface
PM3	Parametric model number 3
PTGS	Prostaglandin-endoperoxide synthase
QMC	Quantum Monte-Carlo
QTAIM	Quantum theory of atoms in molecule
RBZ	Ricobendazole
RMSD	Root mean square deviation
SCF	Self consistent field
SEP	Single point energy
STO	Slater-type orbital
TF	Thomas and Fermi
TD-DFT	Time dependent density functional theory
TFD	Thomas-Fermi-Dirac
TU	Tribhuvan University
USA	United States of America
WHO	World Health Organization
WLS	Wavenumber linear scaling
XC	Exchange correlation

LIGPLOT	A computer program that generates schematic 2-D representations of protein-ligand complexes from standard PDB file input
RAM II	A module used in FT-Raman and FT-IR research
UCSF Chimera	Program for interactive visualization and analysis of molecular structures and related data
1NU6	PDB code of Dipeptidyl peptidase IV Protein
1N1M	PDB code of Dipeptidyl peptidase IV Protein
1J2E	PDB code of Dipeptidyl peptidase IV Protein
5IKT	PDB code of Human Cyclooxygenase-2 Protein
5IKV	PDB code of Human Cyclooxygenase-2 Protein
5KIR	PDB code of Human Cyclooxygenase-2 Protein
3E34	PDB code of Farnesyltransferase Protein
1O1R	PDB code of Farnesyltransferase Protein
4IAQ	PDB code of serotonin 1b (5-Hydroxy Triptamide 1B) receptor Protein
5V54	PDB code of serotonin 1b (5-Hydroxy Triptamide 1B) receptor Protein
6G79	PDB code of serotonin 1b (5-Hydroxy Triptamide 1B) receptor Protein
1UK1	PDB code of Poly [ADP-ribose] polymerase-1(PARP) Protein
2PAW	PDB code of Poly [ADP-ribose] polymerase-1(PARP) Protein
6I8M	PDB code of Poly [ADP-ribose] polymerase-1(PARP) Protein
3BX5	PDB code of MAP kinase p38 alpha (MAPK) Protein
3LFA	PDB code of MAP kinase p38 alpha (MAPK) Protein
3LFB	PDB code of MAP kinase p38 alpha (MAPK) Protein
3PWH	PDB code of Adenosine A2a receptor Protein
3QAK	PDB code of Adenosine A2a receptor Protein

LIST OF TABLES

LIST OF FIGURES

TABLE OF CONTENTS

Page No.

CHAPTER 1

1. INTRODUCTION

In 1828, Friedrich Wöhlar proved that the organic compound can be created artificially in the laboratory by synthesizing the organic compound urea (Clayden, 2000). This idea of synthesis motivates to produce the new series of organic compounds. Initially, it was assumed that the formation of life is due to chemical compounds and the existence of life is due to morphology of cells which is produced by living organisms (Voet & Voet, 2004). The biological active compound produced by living organisms initiate in nature that commonly has a pharmacological or natural activity which has prospective use in the pharmaceutical drug discovery and design. Especially these compounds are important in the treatment of life-threatening conditions. The global trouble of progressive bacterial resistance to newer drugs has led to renewed interest in the structure-activity of drug compositions. So, it is proposed to study the structural, electrostatic, thermodynamic properties, non-linear optical (NLO) properties, ligand-protein interaction with the predicted targets and electron transport properties of some biological active molecules like: ricobendazol (RBZ), cefradine and frovatriptan. Natural products have been the subject of research for many reasons, as they have got wide applications, such as antibiotics in human or animal medicine (Newman & Cragg, 2007). The term natural product today is rather ordinarily implicit to refer as herbs, herbal concoctions, dietary supplements, traditional Chinese medicine or alternative medicines (Holt & Chandra, 2002). The discovery and development of drugs may have been based on herbs, folklore (or traditional) and alternative medicines. The investigation and disclosure along with the development of herbal remedies or dietary supplements typically present other challenges with their skilled goals (Lang & Wai, 2001). Natural products are generally either of the prebiotic origins or originated from microbes, plants or animal sources. History of medicine dates back practically to the existence of human civilization. The actual accepted modern medicine or allopathy has gradually developed over the years by scientific and observational efforts of scientists. In this regard, we have focused on the drugs like RBZ, cefradine and frovatriptan.

1.1 Ricobendazole

Ricobendazole (RBZ), which is popularly known as albendazole sulphoxide, is an active metabolite of albendazole (ABZ). The chemical formula of RBZ is $C_{12}H_{15}N_3O_3S$ and denominated by IUPAC as methyl N-(6-propylsulfinyl-1H-benzimidazol-2-yl) carbamate having molecular weight (MW) 281.33 g/mol. The chemical structure of RBZ

is presented in Figure 1. There are two rings in the compound, one is benzene ring R1 and another is imidazole ring R2. Two methyl (CH_3) groups are present in the compound. Moreover, two amine (N-H) groups: one is attached at the imidazole ring R2 and the other is in the chain. The carbonyl (C=O) and sulphinyl (S=O) groups are the main groups that take part in hydrogen bonding (intra/inter molecular hydrogen bonding). The hydrogen bonds in the solid molecules play vital roles in crystal packing. This compound is a benzimidazole drug which is widely utilized in veterinary medicine for the hinderance and treatment of parasitic diseases of worms and behaves as most efficient anthelmintic agents (McKellar et al., 1990; Z. Wu et al., 2010; Dib et al., 2015). The pharmacological response of RBZ support in the blockage of glucose uptake that produce reduction of glycogen stores and decrease the adenosine triphosphate (ATP) formation in the larval and adult stages of parasites (Bongioanni et al., 2018; Formentini et al., 2001; Riviere & Papich, 2018; García et al., 2013; Priotti, Baglioni, et al., 2018; Stuchlíková et al., 2018). RBZ is soluble in a mixture of water and methanol (50% + 50%). It is feebly soluble in the other solvents like: ethanol, benzene, etc. RBZ has low solubility and high permeability, so it lies in class II of the Biopharmaceutical Classification Systems (BCS) (Z. Wu et al., 2005; Priotti, Leonardi, et al., 2018). The speed of absorption is greater than that of dissolution, where the dissolution controls the speed of absorption. Thus, absorption and bio-availability are limited by the rate of dissolution of the drug (Kawabata et al., 2011). The BCS was formed to guide the correlation between drug dissolution *in vitro* and bio-availability *in vivo* (C.-Y. Wu & Benet, 2005). From these two criteria, the drugs oral absorption have been classified into four classes, based on BCS classification system as presented in Figure 2. The 30% of commercially formulated drugs lie in class II and show limitations for oral medication due to their low solubility (Amidon et al., 1995).

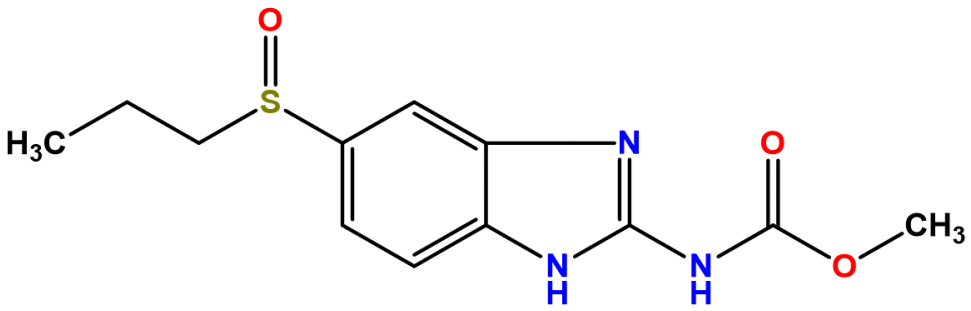

Figure 1: Chemical structure of ricobndazole (PubChem Compound Database, 2019a).

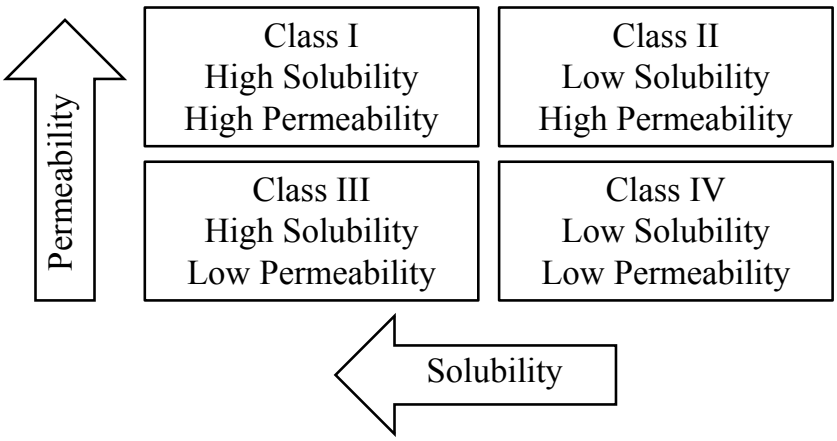

Figure 2: Biopharmaceutical Classification Systems

1.2 Cefradine

The cefradine with molecular formula $C_{16}H_{19}N_3O_4S$ and IUPAC name, (6R,7R)-7-[[-(2R)-2-amino-2-cyclohexa-1,4-dien-1-ylacetyl]amino]-3-methyl-8-oxo-5-thia-1-azabicyclo[4.2.0]oct-2-ene-2-carboxylic acid, is the first generation, β-Lactam, cephalosporin antibiotic. The structure of cefradine is similar to that of cephalexin. The molecular weight of cefradine is 349.4 g/mol and its chemical structure is presented in Figure 3. It is a new cephalosporin antibiotic which is utilized to treat urinary, bronchopulmonary and wound infections in patients presenting a disseminated cancer. The effectiveness of cefradine is more while treating the infections of urinary tract, respiratory tract, soft tissue and wound infections. *In vitro* tests showed that cefradine inhibited most strains of *Pneumococcus Staphylococcus* and *Streptococcus pyogenes* (Klastersky et al., 1973). Cefradine is agile against gram-positive and gram-negative bacteria as well as agile against most strains of penicillinase-producing *Staphylococci* (Du & Luo, 2010).

The solubility of cefradine in most solvents is low, resulting in limited bio-availability and/or erratic absorption (Zhong et al., 2005). In general, it crystallizes in dihydrate form. The structure from single-crystal X-ray data was described in 1976 while atomic co-ordinates were published by Van de Streek et al. (2013). The crystallization mainly includes precipitate crystallization, dilution crystallization and reaction crystallization. The crystallization of cefradine belongs to the reaction crystallization procedure which is hard to control because of its high reaction rate (Du & Luo, 2010; Meseguer et al., 1994; Palomo-Coll & Palomo-Coll, 1983). Cefradine has two benzene rings R1 and R3 and one β-lactam ring R2. The carbonyl (C=O) group in β-lactam ring is active for hydrogen bonding with neighboring molecule. Besides that two more carbonyl (C=O) groups are active for intra/intermolecular hydrogen bonding. Two amine (N-H) groups and one hydroxyl (OH) group have major role in hydrogen bonding in the crystal packing.

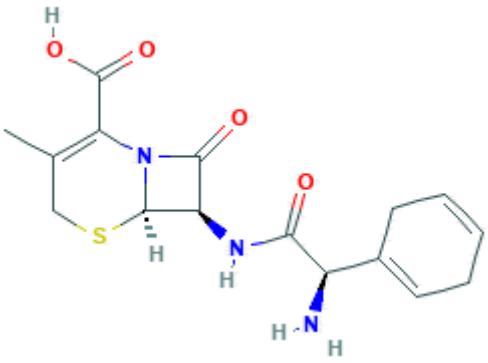

Figure 3: Chemical structure of cefradine (PubChem Compound Database, 2019b).

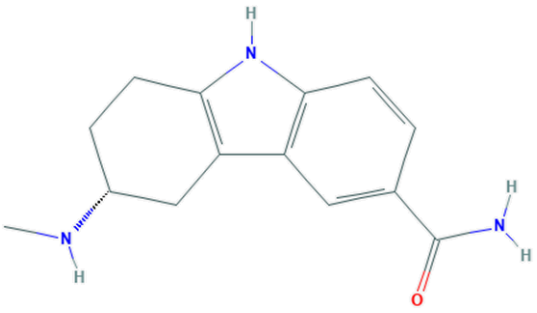

Figure 4: Chemical structure of frovatriptan (PubChem Compound Database, 2019c).

1.3 Frovatriptan

The frovatriptan having molecular formula $C_{14}H_{17}N_3O$ and molecular weight 243.3 g/-mol is a triptan drug which is widely used to treat menstrual migraine. The IUPAC name of frovatriptan is (6R)-6-(methylamino)-6,7,8,9-tetrahydro-5H-carbazole-3-carboxamide and its chemical structure is presented in Figure 4. Two benzene rings R1, R3 and one imidazole ring R2 are present in the compound. The carbonyl (C=O) and amine (N-H) groups are the main functional group that take part in the intermolecular hydrogen bonding in crystal packing as well as with the surrounding protein.

From the World Health Organization (WHO) data, migraine is the 19^{th} leading cause of years lived with disability for both sexes, however, the ranked for women is 12^{th}. The menstrual migraine in female is reported to be more severe, longer lasting, more likely to relapse and less responsive to acute treatment than migraines occurring at other times in the menstrual cycle (MacGregor et al., 2010; Leonardi et al., 2005; Granella et al., 2004; MacGregor & Hackshaw, 2004). Frovatriptan is suitable for the serotonin 5-HT_{1B} agonists class of receptors which has broad covering in the attention of migraine and vascular headaches, particularly in women at the time of menstruum. Frovatriptan dilates the arteries and veins so that blood can well arrive to the brain (Markus & Mikko, 2007; Ferrari et al., 2001).

1.4 Rationale of the study

The growing urbanization, alarming pollution and population growth, mostly in the cities in Nepal as well as globally have put a great challenge to the public health. The epidemic and endemic problems are claiming the lives of poor people in the remote areas and even in the cities very often. As a result, the widespread use of medicine is a common trend in our country or worldwide in the recent years. Despite the significant growth of the pharmaceutical industries in Nepal, it has not yet been dependent only on the medicines produced by these industries. Quality health service is the fundamental right of the

people as defined by the constitution of Nepal. However, the efficiency and efficacy of the drugs being supplied for the treatment of various diseases are still in question. In this light, this research will certainly contribute to ensure the quality of drugs produced by Nepalese/worldwide as well as help for the development of new series of drug in the pharmaceutical industries and help in the quality health service to the public.

This research focuses on the properties of biological active molecules like: RBZ, cefradine and frovatriptan. RBZ drug is widely used in veterinary medicine for the prevention and treatment of parasitic diseases. Cefradine is one of the several hundred different antibiotic substances used in human and veterinary medicine. It is useful for the treatment infections of urinary tract, respiratory tract, skin tissue and soft tissue. Frovatriptan lies in the serotonin 5-HT_{1B} agonists class of receptors which has the curative use to treat the migraine and vascular headaches, particularly in women during menstruation period.

The geometry optimization, minimum energy structure as well as physicochemical properties including the ligand-protein interaction has not been performed yet. These physical quantities enhance the potential of drugs in terms of stable structure, hydrogen bonding with residue of targets together with the chemical reactive sites with the surrounding protein which might help to improve the quality of drugs in the field of pharmacology and medicine. The global problem of advancing bacterial resistance to improve the quality of drugs has led to focus on the structural activity of the drug compositions. Considering the necessity of appropriate drug composition, this research focus on the structural, thermodynamic and electronic properties of some of the biologically active molecules. Therefore, the findings of this research might contribute to the pharmaceutical industries for strengthening the quality of drugs RBZ, cefradine and frovatriptan, and help to enhance the field of medicine.

1.5 Objectives

The objectives of this research are split into two parts.

1.5.1 General objective

The general objective is to study the structural parameters of ricobendazole and cefradine.

1.5.2 Specific objectives

The specific objectives are as follows:

1. To investigate the vibrational modes (infrared [IR] and Raman bands) of ricobendazole and cefradine and compare them with the experimental values.

2. To study the polarizability, hyperpolarizability and thermal properties (like: specific heat, entropy and enthalpy) of ricobendazole and cefradine molecules.
3. To study the molecular electrostatic potential with dipole moments and partial charges.
4. To study the reactive sites of ricobendazole and cefradine molecules.

1.6 Organization of the thesis

The structure of this thesis is organized as follows:

Chapter 1: Introduction

This chapter encircles the introduction of biological active molecules or active pharmaceutical ingredient (API). Moreover, the rationale of the research objectives has been incorporated.

Chapter 2: Literature Review

This chapter encircles the available literature related to the present work. The motive to identify the research problems and the justification of objectives of the present work has been incorporated in this chapter.

Chapter 3: Materials and Methods

This chapter encircles the basic introduction of density functional theory, the theoretical basis of quantum chemical calculation, necessary formula and algorithm that we have used during the entire work. Moreover, the various functional and basis set combination used in Gaussian 09 program are also presented in this chapter. We have also included the IR and Raman spectroscopy to justify the objectives of our present work.

Chapter 4: Results and Discussion

In this chapter, the main findings of the present work have been incorporated.

Chapter 5: Conclusions and Recommendations

This chapter includes the conclusion of the present work along with the possible extension in future study.

Chapter 6: Summary

A brief overview of the entire research has been incorporated in this chapter.

Finally, the references are listed before closing this document.

CHAPTER 2

2. LITERATURE REVIEW

During the last few decades, many research works were performed in the improvement of crystalline structure, solubility, thermodynamic as well as physicochemical properties of different biologically active molecules (antibiotics, anti-oxidants, cytotoxics, etc.) including alkaloids, peptides, etc. At present, many research works by different groups are focused on the study of solubility, polarizability, physicochemical properties with charge delocalization to insight the stability of biologically active molecules including RBZ, cefradine, frovatriptan, sitagliptin and carisoprodol for the enhancement of the drug potential. The history of medicine dates back practically to the existence of human society. The current established advanced medicine or allopathy has step by step formulation over the years by scientific and experimental efforts of scientists.

A literature survey reveals that the natural products chemistry began an important part of research 5000 years ago, probably with the work of Serturner, who first isolated morphine opium poppy (*Papaver somniferum*) (Patwardhan et al., 2004). Quinine had its origin in the royal households of the South American Incas. Indian fever bark (in the early 1500s) was one of the first medicinal plants to find appreciative consumers in Europe, taken from the cinchona tree (*Cinchona officinalis*). In 1860, a German chemist Carl Koler isolated cocaine, a chemical responsible for the biological activity. The Greek physician Galen (129-200 AD) devised the first pharmacopeia describing the appearance, properties and use of many plants of his time (Connolly, 1997). Many plants produce a variety of compounds, including biologically active proteins. Some of these compounds are even shared with other organisms and they include chemical families such as lectins, defensins, cyclotides and ribosome-inactivating proteins (Connolly, 1997).

Triptans, a family of tryptamine, have curative behavior for the treatment of migraines and cluster headaches. The efficacy of sumatriptan and naproxen sodium for the acute treatment of migraine has been investigated. The efficacy responses of sumatriptan and naproxen sodium in combined way produce more efficiency than the monotherapy. This decrease in bio-availability in monothreapy with sumatriptan is due to the chance in pharmacokinetic during encapsulation of the sumatriptan (Smith et al., 2005). Triptans drugs act as agonists for serotonin 5-$HT_{1B/1D}$ receptors at blood vessels and nerve endings in the brain. Sumatriptan was the first clinical drugs of the triptan family which has been marketed since 1991. There are many members of triptans family. Few of them are sumatriptan, naratriptan, zolmitriptan, rizatriptan, almotriptan, eletriptan and frovatriptan (Ferrari et al., 2001). The bio-availability and pharmacokinetics for drug

has major contribution in checking the drug potential and their values for RBZ in sheep is more when injecting through subcutaneous than intravenous and intraruminal route (Formentini et al., 2005, 2001). Moreover, the physicochemical properties of RBZ such as solubility in some pharmaceutical solvent, pH-solubility as well as ionization properties has been characterized (Z. Wu et al., 2005). Sitagliptin lies in dipeptidyl peptidase-4 (DPP-4) inhibitors class of drug. Pharmacologic characteristics of sitagliptin in humans were studied by Herman et al. (2005) which concluded that inhibition of plasma DPP-IV activity, the postprandial rise in active glucagon-like peptide 1 concentrations without causing hypoglycemia in normoglycemic healthy male volunteers. Cefradine, a member of cephalosporin antibiotics, is used to treat the bacterial infections regarding the respiratory and urinary tracts, ear and skin of soft tissues. Du & Luo (2010) studied the crystallization of cefradine under different conditions keeping dissolving temperature, 15 °C; initial temperature in crystallization, 30 °C; cooling temperature in crystallization, 0 °C; and adding 1,2-propanediol as an adjuvant agent with a volume ratio 0.2 of water solution. The yield of cefradine crystallization was about 92 % under these conditions. Oncocalyxone A has pharmaceutical use in antitumor, analgesic, antioxidant and causative of inhibition of platelet activation. The structural properties of Oncocalyxone A on the basis of conformer analysis and from vibrational spectroscopy (Fourier transform infrared [FT-IR] and Fourier transform Raman [FT-Raman]) were studied by Joshi, Srivastava, Honorato, et al. (2013). The molecular stability of Oncocalyxone A has been scrutinized from the potential energy surface (PES) scan analysis and the delocalization of charge from hyperconjugative interaction from the natural bond orbital (NBO) analysis by using the *ab initio* Hartree–Fock (HF) and the density functional theory (DFT/B3LYP) method with 6-311++G(d, p) basis set. A. Srivastava et al. (2010) studied the polymorphism in imatinib mesylate and compared the calculated and the observed IR and Raman spectra. They found that imatinib mesylate exists in two polymorphic forms α and β. However, β-form is more stable than the α-form. They have presented a detailed vibrational spectroscopic investigation of β-form by using the FT-IR and the FT-Raman spectra. The vibrational study (FT-IR and FT-Raman) of polymorphic β-form of imatinib mesylate has been studied on the basis of DFT by using the functional B3LYP/6-311G(d,p) basis set. The energy gap between the highest occupied molecular orbital and the lowest unoccupied molecular orbital i.e., HOMO-LUMO energy gap has been analyzed and the structure of polymorphic β-form is more stable than the α-form (A. Srivastava et al., 2013). Mishra et al. (2010) studied the structure and vibrational spectra of an anti-HIV agent; efavirenz. The molecular geometry parameters, calculated by DFT, were found in good agreement with the experimental values. Information on the size, shape, charge density distribution and site of chemical reactivity of the molecule has been obtained by mapping electron density iso-surface with the PES scan. The Raman spectra were recorded and the vibrational bands were assigned based on the DFT calcu-

lations with the dipole moments and the electrostatic potential surface. Joshi, Srivastava, Gupta, et al. (2013) studied the geometry optimization, electrostatic potential surface, frontier orbital energy gap and vibrational wavenumbers of aristolochic acid I (AA I) using the HF and the DFT methods. These works give relevant facts on the structural and the electronic properties of some biologically active natural products. Carisoprodol is a centrally acting skeletal muscle relaxant but it has also the abuse potential similar to that of benzodiazepines. The abuse potential of carisoprodol, the associated withdrawal syndrome and its implications was studied by Reeves & Burke (2010).

RBZ lies in benzimidazole group of drugs, has great attention towards the veterinary medicine mainly in livestock against internal parasites e.g., roundworms, tapeworm and liver flukes (Walter & Ahmed, 2018; Woodgate et al., 2017). Different types of worms producing the helminthic infections affect millions of people globally. The benzimidazole compounds such as RBZ has great attention to treat helminthiasis. However, its low aqueous solubility leads to the lack of efficacy towards poor gastrointestinal dissolution and absorption. A comparative study of pharmacokinetic and physicochemical behavior of RBZ-NCs has been performed in dogs (Stuchlíková et al., 2018). Literature survey reveals that the structural properties of RBZ from geometry optimization as well as from conformational analysis in terms of one dimensional PES scan has not been conducted so far. Moreover, the chemical reactivity descriptor of RBZ in terms of molecular electrostatic potential (MEP) surface, global and local reactivity descriptor as well from the HOMO-LUMO energy gap are still the interest of study. Besides that the drug potential as well as the inter/intramolecular hydrogen bonding from the IR and the Raman spectra are the major interest of study.

Busulfan is used to treat chronic myeloid leukemia. The chemical reactivity analysis on the basis of electrophilic/ nucleophilic sites, MEP, quantitative analysis on the distribution of charge on the atom in the molecule as well as the binding sites of busulfan has been carried out from the molecular docking and the quantum chemical calculation approach (Karthick & Tandon, 2016). Cephalosporin, discovered in 1945, is a class of β-lactam antibiotics that is originated from the fungus, Acremounium, which was initially known as cephalosporium. It is suitable for the upper respiratory tract infections and popularly known as sinusitis, pharyngitis, tonsillitis and laryngo-tracheo bronchitis (Sayed et al., 2016; Weliky et al., 1974). Cefadroxil is a β-lactam antibiotic drug which lies in the cephalosporin class of drugs having curative behavior similar to the cefradine. The comparative studies of experimental FT-IR and FT-Raman with simulated data were analyzed. Moreover, the reactive nature of cefadroxil in terms of the MEP surface analysis and the HOMO-LUMO energy gap has been studied by Muthu et al. (2015). But the chemical reactivity of cefradine in terms of MEP surface, global and local reactivity descriptor has not been studied in the literary study survey. The structure

of cefradine dehydrate was described with singlecrystal X-ray in 1976 without reporting the atomic coordinates. The atomic coordinate has been published from dispersion-corrected density functional theory (DFT-D) by Van de Streek et al. (2013) but the drug potential cefradine in terms of molecular docking has not been performed. Fakhri et al. (2016) studied the normative batch adsorption of cefotaxime, cefradine and cefazolin with CdS-MWCNT nanocomposites. It reveals that the adsorption capacity increases with increasing the pH value and decreasing the temperature. Structures and physic-ochemical characteristics of five new cefradine drug complexes were characterized by spectroscopic methods like IR, Raman and ultraviolet-Visible spectra, scanning electron microscopy and transmission electron microscopy methods and the antibacterial activity of the complexes were tested against some kinds of bacteria and fungi strains (Al-Khodir & Refat, 2017). However, the analysis of cefradine in terms of inter and intra molecular hydrogen bonding from spectroscopic behavior (IR and Raman) has not been studied. The environment and human health is highly affected from the antibiotic pollutants in the wastewater. The adsorption capacity of tetracycline and cefradine from biochar was studied, which infer that the Columbic interaction and π-π electron-donor-acceptor interaction between cornstalk biochar and cefradine/tetracycline molecules contribute the vital role (Al-Khodir & Refat, 2017; Ali et al., 2020; Zhao et al., 2018; Song et al., 2019). A. K. Singh et al. (2014) analyzed the corrosion inhibition properties of cefradine for mild hydrogen chloride solution. This study revealed that cefradine acted as mixed type inhibitor. Moreover, the adsorption mechanism has been elaborated in terms of various thermodynamic parameters. However, the structural parameters of cefradine from geometry optimization as well as electron transport properties in terms of HOMO-LUMO energy gap are still the interest of study.

Initially, frovatriptan was used as drug in 1990. Tension type headache is not treated by triptans drugs. Migraine, a public health problem that affects both the individual and society, is a neurovascular disorder that arises due to activation of the trigeminovascular system and cranial vasodilation mediated by the release of calcitonin gene-related peptide (CGRP). Triptans, 5-$HT_{1B/1D}$ receptor agonists, have therapeutic use for acute migran pain as gold standard (Rubio-Beltrán et al., 2018). The adsorption of sumatriptan drug onto graphene oxide was studied using DFT which signifies the intense interactions between the positively polarized parts of the sumatriptan (i.e., hydrogen atoms of the–OH and –NH parts) and the negatively polarized oxygen atoms of the graphene oxide. Moreover, graphene oxide can acts as a promising carrier/sensor for sumatriptan drug in practical applications. The frontier molecular orbital, NBO, and the dipole moment were investigated. The global indices such as hardness, softness, chemical potential and electrophilicity of triptan drugs were calculated and compared (Jafari et al., 2021). Frovatriptan succinate as orally disintegrating tablets was formu-

lated in terms of Sodium Starch Glycolate, croscarmellose sodium and crospovidone as well as its bio-availability has been compared from conventional tablets. The effective frovatriptan succinate orally disintegrating tablet form to treat acute migraine attack was generated by direct compression technique (Thulluru et al., 2016). Migraine affects 18% of women and 6% of men. Generally migraine attacks are observed, more than 50% of women migraineurs, during the perimenstrual period. Allais et al. (2018) studied the menstrual migraine based on the Medline database of June 2017. They revealed that the treatment of menstrual migraine is highly complex to evaluate for target therapy, however, the triptans drugs are appropriate for the menstrual migraine (Mayans & Walling, 2018). A conventional therapy is not suitable for treatment regarding the menstrually associated migraine. So, the randomized investigation of frovatriptan, $5HT_{1B/1D}$ receptor agonist, having long half-life and good tolerability for the intermittent inhibitor of menstrual migraine has been done and it has been found to reduce the occurrence of menstrually associated migraine headache (Silberstein et al., 2004; Markus & Mikko, 2007; Maasumi et al., 2017). The comparative study for clinical administration of frovatriptan with sumatriptan, almotriptan, rizatriptan and zolmitriptan has been done which inferred that the effectiveness of frovatriptan against the acute treatment of severe migraine attacks is more due to its favourable tolerability profile than the other comparators (Sanford, 2012). The locomotor activity in female rats has been studied with the impression of frovatriptan and almotriptan in nitroglycerin-induced migraine which concluded that frovatriptan possesses high agonistic activity to $5\text{-}HT_{1B/1D}$ receptors (Saracheva et al., 2019). Polymeric nanoparticles of frovatriptan succinate for brain targeting through nasal route has been developed by Deepika et al. (2019). This research has predicted that the hydrophilic drug, frovatriptan succinate can be successfully entrapped in polymeric nanoparticles to target brain via nasal delivery and the bio-availability of frovatriptan succinate has been increased. The correlative study of the second-generation $5\text{-}HT_{1B/1D}$ agonists (almotriptan, eletriptan, frovatriptan, naratriptan, rizatriptan and zolmitriptan) has been done by Deleu & Hanssens (2000). This study has been compared in terms of *in vitro* pharmacological properties, pharmacokinetics, clinical efficacy, drug interactions and adverse effects with the golden standard in the treatment of acute migraine, sumatriptan. The binding activities of frovatriptan with protein from the molecular docking approach has not been studied. Moreover, the chemical reactivity in terms of global and local reactivity parameters as well as the conformational analysis and the geometry optimization are the major interests of research. Literature survey revealed that the NLO and the thermodynamical study of frovatriptan has not been conducted so far.

Sitagliptin with trade name januvia is used to suppress blood sugar level in patient with type 2 diabetes mellitus. Sitagliptin reproduce the amounts of certain natural substances which subside the blood sugar level in the patient. The potential advantage of

sitagliptin via oral administration is more in comparison to the other antihyperglycaemic agents like voglibose, metformin, pioglitazone (Dhillon, 2010). The structural properties of sitagliptin from the vibrational spectroscopic (FT-IR and FT-Raman) approach as well as the electronic properties regarding the NBO analysis, Mullikan atomic charge, electronic absorption properties in terms of HOMO-LUMO have been studied by Rajesh et al. (2018). The adverse effect of sitagliptin and metformin has been studied by Williams-Herman et al. (2010) in 246 patients for type 2 diabetes and it has been concluded that sitagliptin does not contribute major adverse cardiovascular system and well tolerated in clinical trials up to 2 years duration (Scott et al., 2008; Raz et al., 2008). Efficacy of sitagliptin is found to be more for the significant reduction of HbA_{1c} when added to insulin therapy in patients with type 2 diabetes than the metformin but adverse effect in gastro intestine was observed with sitagliptin (Vilsbøll et al., 2010; Aschner et al., 2010). The histological and immunohistochemical effects of sitagliptin on both endocrine and exocrine pancreases in a rat model of type 2 diabetes mellitus were studied and the outcomes have been correlated with the biochemical findings. Furthermore, a possible synergistic effect of sitagliptin in combination with metformin was also evaluated (Shawky et al., 2020; Green & Feinglos, 2008). The efficacy and safety of sitagliptin as monotherapy in Chinese, Indian and Korean patient with type 2 diabetes were evaluated and this research signifies that sitagliptin has good characteristic in glycemic control and well-tolerated (V. Mohan et al., 2009). But the binding activity of sitagliptin with residue of protein has not been conducted so far. Moreover, the molecular stability in terms of NBO analysis is major interest of research.

Carisoprodol, popularly known as soma, is effective as muscle relaxer which stops the pain sensation between the nerves and the brain. In 2017, carisoprodol was the 255^{th} commonly prescribed drug from more than one million prescriptions. Carisoprodol and its major metabolite meprobamate have central nervous system sedating effects similar to benzodiazepines or alcohol which my produce adverse effects in human beings such as drowsiness, confusion, poor balance and coordination. This is due in part to the common co-administration of other central nervous system depressants, hypnotics or narcotic drugs and the lack of routine testing for carisoprodol and meprobamate in the human performance toxicology laboratory (Robertson & Marinetti, 2003). Texas poison centers during 1998-2009 identified 1,295 poisoning cases due to misuse of hydrocodone, carisoprodol and alprazolam which caused the suicidal death in human (Forrester, 2011). The quantum chemical calculation of cyclobenzaprine such as the geometry optimization, study of the IR and the Raman spectra, the hyperconjucative interaction in terms of the natural bond orbital analysis, the HOMO-LUMO energy gap having similar curative properties like carisoprodol were studied by Mary et al. (2014). The bioavailability of carisoprodol was studied by Carbonaro et al. (2020), which clarified that carisoprodol

penetrates into brain tissue and directly produces behavioral effects without being metabolized to meprobamate. The biomolecular interactions of carisoprodol with bovine serum albumin have been studied by Bolattin et al. (2016), which signifies the binding of carisoprodol to bovine serum albumin induced conformational changes in bovine serum albumin. Moreover, the binding sites and interaction of carisoprodol with amino acid residues has been scrutinized. The structure of the impurity of carisoprodol observed during the optimization and bulk synthesis has been identified by Kumar et al. (2017). The impurity was synthesised, characterised and co-injected with carisoprodol sample to verify the retention time in high performance liquid chromatography. The histopathological and histochemical changes in liver tissue of pregnant rats and their fetuses after treatment with carisoprodol were studied by Abouel-Magd (2018). The treatment of pregnant rats with carisoprodol led to many dystrophic changes in maternal and fetal liver tissue. The treated groups showed lots of degenerative changes post-treatment with carisoprodol. The polymorphism in carisoprodol was analyzed by Diogo et al. (2018). A metastable polymorph, B, was detected. The estimated melting enthalpy signified that a monotropic relation with the most stable polymorph, A. This study revealed that carisoprodol showed a strong glass forming ability with a glass transition temperature $T_g = -8$ °C, which intensify that it can exist as a metastable liquid at room temperature as well as crystallizes isothermally at room temperature over long duration and illustrate cold crystallization at about 60 °C when heated on slow ramps (Diogo et al., 2018). But the molecular docking analysis is still the interest of research to check the drug potential of carisoprodol. Literature survey reveals that the geometry optimization, chemical reactivity behavior in terms of the local and the global reactivity descriptor has not been analyzed. Moreover, the arrangement of charge around the molecule in terms of the MEP surface has not been studied and these are the major interest of research.

Research Gap

Many experimental and theoretical works have been performed by different research groups to enhance the potential of drugs: RBZ, cefradine and frovatriptan. However, many things are still the interest of study. The structural properties of biological active molecule has great attention in drug discovery and drug design. The conformational analysis of drug molecules like: RBZ, cefradine and frovatriptan in terms of bond length, bond angle and dihedral angle from one dimentional potential energy surface analysis is the interest of study. The spectroscopic technique for example IR and Raman analysis is used to study the structural behavior of drug molecules to identify the functional group present in the molecular system as well as the finger print region. The comparative study of simulated spectra with experimentally recorded spectra has not been conducted so far. The spectroscopic technique is also used to predict the hydrogen bonding in crystal packing. The distribution of charge in space around the molecular system has great

importance to predict the reactive binding sites in drug molecule. This can be done by using the MEP surface analysis. This analysis has not been done by any research group. The molecular stability of the molecular system can be scrutinized from the HOMO-LUMO energy gap as well as from the global reactivity behavior. This is still the interest of study. To identify the chemical reactivity of the drug molecule which can be checked from the local reactivity behavior in terms of Fukui function (FF) which is measured in terms of Hirshfeld partial charge analysis is not presented in the literature. Non-linear optical as well as the thermodynamic parameters (specific heat, entropy and enthalpy) of these drug molecules have not been studied by any research group. The protein-ligand binding activity of these drug molecules with predicted targets protein have not been carried out by any research group.

CHAPTER 3

3. MATERIALS AND METHODS

3.1 Introduction

Active pharmaceutical ingredient (API) has a wide range of applications in medical science due to its biological activity. The molecular activity of API is determined by the electronic and the nuclear properties in the molecular system. The quantum chemical calculation is the fundamental way to insight the microscopic study of the molecular structure along with the electron transport properties. The molecular interaction and its properties are the concern of chemical science. Electrons and nuclei are the building block of the molecule and their locomotive is explained by the laws of quantum mechanics. In quantum mechanics, the fundamental properties of a system are described by wave function which depends on the co-ordinates of particle and time. The molecular properties such as molecular structure, reactivity, distribution of electronic charge around the molecule, electron transport properties, spectroscopic vibrational phenomenon etc. are included in quantum chemistry. The calculation from the First principle/*ab initio* is used for a better understanding of the molecular structure and its properties.

In this chapter, we have discussed the fundamental way of theory for calculation regarding the optimized energy, geometry optimization, chemical reactivity, molecular stability, modes of vibration, molecular docking and intramolecular hydrogen bonding of investigated drug molecules (RBZ, cefradine and frovatriptan) as well as the experimental techniques for the determination of the IR and the Raman spectra of RBZ and cefradine to study the functional group present in the molecular system and the prediction of intermolecular hydrogen bonding in the crystal structure.

3.2 Experimental technique

In this section, we have focused on the experimental details used in this thesis. We have mainly discussed the FT-Raman and the FT-IR. Moreover, we have also explained the principle regarding the IR and the Raman spectroscopy. The API has been characterized in terms of spectroscopic technique. The FT-IR and the FT-Raman spectroscopy provides the functional group identification and the vibrational characteristics of the biological active molecules. Moreover, the quantum chemical calculation provides better understanding regarding the mixed mode of vibrations through the normal coordinate procedure. In the present chapter, the experimental setup such as FT-IR and FT-Raman used for study of RBZ and cefradine are given in detail.

3.2.1 Vibrational spectroscopy

Vibrational spectroscopy is a well established technique which is applicable for solid (amorphous/crystalline), liquid/solution, gas and film samples. Vibrational spectroscopy such as IR and Raman has prominent role in the analysis of chemical structure and vibrational features of organic molecules. It gathers the information regarding the inter and intramolecular forces, identification of molecular structure and identification and characterization of new molecules. The signature of IR spectroscopy at a particular wavenumber is due to the change in the molecular dipole moment of the molecular system. The peak that appears in Raman spectroscopy is due to the change in the polarizability of the molecular system. These two methods produce parallel results about the molecular vibration. These two processes help to insight into the normal modes of vibration of the molecules. This work incorporates both the IR and the Raman spectroscopy to scrutinize the vibrational features of the RBZ and the cefradine drug molecules. The mixed mode of vibration has been analyzed more accurately from normal coordinate analysis to obtain the potential energy distribution result. So, qualitative and quantitative analysis can be performed with spectroscopy method for the vibrational analysis (Bumbrah & Sharma, 2016; Raman & Krishnan, 1928; Skoog et al., 2017; Settle, 1997).

3.2.2 Raman spectroscopy

Raman spectroscopy is useful to analyze the atomic position, electron distribution and intermolecular forces in the molecular system and gathers informations regarding the biochemical composition of drug molecules (Willard et al., 1989). In Raman spectroscopy, the scattered light is obtained from the interacting sample with a monochromatic laser light. The Raman spectrum is due to the inelastic scattering of light having frequency differing from the incident light. The active Raman peak in the spectrum is due to the change in the polarizability of sample during the molecular vibrations. The Raman spectrometers may be dispersive or non-dispersive. Raman spectroscopy becomes easier and more practicable when FT-Bruker IFS 55 Equinox spectrometer is introduced in the field of spectroscopy, which gives rapid and reliable analysis. It is quite helpful to study the material which is difficult to analyze with fluorescence and insure about the easy data handling facilities which is available in commercial FT-IR spectrometer (Chase & Rabolt, 1994; Keller et al., 1993). It is also benefitted in terms of spectral resolution and wavelength accuracy.

The RBZ in solid form of whiteness level more than 98% was procured from the Merck & Co., multinational pharmaceutical company, USA. Whereas, the solid form cefradine of whiteness level more than 98% was procured from the Antibiotics do Brazil Ltd (ABL), Brazil. The purity level of compounds is at analytical standard so without making any

further cleaning, the Raman spectra of compounds (RBZ and cefradine) were recorded at room temperature. The signature of Raman spectrum of the RBZ and the cefradine compounds was documented in the range of (100 to 3500) cm^{-1} from RAM II module and its working is based on diode-pumped Nd: YAG laser. The laser generated is capable of emitting the radiation of 1064 nm wavelength at low power (100 mW).

3.2.3 Infrared spectroscopy

The most common spectroscopic technique that is used in society of chemistry is IR spectroscopy. It measures the absorbance of different IR frequencies from a sample in the path of an IR beam of light. The principle involved in IR spectroscopy is due to the change in the molecular dipole moment of the molecular system when IR light is incident on the vibrating particles. The major work of IR spectroscopy is to analyze the functional group present in the sample. The different functional groups absorb the different frequencies of IR radiation. The IR spectrum can be categorized into two regions, one is called the functional group region and another is called the fingerprint region. The wavenumber in the regions (1500 to 4000) cm^{-1} is considered as functional group region whereas the wavenumber below 1500 cm^{-1} is taken as fingerprint region which is the characteristic of molecular system. The fingerprint region involves the stretching and the bending vibration of different bonds in the molecular system which is unique for a given molecular system. This signifies the molecular system more precisely. Thus, both the regions are very helpful to produce the confidence about the structure of chemical species. This is usually recognized by a comparison of spectrum of known sample. The peaks of stretching vibrations characterize the functional group of organic sample.

The purity level of compounds (RBZ and cefradine) is at analytical standard so without making any further cleaning, the infra red signature was recorded at room temperature. The FT-IR spectrum of compounds was reported with Bruker Vertex 70 FT-IR spectrometer. For the spectral measurement, the pellet was formed by mixing the compound with KBr in the ratio $1 : 200$ which reduces the signal to noise ratio.T he spectrum was measured in the range of (400 to 4000) cm^{-1} with a resolution of 4 cm^{-1}.

3.3 Theoretical background

The objective of any theory of molecular system is to provide some insight into the various physical laws governing the chemical constitution of molecules in terms of more fundamental universal physical laws guiding the motions and the interactions of the constituent atomic nuclei and electrons. In quantum mechanics, the physical properties of a system can be obtained from the wave function, a function depending upon the coordinates of the particles and time. The application of the laws of quantum

mechanics which deals with the chemical structure and reactivity is a branch of quantum chemistry. Many computational methods have been developed to study the chemical and the physical knowledge in the molecular world with computational science that enhance our understanding of structure and function of molecules.

Electronic properties are essential to understand the fundamental concept of physics, chemistry and biology of drug molecules. So, one can consider the atomistic level of study to interpret the microscopic properties of API, where the separate identity of electrons is neglected. In the present work, the electronic structure has been calculated from DFT. The structure of drug molecules that expected to exist at room temperature obtained from one dimensional PES scan and optimized parameters has been determined from geometry optimization and quantum chemical procedure. In addition, the atomistic level of calculations to investigate the inter and intra molecular hydrogen bonding has been analyzed. Moreover the most reactive part in the drug molecule has been scrutinized and the protein-ligand interaction has been examined on the basis of molecular docking. Electronic structure of a drug molecule has important role to identify the physical, chemical and biological properties. In many body particles, electrons and nuclei are considered as interacting particles and their solution has been estimated by using Schrödinger equation.

1. Nuclear and electronic equations are separated from Born-Oppenheimer approximation (BOA) including external potentials wherever necessary.
2. The outcome of DFT, functional of electron density, is superior in many aspects in comparison to many body wave-functions.
3. In the wave-function as well as in the DFT, the calculations are performed by converting interacting many body problem into non-interacting single particle problem.

In computational quantum chemistry, the method can be classified into two categories: semi-empirical and *ab initio* electronic structure theory. The semi-empirical methods are relatively faster in terms of computational cost as they solve an approximate form of the Schrödinger equation that uses experimentally derived parameters to simplify the work. The various semi-empirical methods are AM1, PM3 etc. The *ab-initio* methods (or first principles) are governed by the laws of quantum mechanics and a few physical constants but no experimental parameters are included and the solution has been obtained from the Schrödinger equation. Moreover, rigorous method is used to find the exact solutions for chemical systems different from hydrogen-like atom. So, methods such as Hartree-Fock (H-F), Møller-Plesset (MP), coupled cluster (CC) and configuration interaction (CI) approaches have been developed to approximate the solution of the Schrödinger equation. Despite the use of some approximations, the *ab initio* methods generally give

more accurate results than the semi-empirical methods, especially when calculations are performed at higher levels of theory. As expected with all strategies, higher the approximation, the more accurate the results and the computational cost will be high and vice versa. The computational *ab initio* quantum chemistry is aimed to calculate the structures and the properties of molecules. In this thesis, the computational calculation is based on the DFT methods and the theoretical background is briefly explained below.

3.3.1 Born-Oppenheimer approximation

The electronic structure of molecular system reflects many physical, chemical and biological phenomena such as magnetic, optical, transport and chemical reactivity of materials. The electronic structure calculation is a difficult task because the electronic interactions in matter are quantum mechanical in nature and its description becomes tedious with the increasing number of the electrons which leads to the idea of many body problem. For N particles system, there are $3N$ variables which create the complexity in the equations. The solution can be obtained from the Schrodinger equation:

$$\hat{H}\Psi = E\Psi \tag{3.1}$$

The Hamiltonian for a molecular system of N-electrons and M-nuclei can be written as

$$\hat{H} = -\frac{\hbar^2}{2m_\mathrm{e}}\sum_{i=1}^{N}\nabla_i^2 + \frac{1}{2}\sum_{i\neq j}\frac{e^2}{|\mathbf{r}_i - \mathbf{r}_j|} - \frac{1}{2}\sum_{i,I}\frac{Z_I e^2}{|\mathbf{r}_i - \mathbf{R}_I|} - \sum_{I=1}^{M}\frac{\hbar^2\nabla_I^2}{2M_I} + \frac{1}{2}\sum_{I\neq J}\frac{Z_I Z_J e^2}{|\mathbf{R}_I - \mathbf{R}_J|} \tag{3.2}$$

In short notation, the Hamiltonian can be written as

$$\hat{H} = \hat{T}_\mathrm{e} + \hat{V}_\mathrm{int} + \hat{V}_\mathrm{ext} + \hat{T}_\mathrm{N} + \hat{V}_\mathrm{II} \tag{3.3}$$

where,

$$\hat{T}_\mathrm{e} = -\frac{\hbar^2}{2m_\mathrm{e}}\sum_{i=1}^{N}\nabla_i^2 \qquad \text{K. E. of electrons}$$

$$\hat{V}_\mathrm{int} = \frac{1}{2}\sum_{i\neq j}\frac{e^2}{|\mathbf{r}_i - \mathbf{r}_j|} \qquad \text{Electron-electron Coulomb repulsion energy}$$

$$\hat{V}_\mathrm{ext} = -\frac{1}{2}\sum_{i,I}\frac{Z_I e^2}{|\mathbf{r}_i - \mathbf{R}_I|} \qquad \text{Electron-nuclei Coulomb attraction energy}$$

$$\hat{T}_\mathrm{N} = -\frac{1}{2}\sum_{I=1}^{M}\frac{\hbar^2\nabla_I^2}{M_I} \qquad \text{K. E. of nuclei}$$

$$\hat{V}_{\mathrm{II}} = \frac{1}{2}\sum_{I\neq J}\frac{Z_I Z_J e^2}{|\mathbf{R}_I - \mathbf{R}_J|} \qquad \text{Nuclei-Nuclei Coulomb repulsion energy}$$

Here, m_{e} and M_{I} stands for the masses of electrons and nuclei whereas i, j and I, J run over the electrons and nuclei respectively.

For the total wave-function $\Psi(\mathbf{R}, \mathbf{r})$ of the system, Schrödinger equation becomes

$$\hat{H}\Psi(\mathbf{R}, \mathbf{r}) = E\Psi(\mathbf{R}, \mathbf{r}) \tag{3.4}$$

The solution of this equation gives every information. Due to huge computational cost, the exact solution of the Schrödinger equation even for a small system is practically impossible. The mass of electron is 1837 times lighter than the mass of the lightest nuclei. So, the motion of electron is much faster in comparison to the nuclear motion. It means nuclei remains instantaneously at rest in the time scale of the electronic motion and their motion can be separated from each other. Thus the nuclear kinetic energy is negligible and the repulsion between nuclei is constant. This principle was introduced by Born & Oppenheimer (1927) which is called the Born-Oppenheimer approximation (BOA). Thus by separating the nuclear and the electronic parts of the wave-function, the Schrödinger equation becomes

$$\Psi(\mathbf{R}, \mathbf{r}) = \chi(\mathbf{R}) \cdot \Phi(\mathbf{R}, \mathbf{r}) \tag{3.5}$$

where $\chi(\mathbf{R})$ describe the nucleus and $\Phi(\mathbf{R}, \mathbf{r})$ describe the electron. Thus the electronic Hamiltonian which describe the electronic motion under the influence of static external nuclear potential, can be written as

$$\hat{H}_{\mathrm{e}} = -\frac{\hbar^2}{2m_{\mathrm{e}}}\sum_{i=1}^{N}\nabla_i^2 - \frac{1}{2}\sum_{i,I}\frac{Z_I e^2}{|\mathbf{r}_i - \mathbf{R}_I|} + \frac{1}{2}\sum_{i\neq j}\frac{e^2}{|\mathbf{r}_i - \mathbf{r}_j|} \tag{3.6}$$

So, the Schrödinger equation for the electrons and the nuclei can be separately written as

$$\left[-\frac{\hbar^2}{2m_{\mathrm{e}}}\sum_{i=1}^{N}\nabla_i^2 - \frac{1}{2}\sum_{i,I}\frac{Z_I e^2}{|r_i - R_I|} + \frac{1}{2}\sum_{i\neq j}\frac{e^2}{|\mathbf{r}_i - \mathbf{r}_j|}\right]\Phi(\mathbf{R}, \mathbf{r}) = V(\mathbf{R})\Phi(\mathbf{R}, \mathbf{r}) \tag{3.7}$$

$$\left[-\sum_{I=1}^{M}\frac{\hbar^2\nabla_I^2}{2M_I} + V(\mathbf{R})\right]\chi(\mathbf{R}) = \mathrm{E}'\chi(\mathbf{R}) \tag{3.8}$$

The solution of these two equations gives the information of total energy of the system.

3.3.2 Hatree-Fock approximation

The electronic and the nuclear parts of the Hamiltonian are separated by BOA which reduces the complexity of the Schrödinger equation. But the solutions are still complicated due to unknown electron-electron interactions. Each electron moves under the influence of effective potential created by the nuclei and the remaining electrons. This idea motivates towards the single electron/particle approximation. There are two approaches to resolve the independent particle approximation instead of the many body problems and they are (i) the wave-function method and (ii) the DFT method.

Initially, the independent electron approximation was introduced by Hartree (1928), where the electrons are uncorrelated to each other and every electron moves under the effective potential of average Coulomb interactions. The total wave-function of electrons is the product of N one-electron wave-functions and is given by

$$\Psi\left(r_1, r_2, \ldots, r_n\right) = \phi_1\left(r_1\right)\phi_2\left(r_2\right)\ldots\phi_n\left(r_n\right) \tag{3.9}$$

which is known as Hartree product. Thus, the energy of the system is

$$H\Psi\left(r_1, r_2, \cdots, r_n\right) = E\Psi\left(r_1, r_2, \cdots, r_n\right) \tag{3.10}$$

The solution can be obtained from self-consistent variational method. The Hartree approximation reduces the complexity of interacting many electron approach, however, the anti-symmetric electronic wave-function was not included. Moreover, the exchange and the correlation terms were not incorporated.

The anti-symmetric nature of electronic wave was incorporated by Fock (1930) which obey the Pauli-exclusion principle. The Hatree and the Fock approximation are together called the Hatree-Fock (H-F) approximation (Hartree, 1928; Fock, 1930). In the H-F approximation, the wave functions are expressed in terms of a single Slater determinant of N spin-orbitals (Slater, 1937):

$$\Psi_{\mathrm{HF}} = \frac{1}{\sqrt{N!}}\begin{vmatrix} \phi_1\left(r_1, s_1\right) & \phi_2\left(r_1, s_2\right) & \cdots & \phi_n\left(r_1, s_n\right) \\ \phi_2\left(r_2, s_1\right) & \phi_2\left(r_2, s_2\right) & \cdots & \phi_n\left(r_2, s_n\right) \\ \vdots & \vdots & & \vdots \\ \phi_n\left(r_n, s_1\right) & \phi_n\left(r_n, s_2\right) & \cdots & \phi_n\left(r_n, s_n\right) \end{vmatrix} \tag{3.11}$$

Thus the Hamiltonian in the form of $\phi_i(r)$ becomes

$$\left(-\frac{\nabla^2}{2}+V_{\text{ext}}\right)+\int \mathrm{d}^3r'\frac{1}{|r-r'|}\left[\sum_{j\neq i}\phi_j^*(r')\phi_j(r')\phi_i(r)\right.$$
$$\left.-\delta_{s_is_j}\sum_{j\neq i}\phi_j^*(r')\phi_i(r')\phi_j(r)\right]=\varepsilon_i\phi_i(r) \tag{3.12}$$

where the exchange potential is defined as

$$V_x=-\int \mathrm{d}^3r'\sum_{j\neq i}\frac{1}{|r-r'|}\phi_j^*(r')\phi_i(r')\phi_j(r) \tag{3.13}$$

This term was absent in Hartree equations. With the inclusion of the Hartree and the exchange terms in the screening potential, the H-F approximation becomes

$$\left(-\frac{\nabla^2}{2}+V_{\text{ext}}+V_{\text{sc}}\right)\phi_i=\varepsilon_i\phi_i \tag{3.14}$$

where

$$V_{\text{sc}}=V_{\text{H}}+V_{\text{X}} \tag{3.15}$$

In the left side of Equation (3.12), the first term stands for kinetic energy of electrons and the second term represents the electron-ion interaction energy. The electrostatic interactions in between the electrons are represented by the third term which contains the self-interaction term (when $j=i$). This obeys the Pauli-exclusion principle in which the like-spin is not included. The important term in the real system is the correlation between the electrons which is still missing in the H-F approximation which is understood from the difference between the exact ground state energy of the many body system and the H-F energy ($E^0_{\text{exact}}-E^0_{\text{HF}}\neq 0$).

Both, the Hartree and the H-F methods are based on the wave function method and require huge computational cost for large system size because there are $4N$ variables for N-particle system in which $3N$ are space coordinates and N are spin coordinates. Moreover, the correlation term is not included in the H-F approximation. The electron density has great importance in the reduction of degree of freedom which reduces the computational cost to a great extent. The electron density is used as variable to solve many body Schrödinger equation in condensed matter physics and material science in recent era which is called the DFT.

3.4 Density functional theory

For the N-electrons system of a molecule there are 3N degree of freedom for space and N degrees of freedom for spin in the electronic wave function. The DFT assumes that a single variable can describe many body interacting particles and this variable is called the ground state density $n_0(\mathbf{r})$. Thus, the electronic density includes all the information of many body wavefunctions and helps in the reduction of the degree of freedom and the way of calculation to obtain ground state properties becomes easier. So, the ground state as well as the excited state electronic properties of molecular systems can be explained by the functional of electron density. The basic concept of DFT was first imported by Thomas (1927) and Fermi (1927). But it was applicable when the exchange and the correlation terms were introduced by Dirac (1930). So, the approximation is called the Thomas-Fermi-Dirac (TFD) approximation. The TFD approximation gain popularity after the breakthrough of the Hohenberg-Kohn theorems (Hohenberg & Kohn, 1964) and the Kohn-Sham (K-S) approximation (Kohn & Sham, 1965).

3.4.1 Thomas-Fermi-Dirac approximation

The Thomas and Fermi (TF) model (Thomas, 1927; Fermi, 1927) uses electron density as basic variable to solve the system of non interacting particle instead of wavefunctions. The total energy of a system from the TF model i.e., E_{TF} in terms of electron density $n(\mathbf{r})$ under the action of external potential $V_{\mathrm{ext}}(\mathrm{r})$ can be written as.

$$E_{\mathrm{TF}}[n(\mathbf{r})] = C_1 \int \mathrm{d}^3 r\ [n(\mathbf{r})]^{5/3} + \int \mathrm{d}^3 r\ V_{\mathrm{ext}}(\mathbf{r})[n(\mathbf{r})]^{5/3} + \frac{1}{2} \iint \frac{n(\mathbf{r})n(\mathbf{r}')}{|r_i - r_j|}\, \mathrm{d}^3\mathbf{r}\mathrm{d}^3\mathbf{r}' \tag{3.16}$$

In the right hand side, the first term represents the kinetic energy (K. E.) of the non-interacting electrons in the homogeneous electron gas (HEG) where $C_1 = \frac{3}{10}\left(3\pi^2\right)^{2/3}$ in atomic unit ($m_{\mathrm{e}} = e = \hbar = 4\pi/\epsilon_0 = 1$). The middle term represents the nuclei-electrons interaction which is called the external potential whereas the third term represents the electrostatic repulsion energy between the electrons which is also called the Hartree energy.

The K. E. of homogeneous electron gas can be determined from the relation

$$T_0[n(\mathbf{r})] = \frac{2}{(2\pi)^3} \int 4\pi k^2\, \mathrm{d}k = C_1[n(\mathbf{r})]^{5/3} \tag{3.17}$$

where k is the wave vector. However, the exchange and the correlation terms were not included in Thomos-Fermi model. The exchange term: $C_2 \int [n(\mathbf{r})]^{4/3}\, \mathrm{d}^3\mathbf{r}$, where $C_2 = -\frac{3}{4}\left(\frac{3}{\pi}\right)^{1/3}$ was introduced by Dirac (1930). The Thomos-Fermi- Dirac equation

then becomes

$$E_{\mathrm{TFD}}[n(\mathbf{r})] = C_1 \int \mathrm{d}^3\mathbf{r}\ [n(\mathbf{r})]^{5/3} + \int \mathrm{d}^3\mathbf{r}\ V_{\mathrm{ext}}(\mathbf{r})[n(\mathbf{r})]^{5/3} + \frac{1}{2}\iint \frac{n(\mathbf{r})n\,(\mathbf{r}')}{|r_i - r_j|}\,\mathrm{d}^3\mathbf{r}\mathrm{d}^3\mathbf{r}' + C_2 \int [n(\mathbf{r})]^{4/3}\,\mathrm{d}^3\mathbf{r} \tag{3.18}$$

The ground state energy and density can be obtained by minimizing the above energy functional for all possible $n\,(\mathbf{r}')$ where $\int n\,(\mathbf{r}')\,\mathrm{d}\mathbf{r}' = N$ (total number of electrons) Lagrange multiplier is used for the minimization of the functional and is given by

$$\delta\left[E_{\mathrm{TFD}}[n(\mathbf{r})] - \mu\left(\int n(\mathbf{r})\mathrm{d}^3\mathbf{r} - N\right)\right] = 0 \tag{3.19}$$

where μ is the Lagrange multiplier and it is also called the chemical potential. It's value is same as Fermi energy at 0 K. By using the stationary functional, the TFD equation becomes

$$\frac{5}{3}C_1[n(\mathbf{r})]^{2/3} + V_{\mathrm{ext}}(\mathbf{r}) + \int \frac{n\,(\mathbf{r}')}{|r_i - r_j|}\,\mathrm{d}^3\mathbf{r}' + \frac{4}{3}C_2[n(\mathbf{r})]^{1/3} - \mu = 0 \tag{3.20}$$

Thus the ground state density can be determined by solving the above equation. This model has drawback to describe the shell structure of atoms and the binding between the molecules. So, this model unable to describe the electrons in the molecular system.

3.4.2 Hohenberg-Kohn theorems

The H-F theory uses the approximation of one-electron spin orbitals for the solution of many-electrons Schrödinger equation and the correlation term was not incorporated. In the DFT, the solutions to many-electrons Schrödinger equation depend upon the electron density which is the fundamental approach of the DFT. In the DFT, the electron correlation has been incorporated for the calculation of exchange-correlation potential. The Hohenberg-Kohn (H-K) theorems are the basic foundations of the modern DFT in which electron density is the fundamental variable and this concept is applicable to any system of interacting particles under the influence of external potential (Hohenberg & Kohn, 1964). There are two H-K theorems and they are discussed below.

Theorem I: *The external potential $V_{\mathrm{ext}}(r)$ is a unique functional of ground state electron density $n_0(\boldsymbol{r})$.* This implies that all the properties of the system can be obtained if the ground state density $n_0(\mathbf{r})$ is known.

If the different external potential $V_{\mathrm{ext}}(r)$ gives the same ground state electron density then let us consider that $V_1(r)$ and $V_2(r)$ are the two external potential corresponding to the same ground state density of N-electron systems. Then, there should be two

respective Hamiltonians H_1 and H_2 given by

$$H_1 = T + U + \sum_i V_1(r_i)\,, \quad H_2 = T + U + \sum_i V_2(r_i)$$

where

$$T = -\frac{1}{2}\sum_i^N \nabla_i^2 \quad \text{and} \quad U = \frac{1}{2}\sum_{i\neq j} \frac{1}{|\mathbf{r}_i - \mathbf{r}_j|}$$

If E_1 and E_2 be the eigenvalues having the corresponding eigenfunctions Ψ_1 and Ψ_2 then the Schrödinger equations are $H_1\Psi_1 = E_1\Psi_1$ and $H_2\Psi_2 = E_2\Psi_2$. If Ψ_2 is not the ground state of H_1 which gives the same electron density as

$$n(\mathbf{r}) = N \int \Psi^*_{1|2}\left(\mathbf{r}_1, \mathbf{r}_2, \ldots, \mathbf{r}_N\right) \Psi_{1|2}\left(\mathbf{r}, \mathbf{r}_2, \ldots \mathbf{r}_N\right) \mathrm{d}\mathbf{r}_2\, \mathrm{d}\mathbf{r}_3 \ldots \mathrm{d}\mathbf{r}_N \tag{3.21}$$

Then, from the variational principle, we have

$$\begin{aligned} E_1 &= \langle \Psi_1 | H_1 | \Psi_1 \rangle \leq \langle \Psi_2 | H_1 | \Psi_2 \rangle \\ &\leq \langle \Psi_2 | H_2 | \Psi_2 \rangle + \langle \Psi_2 | H_1 - H_2 | \Psi_2 \rangle \\ &\leq \mathrm{E}_2 + \int \mathrm{d}r\; n(r)\left[V_1(\mathbf{r}) - V_2(\mathbf{r})\right] \end{aligned} \tag{3.22}$$

Similarly, it can be verified that

$$E_2 \leq E_1 + \int \mathrm{d}r\; n(r)\left[V_2(\mathbf{r}) - V_1(\mathbf{r})\right] \tag{3.23}$$

Adding the above two equations, we get

$$E_1 + E_2 \leq E_2 + E_1 \tag{3.24}$$

The above inequality leads to the conclusion that the same ground state density $n_0(\mathbf{r})$ unable to determine from two different external potentials $V_{\text{ext}}(\mathbf{r})$. Thus, there is a single external potential corresponding to the given ground state density. So, the external potential $V_{\text{ext}}(\mathbf{r})$ fixes the Hamiltonian and its wave function from the solution of the Schrödinger equation. Since, the wave function is a functional of density, the ground state density determines the ground state wavefunction and the energy functional $E_v[n(\mathbf{r})]$ for a given external potential $V_{\text{ext}}(\mathbf{r})$.

Theorem II: The functional $F[n_0(\mathbf{r})]$, that gives the ground state energy of the system, provides the lowest energy if and only if the initial density is the true ground state density $n_0(\mathbf{r})$ i.e., for every trial density function $n(\mathbf{r})$ that satisfies $\int n(\mathbf{r})d\mathbf{r} = N$ and $n(\mathbf{r}) \geq 0$ and which is connected to external potential $V_{\text{ext}}(\mathbf{r})$.

The H-K energy functional for a given external potential can be defined as

$$E^{(\mathrm{HK})}\,[n(\mathbf{r}), V_{\mathrm{ext}}] = \mathrm{T}[n(\mathbf{r})] + E_{\mathrm{int}}[n(\mathbf{r})] + \int V_{\mathrm{ext}}(r) n(\mathbf{r})\,\mathrm{d}r \tag{3.25}$$

In the right hand side, the first term stands for the kinetic energy whereas, the middle term represents the Coulomb potential energy of the interacting electrons. These terms are not dependent on any external potential and it is defined by a universal functional of density $F[n(\mathbf{r})]$:

$$F[n(\mathbf{r})] = T[n(\mathbf{r})] + E_{\mathrm{int}}[n(\mathbf{r})] \tag{3.26}$$

The last term in Equation (3.25) determines the electron-nuclei interactions. Thus the universal energy functional F[n($\mathbf{r}$)] can be expressed as

$$E^{(\mathrm{HK})}\,[n(\mathbf{r}), V_{\mathrm{ext}}] = F[n(\mathbf{r})] + \int V_{\mathrm{ext}}(r) n(\mathbf{r})\,\mathrm{d}r \tag{3.27}$$

The density which minimizes the energy functional is the exact ground state density. This is the second H-K theorem. Thus the minimization of Equation (3.27) with the variations of electron density gives the exact ground properties. But it is difficult to obtain the exact energy functional. The universal functional $F[n(\mathbf{r})]$ is mainly concerned with the kinetic energy of the electrons which depends on the gradient of the electronic positions and it is difficult to find as a functional of the electron density. Moreover, the electron-electron interaction term $E_{\mathrm{int}}[n(\mathbf{r})]$ is not known. By gaining the ideas from the H-K theorems, the problem has been resolved by Kohn & Sham (1965).

3.4.3 Kohn-Sham approach

To study the electronic calculation of molecular system, Kohn & Sham (1965) proposed a mathematical model based on the H-K theorems which give the exclusive revolution in the modern DFT. The non-interacting particle approximation instead of the interacting many body problems has been considered in the Khon-Sham equations which give the exact ground state density as given by real interacting system. Moreover, the Khon-Sham approach includes the self-consistent equations for homogeneous mathematical model to study the exchange and the correlation effects in the H-K theorems. But the accuracy of calculations depends on the approximations used in the exchange-correlation functionals. The local density approximation (LDA) and the generalized gradient approximation (GGA) are the basic exchange-correlation functionals, which gives accurate result for the molecular systems having covalent as well as ionic bonding (R. M. Martin, 2020). Furthermore, hybrid functionals B3LYP is used to study the van der Waals interactions (Becke, 1988; Lee et al., 1988).

In the K-S assumption, the electrons move under the effective K-S single-particle potential $V_{\mathrm{KS}}(\mathbf{r})$ instead of the potential of interacting particles. The Hamiltonian for a non-interacting reference system made from the set of orbitals introduced by Kohn & Sham (1965) is given by

$$\hat{H}_{\mathrm{KS}} = -\frac{1}{2}\nabla_i^2 + V_{\mathrm{KS}}(\mathbf{r}) \tag{3.28}$$

For the i^{th} independent electron, the i^{th} Schrödinger wave equation is developed, which is

$$\left[-\frac{1}{2}\nabla_i^2 + V_{\mathrm{KS}}(\mathbf{r})\right]\psi_i = \epsilon_i\psi_i \tag{3.29}$$

The solution of this equation gives the ground state energy densities in which each of the electron will occupy the orbital of lowest possible eigen values ϵ_i. The density of the auxiliary system is

$$n(\mathbf{r}) = \sum_{i=1}^{N} |\psi_i|^2 \tag{3.30}$$

The universal energy functional for a system of independent-particles is

$$F[n(\mathbf{r})] = T_{\mathrm{s}}[n(\mathbf{r})] + E_{\mathrm{H}}[n(\mathbf{r})] + E_{\mathrm{XC}}[n(\mathbf{r})] \tag{3.31}$$

The first term in the right hand side is the K. E. of the independent-particle, the middle one is the classical electrostatic energy of the electron and the last term is the exchange correlation (XC) energy. The XC energy is unknown and needs approximations for self-consistent solution. The exchange correlation term contains the difference in the exact kinetic energy and the non-interacting K. E. of the K-S approach as well as all the remaining many body interactions in between the electrons like the exchange and the correlation energies which are not included in the Hartree term. Thus the ground state energy functional for the many body interacting system using the K-S model becomes

$$E[n(\mathbf{r})] = T_{\mathrm{s}}[n(\mathbf{r})] + E_{\mathrm{H}}[n(\mathbf{r})] + E_{\mathrm{XC}}[n(\mathbf{r})] + V_{\mathrm{ext}}(r)n(\mathbf{r}) \tag{3.32}$$

The last term includes the external field and the potential due to nuclei. The energy functional corresponding to the ground state can be obtained by minimizing the equation with respect to the electron density by keeping the number of electrons constant. Thus, the corresponding K-S one-particle potential can be calculated from the relation:

$$V_{KS}(\mathbf{r}) = V_{\mathrm{ext}}(\mathbf{r}) + V_{\mathrm{H}}(\mathbf{r}) + V_{\mathrm{XC}}(\mathbf{r}) = V_{\mathrm{ext}}(\mathbf{r}) + \frac{\partial E_{\mathrm{H}}[n(\mathbf{r})]}{\partial n(\mathbf{r})} + \frac{\partial E_{\mathrm{XC}}[n(\mathbf{r})]}{\partial n(\mathbf{r})} \tag{3.33}$$

where $V_{\mathrm{XC}} = \frac{\partial E_{\mathrm{XC}}[n(\mathbf{r})]}{\partial n(\mathbf{r})}$ is the XC potential and $V_{\mathrm{H}} = \frac{\partial E_{\mathrm{H}}[n(\mathbf{r})]}{\partial n(\mathbf{r})}$ is the Hartree potential.

Equations (3.29), (3.30) and (3.33) are called the Kohn-Sham equations which can be solved self-consistently. The K-S potential V_{KS} depends on the electron density and the same potential is used to solve the K-S equations to find the electron density. The important term which controls the accuracy of the calculation is the XC which requires approximations to solve the K-S density functional theory.

3.5 Exchange-correlation functional

To obtain the independent-particle kinetic energy, the Hartree energy and the exchange-correlation energy terms are very obvious from the independent particle equations for a system of many body interacting particles. These terms are the functionals of density and the calculation of charge density is a crucial task in the K-S theory. Self consistent method is an important way to obtain the charge density which needs the K-S potential. The K-S potential is composed of many ingredients among which the exchange-correlation term is very complex and requires approximations. The LDA and the GGA are the most widely used approximations for the exchange-correlation functionals.

3.5.1 Local density approximation

The LDA is appreciable for a system in which the distribution of electron is uniform (i.e., $n(\mathbf{r})$ varies extremely slowly) and the exchange-correlation energy functional $E_{\mathrm{xc}}[n(\mathbf{r})]$ depends only on the local value of density $n(\mathbf{r})$ as verified by Hohenberg & Kohn (1964). The LDA gives better result than the expected value for a system in which $n(\mathbf{r})$ varies extremely slow as well as for systems where either the electronic system is not too strongly correlated or the electrons in the system are under the influence of a uniform/constant external potential. The concept of HEG was illustrated by the Thomas-Fermi model (Fermi, 1928) and it is implemented by the H-K theorems (Hohenberg & Kohn, 1964) in LDA for geometric optimization and electronic structure calculations. The total exchange-correlation functional $E_{\mathrm{XC}}^{\mathrm{LDA}}[n(\mathbf{r})]$ for homogeneous electron gas can be written as

$$E_{\mathrm{XC}}^{\mathrm{LDA}}[n(\mathbf{r})] = \int n(\mathbf{r})\varepsilon_{\mathrm{XC}}[n(\mathbf{r})]\,\mathrm{d}\mathbf{r} \tag{3.34}$$

where $\varepsilon_{\mathrm{XC}}[n(\mathbf{r})]$ is the XC energy per electron in a HEG and $n(\mathbf{r})$ is the electron density. The exchange correlation functional $E_{\mathrm{XC}}[n(\mathbf{r})]$ in terms of the exchange functional $E_{\mathrm{X}}[n(\mathbf{r})]$ and the correlation functional $E_{\mathrm{C}}[n(\mathbf{r})]$ can be written as

$$E_{\mathrm{XC}}[n(\mathbf{r})] = E_{\mathrm{X}}[n(\mathbf{r})] + E_{\mathrm{C}}[n(\mathbf{r})] \tag{3.35}$$

The mathematical expression for exchange energy functional is given by Dirac (1930) as

$$E_{\mathrm{X}}^{\mathrm{LDA}}[n(\mathbf{r})] = \int n(\mathbf{r})\varepsilon_{\mathrm{X}}[n(\mathbf{r})]\,\mathrm{d}\mathbf{r} \tag{3.36}$$

where

$$\varepsilon_X[n(\mathbf{r})] = -\frac{3}{4}\left(\frac{3}{\pi}\right)^{1/3}[n(\mathbf{r})]^{1/3} \tag{3.37}$$

The analytical presentation of correlation energy density is very problematic and is present in terms of high and low density limits. The correlation energy can be treated as electrostatic energy of point charges and dominates over the exchange energy for low density limit. Whereas, the correlation energy becomes less important over the exchange energy for high density limit. The correlation energy for moderate density has been calculated more precisely from the quantum Monte-Carlo (QMC) simulations (Ceperley & Alder, 1980).

3.5.2 Generalized gradient approximation

The LDA is suitable for homogeneous electron gas which is not found in real system. To overcome the limitations of the LDA of real system for inhomogeneous electron gas, GGA is suitable in which the exchange-correlation functional $E_{\mathrm{xc}}[n(\mathbf{r})]$ incorporates density gradient corrections. The $E_{\mathrm{xc}}[n(\mathbf{r})]$ in GGA is written as:

$$E_{\mathrm{XC}}^{\mathrm{GGA}}[n(\mathbf{r})] = \int f[n(\mathbf{r}), \nabla n(\mathbf{r})]\mathrm{d}\mathbf{r} \tag{3.38}$$

where f stands for some functional of $n(\mathbf{r})$ and it's gradient $\nabla n(\mathbf{r})$. The exchange-correlation energy $E_{\mathrm{XC}}^{\mathrm{GGA}}$ of GGA contains exchange ($E_{\mathrm{X}}^{\mathrm{GGA}}$) and correlation ($E_{\mathrm{C}}^{\mathrm{GGA}}$) parts:

$$E_{\mathrm{XC}}^{\mathrm{GGA}} = E_{\mathrm{X}}^{\mathrm{GGA}} + E_{\mathrm{C}}^{\mathrm{GGA}} \tag{3.39}$$

The exchange-correlation functionals $f[n(\mathbf{r}), \nabla n(\mathbf{r})]$ are obtained from different methods proposed by many research groups. Some of the popular functionals among them are given by Perdew & Wang (1992) and by Perdew et al. (1996). Further, the Becke's formula (Becke, 1988) for the exchange part was combined with Perdew's formula (Perdew, 1986) of correlation and also with the correlation functional of Lee, Yang and Parr (Lee et al., 1988) to give BP88 and BLYP type of GGA functionals. All these functionals are generally suitable for the materials having chemical bonding like covalent, ionic, metallic or hydrogen. For van der Waals interactions, we have to adopt some hybrid

functionals.

Including LDA and GGA in DFT expression of exchange-correlation functional $E_{\mathrm{XC}} = E_{\mathrm{X}} + E_{\mathrm{C}}$ a weighted contribution of the expression which gives a HF/DFT exchange-correlation functional, which is called a hybrid DFT functional. The most popular hybrid functional is developed by Becke (1988) for the exchange-energy functional which is coupled with the correlation-energy functional by Lee et al. (1988). This exchange-correlation functional, called the Becke3LYP or the B3LYP functional is:

$$E_{\mathrm{XC}}^{\mathrm{B3LYP}} = \alpha \cdot E_{\mathrm{X}}^{\mathrm{HF}} + (1-\alpha) \cdot E_{\mathrm{X}}^{\mathrm{HF}} + \beta \cdot \Delta E_{\mathrm{X}}^{\mathrm{Becke}} + E_{\mathrm{C}}^{\mathrm{local}} + \gamma \cdot \Delta E_{\mathrm{C}}^{\mathrm{LYP}} \tag{3.40}$$

The first two terms represents the K-S orbital-based H-F exchange energy functional, the third term is the Becke 88 exchange functional, the fourth is accurate correlation part for the homogeneous electron gas in the LDA and the last term is the LYP correlation functional. The three parameters α, β and γ are those that give the best fit of the calculated energy to molecular atomization energies. This is thus a gradient-corrected, hybrid functional.

3.6 Basis set

The *ab-initio* quantum chemical procedures gather the information by solving the Schrödinger equation without including the experimental data. In this calculation, the introduction of basis set is very fundamental and essential. A basis set is a mathematical representation of the molecular orbitals (MOs) which is a set of basis functions that comprise the molecular orbital from the linear combination of atomic orbitals (LCAO) approach. For convenience, these functions are generally atomic orbitals centered on atoms. To explore the electronic states of molecules, we formulate the electronic wave functions on the basis of molecular orbital which are the approximate solutions of the Schrödinger equation. For a molecular orbital, a mathematical wave function (Φ_i) is formulated in terms of basis function (χ_j):

$$\Phi_i = \sum_{j=1}^{N} c_{ji}\chi_j \tag{3.41}$$

where c_{ji} is the MO expansion coefficients and $\chi_i \ldots \chi_N$ are the normalized basis functions. The frequently used basis orbitals are Slater-type orbital (STO) and Gaussian-type orbital (GTO). The STO provides more accurate result than the GTO, however, the computational cost is high, whereas the calculation is easy as given by the GTO.

3.6.1 Slater and Gaussian-type orbitals

In more confident voice, atomic orbitals are solutions of the H-F equations for the atom, i.e., wave functions of a single electron in the atom. Subsequently, the term atomic orbital was retrieved by basis function or contraction. Previously the Slater type orbitals (STOs) were used as basis functions due to their similarity to atomic orbitals of the hydrogen atom. Two types of basis functions are commonly used: Slater Type Orbitals (STO) and Gaussian Type Orbitals (GTO).

Slater-type orbitals are defined as

$$\Phi_{\mathrm{abc}}^{\mathrm{STO}}(\mathrm{x},\mathrm{y},\mathrm{z}) = Nx^a y^b z^c e^{-\xi r} \tag{3.42}$$

where N is the normalization constant, ξ is called the orbital exponent which controls the width of orbitals. Small ξ gives diffuse function whereas large ξ gives tight function. The sum of a, b and c gives the central angular momentum L i.e., $a + b + c = L$.

In STO, the exponential term has a more important role to play. The exponential dependence on the distance between the nucleus and the electron mirrors, the exact orbitals for the hydrogen atom. The exponential dependence ensures a fairly rapid convergence with increasing number of functions. The STOs are mainly used for atomic and diatomic systems and in semi-empirical methods. The GTOs are defined as

$$\Phi_{\mathrm{abc}}^{\mathrm{GTO}}(x,y,z) = Nx^a y^b z^c e^{-\xi r^2} \tag{3.43}$$

where N is the normalization constant and $r^2 = x^2 + y^2 + z^2$. Unlike the GTO functions, the STOs exhibits the correct cusp behavior at nucleus ($r \rightarrow 0$) with a discontinuous derivatives while the GTO has zero slope at the nucleus and the desired exponential decay in the tail regions ($r \rightarrow \infty$) from nucleus, GTO falls off too rapidly (Pople et al., 1989; Ditchfield et al., 1971).

3.6.2 Contracted Gaussian type orbitals

Contracted Gaussian type orbital (CGTO) is mainly used to describe the core electrons. The combination of full set of basis functions into smaller set of functions by constructing fixed linear combinations is called basis set contraction and the resulting functions is called the CGTOs. Contracting a basis set significantly reduces the computational cost but the energy increases by reducing the flexibility of basis set (Hehre et al., 1972; Pople & Hehre, 1978). The degree of contraction varies from 1 to 10. The CGTOs are given

by

$$\Phi_{\text{abc}}^{\text{CGTO}}(x, y, z) = N \sum_{i=1}^{n} c_i x^a y^b z^c e^{-\xi r^2} \tag{3.44}$$

3.6.3 Classification of basis set

3.6.3.1 Minimal basis set

The simplest basis set is the minimal basis set that contains the atomic orbital occupied by electrons at ground state. For example, hydrogen atom has 1s atomic orbital. So there is one (STO, GTO or CGTO) basis function. For carbon atom, there are 1s, 2s and 2p orbitals. So there are all together five basis functions (1s, 2s, $2p_x$, $2p_y$, $2p_z$). The description of electron distribution in different directions can be made by increasing the size of the basis function. The minimal basis set can be improved by doubling the number of basis function i.e., there are two functions for each atomic orbital so it is called double-zeta basis set. Similarly, in tripal-zeta basis set, there are three times as many functions as compared to minimal basis set.

3.6.3.2 Split valence basis set

The core and the valance electrons are described separately in split valence basis set. Popel and his coworkers developed the Gaussian basis set such as n-ijG and n-ijkG. In this basis set, two or more different sizes of basis functions are included for each valence orbital (Binkley et al., 1980). n-ijG is called double-zeta split valence basis set in which the core orbital is a CGTO made of n- Gaussian (functions) whereas valence orbitals is described by two orbitals, one CGTO made of i-Gaussian another one made of j-Gaussian. n-ijkG is called the tripal- zeta split valence basis set. The examples of split valence basis set are 3-21G, 6-31G, 6-311G, etc. In 6-31G basis set, the core orbital is a CGTO made of 6-Gaussain (function) and the valence is described by two orbitals, one is CGTO made of 3-Gaussian and another is CGTO made of 1-Gaussian.

3.6.4 Polarization function

In split valence basis set, the shape of the orbital remains same but it affects the size of the orbital. This limitation is removed by polarized basis set by adding orbital with angular momentum. When one atom moves towards another atom, the orbital might want to shift to one side or the other (polarization). s orbital can polarized in one direction as it is mixed with a p orbital. Similarly, p orbital can be polarized when it is mixed with d orbital. To polarize a basis function with angular momentum l, it is mixed with a basis function of angular momentum $l + 1$. In polarized basis set, d

functions are added for heavy atoms whereas p functions are added for hydrogen atoms. 6-31G*/6-31G (d) is the example of polarized basis set with d functions added for heavy atoms whereas 6-31G**/6-31G(p,d) represent the basis set with p functions added to the hydrogen atoms in addition to the d functions added to heavy atoms, where * represents polarization functions added to heavy atoms but ** stands for polarization functions added to the hydrogen atoms instead of the heavy atoms.

3.6.5 Diffuse function

The Gaussian functions with small (0.01 to 0.1) orbital exponents that fall off extremely slow with distance from the nucleus is called diffuse functions. Diffuse functions are suitable for the system having sufficient accumulation of charge far from the nucleus. For example, the system with lone pair, anions, system with significant negative charge, and system with low ionization potential. Generally, s and p functions are diffuse functions and it is denoted by + and ++ before G in Popel's basis set. The first + indicates the diffuse function added for heavy atoms and the second + stands for the diffuse function added for hydrogen atoms instead of heavy atoms. The examples of diffuse function basis set is 6-311++G(d,p) in which the diffuse function is added for the heavy atoms as well as for the hydrogen atoms in the triple-zeta valence polarization basis set 6-311G(d,p) (Krishnan et al., 1980).

3.7 Potential energy surface and geometry optimization

The PES in computational chemistry has a key role to illustrate the relation between the energy of a molecule with its geometry. According to BOA (Born & Oppenheimer, 1927), the nuclei in the molecules are almost stationary compared to the electrons. This concept of BOA is useful to create the ideas regarding the molecular shape/geometry, concept of PES, and solve the Schrödinger equation to the molecules for the electronic energy which is added to the nuclear repulsion energy. The concept of PES elaborates the idea of geometry optimization and the nature of the transition state. The total energy of a molecular system changes with a small change in its structure which is explored from its PES. The PES may have 1D, 2D or 3D representations. The 3D potential energy surface is presented in Figure 5. The valleys of a potential energy surface stand for reactant, intermediate and product of the reaction. The stable structure of the molecular system is represented by the minimum position in the valley of the PES as well as it also predicts the vibrational spectrum. The apex point in the valley identifies the instability of the molecule (transition stage for reaction). The individual electronic state of a molecule has separate PES and the separation between these surfaces produces the electronic spectrum. The PES is related to the energy and the geometry of a molecule.

Single point energy (SEP) is the potential energy of a molecule for a given configuration

of atoms in the molecule. It has the distinct numerical value of energy corresponding to each point in PES. The calculations of single-point energy characterize the properties of the molecule for a given configuration and signify its related properties. As a single point is a key point it is assumed that the geometry of the molecule does not change during the calculation procedure. The calculation of single point energy aims to obtain the basic informations about the molecule, to compute very accurate values of energy and other properties of molecular structure optimized at a lower level of theory.

The points on PES where $\partial E/\partial q = 0$ for all geometrical parameters (q) are called stationary points. The chemical significance of stationary points are minima $\left(\frac{\partial^2 E}{\partial q_i \partial q_j} > 0\right.$ for all q) and transition state/first-order saddle points$\left(\frac{\partial^2 E}{\partial q_i \partial q_j} < 0\right.$ for one q, and > 0 for all q).

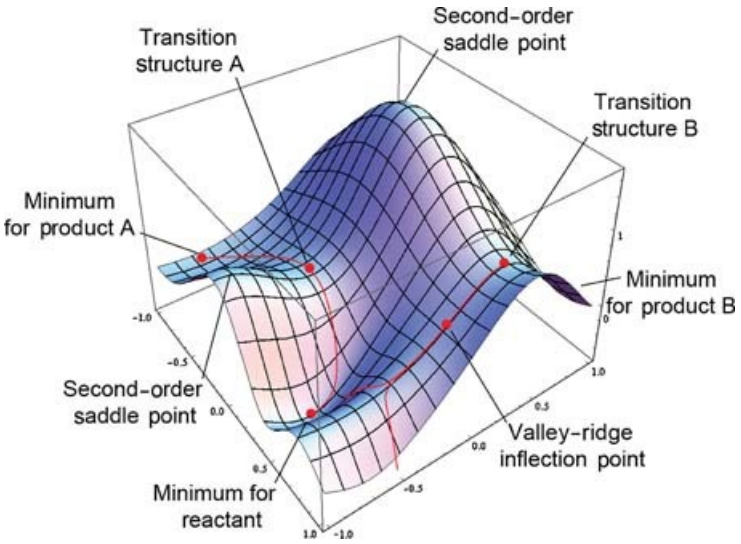

Figure 5: 3D potential energy surface (K. Srivastava, 2019).

The geometry optimization of molecular system in computational chemistry is the initial stage of the *ab initio*/DFT calculation procedure to obtain the minimum energy structure of molecule as well as the frequency of molecular vibration. The frequency calculation is used to justify the stable structure of molecule with minimum energy. In the geometry optimization, the measured physical parameters are bond length in (Å), bond angle in (°) and dihedral angle in (°). The main motive of geometry optimization is to obtain the atomic arrangement that ensure the stable molecular structure. The stability of molecule is obtained in terms of minimum energy value. So, various types of testing have been performed to obtain the lowest energy value. The PES scan is the most suitable procedure to check the molecular geometry in terms of the global and the local minima and their corresponding single point energies. The PES is visualized in a 3-D figure that represents the bond angle, the bond length and the energy.

3.8 Atoms in molecule and molecular docking

The Quantum theory of atoms in molecule (QTAIM) was initially introduced by Bader and his coworkers (R. F. Bader & Matta, 2004) that provides the opportunity to insight the all possible interactions of intramolecular hydrogen bonding. The crucial parameters that determine the nature and the strength of the hydrogen bonding are electron density (ρ) and Laplacian of the electron density ($\nabla^2\rho$) at bond critical point (BCP). Furthermore, the electron kinetic energy density (G_{BCP}), the electron potential energy density (V_{BCP}), the total electron energy density (H_{BCP}), the interaction energy (E_{int}) at BCP also play a vital role that signifies the nature and strength of the intramolecular hydrogen bonding. For the existence of hydrogen bond, Koch & Popelier (1995) suggested that the electron density (ρ) between the proton (H) and the acceptor (A) should be in the order (0.002 to 0.040) a.u and the Laplacian ($\nabla^2\rho_{\mathrm{BCP}}$) of the electron density should be in the order (0.024 to 0.139) a.u. The following are the criteria developed by Rozas et al. (2000) which signifies the nature and the strength of hydrogen bond interactions.
i) If $\nabla^2\rho_{\mathrm{BCP}} > 0$ and $H_{\mathrm{BCP}} < 0$, then hydrogen bond is partially covalent.
ii) If $\nabla^2\rho_{\mathrm{BCP}} < 0$, and $H_{\mathrm{BCP}} < 0$, then hydrogen bond strong and covalent in nature.
iii) If $\nabla^2\rho_{\mathrm{BCP}} > 0$ and $H_{\mathrm{BCP}} > 0$, then hydrogen bond is weak and ionic in nature.

Molecular docking is the structure-based drug design that predicts the binding affinity, the binding strength and the area of binding sites. Furthermore, molecular docking predicts the stable form of complexes when ligand (small molecule) binds with protein (large molecule) and guesses the suitable orientations between the ligand and the protein during the formation of stable complexes (Trott & Olson, 2010). Molecular docking appreciates the opportunity to check the curative behavior of the biologically active molecules with the selected target protein. Molecular docking simulation between the ligand and the selected targets to obtain the binding energy and the binding efficiency was performed by using AutoDock 4.2 software (Studio, 2009) and the visualization of the binding regions and the binding strength of ligand with protein residue has been analyzed with Discovery Studio Visualizer 4.5 (Kitchen et al., 2004).

3.9 Non-linear optical analysis

NLO materials have wide applications in optoelectronics and optical communication devices. Moreover, the NLO effects have been implemented for more specific applications for example optical switching, photo-refraction, optical memories, optical signal processing and many more (Günter, 2012). Many small organic molecules, organic single-crystalline materials, polymers and inorganic species exhibit noticeable NLO response against the incident light (L. Guo et al., 2018; Kalinin et al., 2017). The characteristics of material changes with the intensity of the incident electromagnetic wave.

The study of change in properties of the material with high-intensity incident light is called non-linear optics. The induced polarization (P_i) is observed in the material due to the interaction of the electromagnetic field with ions and electrons of species and there is formation of oscillating dipole within the material. A linear relationship between the induced polarization and an interacting electric field is observed for moderate field strength whereas the response becomes non-linear for intense/laser light. For the intense field, the relation between the applied electric field (E) and the polarization (P) is given by the power series expansion

$$P = \alpha E + \beta E^2 + \gamma E^3 + \cdots \tag{3.45}$$

where E is the electrical component of incident laser light, α is the linear polarizability, β and γ are the first and the second-order hyperpolarizability which gives the non-linear optical response.

To investigate the non-linear optical properties of the material under the influence of the external electric field is due to polarization of the molecule and the formation of the dipole. For weak polarization, as the molecule is subjected to the static electric field (F), the energy (E) is given by the Taylor series expansion:

$$E = E^0 - \mu_i F^i - \frac{1}{2}\alpha_{ij} F^i F^j - \frac{1}{6}\beta_{ijk} F^i F^j F^k - \frac{1}{24}\gamma_{ijkl} F^i F^j F^k F^l - \cdots \tag{3.46}$$

where

$$\begin{aligned} E^0 &= \text{energy of a molecule in the absence of electric field} \\ \mu_i &= \text{components of the dipole moment} \\ \alpha_{ij} &= \text{polarizability} \\ \beta_{ijk},\ \gamma_{ijkl} &= \text{first and second-order hyperpolarizability} \end{aligned}$$

The total static dipole moment can be calculated from the x-, y- and z-components of μ and is given by Jiang et al. (2012):

$$\mu_0 = \left(\mu_x^2 + \mu_y^2 + \mu_z^2\right)^{1/2} \tag{3.47}$$

The distortion in the charge density due to the implementation of the external electric field of a molecule is measured in terms of static electric polarizability (α) which is the average of diagonal elements in polarization tensor

$$|\alpha_0| = \frac{1}{3}(\alpha_{xx} + \alpha_{yy} + \alpha_{zz}) \tag{3.48}$$

The anisotropy of polarizability is given by

$$\Delta\alpha = 2^{-1/2}\left[\left(\alpha_{xx}-\alpha_{yy}\right)^2+\left(\alpha_{yy}-\alpha_{zz}\right)^2+\left(\alpha_{zz}-\alpha_{xx}\right)^2+6\alpha_{xx}^2\right]^{1/2} \tag{3.49}$$

The first order hyperpolarizability (β) is a third-ranked tensor which can be explained by a 3×3×3 matrix. The 27 components of the 3D-matrix can be reduced to 10 components from the Kleinman symmetry (Wortmann et al., 1993) and the first hyperpolarizability can be calculated from the equation

$$\beta_0 = \left[\left(\beta_{xxx}+\beta_{xyy}+\beta_{xzz}\right)^2+\left(\beta_{yyy}+\beta_{xxy}+\beta_{yzz}\right)^2+\left(\beta_{zzz}+\beta_{xxz}+\beta_{yyz}\right)^2\right]^{1/2} \tag{3.50}$$

3.10 Frontier molecular orbital and global reactivity descriptors

In the molecular system, the main orbital that takes part in chemical reactions is the frontier molecular orbitals and they are HOMO and LUMO. According to Koopmans theorem (Manne & Åberg, 1970; Heinrich et al., 1986), HOMO has a high value of ionization potential (I) and LUMO has a greater value of electron affinity (A). The electron transport property has been analyzed based on the HOMO energy (E_{H}) and the LUMO energy (E_{L}). Higher value of the energy gap $\Delta E_{\text{L-H}}$ between HOMO and LUMO reveals that the molecule is more stable whereas the lesser value of $\Delta E_{\text{L-H}}$ represents that the molecule is more chemically reactive and less stable. The global reactivity descriptor parameters are electronegativity (χ), chemical potential (μ), hardness (η), electrophilicity index (ω) and softness (S). These parameters are measured in terms of E_{H} and E_{L} (P. Chattaraj et al., 2003).

$$\chi = -\frac{1}{2}\left(E_{\mathrm{HOMO}}+E_{\mathrm{LUMO}}\right) \tag{3.51}$$

$$\mu = -\chi = \frac{1}{2}\left(E_{\mathrm{HOMO}}+E_{\mathrm{LUMO}}\right) \tag{3.52}$$

$$\eta = \frac{1}{2}\left(E_{\mathrm{LUMO}}-E_{\mathrm{HOMO}}\right) \tag{3.53}$$

$$S = \frac{1}{2\eta} \tag{3.54}$$

$$\omega = \frac{\mu^2}{2\eta} \tag{3.55}$$

Chemical potential (μ) which is negative of electronegativity (χ) measures the escaping behavior of electrons from the molecules. DFT signifies that the electron flow from higher chemical potential to lower chemical potential up to the region of a constant level of chemical potential in space. The chemical potential (μ) of a system is the first-order partial derivatives of energy (E) with respect to the number of electrons (N) at constant

external potential $V(r)$:

$$\mu = \left(\frac{\partial E}{\partial N}\right)_{V(r)} = -\chi \tag{3.56}$$

The words hardness (η) and softness (S) were first introduced by Pearson to check the direction of acid-base reaction as well as to gain the stability of product. From the Koopmans theorem, η is half of the energy gap between HOMO and LUMO which signifies to bear the resistance of the system to take or give up electrons. The global hardness which is the inverse of softness is the second-order derivative of energy (E) with respect to the number of electrons (N) at constant external potential $V(r)$.

$$\eta = \frac{1}{2}\left(\frac{\partial^2 E}{\partial N^2}\right)_{V(r)} = \frac{1}{2}\left(\frac{\partial \mu}{\partial N}\right)_{V(r)} \tag{3.57}$$

Electrophilicity index (ω) is introduced by Parr et al. (1999) which is a global reactivity descriptor. It is the characteristics of atoms that include the reduction of energy procedure during the absorption of electrons from the donors. The chemical reactivity of the molecule is analyzed in terms of the electrophilicity index (ω). It measures the stabilization in energy as the molecule gain external electronic charge from neighboring donor species.

The maximum electronic charge ($\Delta N_{\max}$) that an electrophile can accept from the environment is given by

$$\Delta N_{\max} = -\frac{\mu}{\eta} \tag{3.58}$$

For two molecules A and B heading towards each other, the amount of charge transfer between them is measured in terms of electrophilicity based charge transfer (ECT) which is given by

$$\text{ECT} = (\Delta N_{\max})_A - (\Delta N_{\max})_B \tag{3.59}$$

3.11 Local reactivity descriptor

The global reactivity parameters like electronegativity (χ), hardness (η), softness (S), and electrophilicity index (ω) give the information of the overall reaction mechanism, however, the local reactivity parameters describe the particular site of a molecular species based on the electron density $\rho(\vec{r})$, The Fukui function $f(\vec{r})$ or the local softness. These quantities have great importance to predict the site selectivity of a chemical reaction. According to Ayers & Parr (2000), the Fukui function (FF) is more when attracted by soft reagent and its value is small when attracted by hard reagent. The Fukui functions

$f(r)$ can be solved from the following functions as given by Parr & Yang (1984).

$$f^{+}(r) = \left(\frac{\partial \rho(r)}{\partial N}\right)_{v}^{+} \qquad \text{for nucleophilic attack} \tag{3.60}$$

$$f^{-}(r) = \left(\frac{\partial \rho(r)}{\partial N}\right)_{v}^{-} \qquad \text{for electrophilic attack} \tag{3.61}$$

$$f^{0}(r) = \left(\frac{\partial \rho(r)}{\partial N}\right)_{v}^{0} \qquad \text{for neutral attack} \tag{3.62}$$

It is difficult to calculate the values of $f(r)$. So, condensed Fukui function f_k is calculated by an easy procedure as suggested by Yang & Mortier (1986). In a system having N electrons, independent calculations were performed for the corresponding $N-1$, N and $N+1$ electron system having the same geometry. The expression of condensed Fukui function for k^{th} atom in a molecule from Mulliken population analysis is given by

$$f_k^{+} = q_k(N+1) - q_k(N) \qquad \text{for nucleophilic attack} \tag{3.63}$$

$$f_k^{-} = \frac{1}{2}\left[q_k(N) - q_k(N-1)\right] \qquad \text{for electrophilick attack} \tag{3.64}$$

$$f_k^{0} = \frac{1}{2}\left[q_k(N+1) - q_k(N-1)\right] \qquad \text{for radical attack} \tag{3.65}$$

The local softness $(s_k^{+}, s_k^{-}, s_k^{0})$ and the local electrophilicity indices $(\omega_k^{+}, \omega_k^{-}, \omega_k^{0})$ are given by the relations:

$$s_k^{+} = S f_k^{+}, \quad s_k^{-} = S f_k^{-}, \quad s_k^{0} = S f_k^{0}$$

and

$$\omega_k^{+} = \omega f_k^{+}, \quad \omega_k^{-} = \omega f_k^{-}, \quad \omega_k^{0} = \omega f_k^{0}$$

where +, − and 0 sign represents nucleophilic, electrophilic and radical attack respectively. The extremum value of $(f_k^{+}, s_k^{+}, \omega_k^{+})$ and $(f_k^{-}, s_k^{-}, \omega_k^{-})$ infer the most nucleophilic and electrophilic sites in the molecule respectively.

3.12 Molecular electrostatic potential surface

MEP surface is a useful tool to analyze the distribution of charge, the formation of dipole moment, and reactive parts (electrophilic and nucleophilic region) in the molecular system (Sjoberg et al., 1990). The active region in the biologically active molecule which may take part in a chemical reaction with the surrounding protein can be predicted in terms of color code. The red color represents the most negative potential, the blue color represents the most positive potential, whereas the green represents the zero potential.

The potential increases in terms of color as red < yellow < green < blue. The molecular electrostatic potential $V(r)$ generated around the molecule due to the cumulative effect of negative and positive charges related to electrons and nuclei is obtained from the expression (Weiner et al., 1982; Haddon & Fukunaga, 1980)

$$V(r) = \sum_{A} \frac{Z_A}{|\vec{R}_A - \vec{r}|} - \int \frac{\rho(\vec{r'})}{|\vec{r'} - \vec{r}|} \tag{3.66}$$

where Z_A is the charge on nucleus A present at R_A and $\rho(\vec{r'})$ is the electronic density function of the molecule. The first term gives the potential due to nuclei whereas the second term provides the potential due to electrons and $V(r)$ is the resultant potential due to the nuclei and the electrons.

3.13 Natural bond orbital analysis

The hyperconjucative interaction between filled and vacant orbital has great attention for the charge transfer. The distribution of charge from donor orbital to acceptor orbital which infer the stability of molecular system has been examined on the basis of NBO criticism (Chandran et al., 2012). The interaction between donor and acceptor orbitals has been studied in terms of interaction energy $E^{(2)}$ which is given by second order perturbation theory (Schwenke & Truhlar, 1985; Gutowski et al., 1993). Higher the value of stabilization energy $E^{(2)}$, stronger the interaction between the donor and the acceptor orbitals and vice versa.

$$E^{(2)} = E(i,j) = -q_i \frac{\left(F_{ij}\right)^2}{E_j - E_i} \tag{3.67}$$

where F_{ij} is the diagonal element of Fock-matrix, q_i is the occupancy of donor orbital and E_i and E_j are the energies of the real and the virtual orbitals.

3.14 Vibrational analysis

The contribution of potential energy distribution (PED) of normal modes of vibration (stretching and bending) has been obtained by using the software Gar2Ped (J. M. L. Martin & Van Alsenoy, 1995). The internal coordinates of normal modes of vibrations have been implemented as suggested by Pulay's recommendation (Pulay et al., 1979). DFT calculations always produce the Raman amplitude but not the Raman intensities. The Raman intensity was calculated for each normal mode of vibration in terms of the Raman scattering cross-section $\partial\sigma_j/\partial\Omega$ (Polavarapu, 1990; Guirgis et al., 2003) and is given

by the relation:

$$\frac{\partial \sigma_j}{\partial \Omega} = \left(\frac{2^4 \pi^4}{45}\right) \frac{\left(\nu_0 - \nu_j\right)^4}{1 - \exp\left[-hc\nu_j/(kT)\right]} \left(\frac{h}{8\pi^2 c \nu_j}\right) S_j \tag{3.68}$$

where S_j = scattering activities, ν_j = expected wavenumbers for j^{th} normal mode, ν_0 = wave number of Raman activated state and h, c and k are universal constants. A Lorentzian line shape (FWHM = 8 cm^{-1}) is exploited to develop artificial spectra from the measured Raman and IR intensities by convoluting the expected vibrational mode.

3.15 Computational details

The properties like: optimized geometrical parameters, interaction energy, chemical reactivity parameters, vibrational wavenumbers and intramolecular charge transfer of selected molecules have been incorporated on the basis of DFT. Gaussian 09 software package (M. J. Frisch et al., 2009) was used for geometry optimization, vibrational frequency and optimized energy by using the basis set 6-311++G(d,p) (Peterson et al., 1994; Hehre, 1976; Becke, 1993) by implementing the hybrid exchange-correlation functional B3LYP (Lee et al., 1988; Parr & Yang, 1989a) and the dispersion corrected functional ωB97XD (Chai & Head-Gordon, 2008). The insight of pictorial presentation of accumulation of charge around the molecule in space has been visualized with GaussView 05 (A. Frisch et al., 2005). The molecular docking simulation was carried out to insight the ligand–protein interaction from AutoDock Tools (ADT) version 1.5.4 (G. Morris et al., 2009) and the visualization of binding sites of ligand with residue of protein was done with Discovery Studio Visualizer 4.5 (Studio, 2009). The hyperconjucative interaction to insight the distribution of charge from donor to acceptor level within the molecule was studied on the basis of NBO analysis. The strength and the nature of the intramolecular hydrogen bonding of investigated molecules were studied on the basis of QTAIM with the help of Atoms in molecule (AIM) all software package and pictorial presentation has been done with AIM 2000 (Keith & AIMALL, 2009). The reactive part in the molecules has been predicted from the MEP surface, the Hirshfeld charge analysis and the global reactivity descriptors.

CHAPTER 4

4. RESULTS AND DISCUSSION

4.1 Introduction

In this chapter, the main findings of research have been analyzed and discussed. This research is concerned with the combined study of experimental and DFT computational approach of API such as RBZ and cefradine. Moreover, the first principles calculation of dug molecule has been performed on frovatriptan. The findings of the present work will encircle the following topics.

1. RBZ has potential use to treat as antiparasitic drug. The conformational analysis of RBZ has been carried out from the one dimensional PES scan to obtain the stable conformers at room temperature. The geometry optimization of RBZ has been carried out which helps to obtain the optimized parameters like bond length, bond angle and dihedral angle. Different modes of vibration (stretching and bending) of RBZ have been obtained from the DFT calculation and their vibrational frequency has been compared with the experimental data. The analysis of chemical reactivity of RBZ has been scrutinized from the local and the global reactivity as well as the intra molecular hydrogen bonding has been predicted from the MEP and the AIM study. The drug potential of RBZ in terms of ligand-protein interaction and drug-likeness is explained. The potential use of RBZ as NLO material has been discussed. Moreover, the effect of temperature on thermodynamic parameters like entropy, enthalpy and specific heat capacity has been discussed.

2. The possible conformers of cefradine that likely to exist at room temperature as well as geometry optimization to obtain the minimum energy structure has been discussed. The comparison of possible conformers with the Vandee Stick structure has been discussed. The intra molecular hydrogen bonding in the cefradine has been analyzed from the study of QTAIM. The different modes of vibration obtained from the DFT calculation have been compared with the observed IR and Raman spectra for the functional group study and the intermolecular hydrogen bonding. The molecular docking study as well as the drug-likeness of cefradine which signifies the drug potential in terms of binding strength between ligand and residues of predicted target protein has been elaborated. The variation of thermodynamic parameters like entropy, enthalpy and specific heat capacity of cefradine with temperature have been justified. The NLO properties of cefradine from the DFT calculation have been carried out.

3. The conformational analysis and geometry optimization of frovatriptan with the functional B3LYP and ωB97XD has been discussed. The chemical reactivity in terms of Hirshfeld charge analysis, frontier molecular orbital energy gap and MEP map has been studied in detail. The ligand-protein interaction which signifies the drug potential of API molecule has been examined from the molecular docking approach. Moreover, the dipole moment, the polarizability and the hyperpolarizability of frovatriptan which are the measure the NLO properties have been carried out. Moreover, the variation of thermodynamic parameters like specific heat capacity, entropy and enthalpy with temperature have been studied.

4.2 Ricobendazole

The RBZ is an active metabolite of ABZ, which is also called albendazole sulfoxide, has therapeutic use to treat as anthelmintic against round worms, tape worms etc. In the present work, we discuss the electronic and the structural behavior of RBZ.

4.2.1 Conformational analysis of ricobendazole

Before entering into the drug potential of RBZ, its molecular stability with minimum energy structure has great importance. Initially, the three dimensional electronic structure of RBZ has been taken from PubChem data base (PubChem Compound Database, 2019a) and the geometry optimization has been performed with DFT by using the exchange functional composed of three parameters: Local, non-local and Hartree-Fock (Becke, 1993) coupled with correlation functional Lee-Yang-Parr (Lee et al., 1988; Parr & Yang, 1989b) with basis set 6-311++G(d,p) (Dunning, 1989; Dunning & Woon, 1995). The optimized structure of RBZ along with atom numbering system is presented in Figure 6.

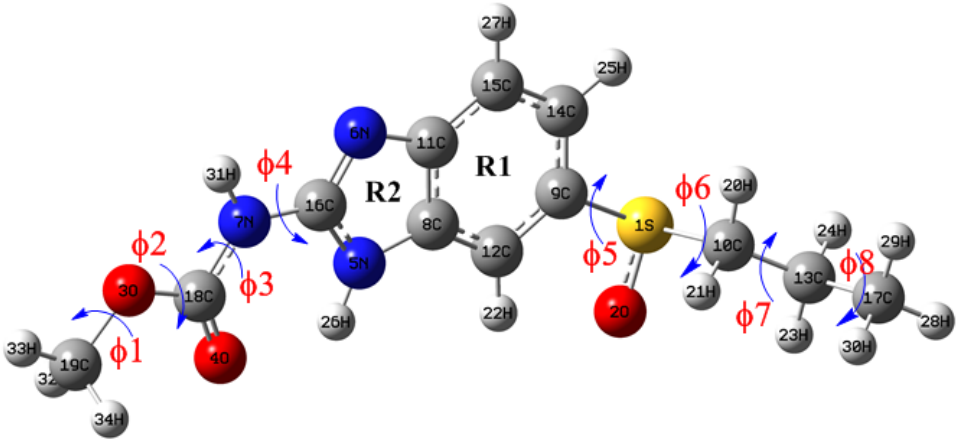

Figure 6: 3D optimized electronic structure of RBZ with atom numbering scheme.

To obtain the minimum energy structure of RBZ, one dimensional PES scan has been incorporated from the quantum mechanical approach across the flexible bonds by using the same functional B3LYP/6-311++G(d,p) as optimization.

The rotatable bonds are C19-O3, O3-C18, C18-N7, N7-C16, C9-S1, S1-C10, C10-C13, and C13-C17 having related torsional angles ϕ1(H33-C19-O3-C18), ϕ2(C19-O3-C18-N7), ϕ3(O3-C18-N7-C16), ϕ4(C18-N7-C16-N5), ϕ5(C14-C9-S1-O2), ϕ6(C9-S1-C10-C13), ϕ7(S1-C10-C13-C17) and ϕ8(C10-C13-C17-H29). The dihedral angle is varied from 0° to 360° along the selected bond alignment such that the change is taken in regular 36 steps, 10° in each step. The fluctuation of the comparative energy with the torsional angle is presented via scan graph. The scan graph corresponding to all flexible bonds is presented in Figure 7. The structures obtained related to the global and the local minima in PES scan is further optimized at the same level of theory to obtain the possible conformers that exist at room temperature. The PES scan graph suggested that there exist eight conformers related to the global and the local minima. The self consistent field (SCF) energy related to all the conformers are tabulated in Table 1. The optimized structure of the eight conformers of RBZ along with the relative energy in comparison to the minimum energy conformer I are given in Figure 8. Only those conformers of relative energy in comparison to the most stable conformer less than 0.56 kcal/mol which is equal to kT (k = Boltzmann's constant and T = absolute room temperature) are expected to exist at room temperature. This reveals that only three conformers having the relative energy less than 0.56 kcal/mol exist. In this study, they are written as conformer I, conformer II and conformer III and their optimized energies are obtained as −787322.8843 kcal/mol, −787322.7170 kcal/mol and −787322.5046 kcal/mol respectively (M. K. Chaudhary, Prajapati, et al., 2021).

Table 1: Optimized energies of eight conformers of RBZ with functional B3LYP/6-311++G(d,p).

Conformers	Energy		Energy Difference*
	Hartree	kcal/mol	kcal/mol
I	–1254.6978	–787322.8843	0.0000
II	–1254.6976	–787322.7170	0.1673
III	–1254.6972	–787322.5046	0.3797
IV	–1254.6962	–787321.8554	1.0289
V	–1254.6960	–787321.7505	1.1338
VI	–1254.6960	–787321.7290	1.1553
VII	–1254.6926	–787319.5775	3.3068
VIII	–1254.6847	–787314.6393	8.2450

*Energies of the seven conformers relative to the minimum energy conformer I

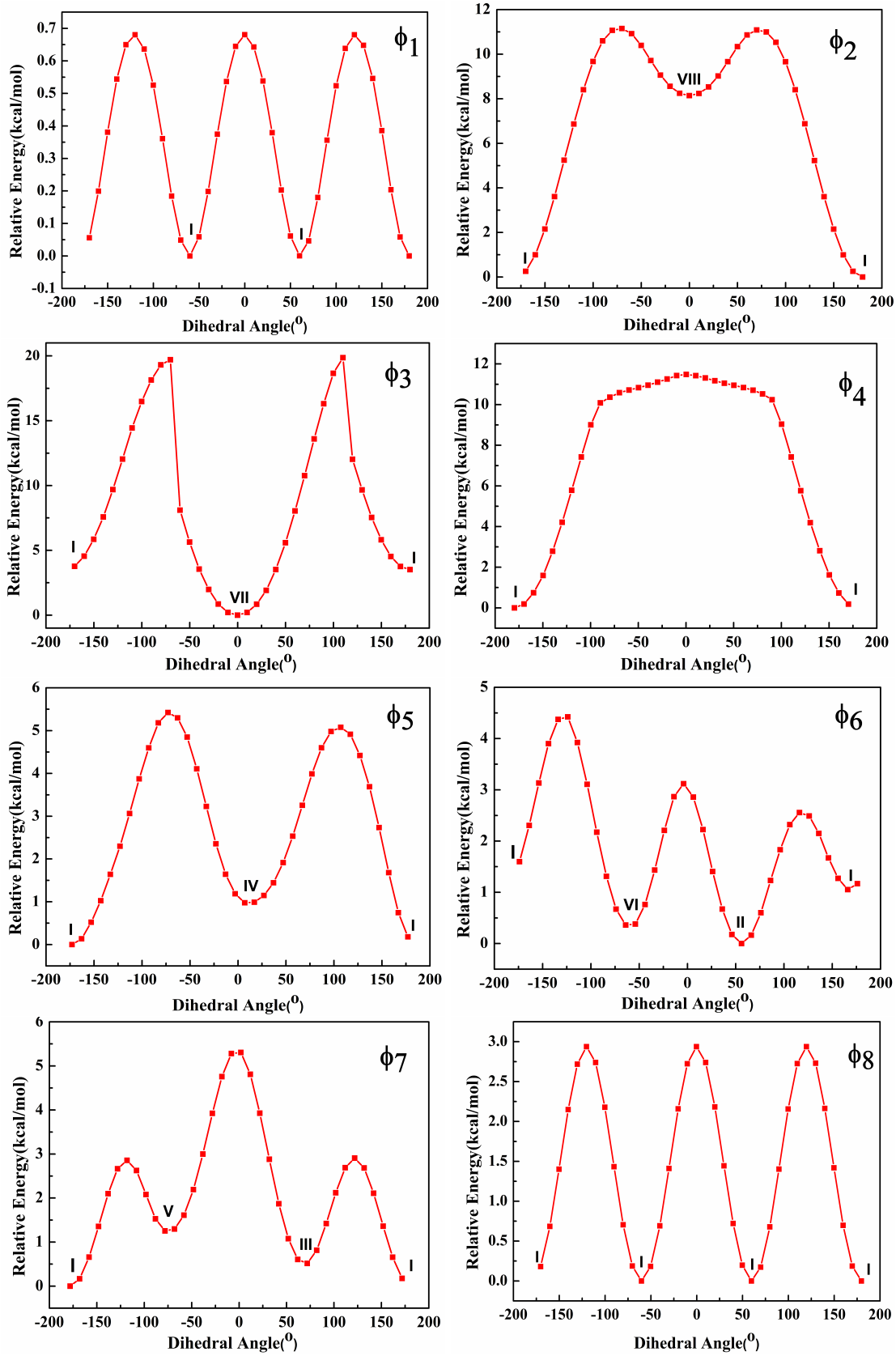

Figure 7: PES scan of RBZ with dihedral angle $\phi 1$, $\phi 2$, $\phi 3$, $\phi 4$, $\phi 5$, $\phi 6$, $\phi 7$, and $\phi 8$.

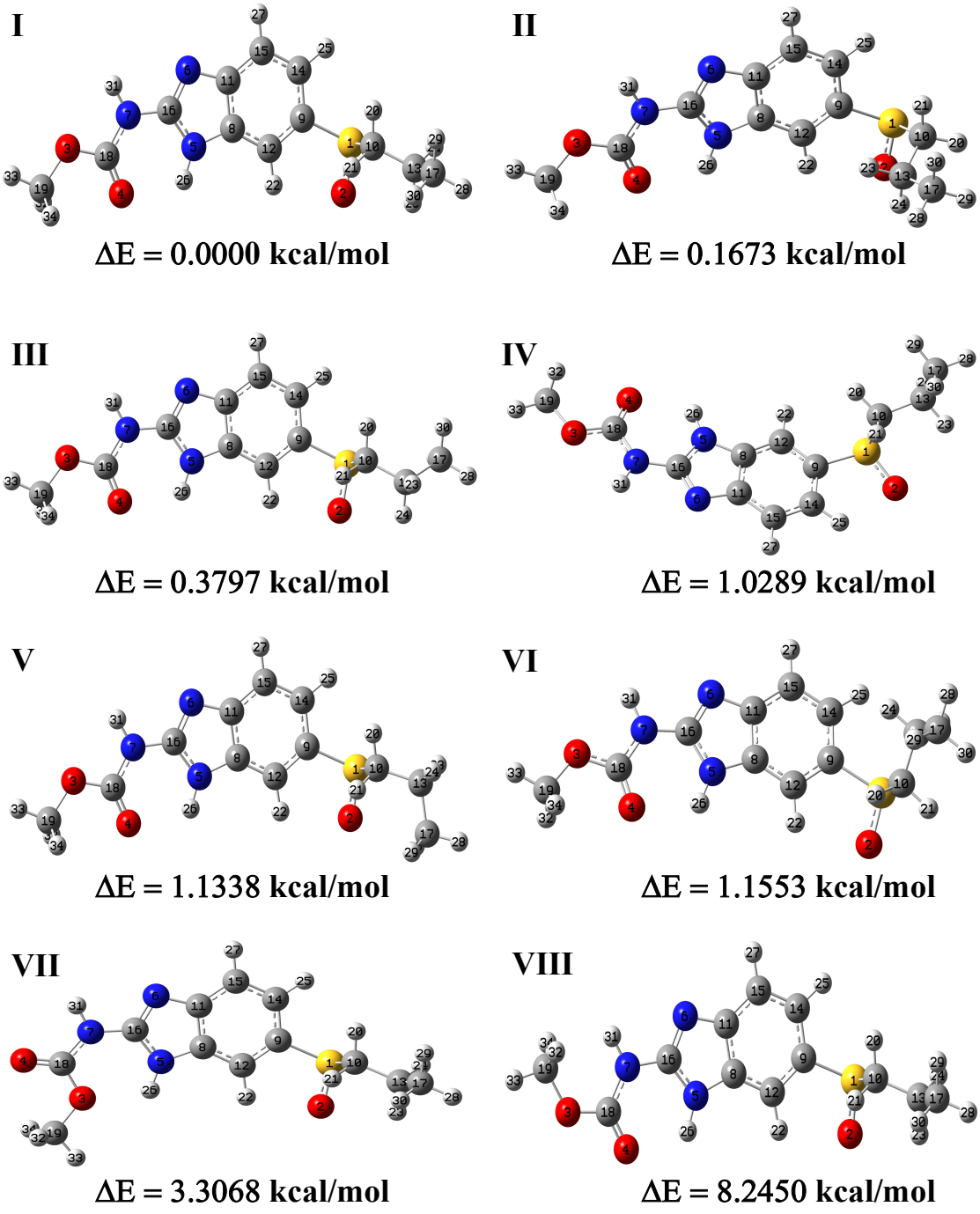

Figure 8: Optimized structure of all the conformers of RBZ along with comparative energy.

4.2.2 Geometry optimization

The relative energy of conformers II and III in comparison to the most stable conformer I is not so large and they are 0.1673 kcal/mol and 0.3797 kcal/mol respectively. So, to check whether their structures are same or different, the overlapping of conformers II and III with most stable structure of conformer I has been done by using the least square algorithm which minimizes the distance between the non-hydrogen atoms. The superimposed body part of conformers II and III with conformer I is presented in Figure 9 (M. K. Chaudhary, Prajapati, et al., 2021).

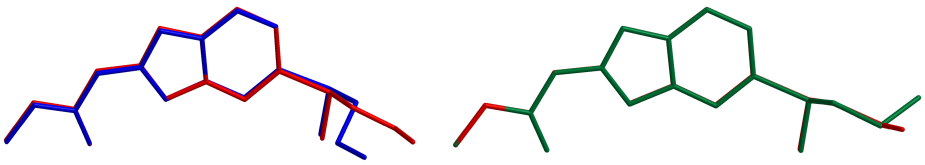

Conformer I and II **Conformer I and III**

Figure 9: Overlapping of conformers II and III with most stable conformer I of RBZ.

From the superimposed structure of conformers I and II, it is seen that the benzene ring R1 and the imidazole ring R2 are overlapped. Moreover, the branch chain containing carbonyl group also coincides. But the side chain containing sulfinyl group is overlapped and the chain -CH_2-CH_2-CH_3 is in different plane. From the overlapping of conformers I and III, it is revealed that the benzene ring R1 and imidazole ring R2 are overlapped in well manner. The side chain containing the carbonyl group and the methyl group are also overlapped. The branch containing sulfinyl group and -CH_2-CH_2-CH_3 are also super imposing but only the functional group -CH_3 is in different plane. The branch chain containing -CH_2-CH_2-CH_3 in the conformers II and III are tilted from the conformer I which is due to intramolecular hydrogen bonding between O2 and H22 which is explained in Section 4.2.11 (M. K. Chaudhary, Prajapati, et al., 2021).

The optimized geometry parameters such as bond distance, bond angle and torsional angle at the same level of calculation is presented in Table 30 (Appendix A). On comparing the bond length of conformers II and III with I, it is found that the significant change in length is 0.0059 Å and 0.0050 Å across the bond S1-C10 in conformers I and II; and conformers I and III, respectively. This difference is due to the interamolecular hydrogen bonding across O2 and H22. The significant change in bond length is not observed in other cases. While comparing the bond angle, the considerable change in the bond angle is determined as 3.1067°, 3.4387° and 1.4376° across S1-C10-H20, S1-C10-C13 and C9-S1-C10 respectively of conformers I and II. In the conformers I and III the significant change in angle is determined as 1.4755° and 2.3585° across C10-C13-H23 and C10-C13-C17. This change in angle is due to the establishment of

intramolecular hydrogen bonding between O2 and H22 (M. K. Chaudhary, Prajapati, et al., 2021).

4.2.3 Experimental vibrational spectra

The solid form of RBZ having whiteness level greater than 98% was procured from the Merck and Co., multinational pharmaceutical company, USA. The purity level of RBZ is at analytical standard. So without making any further cleaning, the IR and the Raman spectra were listed. The pellet is formed with potassium bromide (KBr) in which the ratio of KBr with the sample is 200:1. To reduce the noise, the baseline correction has been implemented with OPUS software. The IR spectra are listed in the range (400 to 4000) cm^{-1} with the help of Bruker Vertex 70 FT-IR spectrometer having resolution 4 cm^{-1}. The RAM II module is used to record the Raman spectrum of RBZ. The spectrum was recorded in the range (100 to 3600) cm^{-1} by using diode-pumped Nd: YAG laser having excitation wavelength of 1064 nm and the laser power is lower than 100 mW (M. K. Chaudhary, Prajapati, et al., 2021).

4.2.4 Modes of vibration and scaling of vibrational wave numbers

For the non-linear molecule having the number of atoms N, the normal modes of vibration is ($3N$-6). In the RBZ there are 34 atoms which give 96 normal modes of vibration. These modes of vibration are both IR and Raman active. The mode of vibration has been determined with Gar2Ped (J. M. L. Martin & Van Alsenoy, 1995) software with the help of Pulay's recommendation (Pulay et al., 1979). The quantum chemical calculation gives Raman amplitude but not the Raman intensity. So the Raman intensity for each mode of vibration is determined from the Raman scattering cross-section $\partial\sigma_j/\partial\Omega$ (Polavarapu, 1990; Guirgis et al., 2003) and is given by the Equation (3.68).

The wavenumber of simulated spectra is more than the experimental wavenumber. The overestimation of the wavenumber in the simulated spectra is due to the presence of anharmonicity in the real system. To compensate this deficiency, the calculated wavenumber were lowered down by wavenumber linear scaling (WLS) procedure and is given by $\left[\nu_{obs}/\nu_{cal} = (1.0087 - 0.0000163 \times \nu_{cal})\,cm^{-1}\right]$, where ν_{obs} is the experimentally recorded wavenumber and ν_{cal} is the simulated wavenumber (Andersson & Uvdal, 2005). After that, the scaled wavenumber showed the good resonance with the experimental one. The unscaled wavenumber, the scaled wavenumber and the observed wavenumber along with the potential energy distribution of each mode of vibration is tabulated in Table 31 (Appendix B). The contribution of PED is considered only those contributions which exhibits equal to or greater than 5% contribution for normal mode of vibration. In this vibration, we have used the following symbols for differ-

ent types of vibration: ν(stretching), ν_a(asymmetric stretching), ν_s(symmetric stretching), δ(deformation and bending), oop(out of plane bending), ω(wagging), γ(twisting), ρ(rocking) and τ(torsion). The comparative study between the observed and the simulated spectra of RBZ has been carried out. The graph of scaled wavenumber of all the conformers (I-III) and the observed wavenumber of infra-red (IR) spectra is plotted in Figure 10. The graph of scaled wavenumber of conformers (I-III) and the experimental wavenumber of Raman spectra is plotted in Figure 11.

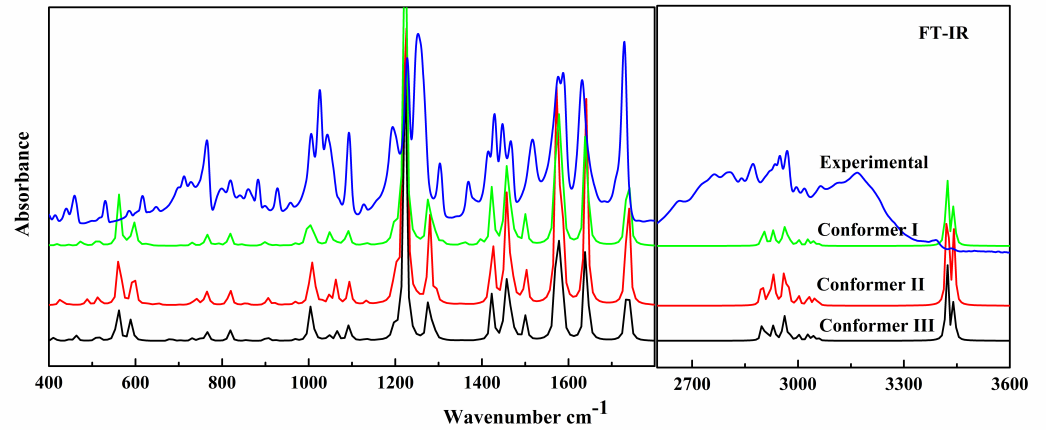

Figure 10: Simulated and experimental infra-red spectra of RBZ in the part (400 to 1800) cm^{-1} and (2601 to 3600) cm^{-1}.

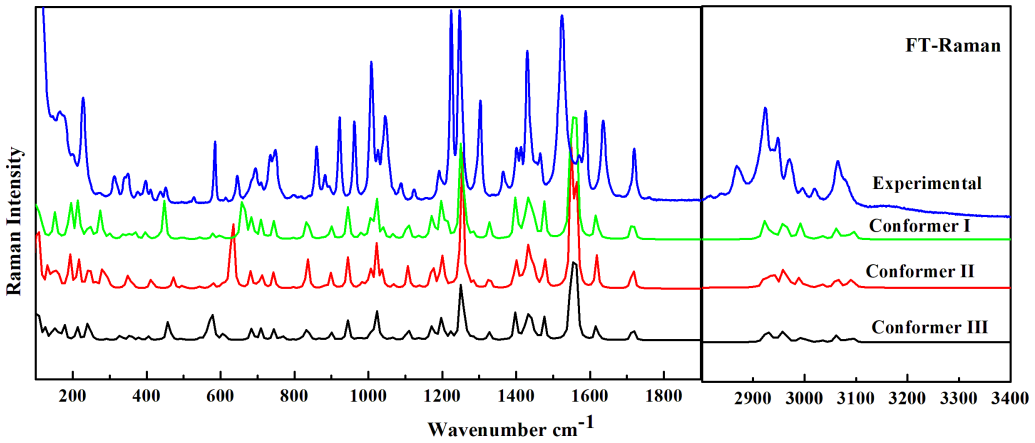

Figure 11: Simulated and experimental Raman spectra of RBZ in the part (100 to 1900) cm^{-1} and (2801 to 3400) cm^{-1}.

4.2.4.1 Vibration of ring R1

The C-H stretching vibration in aromatic compound is discovered in the region (3000 to 3100) cm^{-1} (Varsányi et al., 1973; Thamarai et al., 2020). In the benzene ring of RBZ, many peaks of C-H stretching vibration were observed. The symmetric stretching vibrations were calculated at 3093 cm^{-1} and 3061 cm^{-1} with 99% contribution but these vibrations were determined at 3167 cm^{-1} and 3065 cm^{-1} in the IR spectra and the signature of such vibration was not seen in the Raman spectra. Another C-H stretching

vibration of benzene ring R1 was calculated at 3079 cm^{-1} with 99% contribution and the signature of this spectra was not found in the experimental IR and Raman spectra. The C=C stretching of ring R1 was calculated at 1568 cm^{-1} with 61% contribution but this spectrum was observed at 1587 cm^{-1} in IR spectrum and 1588 cm^{-1} in Raman spectrum. The other C=C stretching spectrum were calculated with mixed mode of vibration at 1551 cm^{-1} but this spectrum is seen at 1575 cm^{-1} in the IR spectra. The another C=C stretching of the ring R1 with 72% contribution was calculated in all the conformers at 1327 cm^{-1} but this is observed at 1303 cm^{-1} in both the IR and the Raman spectrum. The out of plane C-H bending vibration was calculated with 86% contribution at 922 cm^{-1}, 923 cm^{-1} and 921 cm^{-1} in conformers I, II and III respectively and this vibration was determined at 927 cm^{-1} in the IR spectra and 922 cm^{-1} in the Raman spectra. Another out of plane C-H bending vibration with 65% contribution was measured at 883 cm^{-1}, 883 cm^{-1} and 887 cm^{-1} in conformers I, II and III, whereas the corresponding value was observe at 883 cm^{-1} in the IR spectra and 882 cm^{-1} in Raman spectra (M. K. Chaudhary, Prajapati, et al., 2021).

4.2.4.2 Vibration of ring R2

The N-H stretching vibration of imidazole ring R2 with 99% contribution was measured at 3487 cm^{-1}, 3488 cm^{-1} and 3486 cm^{-1} in the conformers I, II and III of RBZ and the corresponding value in IR spectra was seen at 3390 cm^{-1}. There is large difference between the experimental and the calculated wavenumber. This shifting in wavenumber is due to the participation of H26 and O4 atoms in intramolecular hydrogen bonding which is justified in Section 4.2.11. Karabacak et al. (2008) assigned C=N and C-N stretching at 1689 cm^{-1} and 1302 cm^{-1} respectively in the IR spectrum. Sundaraganesan et al. (2007) assigned C-N stretching vibration at 1281 cm^{-1} for benzimidazole. The C=N stretching vibration of respectively ring R2 with 14% contribution was measured at 1618 cm^{-1} in all the conformers of RBZ and the corresponding value was observed at 1631 cm^{-1} and 1635 cm^{-1} in IR/Raman spectra respectively. The stretching vibration of ν(N5C16) with 23% contribution was calculated at 1477 $cm^{-1}$and the corresponding value is observed at 1516 cm^{-1} in the IR spectra and 1524 cm^{-1} in the Raman spectra. There is huge difference between calculated and experimental wavenumber. This difference is due to the participation of O4 and H26 atoms in intramolecular hydrogen bonding as justified in Section 4.2.11. The stretching vibration of ν(N6C11) shows a good resonance between the calculated and the experimental spectra. The calculated spectra was obtained with 27% contribution at 1253 cm^{-1} in all the conformers and the corresponding value in experiment was observed at 1253 cm^{-1} in the IR spectra and 1246 cm^{-1} in the Raman spectra. The N-H bending was calculated in the ring R2 at 1170 cm^{-1}, 1171 cm^{-1} and 1170 cm^{-1} in conformers I, II and III respectively of RBZ and the corresponding signature in experiment was seen at 1158 cm^{-1} in the Raman spectra.

The out of plane bending of N-H was measured at 571 cm^{-1}, 577 cm^{-1} and 576 cm^{-1} in the conformers I, II and III respectively with 62% contribution (M. K. Chaudhary, Prajapati, et al., 2021).

4.2.4.3 CH_2 Vibration

The asymmetric stretching of $C10H_2$ was measured at 3005 cm^{-1}, 3001 cm^{-1} and 3007 cm^{-1} in the conformers I, II and III respectively with 81% contribution whereas asymmetric stretching of $C13H_2$ was measured at 2965 cm^{-1}, 2968 cm^{-1} and 2963 cm^{-1} with a contribution 67% but their corresponding values in experimental part was observed at 2969 cm^{-1} in the IR spectra and 2971 cm^{-1} in the Raman spectra respectively. The symmetric stretching of $C10H_2$ was measured at 2942 cm^{-1}, 29547 cm^{-1} and 2944 cm^{-1} with 93% contribution but the corresponding wavenumber was observe at 2949 cm^{-1} in IR spectra and 2948 cm^{-1} in Raman spectra. Whereas, the symmetric stretching of $C13H_2$ was measured at 2927 cm^{-1}, 2929 cm^{-1} and 2928 cm^{-1} in the conformers I, II and III respectively with 83% contribution but the corresponding value in the experimental IR was observed at 2872 cm^{-1}. The deformation bending δ'_{asym} ($C13H_2$) with 32% contribution was measured at 1461 cm^{-1}, 1461 cm^{-1} and 1456 cm^{-1} in the conformers I, II and III respectively, whereas the corresponding value of wavenumber was seen at 1466 cm^{-1} in the experimental IR spectra. The symmetric deformation $\delta_{sym}(C10H_2)$ bending has been measured at 1214 cm^{-1}, 1227 cm^{-1} and 1222 cm^{-1} in the conformers I, II and III respectively with 57% contribution but it was experimentally seen at 1228 cm^{-1} in the IR spectra and 1224 cm^{-1} in the Raman spectra. The asymmetric deformation bending $\delta_{asym}(C10H_2)$ has been measured at 1200 cm^{-1}, 1197 cm^{-1} and 1197 cm^{-1} in conformers I, II and III respectively and experimentally seen at 1193 cm^{-1} in the IR spectrum and 1191 cm^{-1} in the Raman spectrum (M. K. Chaudhary, Prajapati, et al., 2021).

4.2.4.4 CH_3 Vibration

The stretching vibration of methyl group CH_3 is generally obtained in the higher wavenumber region. In the RBZ, the asymmetric stretching vibration $\nu_a(C19H_3)$ was measured at 3064 cm^{-1} with 99% contribution in all the conformers but the corresponding wavenumber in the experimental Raman spectra was observed at 3065 cm^{-1}. The experimental and the measured spectra have good resonance. Similarly, the asymmetric stretching of $\nu_a(C17H_3)$ was measured at 2991 cm^{-1}, 2989 cm^{-1} and 2996 cm^{-1} for the conformers I, II and III respectively with 98% contribution and observed at 3020 cm^{-1} in both the IR and the Raman spectra. The rocking vibration of $C19H_3$ was measured at 1137 cm^{-1} with 69% contribution in all the conformers and the corresponding value in the experimental IR and the Raman spectra were observed at 1127 cm^{-1} and

1123 cm^{-1} respectively. Similarly, the rocking vibration of $C17H_3$ was measured at 1070 cm^{-1}, 1071 cm^{-1} and 1067 cm^{-1} with 35% contribution in the conformers I, II and III respectively (M. K. Chaudhary, Prajapati, et al., 2021).

4.2.4.5 Carbonyl, Sulfinyl and Amine group Vibration

The vibration of carbonyl group (C=O) is generally found in the region (1670 to 1820) cm^{-1} (Silverstein & Bassler, 1962; Williams, 1963; Myneni et al., 1998). In the RBZ molecule, the stretching of carbonyl group was measured at 1716 cm^{-1} in all the conformers with 67% contribution whereas the corresponding vibration was observed experimentally at 1729 cm^{-1} in the IR spectrum and 1720 cm^{-1} in the Raman spectrum. The stretching vibration of sulfinyl group (S-O) is found at 989 cm^{-1} (Myneni et al., 1998). In the RBZ molecule, the stretching vibration of sulfinyl group was measured at 979 cm^{-1}, 981 cm^{-1} and 975 cm^{-1} in the conformers I, II and III respectively with 82% contribution but it was observed in the experimental Raman spectra at 962 cm^{-1}. Here, the shifting of the wavenumber is due to the formation of intramolecular hydrogen bonding between O2 and H22 which is explained in Section 4.2.11. There is a single aliphatic amine and one aromatic amine in imidazole ring of RBZ. The vibration of aromatic amine has been explained in Section 4.2.4.2 in the vibration of ring R2. The stretching vibration of aliphatic amine is generally observed in the higher wavenumber region. In RBZ, the stretching of N-H was measured with 99% contribution at 3508 cm^{-1}, 3509 cm^{-1} and 3508 cm^{-1} in the conformers I, II and III respectively (M. K. Chaudhary, Prajapati, et al., 2021).

4.2.5 Natural bond orbital investigation

The molecular stability of RBZ has been analyzed from second-order perturbation theory investigation in terms of distribution of charge from donor (filed orbital) to acceptor (vacant orbital). The hyper conjugative interaction or stabilization energy $E^{(2)}$ is the major index to check the intense as well as the weak interaction between the donor Lewis type orbital and the acceptor Lewis type orbital as well as from the lone pair to the acceptor orbital (Foster & Weinhold, 1980; Glendening et al., 1998). The stabilization energy $E^{(2)}$ is determined in terms of second order perturbation theory (Gonohe et al., 1985) and it's value can be measured from Equation (3.67). The interactions between the filled and the vacant orbital of stabilization energy greater than 5 kcal/mol for the conformer I of RBZ is depicted in Table 2.

This reveals that the transition from lone pair (LP) to the antibonding π^*/σ^* orbitals stabilizes the molecule to great extent. The π orbitals have lower occupancies, which show more electron-donor ability in comparison to the σ orbital (Joshi et al., 2011; K. Srivastava et al., 2016). The transitions: LP(2)O3$\rightarrow$ π^*(O4-C18) and LP(1)N7$\rightarrow$ π^*(O4-

Table 2: Second-order perturbation theory analysis of Fock matrix in NBO basis for conformer I of RBZ.

Donor NBO(i)	ED(i)/e	Acceptor NBO (j)	ED(j)/e	$E^{(2)a}$ kcal/mol	E(j) - $E(i)^b$ a.u.	$F(i,j)^c$ a.u.
σ(N6-C11)	1.97364	σ*(N7-C16)	0.03667	8.42	1.18	0.089
σ(N6-C16)	1.98110	σ*(C11-C15)	0.02215	5.34	1.44	0.078
π(N6-C16)	1.86010	π*(C11-C15)	0.42074	20.84	0.35	0.083
π(C8-C12)	1.63923	π*(C9-C14)	0.45257	20.62	0.28	0.069
π(C8-C12)	1.63923	π*(C11-C15)	0.42074	18.19	0.29	0.066
σ(C9-C12)	1.97236	σ*(N5-C8)	0.02573	6.31	1.15	0.076
π(C9-C14)	1.68041	π*(C11-C15)	0.42074	17.39	0.29	0.065
π(C11-C15)	1.60403	π*(N6-C16)	0.40469	13.19	0.25	0.051
π(C11-C15)	1.60403	π*(C8-C12)	0.40965	20.36	0.28	0.067
π(C11-C15)	1.60403	π*(C9-C14)	0.45257	23.08	0.27	0.071
σ(C14-C15)	1.97130	σ*(N6-C11)	0.01787	5.19	1.17	0.070
σ(C19-H32)	1.99540	σ*(C19-H33)	0.00824	7.49	1.18	0.084
σ(C19-H32)	1.99540	σ*(C19-H34)	0.01270	18.63	4.20	0.250
σ(C19-H34)	1.99539	σ*(C19-H33)	0.00824	8.11	1.17	0.087
σ(C19-H34)	1.99539	σ*(C19-H34)	0.01270	21.60	4.19	0.269
LP(2)O2	1.89048	σ*(S1-C9)	0.12617	5.38	0.42	0.042
LP(2)O2	1.89048	σ*(S1-C10)	0.11846	8.36	0.39	0.051
LP(3)O2	1.82449	σ*(S1-C9)	0.12617	12.88	0.41	0.066
LP(3)O2	1.82449	σ*(S1-C10)	0.11846	9.73	0.38	0.055
LP(1)O3	1.96206	σ*(O4-C18)	0.02150	8.24	1.17	0.088
LP(2)O3	1.81638	π*(O4-C18)	0.35949	45.67	0.33	0.114
LP(2)O4	1.83842	σ*(O3-C18)	0.09322	29.73	0.63	0.124
LP(2)O4	1.83842	σ*(N7-C18)	0.07071	22.69	0.70	0.115
LP(1)N5	1.62366	π*(N6-C16)	0.40469	55.06	0.27	0.110
LP(1)N5	1.62366	π*(C8-C12)	0.40965	36.74	0.30	0.095
LP(1)N6	1.92046	σ*(N5-C16)	0.04216	9.41	0.81	0.078
LP(1)N6	1.92046	σ*(C8-C11)	0.03710	5.47	0.91	0.063
LP(1)N7	1.68641	π*(O4-C18)	0.35949	61.96	0.27	0.117
LP(1)N7	1.68641	π*(N6-C16)	0.40469	43.39	0.29	0.103

[a] $E^{(2)}$ means the energy of hyper conjugative interaction (stabilization energy).
[b] Energy difference between donor (i) and acceptor (j) NBOs.
[c] $F(i,j)$ is the Fock matrix element between i and j NBOs.

C18) have major contribution for the stabilization of RBZ molecule with prominent stabilization energy 45.67 kcal/mol and 61.96 kcal/mol respectively. The bonding to the anti-bonding transitions from $\pi \rightarrow \pi^*$ stabilizes the benzine and the imidazole rings. The transitions: π(C11-C15)$\rightarrow$ π^*(N6-C16), π(C11-C15)$\rightarrow$ π^*(C8-C12) and π(C11-C15)$\rightarrow$ π^*(C9-C14) stabilize the molecule with respective interaction energies 13.19 kcal/mol, 20.36 kcal/mol and 23.08 kcal/mol. Similarly, the other transitions which contribute in the stability of the molecule are π(N6-C16)$\rightarrow$ π^*(C11-C15), π(C8-C15)$\rightarrow$ π^*(C9-C14), π(C8-C12)$\rightarrow$ π^*(C11-C15) and π(C9-C14)$\rightarrow$ π^*(C11-C15) with

respective stabilization energy of 20.84 kcal/mol, 20.62 kcal/mol, 18.19 kcal/mol and 17.39 kcal/mol (M. K. Chaudhary, Prajapati, et al., 2021).

The transition from lone pair (LP)→ σ^* also contributes in the stability of molecule. The stability of molecular system due to interaction of LP(2)O4→ σ^*(O3-C18) and LP(2)O4→ σ^*(N7-C18) which contributes the stabilization energy of 29.73 kcal/mol and 22.69 kcal/mol respectively (M. K. Chaudhary, Prajapati, et al., 2021). The hyper conjugative interaction energies of the conformers II and III of RBZ were analyzed and their values are very similar to the conformer I.

4.2.6 Drug-likeness

To be a drug candidate of biological active molecule, it can be predicted theoretically from Lipinski proposed rules (Lipinski et al., 1997). There are several proposed rules which give an idea about the binding property and the lipophilicity for orally intake of drug in human. The improved rule includes (i) Molar Refractivity (MR) should be from (40 to 130) e.s.u (ii) Molecular weight of molecule should be in the range (180 to 500) g/mol and (iii) the number of atoms in the system be in the range 20 to 70. The value of MR is measured from the Lorenz–Lorentz formula (Padron et al., 2002; Verma et al., 2005; Verma & Hansch, 2005):

$$\mathrm{MR} = \left[\frac{n^2-1}{n^2+2}\right]\left(\frac{MW}{\rho}\right) = 1.333\pi\alpha\mathrm{N} \tag{4.1}$$

where N is the Avogadro number and α is the polarizability of the molecular system.

This equation is suitable for both the solid and the liquid states of the molecular system. It is related to the volume of the molecules as well as to the London dispersive forces that act in the drug-receptor interaction. The measured values of MR of conformers I, II and III of RBZ are 41.50 e.s.u, 42.02 e.s.u and 41.37 e.s.u respectively which are in the acceptable range to be a drug. The molecular weight and the number of atoms for RBZ are 281.33 g/mol and 34 respectively. So, RBZ fulfil all the criteria given by Lipinski's rules for being a good drug (M. K. Chaudhary, Prajapati, et al., 2021).

4.2.7 Frontier molecular orbital energy gap ($\Delta E_{\mathrm{L\text{-}H}}$)

The prominent orbitals that participate in the chemical reaction as well as in the stability of the molecular system are the HOMO and the LUMO. The energy of HOMO orbital (E_{H}) and LUMO orbital (E_{L}) and their energy gap $\Delta E_{\mathrm{L\text{-}H}}$ identify the biological activity of the molecule. The HOMO orbital has tendency to donate the electrons so it is called the donor orbital whereas the LUMO orbital has tendency to capture the electrons so it is called the acceptor orbital for the stability of molecule (Atkins, 2001). The electron

transport properties that measure the electron conductivity and the chemical activities of a molecule was observed in terms of HOMO-LUMO energy gap $\Delta E_{\text{L-H}}$ (Fukui et al., 1952; Lewis et al., 1994; Ghosh & Jana, 1999).

The time dependent density functional theory (TD-DFT) calculation in RBZ has been carried out to understand the concentration of electron density in the orbital lobes from TD/B3LYP/6-311++G(d,p) for conformers (I-III). The measured HOMO-LUMO energy gap $\Delta E_{\text{L-H}}$ for the conformers (I-III) are 4.9601 eV, 4.9514 eV and 4.9476 eV respectively. The least value of $\Delta E_{\text{L-H}}$ (4.9476 eV) for conformer III signifies that it is more chemical reactive whereas the highest value of $\Delta E_{\text{L-H}}$ (4.9601 eV) for conformer I explorer that it is more stable. The HOMO-LUMO plot of RBZ for the conformers (I-III) is presented in Figure 12.

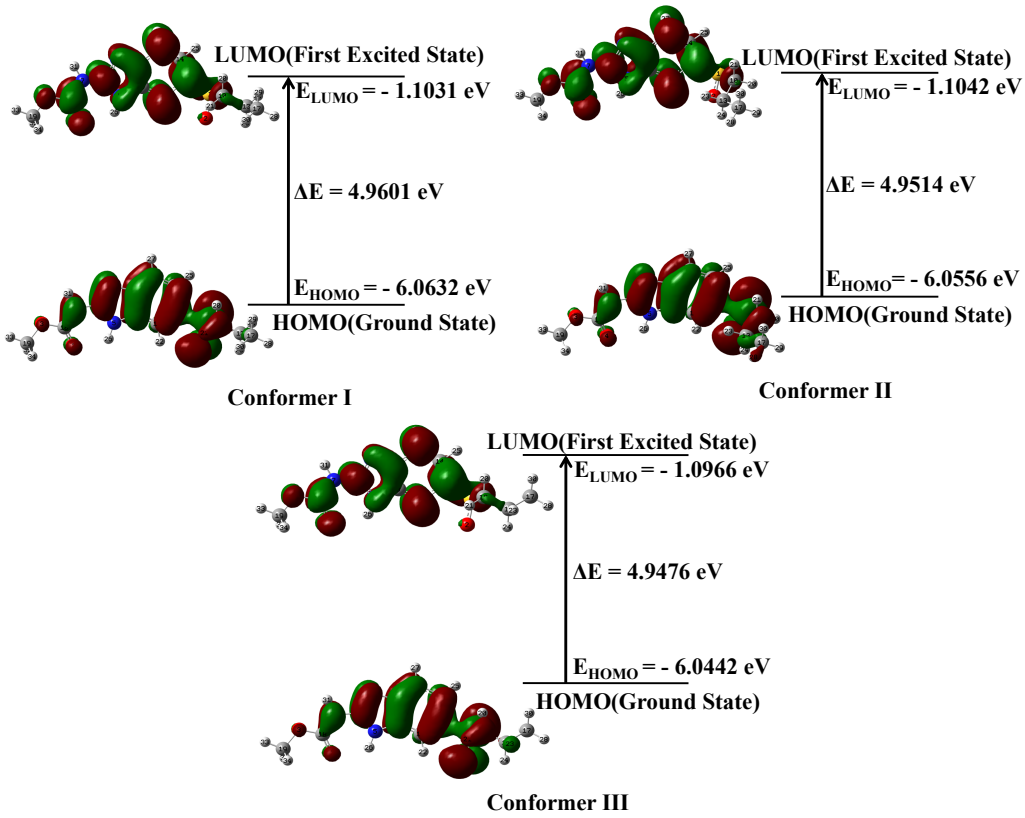

Figure 12: Frontier molecular orbital plot for conformers (I-III) of RBZ.

From the HOMO-LUMO plot it can be identified that the electron density in the HOMO is more in the sulfinyl group and it diverges to aliphatic nitrogen (N7) and rings in the LUMO in all the conformers (I-III) (M. K. Chaudhary, Prajapati, et al., 2021).

4.2.8 Molecular electrostatic potential

It is the fundamental way which identify the electrophilic and the nucleophilic areas in the molecular system for further chemical reaction with the surrounding species. The

molecular electrostatic potential $V(r)$ developed around the molecule is the cumulative impression of the negative and the positive charges related to the electrons and the nuclei and it's value is obtained from the Equation (3.66). It also predicts the inter and intra molecular hydrogen bonding sites.

The electrophilic and the nucleophilic regions are predicted in terms of color code. The red color signifies the electrophilic region whereas the blue color is responsible for the nucleophilic region, however, the green color predicts zero potential (Weiner et al., 1982; Chidangil et al., 1998; Kumru et al., 2015). The three-dimensional MEP surface for all the conformers (I-III) of RBZ is shown in Figure 13. The red color across the sulfinyl group (S1O2) prone to the electrophilic region whereas the blue color across hydrogen atoms in the imidazole ring and N7H31 feasible for nucleophilic region in all the conformers (I-III). This is also verified by the molecular docking as these regions are active binding sites (M. K. Chaudhary, Prajapati, et al., 2021).

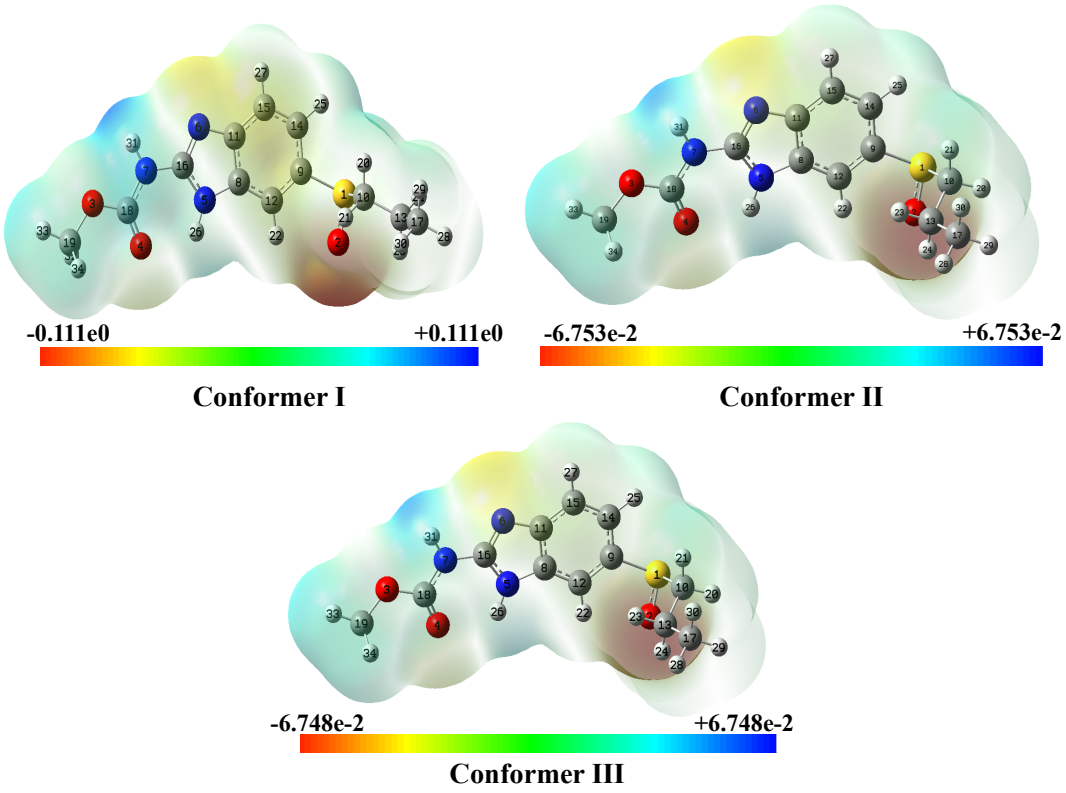

Figure 13: 3D Molecular electrostatic potential of conformers (I-III) of RBZ.

4.2.9 Global reactivity descriptor

The Koopman's theorem (Parr & Pearson, 1983) elaborate the global reactivity descriptor. The physical quantities like: electronegativity (χ), chemical potential (μ), global hardness (η), global electrophilicity index (ω) and global softness (S) are the main indices which measure the reactivity of the molecules globally. These indices are measured in terms of the energies of frontier molecular orbitals E_{HOMO}, E_{LUMO} and are given by

the Equations (3.51)–(3.55) (Pearson, 1989; Padmanabhan et al., 2007; P. K. Chattaraj & Roy, 2007).

The global reactivity index (ω) measures the stabilization energy when the system gains an additional electronic charge (ΔN) from the surroundings species (Parr & Pearson, 1983). Similarly, the electronic chemical potential of the molecule exclusively measures the path of the charge transfer, whereas electrophile is a type of chemical category which can accept the electrons from the surroundings. While accepting the electronic charge from the surrounding, the energy of the system is lowered down and the chemical potential must be negative. The measured values of energies E_{H}, E_{L}, $\Delta E_{\mathrm{L\text{-}H}}$, χ, μ, η, S and ω for all the three conformers (I-III) of RBZ are presented in Table 3. The higher values of ω (2.5885 eV) and $\Delta E_{\mathrm{L\text{-}H}}$ (4.9601 eV) reveal that the conformer I is closer to strong electrophile, is chemically less reactive, is most stable or hardest among all the three conformers. The least values of ω (2.5766 eV) and $\Delta E_{\mathrm{L\text{-}H}}$ (4.9476 eV) signifies that the conformer III is prone to more chemically reactive, least stable or softer than the remaining one (M. K. Chaudhary, Prajapati, et al., 2021).

Table 3: Measured E_{HOMO}, E_{LUMO}, $\Delta E_{\mathrm{L\text{-}H}}$, μ, χ, η, S and ω for conformers (I-III) of RBZ.

Molecule	E_{H} (eV)	E_{L} (eV)	$\Delta E_{\mathrm{L\text{-}H}}$ (eV)	χ (eV)	μ (eV)	η(eV)	S (eV)$^{-1}$	ω (eV)	ΔN_{max}
Conformer I	−6.0633	−1.1032	4.9601	3.5832	−3.5832	2.4801	0.2016	2.5885	1.4448
Conformer II	−6.0557	−1.1042	4.9514	3.5800	−3.5800	2.4757	0.2020	2.5884	1.4460
Conformer III	−6.044	−1.0966	4.9476	3.5704	−3.5704	2.4738	0.2021	2.5766	1.4433

4.2.10 Local reactivity descriptors

The global reactivity descriptor explores the overall reactive picture of the molecular system whereas the local reactive parameter measures the quantitative analysis of particular site in the molecule. The Fukui function (FF) has been used to compute the reactivity of each atom on the basis of the Hirshfeld partial charge analysis from B3LYP/6-311++G(d,p) level of theory in all the conformers (I-III) of RBZ. The atom with more value of FF is more likely to take part in the chemical activity with the surrounding species than the other atoms in the molecule (Parr & Yang, 1984).

The reactivity of each atom in anion, cation and neutral states of the molecule was measured in terms of FF (f_k^+, f_k^-, f_k^0), local softness (s_k^+, s_k^-, s_k^0) and local electrophilicity indices (ω_k^+, ω_k^-, ω_k^0). The Fukui functions were measured through the Equations (3.63)–(3.65) (Fukui, 1982). The FF values for the nucleophilic, the electrophilic and the radical attack of the particular atoms of RBZ are listed in Table 4.

Figure 14 visualizes the comparative study for the nucleophilic attack whereas Figure 15 demonstrates for the electrophilic attack in the conformers (I-III). The findings of this study regarding the local reactivity descriptor signifies that the atoms O2, C12 and S1

Table 4: Measured local reactivity descriptors of the particular atoms using Hirshfeld [B3LYP/6-311++G(d,p)] derived charges for RBZ of conformers (I-III).

Atom	f_k^+	Atom	f_k^-	Atom	f_k^0
Conformer I					
O2	0.17229	C12	0.06433	S1	1.21969
S1	0.08739	C15	0.05609	C18	0.91565
C9	0.06941	C16	0.03264	C16	0.59882
N6	0.06642	C9	0.02996	C8	0.16906
C11	0.06077	S1	0.02748	C11	0.14272
C16	0.05877	C19	0.02713	C15	–0.20397
Conformer II					
O2	0.16948	C12	0.07097	S1	1.22877
S1	0.09063	C15	0.05663	C18	0.91549
C9	0.06938	C16	0.03389	C16	0.59788
N6	0.06500	C9	0.02784	C8	0.16443
C11	0.06094	C19	0.02755	C11	0.14392
C16	0.05864	C10	0.02519	C15	–0.20480
Conformer III					
O2	0.17316	C12	0.06534	S1	1.22151
S1	0.08916	C15	0.05508	C18	0.91645
C9	0.06707	C16	0.03018	C16	0.59980
N6	0.06547	C19	0.02959	C8	0.16398
C11	0.06069	C9	0.02677	C11	0.14493
C16	0.05847	O4	0.02233	C15	–0.20361

are responsible for electrophilic, nucleophilic and radical attack respectively in all the conformers (M. K. Chaudhary, Prajapati, et al., 2021).

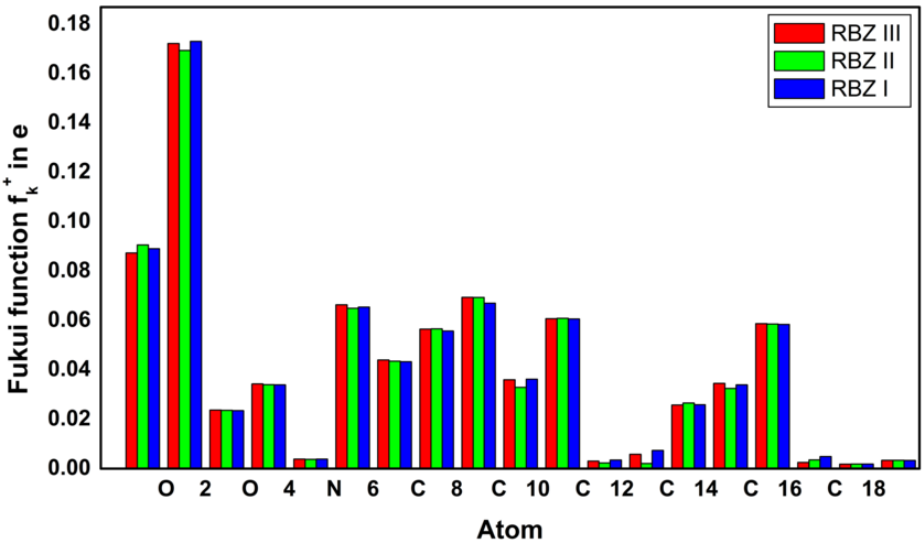

Figure 14: Graphical comparison of Fukui functions (f_k^+) for conformer (I-III) of RBZ.

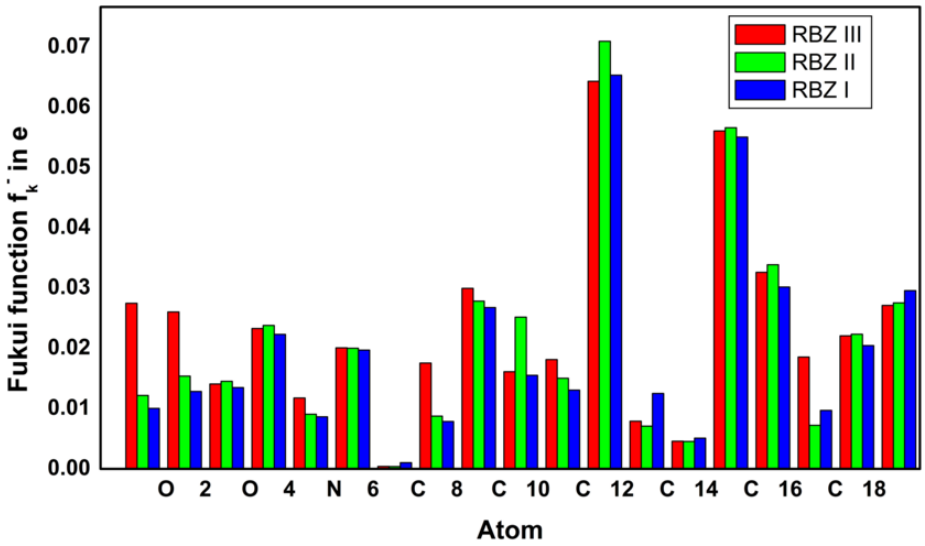

Figure 15: Graphical comparison of Fukui functions (f_k^-) for conformer (I- III) of RBZ.

4.2.11 Atoms in molecule

The intramolecular hydrogen bonding of RBZ has been investigated from QTAIM. The enquiry of AIM is supported by the electron density (ρ_{BCP}) and the Laplacian of electron density $\nabla^2\rho_{BCP}$ at the BCP. The molecular graph of RBZ by using the AIM program is given in Figure 16. The intramolecular hydrogen bond energy for all the conformers (I-III) is tabulated in Tables 5 and 6.

Table 5: Geometrical parameters of RBZ to explain the intramolecular hydrogen bonds in conformers (I-III): bond length, bond angle and the sum of van der Waal radii of interacting atoms ($r_{\mathrm{H}} + r_{\mathrm{A}}$).

D-H...A	D-H (Å)	H...A (Å)	D-H...A (Å)	($r_{\mathrm{H}} + r_{\mathrm{A}}$) (Å)
Conformer I				
C12-H22...O2	1.08446	2.41052	106.15647	2.72
N5-H26...O4	1.01129	2.12395	118.29519	2.72
Conformer II				
C12-H22...O2	1.08434	2.39753	106.37893	2.72
N5-H26...O4	1.01133	2.12673	118.20813	2.72
Conformer III				
C12-H22...O2	1.08449	2.41032	106.25647	2.72
N5-H26...O4	1.01131	2.12586	118.23876	2.72

Table 6: Geometrical parameter (bond length) and topological parameters for bonds of interacting atoms for conformers (I-III) of RBZ: ρ_{BCP}, $\nabla^2\rho_{BCP}$, G_{BCP}, V_{BCP}, H_{BCP} at the BCP and estimated E_{int}.

Interactions	Bond length (Å)	ρ_{BCP} (a.u.)	$\nabla^2\rho_{BCP}$ (a.u.)	G_{BCP} (a.u.)	V_{BCP} (a.u.)	H_{BCP} (a.u.)	E_{int} (kcal/mol)
Conformer I							
O2...H22	2.41052	0.01392	0.05399	−0.00173	−0.01003	−0.01176	−3.14671
O4...H26	2.12395	0.01989	0.07628	−0.00256	−0.01396	−0.01651	−4.37854
Conformer II							
O2...H22	2.39753	0.01421	0.05462	−0.00174	−0.01017	−0.01191	−3.19007
O4...H26	2.12673	0.01978	0.07584	−0.00255	−0.01387	−0.01641	−4.35157
Conformer III							
O2...H22	2.41032	0.01392	0.05396	−0.00173	−0.01003	−0.01176	−3.14624
O4...H26	2.12586	0.01981	0.07597	−0.00255	−0.01389	−0.01644	−4.35927

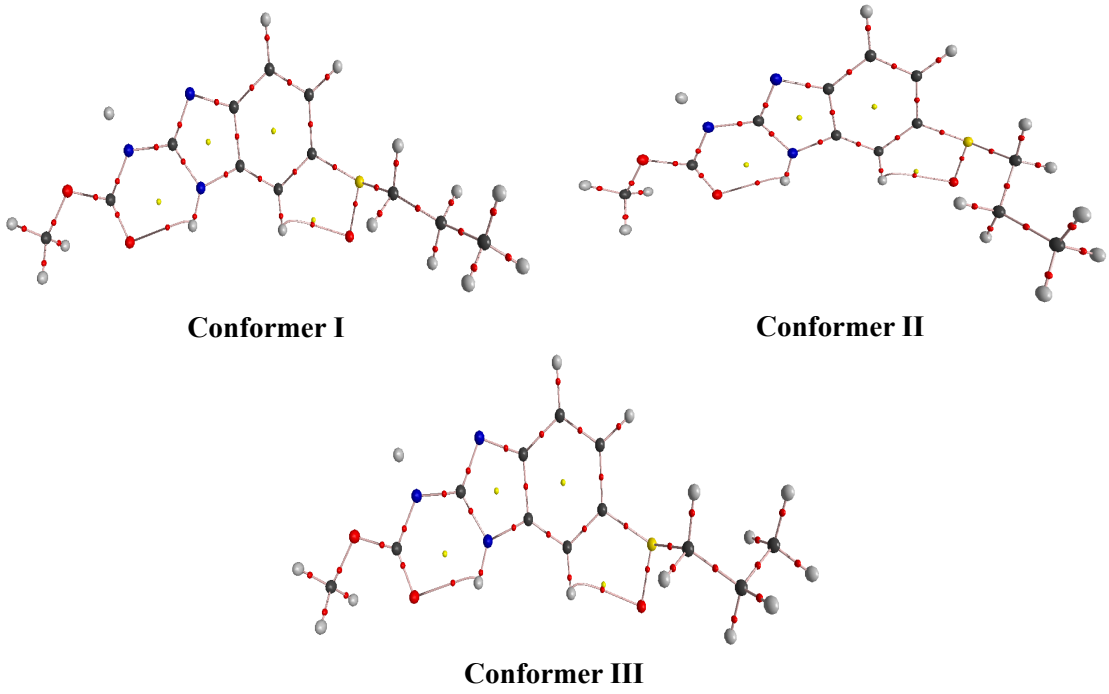

Figure 16: Graphical presentation of atoms in molecule for RBZ of conformers (I-III): bond critical points (small red spheres), bond path (pink lines), ring critical points (small yellow spheres).

According to Koch and Popelier criteria (Koch & Popelier, 1995), the hydrogen bond exists when the electron density (ρ) between the proton (H) and the acceptor (A) lie in the range (0.002 to 0.040) a.u. The Laplacian ($\nabla^2\rho_{BCP}$) of the electron density should be in the order (0.024 to 0.139) a.u. In the RBZ molecule, two intramolecular hydrogen bonds C12-H22. . . O2 and N5-H26. . . O4 have been identified that follow the Koch and Popelier criteria. Furthermore, the nature and the strength of hydrogen bond has been examined by Rozas et al. (2000) in terms of ($\nabla^2\rho_{BCP}$) and the total electron energy density (H_{BCP}). For weak hydrogen bond, the condition should be $\nabla^2\rho_{BCP} > 0$ and $H_{BCP} > 0$. For partially covalent in nature, the criteria should be $\nabla^2\rho_{BCP} > 0$ and $H_{BCP} < 0$. But for strong and covalent nature, the criteria should be $\nabla^2\rho_{BCP} < 0$ and $H_{BCP} < 0$. In the RBZ molecule, both the bonds are partially covalent and medium in nature. The

interaction energy (E_{int}) for O4...H26 is more in comparison to O2...H22 in all the conformers (I-III). So the previous one is stronger than the latter one (M. K. Chaudhary, Prajapati, et al., 2021).

4.2.12 Thermo dynamical properties

The significance of the stability and the reactivity of molecules can be shown in terms of the thermodynamic parameters (V. Choudhary et al., 2019). The total energy, zero-point energy, enthalpy, specific heat capacity, entropy and the rotational constants at 298.15 K temperature for all the conformers (I-III) of RBZ have been measured from the DFT approach at B3LYP/6-311++G(d,p) level of calculation. These values are depicted in Table 7. The variation of enthalpy (H_p°), specific heat ($C_{p,m}^\circ$) and entropy (S_p°) with temperature for the conformer I of RBZ has been studied and the correlation equations are obtained as

$$C_{m,p}^\circ = 9.12952 + 0.22101\,T - 5.92258 \times 10^{-5}T^2 \qquad (R^2 = 0.9998) \qquad (4.2)$$

$$S_m^\circ = 58.16498 + 0.34066\,T - 0.153456 \times 10^{-5}T^2 \qquad (R^2 = 0.9993) \qquad (4.3)$$

$$H_m^\circ = 166.88312 + 0.01279\,T + 9.44106 \times 10^{-5}T^2 \qquad (R^2 = 0.9998) \qquad (4.4)$$

These equations will help in the further study of thermodynamic energies and estimate the direction of chemical reactions from the second law of thermodynamics in thermo chemical field of the RBZ (Joshi et al., 2014; Ott & Boerio-Goates, 2000; Zhang et al., 2010). The variation of H_p°, $C_{p,m}^\circ$ and S_p° with temperature for the conformer I of RBZ is shown in Figure 17, which signifies that their values increases with rise in temperature. It also reveals that the atomic vibration in the molecule increases with temperature and results in the increase of the thermodynamic properties.

Table 7: Theoretically computed total energy, zero-point energy, enthalpy, specific heat, entropy and rotational constants at 298.15 K at the B3LYP/6-311++G(d,p) level for conformers (I-III) of RBZ.

Parameters	Conformer I	Conformer II	Conformer III
Total energy(eV)	−34140.3277	−34140.3205	−34140.3113
Zero point energy(J/mol)	699536.1	700047.3	699421.8
Enthalpy(kcal/mol)	179.085	179.162	179.039
Specific heat(cal/mol-K)	69.573	69.477	69.565
Entropy(cal/mol-K)	145.427	144.913	145.548
Rotational constant(GHz)	0.88858	0.75377	1.06719

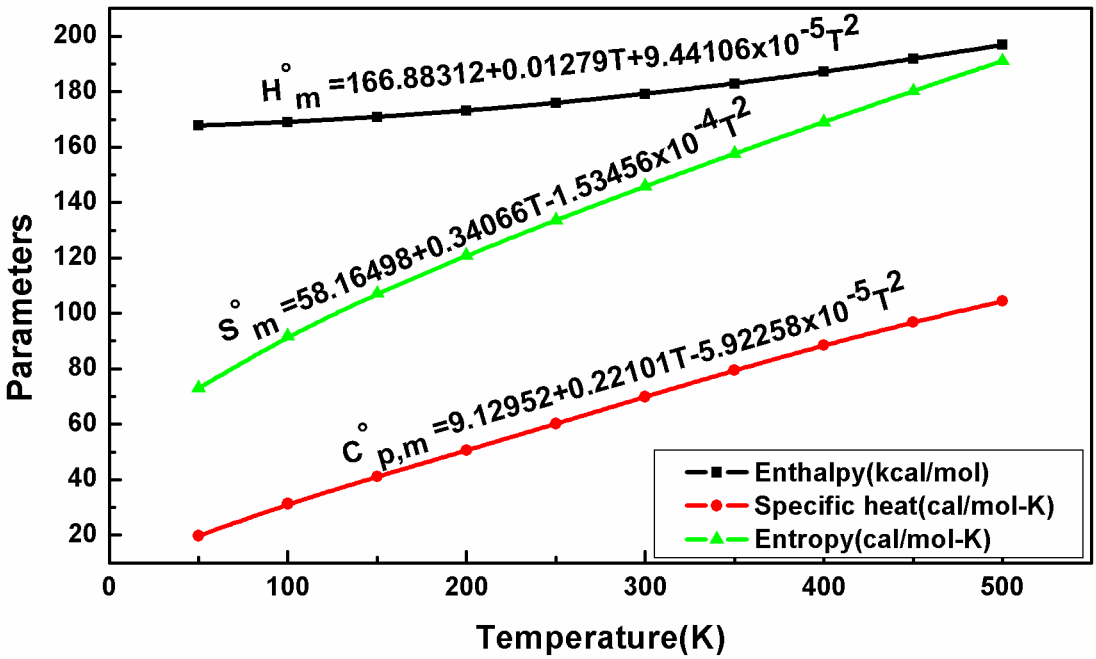

Figure 17: Variation of H°_{m}, $C^{\circ}_{p,m}$ and S°_{m} with temperature for conformer I of RBZ.

4.2.13 Non-linear optical properties

The practical application of NLO substance is in laser technology, optical communication, information processing and optical disk data storage, etc. (Cao et al., 2017; M. K. Mohan et al., 2017; Suresh et al., 2018). The static dipole moment (μ_0), mean polarizability ($\Delta\alpha_0$), anisotropy of polarizability $|\alpha_0|$ and the first hyperpolarizability (β_0) are the fundamental NLO properties of the molecular system and these properties of RBZ has been calculated from the DFT approach at B3LYP/6-311++G(d,p) level of calculation from the Equations (3.47)–(3.50) (Vidya et al., 2011). The delocalization of charge in a particular direction is measured by the component of polarizability in that direction. The static dipole moment (μ_0), mean polarizability ($\Delta\alpha_0$), anisotropy of polarizability $|\alpha_0|$ and the first hyperpolarizability (β_0) are calculated as 4.7071 debye, 84.3080×10^{-24} e.s.u, 31.2624×10^{-24} e.s.u and 1.7353×10^{-30} e.s.u respectively. These values are depicted in Table 8. The values of μ_0, $\Delta\alpha_0$, and β_0 for RBZ are 2.7, 8.6 and 1.8 times more than that of the empirical values of urea (Cassidy et al., 1979) respectively which prompt that the RBZ can be treated as a good NLO substance.

4.2.14 Molecular docking simulation

Molecular docking is the basic tool that insight the binding site of the ligand with residue (i.e., amino acid) of target protein. The docking procedure of RBZ has been performed by using Autodock software (Trott & Olson, 2010). The protein targets which are assumed to bind with ligand (RBZ) are predicted from online Swiss Target Prediction (Daina et al., 2019). Three proteins have been selected and their protein data bank (PDB) code

Table 8: The measured dipole moment (μ_0), mean polarizability$|\alpha_0|$, anisotropy of polarizability ($\Delta\alpha$) and first hyperpolarizability (β_0) of RBZ at B3LYP/6-311++G (d,p).

Dipole moment (debye)		Polarizability ($\times10^{-24}$ e.s.u.)		Hyperpolarizability ($\times10^{-30}$ e.s.u.)	
μ_x	−3.6195	α_{xx}	46.6039	β_{xxx}	1.8285
μ_y	1.0487	α_{xy}	0.7624	β_{xxy}	−0.9924
μ_z	2.8207	α_{yy}	27.2697	β_{xyy}	−0.9858
μ_0	4.7071	α_{xz}	−0.5937	β_{yyy}	0.9728
μ_0(urea)	1.7410	α_{yz}	1.5497	β_{xxz}	−0.4565
		α_{zz}	19.9136	β_{xyz}	−0.2356
		$\|\alpha_0\|$	31.2624	β_{yyz}	0.4193
		$\Delta\alpha$	84.3080	β_{xzz}	0.7311
		$\Delta\alpha$(urea)	9.7710	β_{yzz}	0.4333
				β_{zzz}	0.6399
				β_0	1.7353
				β_0(urea)	0.9279

were downloaded from RCSB PDB (Rose et al., 2010): Poly [ADP-ribose] polymerase-1(PARP) (PDB code: 1UK1, 2PAW, 6I8M); MAP kinase p38 alpha (MAPK) (PDB Code: 3BX5, 3LFA, 3LFB) and Adenosine A2a receptor (PDB Code: 3PWH, 3QAK) to scrutinize the binding site and the effectiveness of RBZ.

The PARP protein is responsible to repair Deoxyribonucleic acid (DNA), programmed cell death and genomic stability (C. Guo et al., 2020) but the MAPK protein is effective in the recovery of osmotic stress, heat shock, metogens (Segalés Dalmau et al., 2016) whereas the Adenosine A2a receptor is effective to control the planning and the initiation of the voluntary movement (Pinna et al., 2017).

The proteins were prepared by removing the co-crystallized ligands and the water molecules using the Discovery Studio Visualizer 4.5 software (Studio, 2009). The protein has been confined in the grid size of 60 Å × 60 Å × 60 Å to identify the residues which bind with the active sites. From the many docked conformations, those which were well-bounded with the active sites were taken into consideration and their pictorial presentation is depicted in Figure 18.

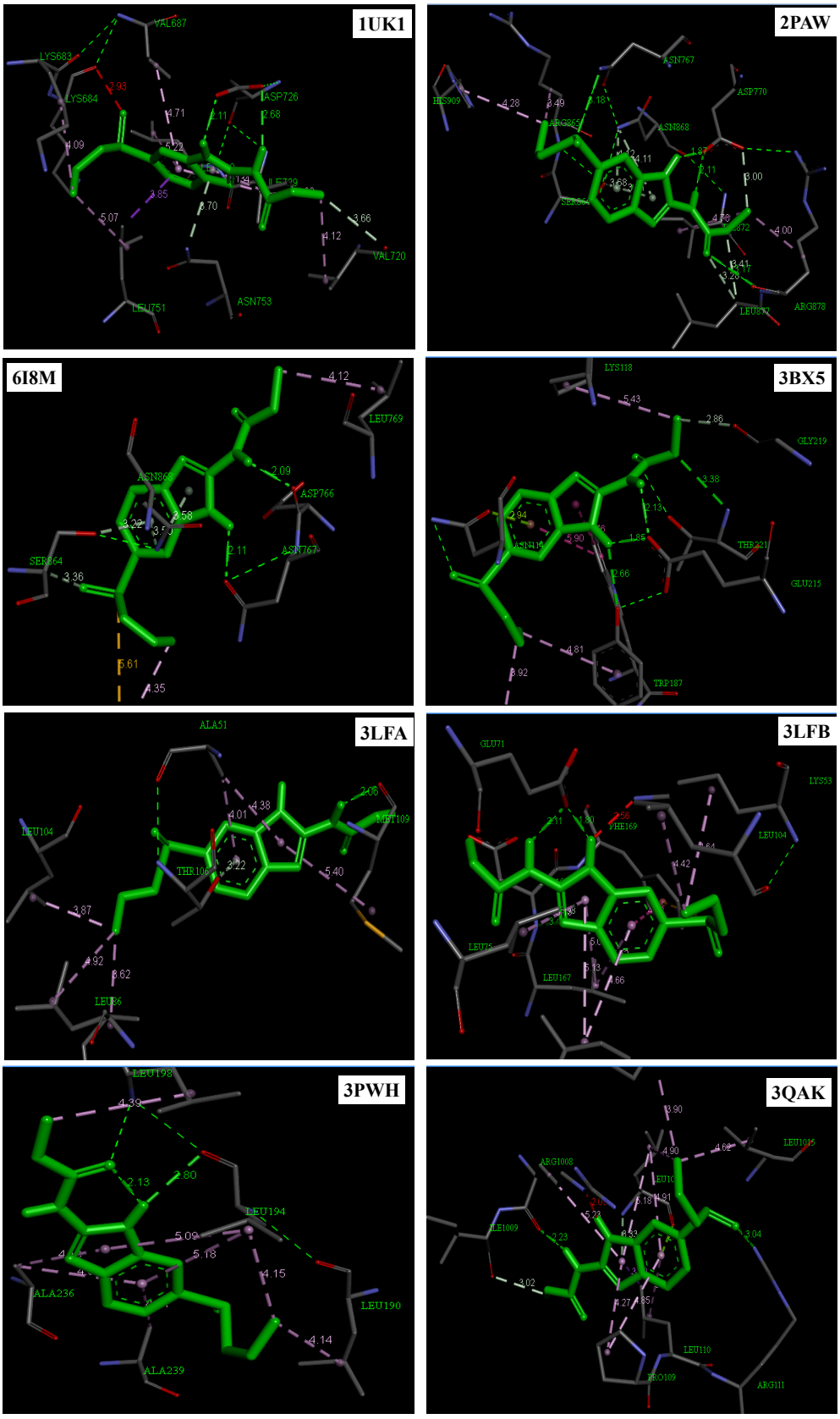

Figure 18: Docking of RBZ with predicted protein targets.

The binding energy of protein-ligand interaction, the bond distance of the hydrogen bond and the ligand efficiency are given in Table 9. The physical phenomenon of 1UK1 exhibit two hydrogen bonds H31 (2.32 Å) and H26 (2.01 Å) with residue ASP:726 with sufficient binding energy −7.60 kcal/mol. Similar type of interactions are found in docked conformer 6I8M with H31 (2.09 Å, ASP:766) and H26 (2.11 Å, ASN:767) with binding energy −7.16 kcal/mol. The docked conformer 2PAW gives four conventional hydrogen bonds, two with H31 (2.11 Å, ASP:770) and H26 (1.87 Å, ASP:770), another with a carbonyl group (3.17 Å, ARG:878) and sulfinyl group (3.18 Å, ASN:767) with binding energy −7.15 kcal/mol. Besides these interactions, the docked conformer 3BX5 exhibits four conventional hydrogen bonds. H26 binds with two residue GLU:215 and TYR: 188 and their bond length are 1.85 Å and 2.66 Årespectively. H31 again binds with GLU:215 with bond distance 2.13 Å and O3 interact with THR:221 having bond distance of 3.88 Å with a binding energy of −5.52 kcal/mol. Furthermore, the docked conformer 3LFA shows the interaction with H31 (2.06 Å, MET:109) with binding energy −5.78 kcal/mol and the docked conformer 3LFB interacts with H31 (2.11 Å, GLU:71) and H26 (1.80 Å, GLU:71) with binding energy −8.07 kcal/mol. 3QAK and 3PWH of Adenosine A2a receptor shows the binding activity with H31 (2.23 Å, ARG:1008) and H26 (2.80 Å, LEU:194) with binding energy −6.39 kcal/mol and −5.81 kcal/mol respectively (M. K. Chaudhary, Prajapati, et al., 2021).

Table 9: Docking parameters of RBZ against predicted protein targets.

Protein	PDB code	Bond length (Å)	Amino acid	Binding energy (kcal/mol)	Ligand efficiency
Poly [ADP-ribose] polymerase-1	1UK1	2.32 2.01	ASP:726 ASP:726	−7.60	−0.40
	2PAW	1.87 2.11 3.17 3.18	ASP:770 ASP:770 ARG:878 ASN:767	−7.15	−0.38
	6I8M	2.09 2.11	ASP:766 ASN:767	−7.16	−0.38
MAP kinase p38 alpha	3BX5	2.13 1.85 2.66 3.38	GLU:215 GLU:215 TYR:188 THR:221	−5.52	−0.29
	3LFA	2.06	MET:109	−5.78	−0.30
	3LFB	2.11 1.80	GLU:71 GLU:71	−8.07	−0.42
Adenosine A2a receptor	3PWH	2.80	LEU:194	−5.81	−0.31
	3QAK	3.04 2.23	ARG:111 ARG:1008	−6.39	−0.34

Thus, the docking simulation of RBZ explores that H31 and H26 are the active sites for protein-ligand interactions. The convenient active binding sites are also explained in MEP surface investigation as explained in Section 4.2.8. However, further *in vitro* and *in vivo* studies have to be performed to support its activities.

4.3 Cefradine

Cefradine is a first-generation cephalosporin having therapeutic use against Gram-positive and Gram-negative bacteria. Our discussion regarding the cefradine is mainly concerned with the electronic and the structural properties from the combined experimental and theoretical (DFT) approach. The main motive of this study to focus on the structural properties from the spectroscopic as well as from the conformational analysis approach which helps to study the drug activity of molecular system (M. K. Chaudhary, Karthick, et al., 2021). The following property of cefradine has been discussed below.

4.3.1 Quantum chemical calculation details of cefradine

The minimum energy structure of cefradine has been obtained from the DFT calculations (Hohenberg & Kohn, 1964) with B3LYP (Lee et al., 1988; Parr & Yang, 1989a) functional by employing the standard 6-311++G(d,p) basis set (Peterson et al., 1994; Hehre, 1976; Becke, 1993) implemented in the Gaussian 09 program package (M. J. Frisch et al., 2009). The PES scans were performed across the rotatable bonds to explore the most stable structure. The vibrational harmonic frequencies calculation of the minimum energy conformer along with the conformers having closely related energies from the B3LYP/6-311++G(d,p) level of approximation were performed. The signatures of normal modes of vibrations were identified by following the normal coordinate analysis procedure recommended by Pulay et al. (1979). The PEDs for the normal modes were estimated by using Gar2Ped program (J. M. L. Martin & Van Alsenoy, 1995). The simulated IR and Raman spectra of cefradine were compared with the experimental spectra. The quantum chemical parameters which signifies the chemical reactivity of the molecule in terms of NBOs, MEP, global and local reactivity descriptors of the molecule were carried out at B3LYP/6-311++G(d,p) level of calculation. The distributions of electron in the molecule were identified from the surface mapping of HOMO, LUMO orbitals and the MEP surfaces and they are generated with the help of GaussView 05 (A. Frisch et al., 2005). The intramolecular hydrogen bond of cefradine has been analyzed from the QTAIM (R. Bader et al., 1979, 1983; R. F. Bader & MacDougall, 1985) by using the AIM all and the AIM 2000 program (Keith & AIMALL, 2009). The inhibition capability of cefradine against certain expected targets were scrutinized from the molecular docking simulations approach. The docked parameters of complexes such as the binding energy, the ligand efficiency and the inhibition constant were obtained by using AutoDock 4.2 (G. Morris

et al., 2009). For ligand-protein interaction, a grid size of 60 Å × 60 Å × 60 Å was chosen and a tolerance value of 2.0 Å was fixed while clustering the conformers. The proteins were cleaned by removing the co-crystallized ligands and the water molecules in the PDB file and then hydrogen atoms and Gasteiger charges were incorporated to the protein residues using UCSF Chimera program (Pettersen et al., 2004). The docking has been performed using the Lamarckian Genetic Algorithm (LGA) (G. M. Morris et al., 1998) which is included in the AutoDock 4.2 program. The ligand-protein interaction has been visualized with the help of LIGPLOT which is included in Discovery Studio software (Studio, 2009).

4.3.2 Conformational studies

The optimized 3D-electronic structure of cefradine with the atom numbering system is illustrated in Figure 19. The ground state optimized geometry was initially obtained by employing the B3LYP/6-311++G(d,p) level of calculation. The minimum energy structure of cefradine at room temperature was obtained by employing the one-dimensional PES scan across the flexible bonds C19-C16, C16-N8, C16-C15, C15-N7, C12-C18, C18-O4, C17-C14 and N7-C10 having corresponding torsional angles ϕ1(C21-C19-C16-N8), ϕ2(C19-C16-N8-H38), ϕ3(C19-C16-C15-O3), ϕ4(C16-C15-N7-C10), ϕ5(N6-C12-C18-O4), ϕ6(C12-C18-O4-H43), ϕ7(H33-C17-C14-C13) and ϕ8(C15-N7-C10-C9) as shown in Figure 20. The geometry obtained corresponding to local and global minima on the PES scan curve was further optimized with same level of calculation as optimization. Twelve conformers were obtained and their energies are presented in Table 10. The PES curves for each rotational bond are presented in Figure 20. The optimized structures of the twelve conformers along with their relative SCF energies are depicted in Figure 21.

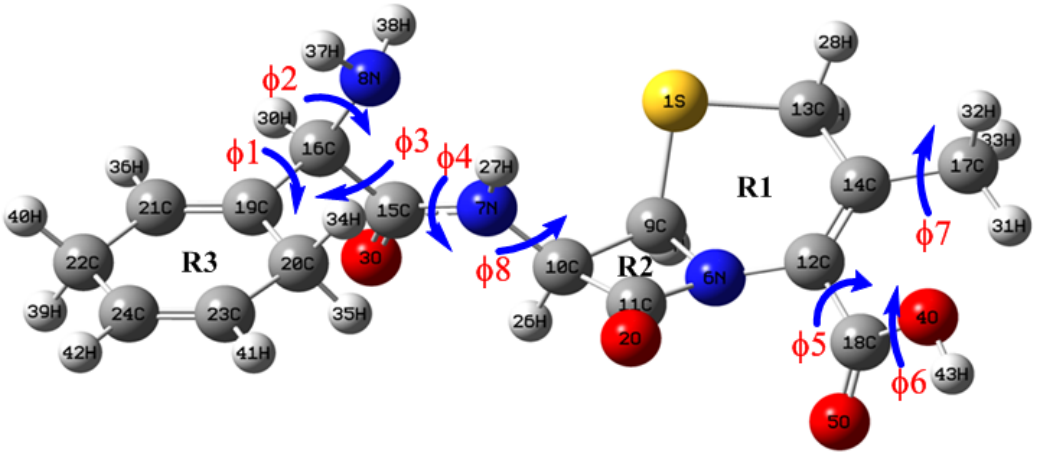

Figure 19: 3D minimum energy electronic structure of cefradine with atom numbering system.

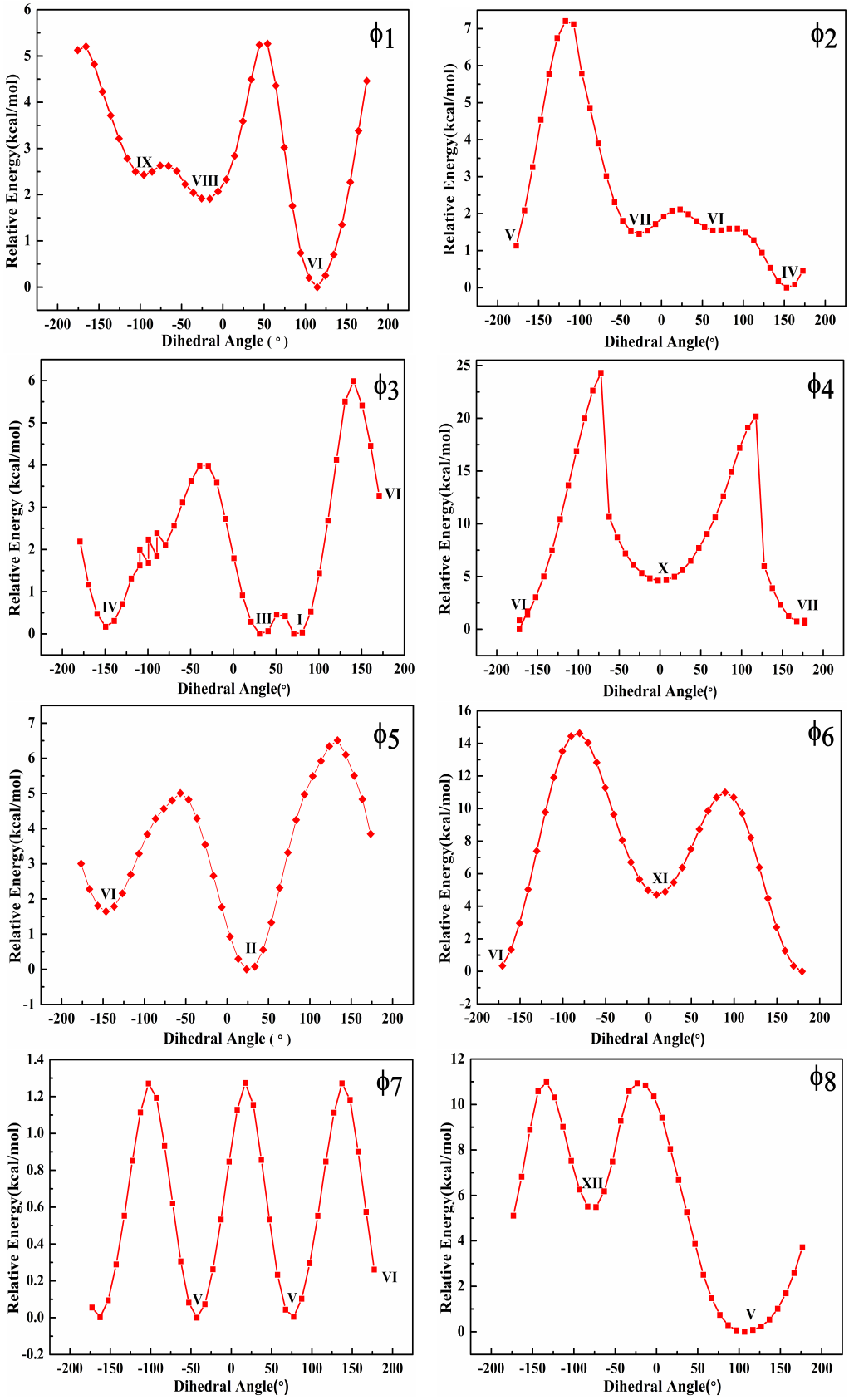

Figure 20: PES scan with varying dihedral angle $\phi 1$, $\phi 2$, $\phi 3$, $\phi 4$, $\phi 5$, $\phi 6$, $\phi 7$, $\phi 8$.

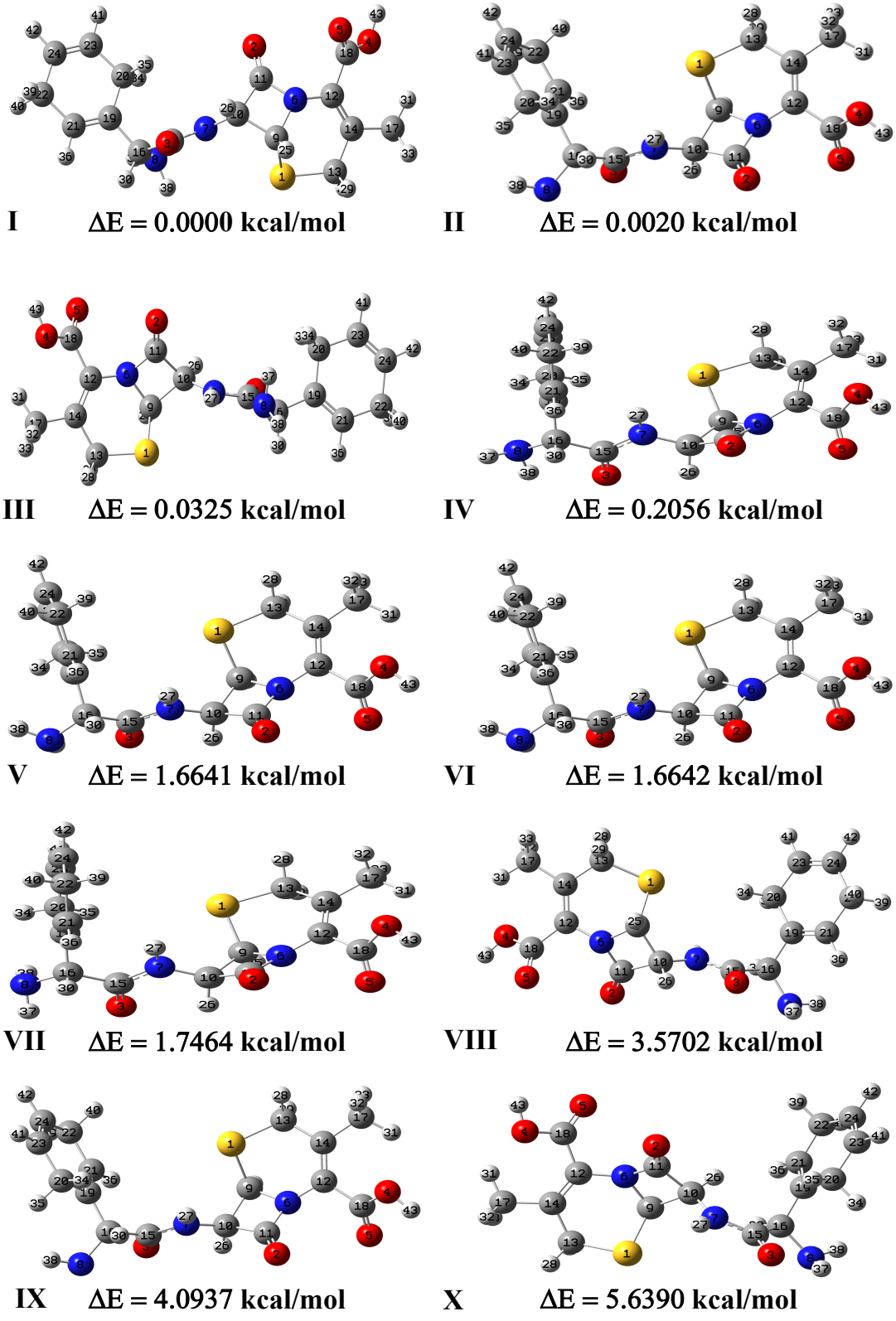

Figure 21: Optimized structure of all the twelve conformers of cefradine along with relative energy.

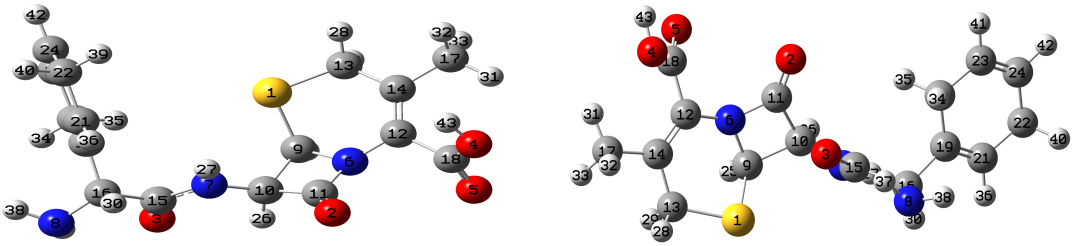

Figure 21: (cont.) Optimized structure of all the twelve conformers of cefradine along with relative energy.

Table 10: The optimized energy and relative energy of all the feasible conformers of cefradine from B3LYP/6-311++G(d,p) level of theory.

Dihedral Angles	Conformers	Energy (Hartree)	Energy (kcal/mol)	Energy Difference* (kcal/mol)
ϕ3(C19-C16-C15-O3)	I	−1484.788724	−931719.0299	0.0000
ϕ5(N6-C12-C18-O4)	II	−1484.788721	−931719.0279	0.0020
ϕ3(C19-C16-C15-O3)	III	−1484.788672	−931718.9974	0.0325
ϕ2(C19-C16-N8-H38)	IV	−1484.788397	−931718.8243	0.2056
ϕ8(C15-N7-C10-C9)	V	−1484.786072	−931717.3658	1.6641
ϕ1(C21-C19-C16-N8)	VI	−1484.786072	−931717.3657	1.6642
ϕ4(C16-C15-N7-C10)	VII	−1484.785941	−931717.2835	1.7464
ϕ1(C21-C19-C16-N8)	VIII	−1484.783035	−931715.4597	3.5702
ϕ1(C21-C19-C16-N8)	IX	−1484.782200	−931714.9362	4.0937
ϕ4(C16-C15-N7-C10)	X	−1484.779738	−931713.3909	5.6390
ϕ6(C12-C18-O4-H43)	XI	−1484.778566	−931712.6558	6.3741
ϕ8(C15-N7-C10-C9)	XII	−1484.777751	−931712.1443	6.8856

*comparative energies of the other eleven conformers in comparison to the minimum energy conformer I.

In the PES scan, the dihedral angle was changed from 0° to 360° by varying 10°in each step along the bond axis. The conformers having relative energy less than 0.56 kcal/-mol (which is equal to kT) in comparison to the minimum energy structure consist at room temperature. The minimum energy (−931719.0299 kcal/mol) of conformer I was obtained from rotation along ϕ3. The conformational analysis signifies that only four conformers known as conformer I, conformer II, conformer III and conformer IV inference to their SCF energies that consist at room temperature (M. K. Chaudhary, Karthick, et al., 2021).

4.3.3 Geometry optimization and optimized parameters

The functional B3LYP is suitable for short-range interaction because it has problems with incorrect $1/r$ activities for long range (i.e., for large r) but the latest functional ωB97XD which is also called the range-separated functional is suitable for both the short-range as well as for the long-range interactions. The four conformers (I-IV) were further optimized with the latest dispersion corrected functional ωB97XD (Chai & Head-Gordon, 2008). The calculated energy using the functional ωB97XD is more than

the energy calculated using the functional B3LYP as tabulated in Table 11. Moreover,

Table 11: Comparison of the energy of conformers (I-IV) of cefradine by using the functional B3LYP and ωB97XD.

Conformers	B3LYP		ωB97XD	
	Energy (Hartree)	Energy (kcal/mol)	Energy (Hartree)	Energy (kcal/mol)
I	−1484.788724	−931719.0299	−1484.427687	−931492.4754
II	−1484.788721	−931719.0278	−1484.429713	−931493.7470
III	−1484.788672	−931718.9974	−1484.426468	−931491.7109
IV	−1484.788396	−931718.8243	−1484.428617	−931493.0595

the bench marking report shows that the result given by the functional B3LYP is nearer to the experimental data (Tortorella et al., 2016). So, the further DFT calculation has been carried out with the functional B3LYP. The superposition of conformers (I-IV) of cefradine has been carried out with the structure presented by Van de Streek et al. (2013) with the support of dispersion corrected functional by using least square algorithm which minimizes the distance of non-hydrogen atom. The superimposed structure is depicted in Figure 22, which signifies that the conformer II is more likely to overlap with the structure as mentioned in the literature (Van de Streek et al., 2013).

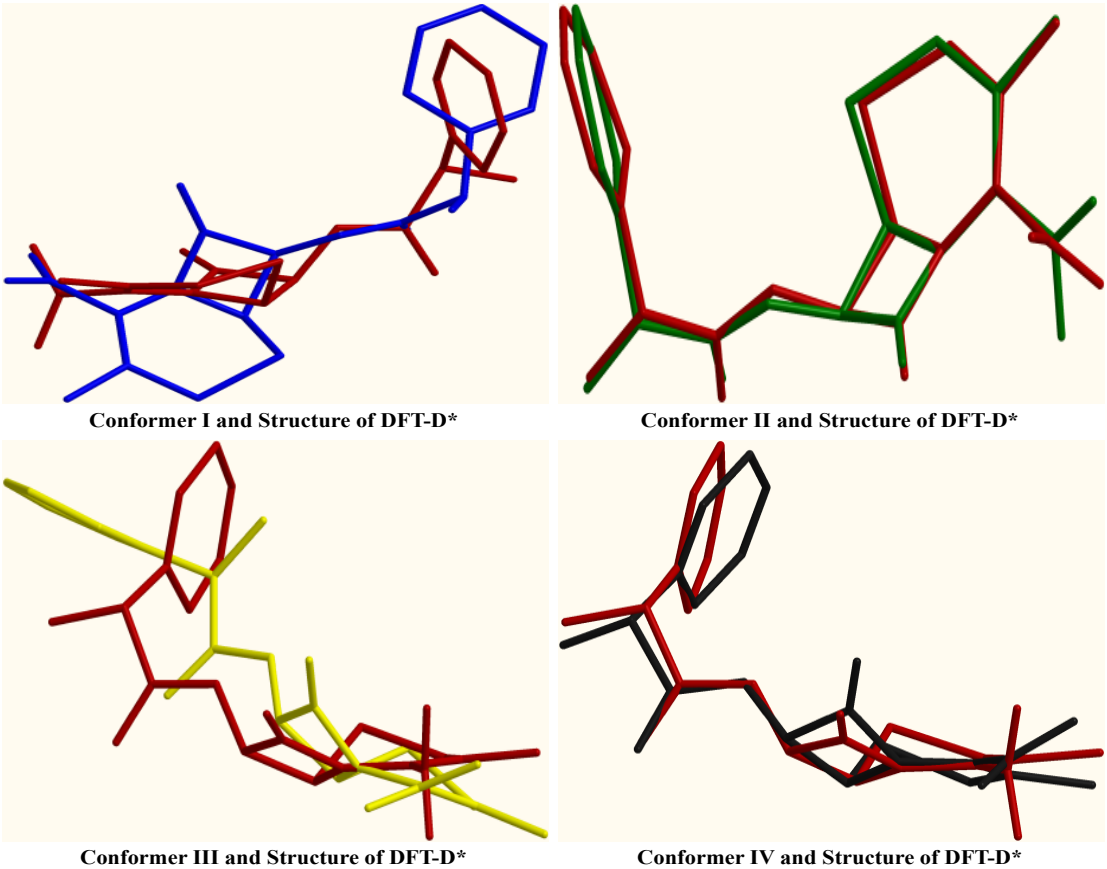

Figure 22: Superimposition of conformers (I-IV) with structure of Ref. DFT-D* (blue: conformer I, green: conformer II, yellow: conformer III, black: conformer IV and red: structure of Ref. DFT-D*) (Van de Streek et al., 2013).

The energy of conformer II is slightly more than the energy of conformer I (~ 0.0020 kcal/-mol). Moreover, the experimental IR and the Raman spectra are closer to the calculated spectra of conformer II. So the further calculation has been conducted for conformer II (M. K. Chaudhary, Karthick, et al., 2021).

The optimized parameters like bond distance, bond angle and torsional angle of all the conformers (I-IV) of cefradine from the B3LYP/6-311++G(d,p) level of calculation are presented in Table 32 (Appendix C). The comparison of bond length between the conformers (I-IV) with the structure of the literature (Van de Streek et al., 2013) signifies that the difference 0.018 Å for the bond N8-C16 in conformers II and IV in comparison to conformers I and III. This change in bond distance is due to the establishment of intramolecular hydrogen bond H27. . . N8. But the bond length of N8-C16 in conformers II and IV appears to be shorter (~ 1.459 Å). The optimized geometry of conformers (I-IV) has been compared with the structure proposed by Van de Streek et al. (2013) which demonstrates that a considerable change in bond distance across C-C, C-O, C-N, C-S, N-H, C-H groups were not determined. The prominent difference is observed to be 0.083 Å across O4-C18 bond in all the conformers and this difference is due to the formation of intramolecular hydrogen bond O4. . . H31. While comparing the bond angle, the major difference was observed to be 7.89°, 9.83°, 7.92° and 7.88° in conformers I, II, III and IV respectively for O5-C18-C12. This is due to the formation of intramolecular hydrogen bonding across O5. . . H33. Another significant difference in angle was seen as 5.86°, 3.27°, 5.56° and 3.93° for C15-N7-H27 in conformers I, II, III and IV respectively. This is due to the formation of intramolecular hydrogen bonding across H27. . . N8 which is explained in Section 4.3.4. Another prominent difference of 6.50° was identified in conformer I across N8-C16-H30 (M. K. Chaudhary, Karthick, et al., 2021).

4.3.4 Atoms in molecule analysis

The QTAIM is used to study the structural changes across the conformers which is based on ρ_{BCP} and $\nabla^2\rho_{BCP}$ at the BCP. This is analyzed in terms of intramolecular hydrogen bonding interactions. The QTAIM topology of all the conformers (I-IV) of cefradine was generated using the AIM 2000 program which is presented in Figure 23. The geometrical and the topological parameters for the intramolecular interactions of conformers (I-IV) of cefradine are presented in Tables 12 and 13.

For the existence of hydrogen bond, Koch & Popelier (1995) suggested that the electron density (ρ) between the proton (H) and the acceptor (A) lie in the range (0.002 to 0.040) a.u and the Laplacian ($\nabla^2\rho_{BCP}$) of the electron density should be in the range (0.024 to 0.139) a.u. Thus, the formation of intramolecular hydrogen bonding H31. . . O4 in conformers I, III and IV; for the hydrogen boding H27. . . N8 in conformers I and III

and for the hydrogen boding H33...O5 in conformer II follow the geometrical criteria suggested by Koch and Popilier. Furthermore, the nature and the strength of hydrogen bond has been scrutinized by Rozas et al. (2000) in terms of $\nabla^2\rho_{BCP}$ and H_{BCP}. For weak hydrogen bond, the condition should be $\nabla^2\rho_{BCP} > 0$ and $H_{BCP} > 0$. For partially covalent in nature, the criteria should be $\nabla^2\rho_{BCP} > 0$ and $H_{BCP} < 0$. For strong and covalent nature, the criteria should be $\nabla^2\rho_{BCP} < 0$ and $H_{BCP} < 0$. So, the interaction H35...S1 in conformers II and IV; the interaction H31...O4 in conformers I, III and IV; the interaction H27...N8 in conformers I and III and the interaction H33...O5 in conformer II follow the criteria $\nabla^2\rho_{BCP} > 0$ and $H_{BCP} < 0$. So there is formation of partial covalent bond. The Bader's theory is used to estimate the hydrogen bond energy (E). Espinosa et al. (1998) proposed a relation between E and V_{BCP} at H...O contact: $E = V_{BCP}/2$. The estimated interaction energy at BCP shows that the interaction H31...O4 in conformers I, III and IV and H33...O5 in conformer II; the interaction H31...O4 is the strongest interaction. Furthermore, the highest value of the interaction energy and the least bond length of H27...N8 in conformer III signify the strongest interaction (M. K. Chaudhary, Karthick, et al., 2021).

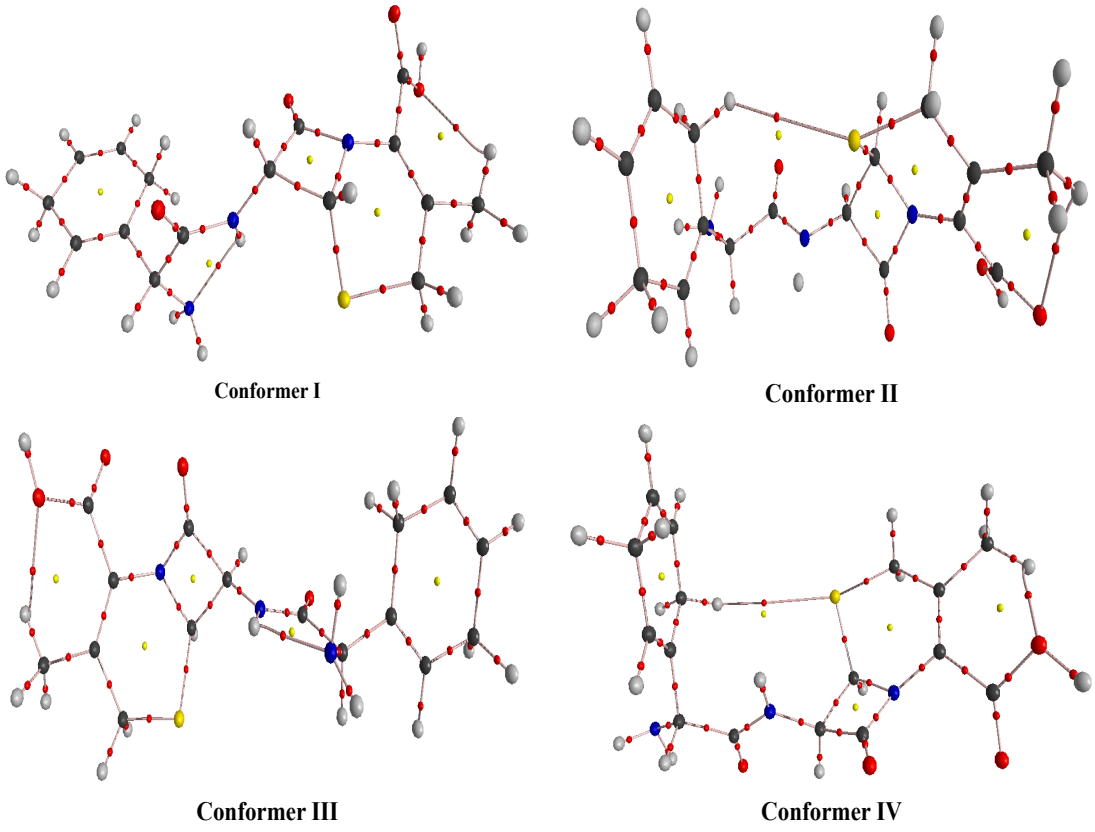

Figure 23: The graphical presentation of atoms in molecules of cefradine for conformers (I-IV) at bond critical points (small red spheres), ring critical points (small yellow sphere) and bond paths (pink lines).

Table 12: Topological parameters for intramolecular interaction in conformers (I-IV) of cefradine: ρ_{BCP}, $\nabla^2\rho_{BCP}$, G_{BCP}, V_{BCP}, H_{BCP} at the BCP and estimated E_{int}.

Interactions	Bond length (Å)	ρ_{BCP} (a.u.)	$\nabla^2\rho_{BCP}$ (a.u.)	G_{BCP} (a.u.)	V_{BCP} (a.u.)	H_{BCP} (a.u.)	E_{int} (kcal/mol)
Conformer I							
H31...O4	2.3326	0.0143	0.0529	−0.0019	−0.0094	−0.0113	–2.9442
H27...N8	2.1652	0.0218	0.0845	−0.0029	−0.0153	−0.0182	–4.7949
Conformer II							
H33...O5	2.2908	0.0154	0.0564	−0.0021	−0.0099	−0.0120	–3.1142
H35...S1	3.7090	0.0014	0.0050	−0.0004	−0.0005	−0.0009	–0.1655
Conformer III							
H31...O4	1.0861	0.0143	0.0529	−0.0019	−0.0094	−0.0113	–2.9446
H27...N8	1.0140	0.0228	0.0874	−0.0029	−0.0161	−0.0189	–5.0368
Conformer IV							
H35...S1	3.4829	0.0021	0.0074	−0.0005	−0.0009	−0.0014	–0.2342
H31...O4	2.3305	0.0144	0.0534	−0.0019	−0.0095	−0.0114	–2.4945

Table 13: Physical parameters: bond angle (°), the sum of van der Waal radii of interacting atoms (r_H + r_A) in Å, and bond distance (Å) of cefradine for conformers (I-IV).

D-H...A	D-H (Å)	H...A (Å)	D-H...A (Å)	(r_H + r_A)) (Å)
Conformer I				
C17-H31...O4	1.0861	2.3326	113.3850	2.72
N7-H27...N8	1.0140	2.1652	108.9447	2.75
Conformer II				
C17-H33...O5	1.0861	2.2908	116.6291	2.72
C20-H35...S1	1.0999	3.7090	130.4821	3.00
Conformer III				
C17-H31...O4	1.0861	2.3329	113.3072	2.72
N7-H27...N8	1.0140	2.1432	109.8265	2.75
Conformer IV				
C20-H35...S1	1.1000	3.4829	140.4263	3.00
C17-H31...O4	1.0860	2.3305	112.9911	2.72

4.3.5 Experimental details for vibrational spectra

The solid form cefradine with whiteness degree more than 98% was procured from the Antibiotics do Brazil Ltd (ABL), Brazil. The purity level of compound is at analytical standard so without making any further cleaning, the signature (Infrared and Raman) was listed. The FT-IR spectrum of cefradine at room temperature was reported with Bruker Vertex 70 FT-IR spectrometer. For the spectral measurement, the pellet was formed by mixing the cefradine compound with KBr in the ratio 1 : 200 which reduces the signal to noise ratio and the spectrum was measured in the range of 400 cm^{-1} to 4000 cm^{-1} with a resolution of 4 cm^{-1}. The signature of Raman spectrum of the cefradine compound was documented in the range 100 cm^{-1} to 3500 cm^{-1} with the help of RAM II module from diode-pumped Nd: YAG laser. The laser source is able to emit a radiation of wavelength

1064 nm at low power (100 mW).

4.3.6 Vibrational spectra

The molecule containing N atoms exhibit $(3N - 6)$ modes of vibration. The cefradine molecule has 43 atoms so there are 123 normal modes of vibrations and all the modes of vibration are both IR and Raman active (M. K. Chaudhary, Karthick, et al., 2021). The assignments of normal modes of vibration along with their PEDs, which is determined from Gar2Ped (J. M. L. Martin & Van Alsenoy, 1995) software with the help of Pulay's recommendation (Pulay et al., 1979) are depicted in Table 33 (Appendix D). The simulated IR and Raman spectra of the conformers (I-IV) of cefradine have been compared with the empirical listed spectra shown in Figures 24 and 25.

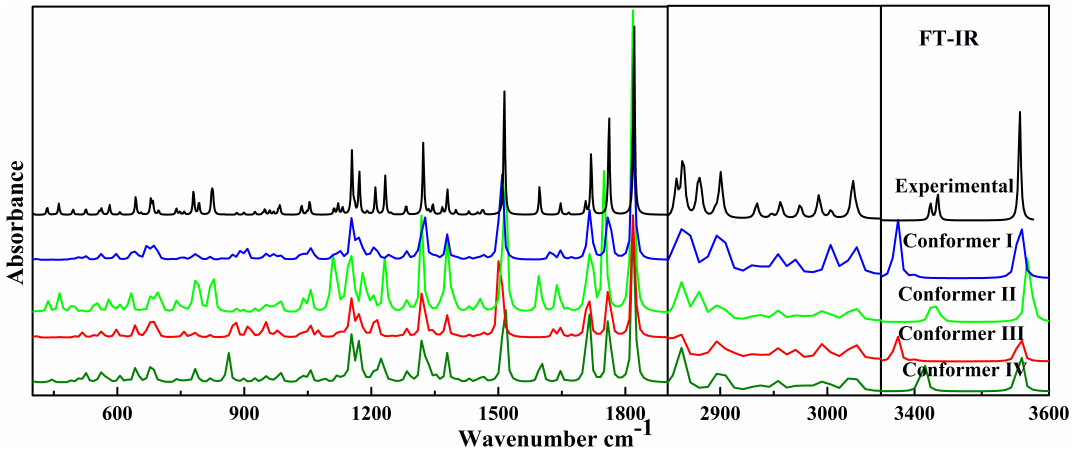

Figure 24: Experimental and simulated infrared spectra of cefradine in the region (400 to 1900) cm^{-1}, (2850 to 3050) cm^{-1} and (3350 to 3600) cm^{-1}.

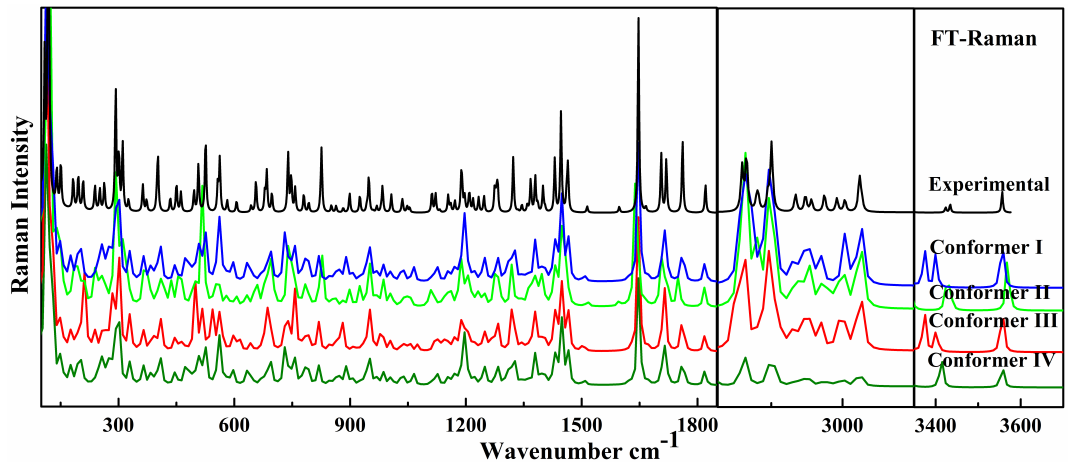

Figure 25: Experimental and simulated Raman spectra of cefradine in the region (100 to 1850) cm^{-1}, (2825 to 3100) cm^{-1} and (3350 to 3650) cm^{-1}.

The quantum chemical calculation gives the Raman amplitude but not the Raman intensity. So the Raman intensity for each mode of vibration is determined from the Raman

scattering cross-section $\partial\sigma_j/\partial\Omega$ (Polavarapu, 1990; Guirgis et al., 2003) and is given by Equation (3.68).

4.3.6.1 Scaling of vibrational wave numbers

The overestimated harmonic frequencies are obtained in the simulated spectra which are due to the anharmonicity present in the real system. The overestimated values of frequencies were lowered down by WLS procedure given by $\nu_{obs}/\nu_{cal} = (1.0087 - 0.0000163 \times \nu_{cal})$ cm^{-1} (Andersson & Uvdal, 2005) and the comparison has been done with the observed spectra (IR and Raman). The experimental and scaled calculated spectra show a good resonance with each other. Here, we have discussed only the scaled simulated spectra. The comparative graph of scaled simulated and experimental spectra is presented in Figures 24 and 25. The simulated spectra of the conformers (I-IV) are in good agreement with the experimental one, however, the signature of the conformer II shown is in good resemblance with the empirical data. This similarity is due to the superposition of the conformer II with the structure of Van de Streek et al. (2013).

The unscaled wavenumber, the scaled wavenumber and the observed wavenumber along with the potential energy distribution of each mode of vibration is depicted in Table 33 (Appendix D). The contribution of PED is taken only those contributions which exhibits equal to or greater than 5% contribution for normal mode of vibration. In this vibration, we have used the following symbols for different types of vibration: ν(stretching), ν_a(asymmetric stretching), ν_s(symmetric stretching), δ(deformation and bending), oop(out of plane bending), ω(wagging), γ(twisting), ρ(rocking) and τ(torsion).

4.3.6.2 O-H Vibrations

The free O-H stretching vibration is found in the range (3640 to 3610) cm^{-1} but the hydrogen bounded O-H stretching vibration is found in the range (3500 to 3200) cm^{-1} (Colthup et al., 1990). There is a single O-H group present in the cefradine. The free O-H stretching vibration is calculated at 3570 cm^{-1} with 100% contribution but experimentally it was recorded at 3557 cm^{-1} in both the IR and the Raman spectra. The bending of O-H group in cefradine was calculated with 24% contribution at 1149 cm^{-1} and experimentally it was recorded at 1154 cm^{-1} in the IR spectrum and 1155 cm^{-1} in the Raman spectrum. The torsion bending of O-H group was calculated at 631 cm^{-1} and it was seen at 643 cm^{-1} in IR spectrum and 642 cm^{-1}in Raman spectrum (M. K. Chaudhary, Karthick, et al., 2021).

4.3.6.3 N-H Vibrations

The asymmetric stretching of $N8H_2$ with 100% contribution was measured at 3434 cm^{-1} whereas it was seen in experimental data at 3435 cm^{-1} in the IR graph and 3433 cm^{-1} in the Raman graph. The simulated and experimental spectra are in good agreement with each other. The stretching of N7H in the simulated spectra with 99% contribution was measured at 3424 cm^{-1}. The scissoring bending of $N8H_2$ was calculated at 1597 cm^{-1} with 95% contribution and experimentally it was seen at same wave number in both the IR and the Raman spectra. This signifies that the experimental and simulated spectra are coinciding with each other. The rocking vibration of $N8H_2$ was calculated at 1116 cm^{-1} with 20% contribution and experimentally it was recorded 1113 cm^{-1} in both the IR and the Raman spectrum. The wagging vibration of $N8H_2$ in the cefradine molecule was calculated at 899 cm^{-1} with 11% contribution which exactly match with the experimental data in the IR spectra and the Raman spectra. Furthermore, an another wagging vibration was measured at 863 cm^{-1} and it was recorded in the experimental data at 881 cm^{-1} in the IR spectrum and 883 cm^{-1} in the Raman spectrum respectively (M. K. Chaudhary, Karthick, et al., 2021).

4.3.6.4 C-H Vibrations

The C-H stretching vibration is generally found in the higher wavenumber region in the range of (3000 to 3100) cm^{-1} (Varsányi et al., 1973). The asymmetric C-H stretching of $C17H_3$ is calculated at 3026 cm^{-1} with 100% contribution and the corresponding value in the experimental data was recorded at 3024 cm^{-1} in both the IR and the Raman spectra. The symmetric C-H stretching corresponding to R3[ν_s(CH)] with 99% contribution was calculated in simulated spectra. The asymmetric stretching of R3[ν_a(CH)] was calculated at 3003 cm^{-1} with 99% contribution and its corresponding value in the experimental data was recorded at same wavenumber in both the IR and the Raman spectra. The C-H stretching vibration corresponding to R2[ν(C10H)] was calculated with 94% contribution in simulated spectra at 2974 cm^{-1} and its corresponding value in the experimental IR and Raman spectra was in good resemblance at the same wave number. Another C-H stretching of R1[ν(C9H)] was found in the calculated spectra at 2955 cm^{-1} with 93% contribution and the corresponding value in the experimental IR and Raman spectra was at the same wavenumber which is in good resonance with each other. The out of plane bending of CH_2 group was calculated at 1429 cm^{-1} and its corresponding value was observed at 1430 cm^{-1} in both the IR and the Raman spectra. The symmetric deformation of $C17H_3$ was found in the calculated spectra at 1397 cm^{-1} and its corresponding wavenumbers were seen experimentally at 1399 cm^{-1} in the IR spectrum and at 1400 cm^{-1} in the Raman spectrum (M. K. Chaudhary, Karthick, et al., 2021).

4.3.6.5 C=O and C=C Vibrations

The stretching vibration of the carbonyl group (C=O) is found in the region (1670 to 1820) cm^{-1} (Silverstein et al., 1981; J. Mohan, 2004). In cefradine molecule, there are three clear peaks recorded in the experimental IR and Raman spectra at 1821 cm^{-1}, 1762 cm^{-1} and 1719 cm^{-1} and their corresponding values in the simulated spectra were found at 1818 cm^{-1}, 1751 cm^{-1} and 1719 cm^{-1} with respective contribution 81%, 78% and 61%. These values correspond to stretching vibration of the carbonyl group C11=O2, C18=O5 and C15=O3 respectively. The wavenumber of stretching vibration of C18=O5 is reduced by 11 cm^{-1}. Moreover, the calculated bond distance of C18=O5 is enlarged by 0.067 Å than the bond length of the Van de Streek structure (Van de Streek et al., 2013). Furthermore, the high value of the Fukui functions (f_k^-) of O5 signifies that there is a formation of intermolecular hydrogen bonding with the neighboring molecule in compact solid form. However, our research is confined for individual molecule in gaseous state (M. K. Chaudhary, Karthick, et al., 2021). The C=C stretching of the ring R3 was found in simulated spectra at 1706 cm^{-1} with 60% contribution and the corresponding value in experimental data is recorded at 1706 cm^{-1} in both the IR and the Raman spectra. Another C=C stretching vibration of the ring R1 is calculated at 1641 cm^{-1} with 71% contribution and the corresponding value is determined at 1647 cm^{-1} in both the IR and the Raman spectra.

4.3.7 Natural bond orbital analysis

NBO is used to discuss the interactions between the bonding/electron lone pair orbital and the antibonding/electron-deficient orbitals. The NBO interactions have been analyzed on the basis of second-order perturbation theory analysis between the bonding/donor and the antibonding/acceptor orbitals. The stabilization energies $E^{(2)}$ (Reed et al., 1988; Glendening et al., 2012) is the major index to study the NBO interaction of the species molecule for their stability and it's value can be determined from Equation (3.67). The second-order perturbation energies $E^{(2)}$ of major donor-acceptor orbital of the conformer II of cefradine has been reported in Table 14. The stability of the molecule has been observed for the delocalization of electrons from σ orbital to σ^* virtual orbital. The interaction energies for the delocalization of $\sigma \rightarrow \sigma^*$ orbitals σ(N6-C9)$\rightarrow$ σ^*(O2-C11)/σ^*(O2-C11), σ(C9-C10)$\rightarrow$ σ^*(N6-C12), σ(C10-C11)$\rightarrow$ σ^*(N6-C12), σ(C23-H41)$\rightarrow$ σ^*(C22-C24), σ(C24-H42)$\rightarrow$ σ^*(C20-C23) which stabilizes the molecular system with respective interaction energies 6.22 kcal/mol, 6.38 kcal/mol, 6.17 kcal/mol, 7.21 kcal/mol, 5.91 kcal/mol and 6.02 kcal/mol. Similarly, the delocalization of electrons between $\pi \rightarrow \pi^*$ orbital is π(C12-C14)$\rightarrow$ π^*(O5-C18) which stabilizes the system with interaction energy 12.73 kcal/mol. The major lone pair to the antibonding interactions (LP$\rightarrow$ σ^*/π^*) such as

LP(2)O2 → σ^*(N6-C11) [$E^{(2)}$ = 30.52 kcal/mol]

LP(2)O2 → σ^*(C10-C11) [$E^{(2)}$ = 24.10 kcal/mol]

LP(2)O3 → σ^*(N7-C15) [$E^{(2)}$ = 25.05 kcal/mol]

LP(2)O3 → σ^*(C15-C16) [$E^{(2)}$ = 20.15 kcal/mol]

LP(2)O5 → σ^*(O4-C18) [$E^{(2)}$ = 33.28 kcal/mol]

LP(2)O5 → σ^*(C12-C18) [$E^{(2)}$ = 61.87 kcal/mol]

play a vital role for the stability of the molecule and they stabilize the molecule. The corresponding stabilization energies are indicated by $E^{(2)}$. The crucial physical phenomenon which gives the apex value of $E^{(2)}$ is LP(1)N7→ π^*(O3-C15) with stabilization energy of about 61.87 kcal/mol (M. K. Chaudhary, Karthick, et al., 2021).

Table 14: Second-order perturbation theory analysis of the Fock matrix in the NBO basis of cefradine (conformer II).

Donor NBO(i)	ED(i)/e	Acceptor NBO (j)	ED(j)/e	$E^{(2)a}$ kcal/mol	E(j) - $E(i)^b$ a.u.	$F(i,j)^c$ a.u.
σ(N6-C9)	1.9772	σ*(O2-C11)	0.0182	6.22	1.38	0.083
σ(C9-C10)	1.9635	σ*(O2-C11)	0.0182	6.38	1.25	0.080
σ(C9-C10)	1.9635	σ*(N6-C12)	0.0441	6.17	1.01	0.071
σ(C10-C11)	1.9648	σ*(N6-C12)	0.0441	7.21	1.01	0.076
π(C12-C14)	1.8819	π*(O5-C18)	0.2250	12.73	0.31	0.057
σ(C17-H32)	1.9721	π*(C12-C14)	0.1608	5.34	0.55	0.050
σ(C23-H41)	1.9764	σ*(C22-C24)	0.0179	5.91	0.94	0.067
σ(C24-H42)	1.9767	σ*(C20-C23)	0.0172	6.02	0.94	0.067
LP(2)O2	1.8169	σ*(N6-C11)	0.1031	30.52	0.66	0.129
LP(2)O2	1.8169	σ*(C10-C11)	0.0953	24.10	0.59	0.109
LP(2)O3	1.8584	σ*(N7-C15)	0.0785	25.05	0.71	0.121
LP(2)O3	1.8584	σ*(C15-C16)	0.0809	20.15	0.61	0.100
LP(1)O4	1.9773	σ*(O5-C18)	0.0208	6.49	1.24	0.080
LP(2)O4	1.8244	π*(O5-C18)	0.2250	40.81	0.36	0.110
LP(2)O5	1.8403	σ*(O4-C18)	0.0995	33.28	0.60	0.129
LP(2)O5	1.8403	σ*(C12-C18)	0.0746	18.93	0.66	0.102
LP(1)N6	1.6578	π*(O2-C11)	0.2343	45.23	0.30	0.107
LP(1)N6	1.6578	π*(C12-C14)	0.1608	18.86	0.32	0.072
LP(1)N7	1.6948	π*(O3-C15)	0.2741	61.87	0.28	0.119
LP(1)N7	1.6948	σ*(C9-C10)	0.0425	9.92	0.56	0.072
LP(1)N8	1.9484	σ*(C16-H30)	0.0299	5.97	0.73	0.059

[a] $E^{(2)}$ means the energy of hyper conjugative interaction (stabilization energy).

[b] Energy difference between donor (i) and acceptor (j) NBOs.

[c] $F(i,j)$ is the Fock matrix element between i and j NBOs.

4.3.8 Frontier molecular orbital energy gap

The prominent orbitals involved in the chemical activity in the molecular system are the HOMO and the LUMO (T. Chaudhary, Chaudhary, & Joshi, 2021). The HOMO orbital donates the electrons whereas the LUMO orbital accept the electrons. The transfer of electrons from HOMO to LUMO orbitals produces molecular stability. The reactivity of the molecular system is determined in terms of the energies of HOMO (E_{H}) and LUMO (E_{L}) orbitals and their energy difference ($\Delta E_{\mathrm{L\text{-}H}}$) (also known as frontier molecular orbital energy gap) (Raafat et al., 2008).

The molecule is much stable or fewer chemical reactive for higher value of $\Delta E_{\mathrm{L\text{-}H}}$ and vice-versa (Fukui, 1982). The TD-DFT calculations for all the conformers (I-IV) were carried out at B3LYP/6-311++G(d,p) to scrutinized the electronic transitions of cefradine. The HOMO and LUMO plots of the conformers (I-IV) of cefradine are depicted in Figure 26. The respective vales of $\Delta E_{\mathrm{L\text{-}H}}$ for conformers (I-IV) are calculated as 4.7454 eV, 4.6978 eV, 4.7731 eV and 4.7661 eV. This calculation signifies that the conformer III is more stable or less reactive than the others. Moreover, the conformer II is less stable or more chemically reactive whose IR and Raman spectra match well with the experimental spectra as explained in Section 4.3.6.1. From the HOMO surface maps, it was noticeable that the orbital lobes are concentrated in the ring R3, C15=O3 and N7 whereas in the LUMO surface maps, the orbital lobes were scattered over the ring R1, R2, carbonyl group (C18=O5), hydroxyl group and $C17H_3$ regions in all the conformers of cefradine (M. K. Chaudhary, Karthick, et al., 2021).

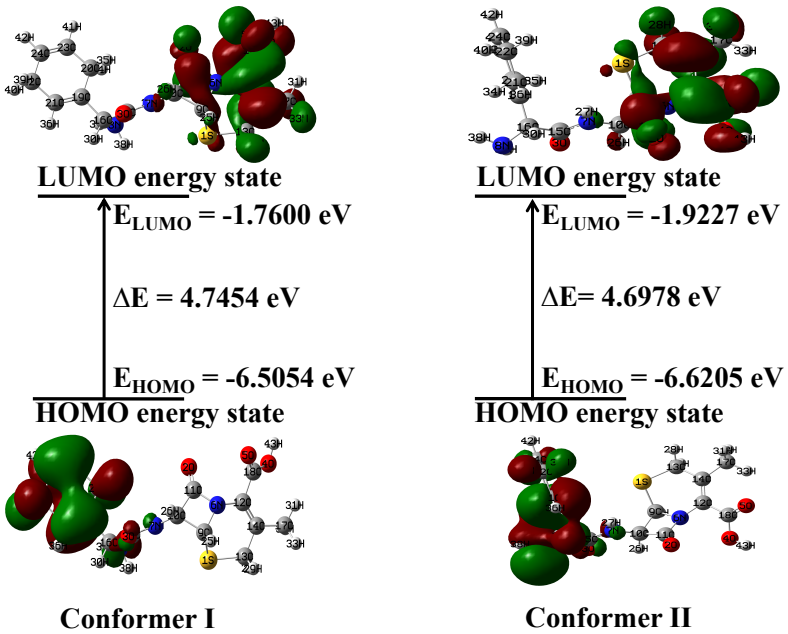

Figure 26: Frontier molecular orbital plot of cefradine for conformers (I-II).

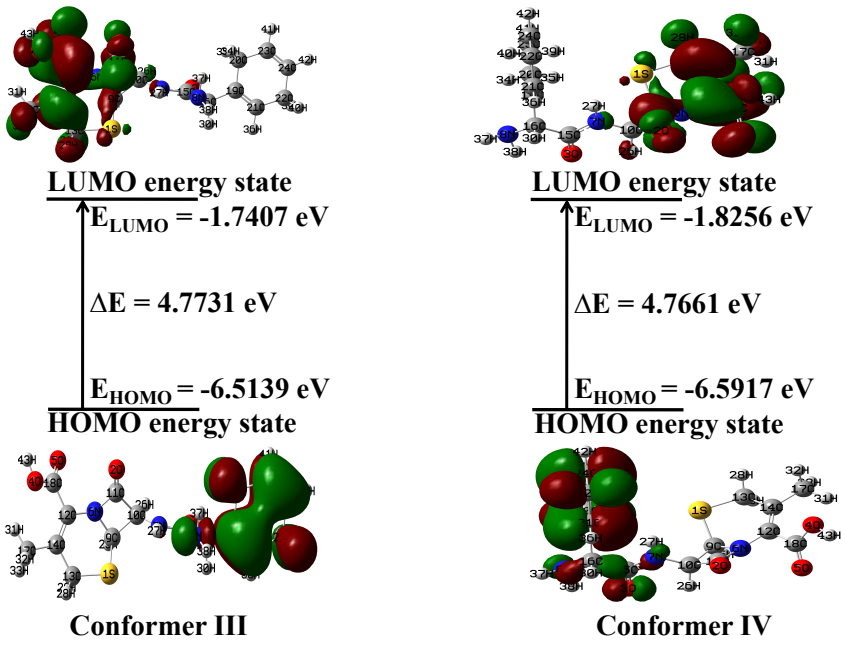

Figure 26: (cont.) Frontier molecular orbital plot of cefradine for conformers (III-IV).

4.3.9 Molecular electrostatic potential

The distribution of charge in space around the molecule is predicted from fitting point charges to the electrostatic potentials (Murray et al., 1992). The various color coding on the MEP surface as shown in Figure 27 indicates the sites feasible for the electrophilic and the nucleophilic attack (Brinck et al., 1993).

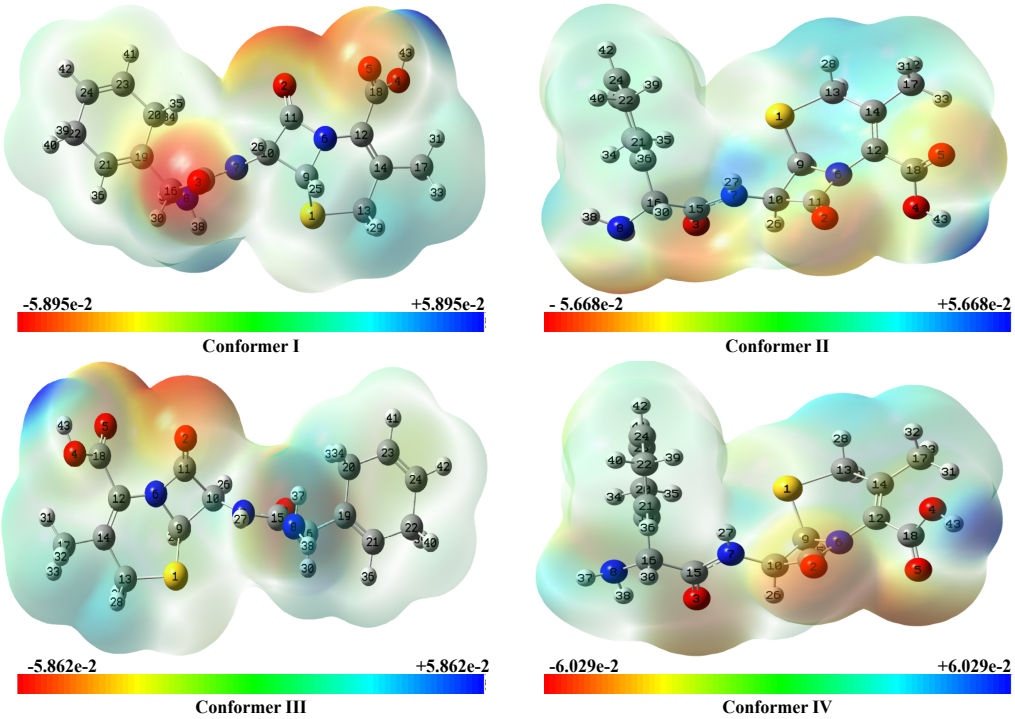

Figure 27: MEP of cefradine for conformers (I-IV) generated by mapping of total density over the electrostatic potential.

In the MEP surface map, the red region represents high electron density and the blue region represents low electron density. The potential in the MEP map increases in the order red < yellow < green < blue. The molecular electrostatic potential $V(r)$ generated in the molecular system which is due to the total effect of the negative and the positive charges corresponding to electrons and nuclei is given by the Equation (3.66). The MEP surface map of cefradine was calculated by using the DFT at the B3LYP/6-311++G(d,p) level. The red color regions around O2, O3 and O5 atoms in all the four conformers of cefradine are the electrophilic region whereas the blue color region across H43 shows less electron density and is a nucleophilic region (M. K. Chaudhary, Karthick, et al., 2021).

4.3.10 Global reactivity descriptors

The major global reactivity descriptors based on the frontier molecular orbital energies E_{L} and E_{H} and their energies difference $\Delta E_{\mathrm{L\text{-}H}}$ is justified by Koopman's theorem (Parr & Pearson, 1983; Parr et al., 1999). The global reactivity descriptors are electronegativity (χ), chemical potential (μ), global hardness (η), global softness (S) and electrophilicity index (ω). Their values can be calculated from the Equations (3.51)–(3.55). The electrophilicity index (ω) measures the stabilization energy when the molecular system acquires more electronic charge from the surrounding species (Parr et al., 1999). The capacity to acquire the additional electronic charge (ΔN) and the resistance of the system to exchange electronic charge with the surrounding is calculated in terms of the electrophilicity index (ω). Moreover, the electron transfer or the chemical potential as well as the molecular stability/hardness of the system are determined from the electrophilicity index. The values of energies E_{L}, E_{H}, energy gap ($\Delta E_{\mathrm{L\text{-}H}}$), χ, μ, η, S and ω for the conformers (I-IV) of cefradine are depicted in Table 15. The chemical stability of a molecular system is scrutinized with the help of global hardness (η) and softness (S). The higher value of energy gap ($\Delta E_{\mathrm{L\text{-}H}}$) stands for harder molecule whereas the smaller value of energy gap ($\Delta E_{\mathrm{L\text{-}H}}$) signifies a softer molecule. The harder molecule is sustainable or less reactive but the softer molecule is more polarizable and reactive. The least value of $\Delta E_{\mathrm{L\text{-}H}} \sim 4.6978$ eV for the conformer II indicates that it is more reactive with the highest electrophilicity index $\omega = 3.8841$ eV which can gain more extra charge $\Delta N = 1.8186$ from the surrounding species than the conformer I, III and IV of cefradine. The highest value of energy gap $\Delta E_{\mathrm{L\text{-}H}} \sim 4.7731$ eV and the least value of electrophilicity index $\omega = 3.5689$ eV for conformer III indicate that it is more stable than the other conformers. Thus conformer II is more sensitive in comparison to conformers I, III and IV but conformer III is harder in comparison to conformers I, II and IV of cefradine (M. K. Chaudhary, Karthick, et al., 2021).

Table 15: Calculated E_{HOMO}, E_{LUMO}, $\Delta E_{\mathrm{L\text{-}H}}$, μ, χ, η, S and ω in the conformers (I-IV) of cefradine.

Molecule	E_{H}	E_{L}	$\Delta E_{\mathrm{L\text{-}H}}$	χ	μ	η	S	ω	$\Delta N_{\max}$
Conformer I	−6.5054	−1.7600	4.7454	4.1327	−4.1327	2.3727	0.2107	3.5991	1.7418
Conformer II	−6.6205	−1.9227	4.6978	4.2716	−4.2716	2.3489	0.2129	3.8841	1.8186
Conformer III	−6.5139	−1.7407	4.7731	4.1273	−4.1273	2.3866	0.2095	3.5689	1.7294
Conformer IV	−6.5917	−1.8256	4.7661	4.2087	−4.2087	2.3831	0.2098	3.7164	1.7661

4.3.11 Local reactivity descriptors

It is used to describe the chemically reactive site in the molecular system. The more chemically reactive (electrophilic and nucleophilic) site in the molecular system is determined in terms of Fukui function $f(r)$. The higher value of FF (f_k^+, f_k^-, f_k^0) prone to the electrophilic and the nucleophilic center in the molecule (Parr & Yang, 1984; K. Srivastava et al., 2016). The value of Fukui functions were calculated for the cations, the anions and the radicals attack from the Equations (3.63)–(3.65). Besides that, the local softness (s_k^+, s_k^-, s_k^0) and the local electrophilicity indices (ω_k^+, ω_k^-, ω_k^0) are also used to explore the reactivity of atoms in the species and are given by relations:

$$
\begin{aligned}
s_k^+ &= S f_k^+, \quad & \omega_k^+ &= \omega f_k^+ \\
s_k^- &= S f_k^-, \quad & \omega_k^- &= \omega f_k^- \\
s_k^0 &= S f_k^0, \quad & \omega_k^0 &= \omega f_k^0
\end{aligned}
$$

where +, − and 0 sign stands for nucleophilic, electrophilic and radical attack respectively. The extremum value of (f_k^+, ω_k^+, s_k^+) and (f_k^-, ω_k^-, s_k^-) infer the most nucleophilic and electrophilic sites in the molecule respectively. The Fukui functions (f_k^+, f_k^-, f_k^0), the local softness (s_k^+, s_k^-, s_k^0) and the local electrophilicity indices ($\omega_k^+, \omega_k^-, \omega_k^0$) for selected atomic sites for the conformers (I-IV) of cefradine is tabulated in Table 16. The prominent sites for the nucleophilic attack are S1 and N8 but the favorable sites for the respective electrophilic and radical attack are C14 and C18 (M. K. Chaudhary, Karthick, et al., 2021). The pictorial view for the distribution of charge for the nucleophilic and the electrophilic attack in various atoms of cefradine are shown in Figures 28 and 29 respectively.

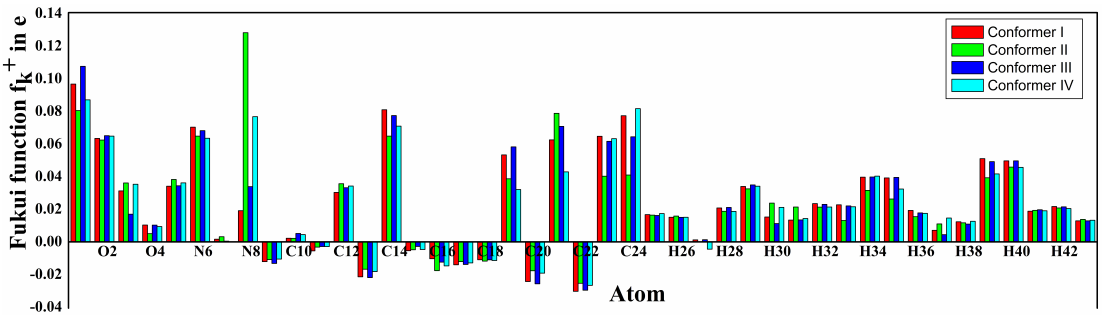

Figure 28: Charge distribution for nucleophilic attack on different atoms of cefradine.

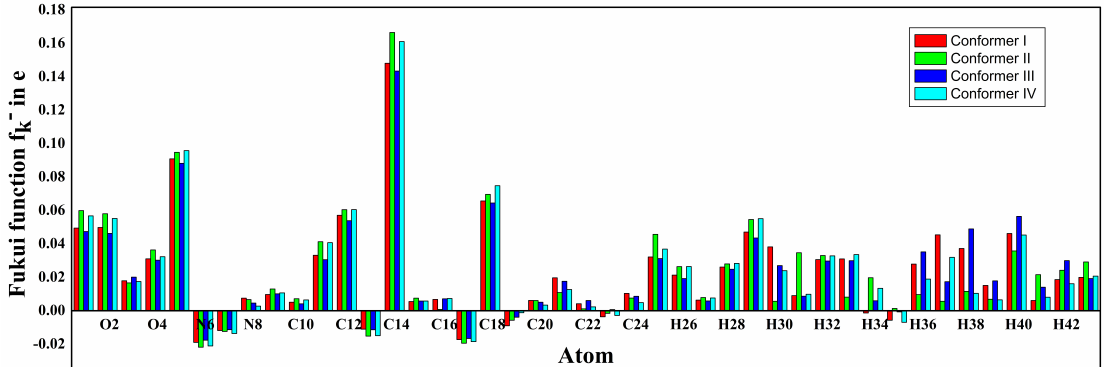

Figure 29: Charge distribution for electrophilic attack on different atoms of cefradine.

Table 16: Calculated local reactivity properties of the selected atoms of cefradine using Hirshfeld charges at B3LYP/6-311++G(d,p) level.

Site	f_k^+	s_k^+	ω_k^+	Site	f_k^-	s_k^-	ω_k^-	Site	f_k^0	s_k^0	ω_k^0
Conformer I											
S1	0.0968	0.0204	0.3483	C14	0.1481	0.0312	0.5330	C18	0.7452	0.1570	2.6821
C14	0.0811	0.0171	0.2917	O5	0.0909	0.0192	0.3273	C11	0.6931	0.1460	2.4944
C24	0.0774	0.0163	0.2785	C18	0.0657	0.0138	0.2365	C15	0.6856	0.1444	2.4674
N6	0.0704	0.0148	0.2534	C12	0.0572	0.0120	0.2058	H43	0.4836	0.1019	1.7404
C23	0.0648	0.0137	0.2332	O2	0.0498	0.0105	0.1793	H27	0.4278	0.0901	1.5397
O2	0.0635	0.0134	0.2285	S1	0.0495	0.0104	0.1782	H38	0.3499	0.0737	1.2593
C21	0.0626	0.0132	0.2253	H29	0.0471	0.0099	0.1696	H37	0.3488	0.0735	1.2554
C19	0.0534	0.0113	0.1922	H40	0.0463	0.0097	0.1665	H26	0.2533	0.0534	0.9116
Conformer II											
N8	0.1283	0.0273	0.4982	C14	0.1665	0.0354	0.6467	C18	0.745	0.1586	2.8935
S1	0.0805	0.0171	0.3128	O5	0.0948	0.0202	0.3684	C15	0.6968	0.1484	2.7065
C21	0.0789	0.0168	0.3063	C18	0.0697	0.0148	0.2707	C11	0.6893	0.1468	2.6773
C14	0.0649	0.0138	0.2521	C12	0.0605	0.0129	0.2349	H43	0.4802	0.1022	1.8650
N6	0.0649	0.0138	0.2521	S1	0.0600	0.0128	0.2329	H27	0.4041	0.086	1.5697
O2	0.0625	0.0133	0.2427	O2	0.0580	0.0124	0.2254	H37	0.3802	0.081	1.4769
H40	0.0459	0.0098	0.1784	H29	0.0546	0.0116	0.2122	H38	0.3556	0.0757	1.3810
C24	0.0411	0.0087	0.1595	H25	0.0458	0.0097	0.1777	H26	0.2499	0.0532	0.9706
Conformer III											
S1	0.1077	0.0226	0.3842	C14	0.1434	0.0301	0.5119	C18	0.7458	0.1563	2.6618
C14	0.0775	0.0162	0.2765	O5	0.0882	0.0185	0.3148	C11	0.6960	0.1458	2.4838
C21	0.0708	0.0148	0.2528	C18	0.0645	0.0135	0.2302	C15	0.6875	0.1440	2.4535
N6	0.0682	0.0143	0.2435	H40	0.0565	0.0118	0.2016	H43	0.4837	0.1013	1.7264
O2	0.0652	0.0136	0.2325	C12	0.0539	0.0113	0.1924	H27	0.4306	0.0902	1.5369
C24	0.0645	0.0135	0.2302	H38	0.0490	0.0103	0.1748	H37	0.3506	0.0735	1.2514
C23	0.0617	0.0129	0.2203	S1	0.0474	0.0099	0.1693	H38	0.3471	0.0727	1.2388
C19	0.0583	0.0122	0.2081	O2	0.0463	0.0097	0.1652	H26	0.2544	0.0533	0.9078
Conformer IV											
S1	0.0871	0.0183	0.3237	C14	0.1611	0.0338	0.5986	C18	0.7400	0.1552	2.7500
C24	0.0817	0.0171	0.3037	O5	0.0958	0.0201	0.3562	C15	0.6975	0.1463	2.5922
N8	0.0768	0.0161	0.2854	C18	0.0749	0.0157	0.2782	C11	0.6898	0.1447	2.5635
C14	0.071	0.0149	0.2639	C12	0.0606	0.0127	0.2251	H43	0.4837	0.1015	1.7975
O2	0.0649	0.0136	0.2412	S1	0.0568	0.0119	0.2111	H27	0.4127	0.0866	1.5337
N6	0.0636	0.0133	0.2363	O2	0.0553	0.0116	0.2053	H38	0.3834	0.0804	1.4248
C23	0.0634	0.0133	0.2354	H29	0.0551	0.0116	0.2049	H37	0.3467	0.0727	1.2886
H40	0.0457	0.0096	0.1700	H40	0.0453	0.0095	0.1684	H34	0.2538	0.0533	0.9433

4.3.12 Thermodynamic properties

The chemical reactivity of biologically active molecule increases with rise in temperature, so it plays a essential role in chemical reactivity of compound (Joshi et al., 2014). The values of $C^\circ_{p,m}$, S°_m and H°_m of conformer II of cefradine obtained from the output file in temperature range 50 K to 450 K is presented in Table 17 and their correlation with

temperature between 50 K to 450 K is shown in Figure 30. The important thermodynamic parameters: specific heat capacity ($C^{\circ}_{p,m}$), entropy (S°_{m}) and enthalpy (H°_{m}) along with total energy, zero point energy and rotational constant of all the conformers (I-IV) of cefradine were measured by using DFT, B3LYP/6-311++G(d,p) at room temperature 298.15 K and the values obtained is illustrated in Table 18. The mathematical equations for conformer II are as follows:

$$C^{\circ}_{m,p} = 10.83131 + 0.26842\,T - 4.06199 \times 10^{-5}\,T^2 \qquad (R^2 = 0.9998) \qquad (4.5)$$

$$S^{\circ}_{m} = 62.30036 + 0.415566\,T - 1.85668 \times 10^{-4}\,T^2 \qquad (R^2 = 0.9994) \qquad (4.6)$$

$$H^{\circ}_{m} = 213.33317 + 0.01272\,T + 1.24585 \times 10^{-4}\,T^2 \qquad (R^2 = 1.0000) \qquad (4.7)$$

These equations are effective for further studies of thermodynamic energies and forecast the direction of chemical reactions according to the second law of thermodynamics in thermo chemical field (Ott & Boerio-Goates, 2000; Zhang et al., 2010) of the cefradine. Figure 30 shows that the effect of temperature increases the thermodynamic parameters.

Table 17: The calculated values of enthalpy, specific heat and entropy at the B3LYP/6-311++G(d, p) level of conformer II of cefradine.

Temperature (K)	Enthalpy (kcal/mol)	Specific Heat (cal/mol-K)	Entropy (cal/mol-K)
50	214.290	24.085	80.936
100	215.847	37.753	103.353
150	218.044	50.047	121.805
200	220.852	62.360	138.428
250	224.287	75.054	154.171
300	228.360	87.870	169.338
350	233.068	100.343	184.145
400	238.382	112.089	198.586
450	244.261	122.893	212.656

Table 18: The calculated values of total energy, zero-point energy, enthalpy, specific heat capacity, entropy and rotational constants at 298.15 K at the B3LYP/6-311++G(d,p) level for conformers (I-IV) of cefradine.

Parameters	Conformer I	Conformer II	Conformer III	Conformer IV
Total energy (eV)	−40401.1011	−40401.1010	−40401.0997	−40401.0922
Zero point energy (J/mol)	893436.0	892232.6	893159.7	892764.7
Enthalpy (kcal/mol)	228.198	227.983	228.134	228.022
Specific heat (cal/mol-K)	87.399	87.930	87.428	87.619
Entropy (cal/mol-K)	168.796	169.100	168.923	167.438
Rotational constant (GHz)	0.48657	0.40634	0.59267	0.37637

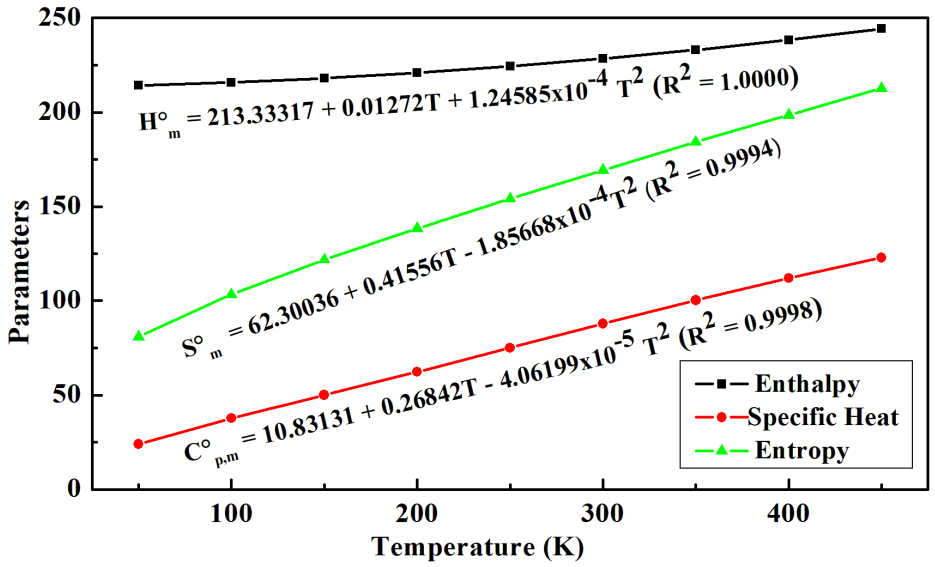

Figure 30: The variation of H°_{m}, $C^{\circ}_{p,m}$ and S°_{m} with temperature for conformer II of cefradine.

4.3.13 Non-linear optical properties

The attractive potential use of NLO material is in optical communication, optical sensing, data storage, computing and many more (Williams, 1984). The total static dipole moment (μ_0), the first hyperpolarizability (β_0), the mean polarizability ($\Delta\alpha_0$) and the anisotropy of polarizability $|\alpha_0|$ of the molecular system have been calculated by using DFT at B3LYP/6-311++G (d, p) level of theory and are given by the Equations (3.47)–(3.50) (Alyar et al., 2007). The considerable delocalization of charge in a specific direction is mentioned by the component of polarizability in that direction. The values of μ_0, $\Delta\alpha_0$, β_0 and $|\alpha_0|$ obtained from DFT calculation is presented in Table 19.

Table 19: The calculated μ_0, $|\alpha_0|$, $\Delta\alpha$ and β_0 of conformer II of cefradine at B3LYP/6-311++G (d,p).

Dipole moment (debye)		Polarizability ($\times10^{-24}$ e.s.u.)		Hyperpolarizability ($\times10^{-30}$ e.s.u.)	
μ_x	2.3805	α_{xx}	47.3759	β_{xxx}	1.3694
μ_y	−3.6631	α_{xy}	−1.1847	β_{xxy}	−0.2378
μ_z	−3.2730	α_{yy}	34.4283	β_{xyy}	0.5065
μ_0	5.4587	α_{xz}	−3.5574	β_{yyy}	−0.7900
μ_0(urea)	1.3732	α_{yz}	0.5480	β_{xxz}	0.0448
		α_{zz}	26.9264	β_{xyz}	0.2517
		$\|\alpha_0\|$	36.2435	β_{yyz}	−0.1720
		$\Delta\alpha$	84.1207	β_{xzz}	−0.3072
				β_{yzz}	−0.5970
				β_{zzz}	−1.0145
				β_0	2.5307
				β_0(urea)	0.3728

These values are more than the values of urea (Cassidy et al., 1979). Therefore, cefradine

shows the non-linear optical response and can be activated as a NLO substance.

4.3.14 Drug-likeness

The drug-likeliness properties of the molecule have been characterized theoretically rather than the spectroscopic characteristics. To be orally active drugs in humans, the range of MR should be in between 40 and 130. The MR value has been calculated in terms of polarizability from the Lorenz-Lorentz relation and is given by the Equation (4.1) (Verma & Hansch, 2005). Moreover, the drug-likeness of the molecule can be evaluated from Lipinski's five-rule (Lipinski et al., 1997). Lipinski's five-rule signifies that to be orally active drug in human, the number of atoms in the molecule should lie between 20 and 70 and the MW should be in the range (180 and 500) g/mol.

For the cefradine molecule, the number of atoms is 43, the MW is 349.40 g/mol and the respective calculated values of MR for the conformers (I-IV) is 57.8479 e.s.u, 57.9478 e.s.u, 53.9818 e.s.u and 56.2732 e.s.u (M. K. Chaudhary, Karthick, et al., 2021). Thus, it can be concluded that all the above-mentioned properties of the cefradine molecule lie within the range of orally accepted drugs.

4.3.15 Molecular docking

The active binding site as well as the ligand-protein interaction has been analyzed to explore the drug potential of the biologically active molecule from molecular docking approach (T. Chaudhary, Chaudhary, Joshi, de Santana, & Ayala, 2021). The curative behavior of cefradine has been investigated from molecular docking simulation by using AutoDock 4.2 software (G. Morris et al., 2009). For the cefradine molecule, three classes of target proteins have been predicted from the Swiss target prediction (Daina et al., 2019) and they are Dipeptidyl peptidase IV (DPP4), Protein farnesyltransferase (FTase) and Human Cyclooxygenase-2. The crystal structures of the predicted proteins were downloaded from the RCSB data bank (Rose et al., 2010). The pictorial view of possible interaction which contains all possible ligand - protein interactions has been presented in LIGPLOT in Figure 31. The parameters of the docked-complex from the large number of conformers which shows good binding behavior have been summarized in Table 20.

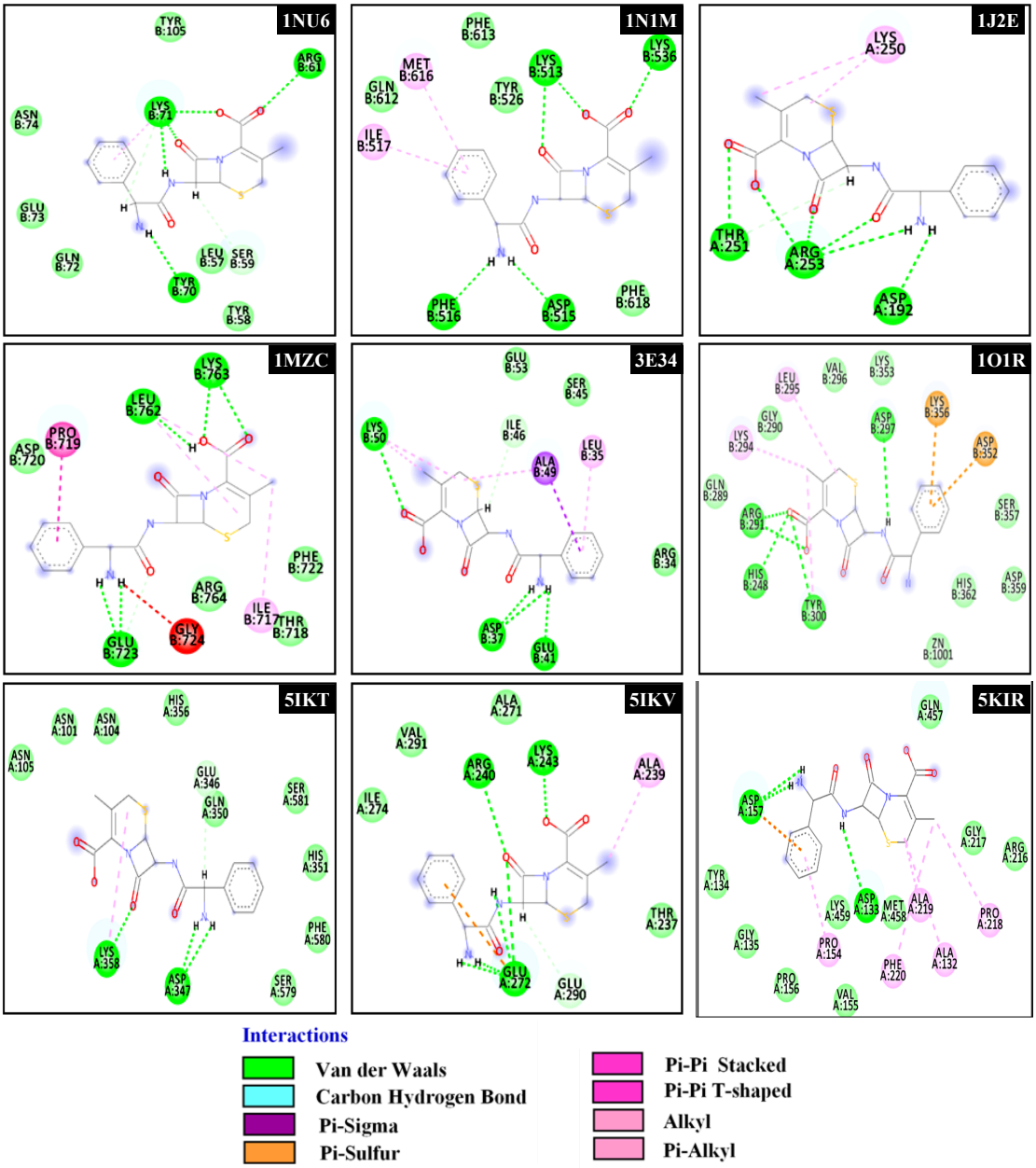

Figure 31: Molecular docking with predicted protein targets of cefradine.

4.3.15.1 Docked complex of cefradine and Dipeptidyl peptidase IV

The significant role of an enzyme DPP4 is to regulate the immune, to degrade the glucose metabolism of incretins (GLP-1) and also support for the development of some tumors (Wesley et al., 2005). The DPP4 inhibitors lie in the oral hypoglycemics class and block the enzyme DPP4. The therapeutic use of DPP4 is mainly in the treatment of type 2 diabetes. To scrutinize the inhibition activity of cefradine against DPP4, the crystal structure of three PDB codes, 1NU6, 1N1M and 1J2E, with a resolution of 2.10 Å, 2.50 Å, 2.60 Årespectively, has been downloaded from RCSB data bank. The superimposition of 1N1M and 1J2E with respect to the high-resolution structure of 1NU6 has been conducted and the root mean square deviation (RMSD) values were

predicted to be 0.586 and 0.577 which is tabulated in Table 20.

Table 20: Docking parameters of cefradine with the estimated protein targets.

Target Proteins	Selected PDB structures with their resolutions	[a]Hydrogen Bonding residues	Ligand efficiency	Inhibition constant (μM)	Binding energy (kcal/mol)	[b]RMSD
Dipeptidyl peptidase IV (DPP4)	1NU6 (2.10 Å)	TYR70, LYS71, ARG61	−0.22	163.53	−5.17	
	1N1M (2.50 Å)	PHE516, ASP515, LYS513, LYS536	−0.25	39.25	−6.01	0.586
	1J2E (2.60 Å)	THR251, ARG253, ASP192	−0.22	111.68	−5.39	0.577
Protein Farnesyl-transferase	1MZC (2.00 Å)	GLU723, LHE762, LYS763	−0.24	69.28	−5.67	
	3E34 (2.05 Å)	LYS50, GLU41, ASP37	−0.2	310.15	−4.79	0.253
	1O1R (2.30 Å)	ASP297, ARG291, HIS248, TYR300	−0.22	111.28	−5.39	0.342
Human Cyclo-oxygenase-2 (COX-2)	5IKT (2.45 Å)	GLU346, ASP347, LYS358	−0.19	387.03	−4.66	
	5IKV (2.51 Å)	ALA239, ARG240, LYS243, GLU272, GLU290	−0.23	90.95	−5.51	0.137
	5KIR (2.70 Å)	ASP157, ASP133, GLN457	−0.24	64.53	−5.72	0.266

[a]The distance between the ligand and the binding residues is given in Angstrom units in the parenthesis.
[b]RMSD value of the superimposition of proteins with respect to the high resolution PDB structure is provided.

From the selected target structures of proteins, the amino acid residues of target 1N1M

of DPP4 exhibit the highest binding energy (−6.01 kcal/mol). Moreover, the inhibition constant (39.25 μM) of cefradine with structure of 1N1M is least and the high value of ligand efficacy (−0.25) than the other two protein structures signifies that the cefradine can probably be a good candidate that can block the enzymatic activity of DPP4 (M. K. Chaudhary, Karthick, et al., 2021).

4.3.15.2 Docked complex of cefradine and Protein Farnesyltransferase (FTase)

FTase is a heterodimer consisting of α and β sub unit shared with geranylgeranyltransferase I and a CaaX prenyltransferase (Maurer-Stroh et al., 2003). The FTase enzyme is active against the posttranslational modification (farnesylation) of proteins containing a carboxy-terminal CaaX motif, including Ras, Ras homologues and other small G proteins which are responsible for anti-parasitic and anti-cancer agents. Thus, certain FTase inhibitors are suitable for the treatment regarding the anti-parasitic and anti-cancer agents.

To examine the binding affinity and the inhibition capability of cefradine against the FTase enzyme, three protein structures such as 1MZC, 3E34 and 1O1R with the resolution of 2.0 Å, 2.05 Å and 2.30 Å respectively were taken into consideration. From the selected targets, the protein structure with PDB codes 3E34 and 1O1R, are superimposed with respect to the higher resolution structure of 1MZC and the respective RMSD value of these superposition structures were calculated to be 0.253 and 0.342 respectively. From the docked complexes of the FTase and the cefradine, higher binding energy (−5.67 kcal/mol) was predicted for 1MZC. Moreover, the residues (GLU723, LHE762, LYS763) of amino acid of 1MZC exhibit the strong ligand-protein interaction by forming strong hydrogen bonds and the predicted inhibition constant is found to be 69.28 μM (M. K. Chaudhary, Karthick, et al., 2021). The docking simulation of cefradine with FTase enzyme signifies that the other two PDB structures 3E34 and 1O1R are loosely bind with the active residues.

4.3.15.3 Docked complex of cefradine and Human Cyclooxygenase-2 (COX-2)

The COX-2 is an enzyme in human encoded by Prostaglandin-endoperoxide synthase 2 (PTGS2) gene. The therapeutic use of COX is helpful in the relief from the symptoms of inflammation and pain (Kurumbail et al., 1996). To examine the active binding sites of cefradine against COX-2, three COX-2 structures such as 5IKT, 5IKV and 5KIR have been selected and the docking has been performed with the AutoDock 4.2 program. The docking result signifies that the residues of target 5KIR provides the strong hydrogen binding with the residues ASP157, ASP133, GLN457 with the ligand (cefradine). The inhibition constant (64.53 μM) of cefradine with structure of 5KIR is least. The ligand efficacy of the structure 5KIR with cefradine is (−0.24) which is higher than the other

two structures 5IKT and 5IKV of COX-2. The corresponding least values of RMSD of 5IKV and 5KIR are 0.253 and 0.266 respectively with respect to the higher resolution structure 5IKT. These values signify that amino acids are aligned with small deviations in their orientation (M. K. Chaudhary, Karthick, et al., 2021).

Thus, the docking study explore that cefradine has useful merit as the inhibitors of DPP4, FTase and COX-2. However, further *in vitro* and *in vivo* studies have to be performed to confirm its activities (M. K. Chaudhary, Karthick, et al., 2021).

4.4 Frovatriptan

Frovatriptan belongs to triptan class of drug which has wide application in the treatment of migraine pain, headache and other migraine symptoms. Frovatriptan is active against the serotonin 5-HT_{1B} agonists class of receptors having the pharmacological activity for the treatment of migraine and vascular headaches, mainly in women during the menstruation period (Markus & Mikko, 2007; Lisotto et al., 2013; Ferrari et al., 2001). The frovatriptan expand the arteries and the veins which can easily transport the blood to the brain and the bold pressure is reduced to a great extent. The ligand-protein interaction of frovatriptan with serotonin 5-HT_{1B} has been discussed to check the drug potential of ligand and the binding sites have been identified (M. K. Chaudhary, Srivastava, et al., 2020). The following characteristic of frovatriptan at microscopic level has been explored from the DFT approach as explained below.

4.4.1 Conformational analysis

The pictorial presentation of the optimized 3D electronic structure of frovatriptan from B3LYP/6-311++G(d,p) level of calculation including atom numbering arrangement is depicted in Figure 32.

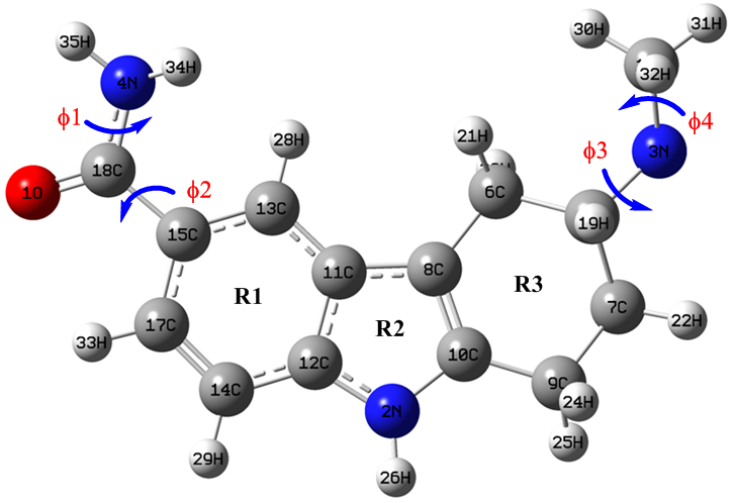

Figure 32: Stable structure of frovatriptan with atom numbering system.

To identify the probable conformers of frovatriptan at room temperature, one dimensional PES scan has been carried out across the soft bonds N4-C18, C18-C15, C5-N3 and N3-C16 having respective torsion angles ϕ1(H35-N4-C18-C15), ϕ2(N4-C18-C15-C17), ϕ3(C7-C5-N3-C16) and ϕ4(H31-C16-N3-C5). The torsion angle is varied from (0° to 360°) at a step size of 10° across the flexible bonds. The relative energy across each flexible bond is shown in the PES graph in Figure 33.

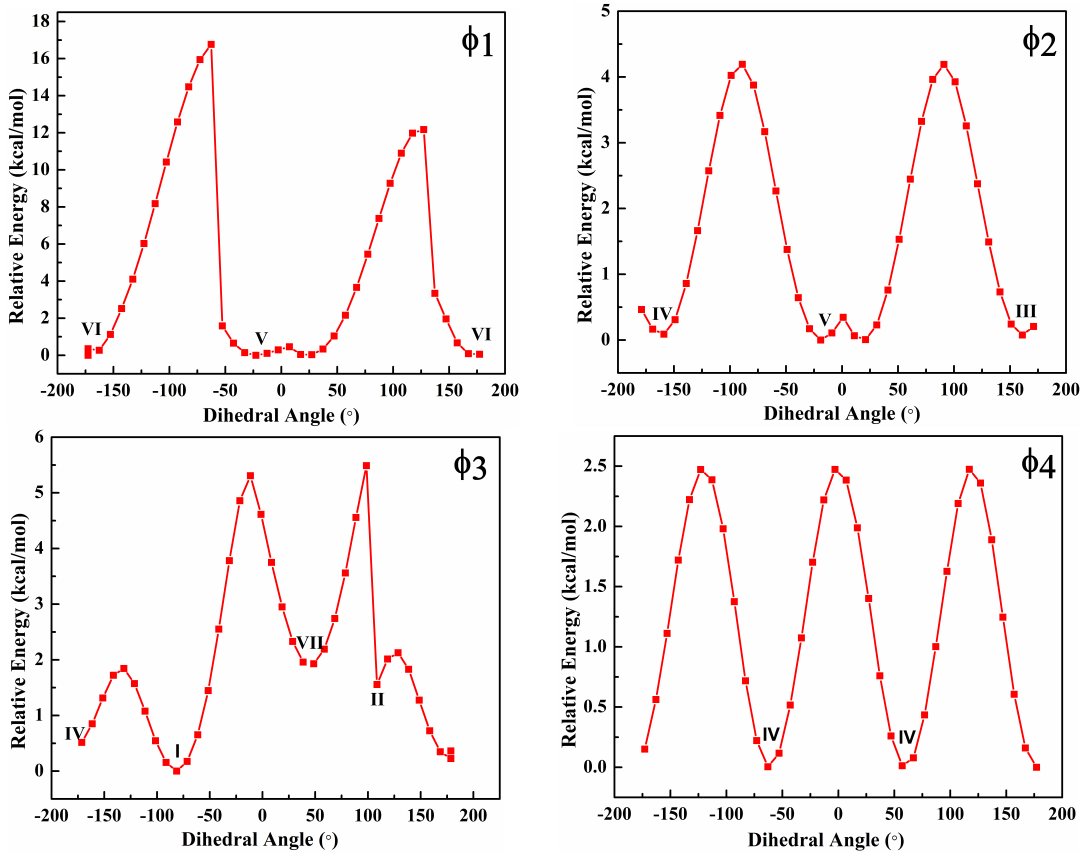

Figure 33: One dimensional potential energy surface scan across the flexible bonds ϕ1, ϕ2, ϕ3, ϕ4 of frovatriptan.

On the basis of SCF energy, six conformers are predicted whose relative energy with respect to the most stable conformer are presented in Table 21. The geometry of all the conformers with their relative energy is depicted in Figure 34. Only those conformers whose relative energies less than 0.56 kcal/mol (equivalent to kT) are likely to exist at room temperature. Thus, only five conformers (I-V) can exist at room temperature (M. K. Chaudhary, Srivastava, et al., 2020). Their structures are further optimized with the ωB97XD functional which measures the dispersion correction (Chai & Head-Gordon, 2008). This signifies that the energy obtained from the functional ωB97XD is more than the energy obtained from the B3LYP which is presented in Table 22. Moreover, the benchmarking report (Tortorella et al., 2016) explore that the functional B3LYP provides correct electronic and spectroscopic data than the ωB97XD functional. So, the remaining electronic results have been obtained from the calculation of B3LYP

functional, which gives convenient experimental data (K. Srivastava et al., 2016; Joshi et al., 2018).

Table 21: Relative energy of six conformers of frovatriptan in comparison to the most stable one.

Conformer	Dihedral angle	Energy (Hartree)	Energy (kcal/mol)	Energy difference (kcal/mol)
I	ϕ3(C7-C5-N3-C16)	−783.453293	−491616.9411	0
II	ϕ3(C7-C5-N3-C16)	−783.453179	−491616.8696	0.0715
III	ϕ2(N4-C18-C15-C17)	−783.452840	−491616.6574	0.2837
IV	ϕ4(H31-C16-N3-C5)	−783.452713	−491616.5777	0.3634
V	ϕ2(N4-C18-C15-C17)	−783.452703	−491616.5714	0.3697
VI	ϕ3(C7-C5-N3-C16)	−783.450265	−491615.0416	1.8995

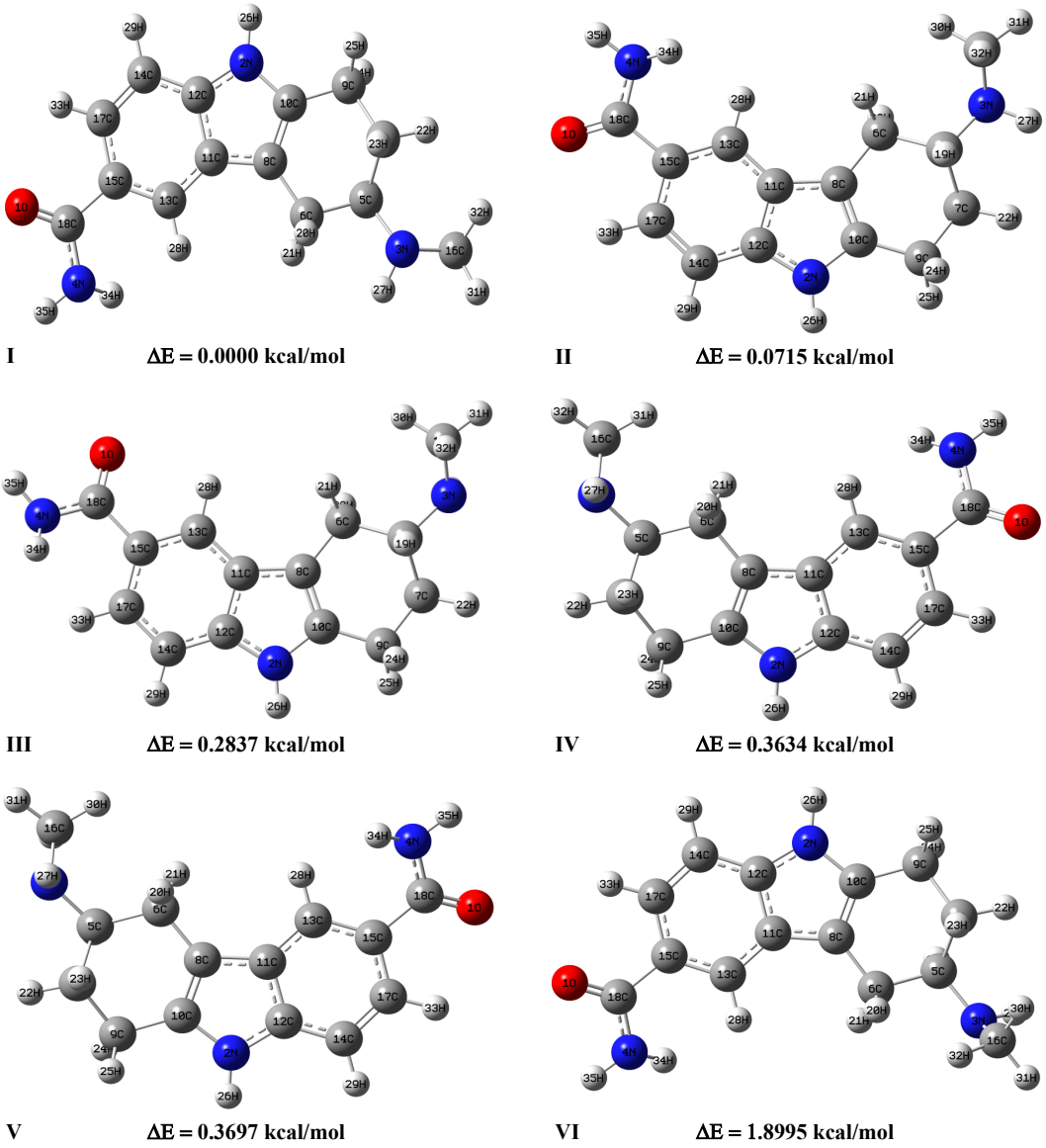

Figure 34: Stable structure of the six conformers of frovatriptan with relative energy.

Table 22: Energy of all the possible conformers of frovatriptan with the functional B3LYP and ωB97XD.

Dihedral Angle	Conformer	B3LYP		ωB97XD	
		Energy (Hrtree)	Energy (kcal/mol)	Energy (Hrtree)	Energy (kcal/mol)
ϕ3(C7-C5-N3-C16)	I	−783.453293	−491616.9411	−783.198347	−491456.9626
ϕ3(C7-C5-N3-C16)	II	−783.453179	−491616.8696	−783.198456	−491457.0314
ϕ2(N4-C18-C15-C17)	III	−783.452840	−491616.6574	−783.198456	−491457.0314
ϕ4(H31-C16-N3-C5)	IV	−783.452713	−491616.5777	−783.198204	−491456.8732
ϕ2(N4-C18-C15-C17)	V	−783.452703	−491616.5714	−783.198230	−491456.8890

4.4.2 Optimized structure specifications

The optimized specifications of frovatriptan such as bond length, bond angle and torsional angle of conformers (I-V) estimated from B3LYP/6-311++G(d,p) level of calculation are represented in Table 34 (Appendix E) and the atom numbering arrangement is presented in Figure 32. The superimposed structure of conformer I with conformers (II-V) has been performed in terms of the least square algorithm, which reduces the distance of the corresponding non-hydrogen atoms are illustrated in Figure 35. From the Figure 35, it is clear that the rings R1, R2 and R3 are co-planer. The branch chain that contains amine group (-$N4H_2$) also present in the same plane. But the other branch which consist of the methyl group (-$C16H_3$) is slightly in another plane. Comparison of the bond length of conformer I with conformers (II-V) signifies that the bond length across C5-C6 is slightly increased by 0.011 Å.

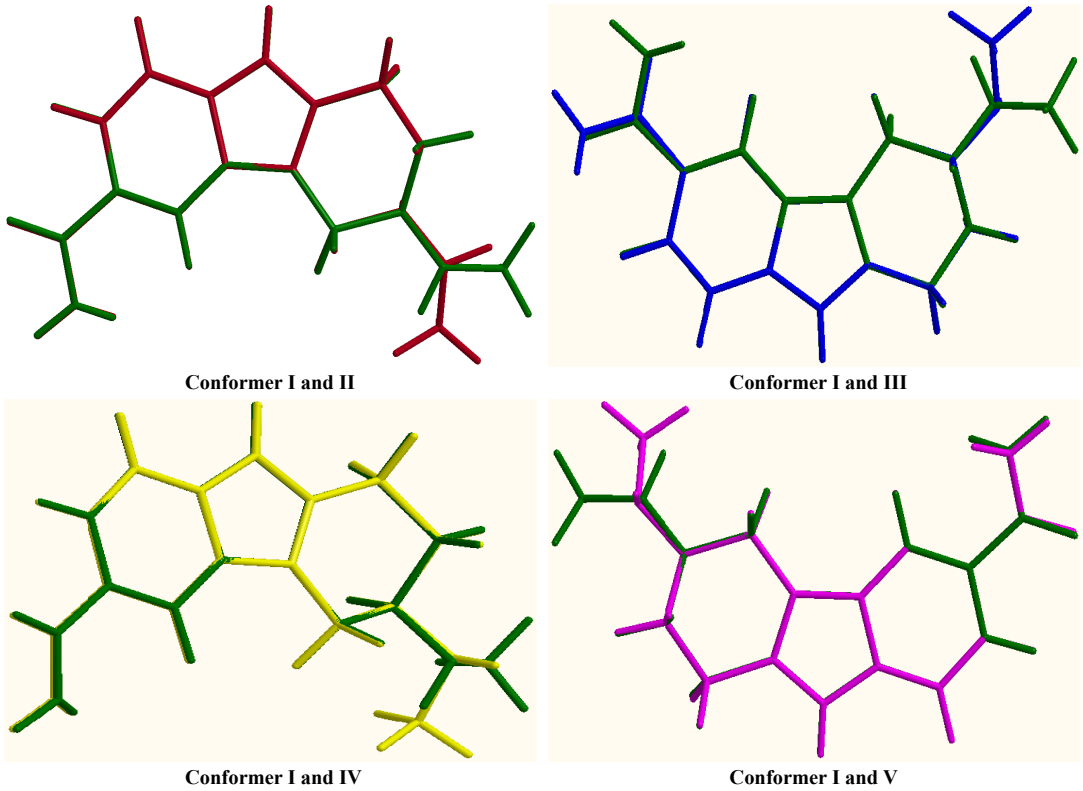

Figure 35: Overlapping of conformers (II-V), with conformer I (green: conformer I, red: conformer II, blue: conformer III, yellow: conformer IV and pink: conformer V).

This increment in the bond distance is due to the attachment of N3 atom with the ring R3 which is involved in the intermolecular hydrogen bonding in the crystal structure. But our calculation is focused on a particular molecule in gaseous form. The significant change in the bond angle in conformer I and II is not observed, however, a small change in bond angle is observed as 4.36°, 4.34°, 4.34° and 5.53°, 4.34°, 5.54° across (N3-C5-H19) and (N3-C5-C16) while comparing the conformer I with the conformers (III-V) respectively. Moreover, the angle 5.51° and 5.94° across C13-C15-C18 and N3-C16-H31 are observed while comparing the conformer I with conformers III and IV respectively. This change in angle signifies that there is formation of intermolecular hydrogen bond in crystal form with N3 and N4 atoms. While analyzing the torsional angles of conformer I with conformers II to V, the prominent variation is observed in atoms which are involved in intermolecular hydrogen bonding in solid state. These atoms are O1, N3 and N4 (M. K. Chaudhary, Srivastava, et al., 2020).

4.4.3 Natural bond orbital analysis

The molecular stability has been scrutinized from the NBO analysis from the distribution of charge from the filled orbital to the vacant orbital (M. K. Chaudhary, Prajapati, & Joshi, 2020). The transition of electrons from donor to acceptor orbital is called bonding-antibonding interaction (R. Singh et al., 2018). The stabilization energy $E^{(2)}$ between the filled orbital (i) and the vacant orbital (j) is the major index which determines the stability of the orbital system. The stabilization energy $E^{(2)}$ of frovatriptan between the prominent donor and the acceptor orbitals has been calculated from the Fock matrix in terms of the second-order perturbation theory (Reed & Weinhold, 1983; Reed et al., 1988; Weinhold & Landis, 2005). The stabilization energy $E^{(2)}$ of frovatriptan are presented in Table 23, which is determined from the Equation (3.67).

The distribution of electrons from $\sigma \rightarrow \sigma^*$ transitions play a prominent role for the stabilization of frovatriptan molecule. The transition of σ electrons from σ(O1-C18)$\rightarrow$ σ^*(C13-C15), σ(N4-C18)$\rightarrow$ σ^*(C13-C15), σ(N4-H34)$\rightarrow$ σ^*(C13-C15) and σ(N4-H35)$\rightarrow$ σ^*(C13-C15) stabilizes the molecular system with 12.73 kcal/mol, 13.89 kcal/-mol, 8.68 kcal/mol and 11.32 kcal/mol energy, respectively. Furthermore, the interactions σ(N2-C10)$\rightarrow$ σ^*(C12-C14), σ(C5-C6)$\rightarrow$ σ^*(C12-C14), σ(C8-C11)$\rightarrow$ σ^*(C12-C14), σ(C13-C15)$\rightarrow$ σ^*(C12-C14), σ(C13-H28)$\rightarrow$ σ^*(C12-C14), σ(C15-C17)$\rightarrow$ σ^*(C12-C14), σ(C15-C18)$\rightarrow$ σ^*(C12-C14) stabilizes the molecule with respetive interaction energy 8.28 kcal/mol, 35.46 kcal/mol, 7.04 kcal/mol, 16.49 kcal/mol, 16.47 kcal/-mol, 9.68 kcal/mol and 77.48 kcal/mol. The transitions LP(1)N4$\rightarrow$ π^*(O1-C18) and LP(1)N2$\rightarrow$ π^*(C11-C12) contribute a vital role for the stability of frovatriptan molecule with $E^{(2)}$ = 37.82 kcal/mol and 35.19 kcal/mol, respectively (M. K. Chaudhary, Srivastava, et al., 2020).

Table 23: Second-order perturbation theory analysis of Fock matrix in NBO basis of frovatriptan (conformer I).

Donor NBO(i)	ED(i)/e	Acceptor NBO (j)	ED(j)/e	$E^{(2)a}$ kcal/mol	E(j) - $E(i)^b$ a.u.	$F(i,j)^c$ a.u.
σ(O1-C18)	1.99369	σ*(C13-C15)	0.02154	12.73	1.53	0.125
σ(N2-C10)	1.98370	σ*(C12-C14)	0.02175	8.28	0.86	0.075
σ(N4-C18)	1.99388	σ*(C13-C15)	0.02154	13.89	1.35	0.123
σ(N4-H34)	1.98736	σ*(C13-C15)	0.02154	8.68	1.19	0.091
σ(N4-H35)	1.98972	σ*(C13-C15)	0.02154	11.32	1.10	0.100
σ(C5-C6)	1.97281	σ*(C12-C14)	0.02175	35.46	0.70	0.141
σ(C5-C6)	1.97281	σ*(C16-H32)	0.01408	8.27	3.52	0.153
π(C8-C10)	1.82776	π*(C11-C12)	0.49429	16.50	0.29	0.067
σ(C8-C11)	1.96457	σ*(C9-C10)	0.02228	5.35	1.07	0.068
σ(C8-C11)	1.96457	σ*(C12-C14)	0.02175	7.04	0.71	0.063
σ(C11-C12)	1.95698	σ*(C6-C8)	0.02037	5.10	1.09	0.067
π(C11-C12)	1.56649	π*(C8-C10)	0.29730	17.19	0.29	0.065
π(C11-C12)	1.56649	π*(C14-C17)	0.30370	16.81	0.29	0.064
σ(C13-C15)	1.97223	σ*(C12-C14)	0.02175	16.49	0.75	0.100
π(C13-C15)	1.70662	π*(O1-C18)	0.27417	18.17	0.30	0.067
π(C13-C15)	1.70662	π*(C11-C12)	0.49429	16.77	0.28	0.064
π(C13-C15)	1.70662	π*(C14-C17)	0.30370	18.99	0.30	0.067
σ(C13-H28)	1.97797	σ*(C12-C14)	0.02175	16.47	0.58	0.088
σ(C14-C17)	1.97515	σ*(N2-C12)	0.02452	6.02	1.15	0.074
π(C14-C17)	1.72166	π*(C11-C12)	0.49429	20.25	0.28	0.071
σ(C15-C17)	1.97122	σ*(C12-C14)	0.02175	9.68	0.74	0.076
σ(C15-C18)	1.97384	σ*(C12-C14)	0.02175	77.48	0.72	0.211
LP(2)O1	1.87062	σ*(N4-C18)	0.06824	24.67	0.68	0.118
LP(1)N2	1.64263	π*(C8-C10)	0.29730	34.34	0.32	0.094
LP(1)N2	1.64263	π*(C11-C12)	0.49429	35.19	0.30	0.094
LP(1)N4	1.78111	π*(O1-C18)	0.27417	37.82	0.34	0.102
LP(1)N4	1.78111	σ*(C17-H33)	0.01295	8.42	2.43	0.135

[a] $E^{(2)}$ means the energy of hyper conjugative interaction (stabilization energy).
[b] Energy difference between donor (i) and acceptor (j) NBOs.
[c] $F(i,j)$ is the Fock matrix element between i and j NBOs.

4.4.4 Molecular electrostatic potential surface

The distribution of charge in the molecular system can be evaluated by MEP analysis (Kumru et al., 2015). This provides the idea of binding sites of biologically active molecules. Moreover, MEP is the visual procedure to identify the distribution of charge density in three dimension around the molecule as well as separation of positive and negative charge in the molecule (Sjoberg et al., 1990; Weiner et al., 1982). The molecular electrostatic potential $V(r)$ around the frovatriptan, which is the cumulative effect of the negative and the positive charges corresponding to electrons and nuclei, is calculated from the Equation (3.66). The electrostatic potential is measured in terms of color code. The red color stands for negative potential, the blue color stands for positive potential and the green color signifies zero-potential region. The allotment of potential in the MEP

map is measured in the order red < yellow < green < blue. The distribution of charge cloud of conformers (I-V) of the frovatriptan in terms of color is presented in Figure 36. This signifies that the hydrogens across the amine group ($N4H_2$), H26 and H27 atoms exhibits intense blue cloud and have the maximum positive potential. These atoms are important for the nucleophilic attack for surrounding species. Whereas, the oxygen in the carbonyl group (C18=O) has a red cloud and exhibits maximum negative potential and is suitable for the electrophilic attack in all the conformers (I-V) of frovatriptan (M. K. Chaudhary, Srivastava, et al., 2020).

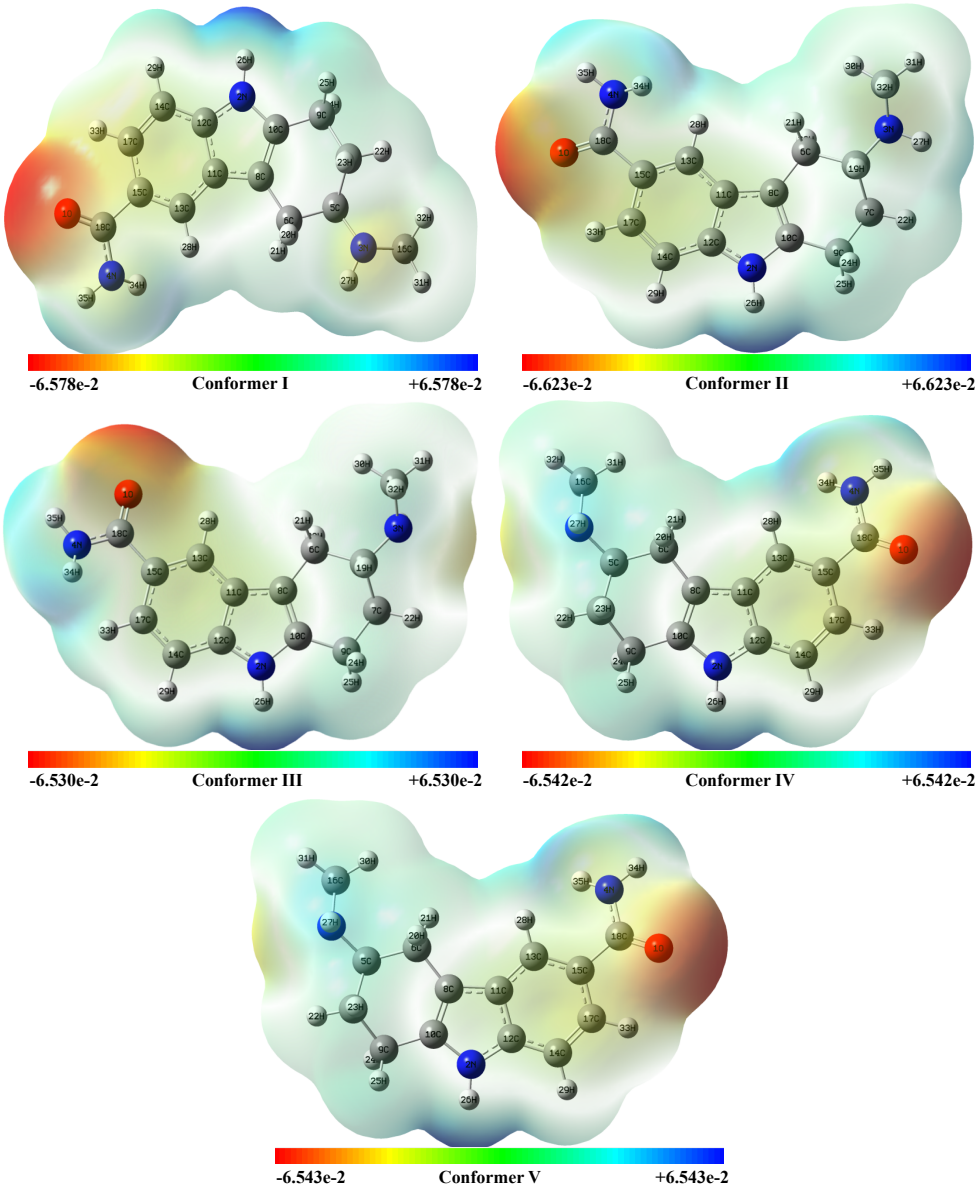

Figure 36: Distribution of charge cloud around the frovatriptan molecule of conformers (I-V) in MEP map obtained from the total density over the electrostatic potential.

4.4.5 HOMO–LUMO energy gap

The frontier molecular orbital plot of frovatriptan for the conformers (I-V) is visualized in Figure 37. The prominent orbitals that take part in the chemical reaction in the molecular system are the HOMO and the LUMO. The HOMO orbital has tendency to donate electrons whereas the LUMO orbital has tendency to accept the electrons. The energies E_{H} and E_{L} of HOMO and LUMO orbitals and their energy difference ($\Delta E_{\mathrm{L\text{-}H}}$) analyze the stability as well as the chemical reactivity of the molecular system.

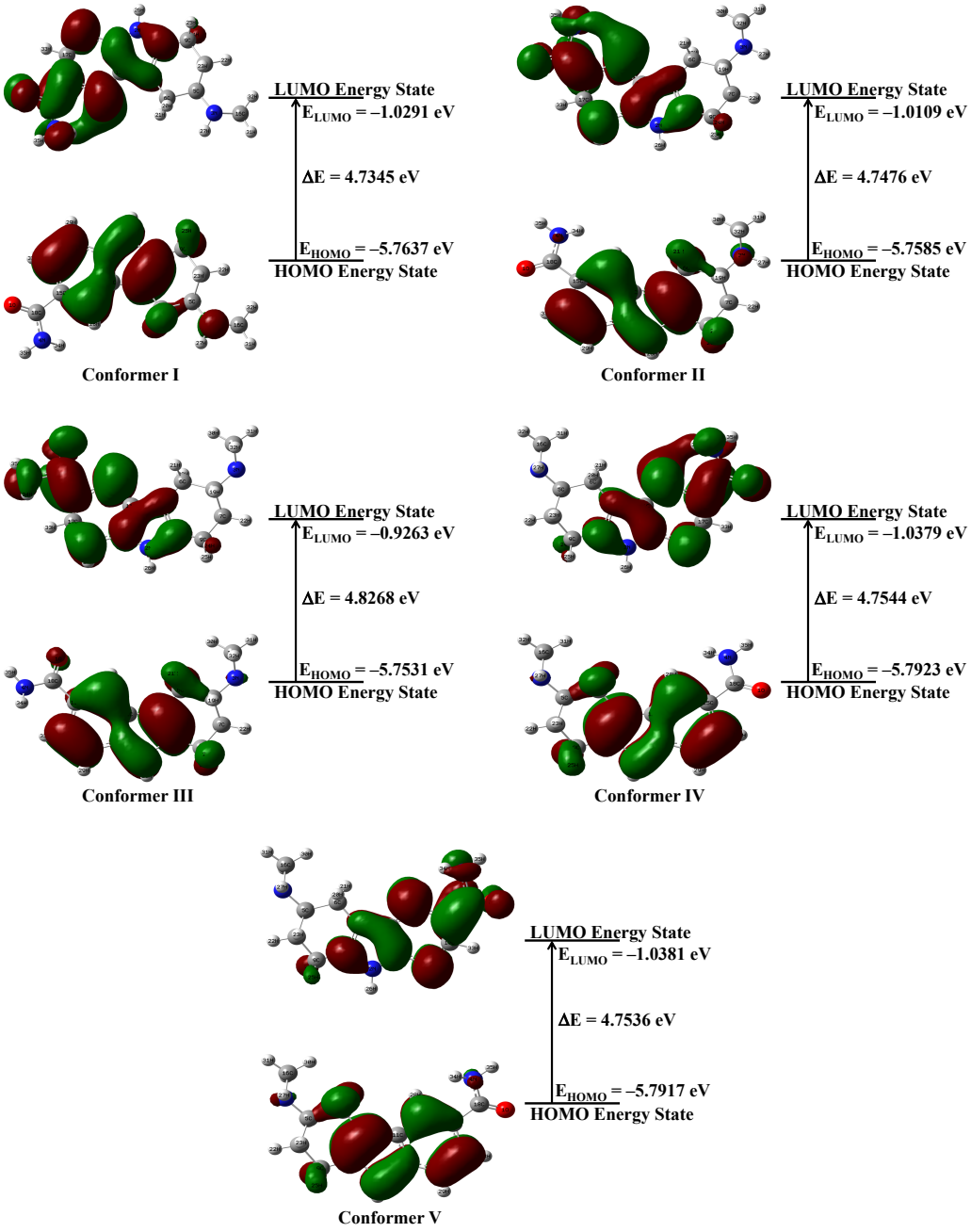

Figure 37: Frontier molecular orbital plot of frovatriptan of conformers (I-V).

The significantly high value of $\Delta E_{\mathrm{L\text{-}H}}$ motivates that the molecule is less chemically

reactive and more stable (Haddon & Fukunaga, 1980; Schmalz et al., 1988; Liu et al., 1992). $\Delta E_{\text{L-H}}$ of the frovatriptan for all the conformers (I-V) is obtained from B3LYP/6-311++G(d,p) level of calculation and their respective values are 4.7345 eV, 4.7476 eV, 4.8268 eV, 4.7544 eV and 4.7536 eV. The highest value of $\Delta E_{\text{L-H}}$ for the conformer III reveals that it is more stable and less chemically reactive whereas the least value of $\Delta E_{\text{L-H}}$ for conformer I infer that it is less stable more chemical reactive (M. K. Chaudhary, Srivastava, et al., 2020). The HOMO-LUMO plot of frovatriptan explore that the charge in HOMO is concentrated in the rings, whereas, the charge in LUMO is scattered to the amine group and the rings.

4.4.6 Global reactivity descriptors

The global reactivity parameters are electronegativity (χ), chemical potential (μ), hardness (η), electrophilicity index (ω) and softness (S) as suggested by Koopman's theorem (Parr & Yang, 1989a). These values are obtained in terms of the HOMO and the LUMO energies E_{H} and E_{L} and are calculated by the Equations (3.51)–(3.55) (Parr et al., 1999; Geerlings et al., 2003).

According to Parr et al. (1999), the value of ω is always positive which depends on μ and η. ω measures the stabilization in energy as the system gains the additional charge (ΔN) from environment species (Shweta et al., 2017). The high value of μ and ω illustrate the good electrophilic nature of the molecules, whereas, their low values show good nucleophilic nature of the molecule (A. Srivastava et al., 2012). The calculated values of E_{H}, E_{L}, $\Delta E_{\text{L-H}}$, χ, μ, η, ω and S of frovatriptan for the conformers (I-V) is illustrated in Table 24. The large value of $\Delta E_{\text{L-H}}$ and η of conformer III signifies that it has more stability and less polarizability (Prajapati et al., 2016).

Table 24: Calculated E_{HOMO}, E_{LUMO}, $E_{\text{L}} - E_{\text{H}}$, μ, χ, η, S and ω for all the conformers of frovatriptan.

Molecule	E_{H}(eV)	E_{L} (eV)	($E_{\text{L}} - E_{\text{H}}$)(eV)	χ(eV)	μ(eV)	η(eV)	S(eV^{-1})	η(eV)	ΔN_{max}
Conformer I	−5.7637	−1.0291	4.7345	3.3964	−3.3964	2.3673	0.2112	2.4365	1.4347
Conformer II	−5.7585	−1.0109	4.7476	3.3847	−3.3847	2.3738	0.2106	2.4131	1.4259
Conformer III	−5.7531	−0.9263	4.8268	3.3397	−3.3397	2.4134	0.2072	2.3107	1.3838
ConformerIV	−5.7923	−1.0379	4.7544	3.4151	−3.4151	2.3772	0.2103	2.4530	1.4366
Conformer V	−5.7917	−1.0381	4.7536	3.4149	−3.4149	2.3768	0.2104	2.4532	1.4368

4.4.7 Local reactivity descriptors

The local reactivity descriptors explain the quantitative study about the reactive sites in the molecular system. The Fukui function, $f(r)$ is main local reactivity parameter which describes the chemical reactivity and the site selectivity (Ayers & Parr, 2000). According to Parr & Yang (1984), the atom with high value of $f(r)$ is responsible for reactive center in the biologically active molecule. The $f(r)$ corresponding to the nucleophilic, electrophilic and the radical attack are f_k^+, f_k^- and f_k^0 respectively. Their

values are determined from the Equations (3.63)–(3.65) (Ayers & Parr, 2000). The signs +, − and 0 indicates the nucleophilic, electrophilic and the radical reactivity behavior respectively. Similarly, the local softness (s_k^+, s_k^-, s_k^0) and the electrophilicity indices (ω_k^+, ω_k^-, ω_k^0) have major role to check the reactivity of atoms in the molecule and are given by the equations:

$$s_k^+ = Sf_k^+, \quad \omega_k^+ = \omega f_k^+$$
$$s_k^- = Sf_k^-, \quad \omega_k^- = \omega f_k^-$$
$$s_k^0 = Sf_k^0, \quad \omega_k^0 = \omega f_k^0$$

The local reactivity parameters of frovatriptan for the specific atoms of conformers (I-V) is depected in Table 25, which shows that the sites C8, C10 and N3 are responsible for the nucleophilic center, whereas, the atoms C13, O1 and C9 are close to the electrophilic center (M. K. Chaudhary, Srivastava, et al., 2020).

Table 25: Local reactivity descriptors of frovatriptan for the specific atoms using Hirshfeld charges at B3LYP/6-311++G(d,p) level of calculation.

Site	f_k^+	s_k^+	ω_k^+	Site	f_k^-	s_k^-	ω_k^-	Site	f_k^0	s_k^0	ω_k^0
Conformer I											
C8	0.1523	0.0322	0.3711	C13	0.0375	0.0079	0.0914	C18	0.6476	0.1368	1.5780
C10	0.1171	0.0247	0.2853	O1	0.0332	0.0070	0.0809	C10	0.2425	0.0512	0.5908
N3	0.0924	0.0195	0.2251	C9	0.0266	0.0056	0.0648	C12	0.1801	0.0380	0.4389
Conformer II											
C8	0.1602	0.0337	0.3865	C13	0.0479	0.0101	0.1155	C18	0.6480	0.1365	1.5636
C10	0.1207	0.0254	0.2914	O1	0.0351	0.0074	0.0846	C10	0.2448	0.0515	0.5906
C17	0.1032	0.0217	0.2491	C15	0.0268	0.0057	0.0648	C12	0.1769	0.0372	0.4268
Conformer III											
C8	0.1563	0.0324	0.3612	C9	0.0203	0.0042	0.0470	C18	0.6556	0.1358	1.5148
N3	0.1015	0.0210	0.2346	O1	0.0186	0.0039	0.0430	C10	0.2386	0.0494	0.5513
C10	0.0998	0.0207	0.2306	C13	0.0173	0.0036	0.0400	C12	0.1771	0.0367	0.4092
Conformer IV											
C8	0.1547	0.0325	0.3794	C11	0.0418	0.0088	0.1025	C18	0.6487	0.1364	1.5914
C10	0.1157	0.0243	0.2838	C10	0.0378	0.0079	0.0927	C10	0.2263	0.0476	0.5552
C17	0.1016	0.0214	0.2492	C13	0.0353	0.0074	0.0867	C12	0.1762	0.0371	0.4323
Conformer V											
C8	0.1533	0.0322	0.3760	C13	0.0455	0.0096	0.1116	C18	0.6478	0.1363	1.5891
C10	0.1157	0.0243	0.2838	O1	0.0348	0.0073	0.0853	C10	0.2409	0.0507	0.5910
C17	0.1016	0.0214	0.2492	C14	0.0262	0.0055	0.0642	C12	0.1773	0.0373	0.4350

4.4.8 Thermodynamic behavior

The temperature plays a vital role in chemical reactivity and in pharmacodynamics (Ott & Boerio-Goates, 2000; Basha et al., 2019). The significant thermodynamic functions such as: total energy, zero-point energy and rotational constant of all the conformers (I-V) of frovatriptan were determined at room temperature 298.15 K and their obtained values are illustrated in Table 26. The thermo dynamical parameters like: heat capacity ($C_{p,m}^\circ$), entropy (S_m°) and enthalpy (H_m°) of the conformer I of frovatriptan determined from the output file in the temperature range (50 to 300) K are presented in Table 27 and their correlation graph is presented in Figure 38. The mathematical equations for $C_{p,m}^\circ$,

S_m° and H_m° of conformer I are as follows:

$$C_{m,p}^\circ = 4.7627 + 0.19258\,T + 2.00071 \times 10^{-5}\,T^2 \qquad (R^2 = 1.0000) \qquad (4.8)$$

$$S_m^\circ = 52.7758 + 0.29455\,T - 1.49029 \times 10^{-4}\,T^2 \qquad (R^2 = 0.9998) \qquad (4.9)$$

$$H_m^\circ = 184.32 + 0.00428\,T + 9.996571 \times 10^{-5}\,T^2 \qquad (R^2 = 1.0000) \qquad (4.10)$$

From the second law of thermodynamics, the above equations are helpful for further studies of thermodynamic energies as well as to estimate the direction of chemical reactions of the frovatriptan (N. Choudhary et al., 2014). Figure 38 explore that the effect of temperature increases the thermodynamic parameters (M. K. Chaudhary, Srivastava, et al., 2020).

Table 26: Zero-point energy, total energy, enthalpy, specific heat, entropy and rotational constant at 298.15 K obtained at B3LYP/6-311++G(d,p) level of calculation of frovatriptan of conformers (I-V).

Parameters	Conformer I	Conformer II	Conformer III	Conformer IV	Conformer V
Total energy (eV)	–21317.76	–21317.76	–21317.75	–21317.75	–21317.75
Zero-point energy (J/mol)	771168.2	771162.2	771035.3	770974.1	771076.5
Enthalpy (kcal/mol)	194.458	194.457	194.452	194.439	194.454
Specific heat (cal/mol-K)	63.982	63.973	64.102	64.090	64.065
Entropy (cal/mol-K)	127.547	127.637	127.820	127.858	127.794
Rotational constant (GHz)	0.8818	0.7689	0.7681	0.7687	0.7672

Table 27: Enthalpy, specific heat and entropy of frovatriptan (conformer I) in the temperature range (50 to 300) K.

Temperature (K)	Enthalpy (kcal/mol)	Specific Heat (cal/mol-K)	Entropy (cal/mol-K)
50	184.781	14.416	66.834
100	185.747	24.251	81.218
150	187.207	34.137	93.724
200	189.161	44.037	105.470
250	191.614	54.132	116.825
300	194.576	64.360	127.957

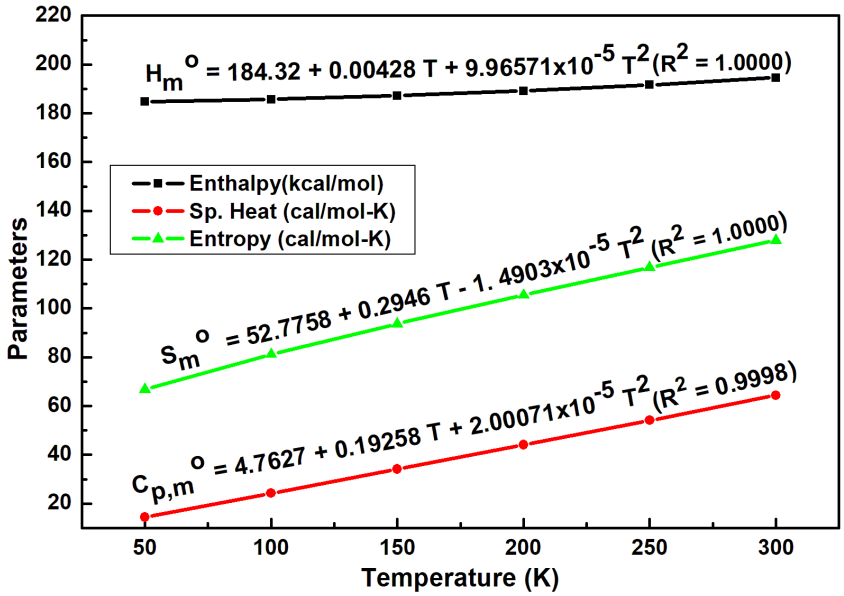

Figure 38: The variation of H_m°, $C_{p,m}^\circ$ and S_m° with temperature for frovatriptan of conformer I.

4.4.9 Non-linear optical components

The specific use of NLO substance is in data storage, sensing, optical communication, computing and many more (Williams, 1984). The NLO behavior of substance are measured in terms of the total static dipole moment (μ_0), the first hyperpolarizability (β_0), the mean polarizability ($\Delta\alpha_0$) and the anisotropy of polarizability $|\alpha_0|$. These properties of frovatriptan is determined from DFT at B3LYP/6-311++G(d,p) level of calculation with the support of Equations (3.47)–(3.50) (Vidya et al., 2011). The delocalization of charge in a specific direction is obtained from the component of polarizability in that direction. The components of μ_0, β_0, $\Delta\alpha_0$ and $|\alpha_0|$ of frovatriptan are tabulated in Table 28. The respective values of μ_0, $\Delta\alpha_0$ and β_0 of frovatriptan are 3.4, 7.5 and 7 times more than the observed values of urea (Cassidy et al., 1979). This signifies that the frovatriptan can be used as a good NLO substance (M. K. Chaudhary, Srivastava, et al., 2020).

4.4.10 Drug-likeness

Besides the clinical activities of the molecular system, the drug-likeliness of the molecule can be evaluated theoretically (Khan et al., 2015). Theoretically, the Lipinski's rule of 5 is used to investigate the drug candidates (Lipinski et al., 1997; Lipinski, 2004). From the Lipinski's hypothesis, the number of atoms in the molecule should be in the range 20 to 70, whereas, the value of molecular weight should be in the range (180 to 500) g/mol. Moreover, the value of MR of the molecule should lie in the range of (40 to 130) e.s.u (Ghose et al., 1999). The value of MR is calculated in terms of polarizability (α) and its value is calculated from the Lorenz-Lorentz formula which is given by the

Table 28: The computed μ_0, $|\alpha_0|$, $\Delta\alpha$ and β_0 of frovatriptan at B3LYP/6-311++G(d,p) level of calculation.

Dipole moment (debye)		Polarizability ($\times 10^{-24}$ e.s.u)		Hyperpolarizability ($\times 10^{-30}$ e.s.u)	
μ_x	−5.4122	α_{xx}	40.9096	β_{xxx}	4.4414
μ_y	−0.5549	α_{xy}	1.4574	β_{xxy}	2.6325
μ_z	−2.4254	α_{yy}	29.6220	β_{xyy}	1.3251
μ_0	5.9568	α_{xz}	0.3010	β_{yyy}	0.5426
μ_0 (urea)	1.7410	α_{yz}	0.2886	β_{xxz}	−0.9551
		α_{zz}	17.8294	β_{xyz}	0.1358
		$\|\alpha_0\|$	29.4537	β_{yyz}	−0.0564
		$\Delta\alpha$	73.7370	β_{xzz}	−0.4309
		$\Delta\alpha$(urea)	9.7710	β_{yzz}	0.0294
				β_{zzz}	−1.1238
				β_0	6.5775
				β_0(urea)	0.9279

Equation (4.1) (Verma & Hansch, 2005). In the frovatriptan, the number of atoms is 35, whereas, the molecular weight is 243.3 g/mol. These values are in the range mentioned by the Lipinski's rule. The MR value of the frovatriptan is calculated as 76.80 e.s.u, 76.66 e.s.u, 76.66 e.s.u, 76.40 e.s.u and 76.40 e.s.u for the conformers (I-V) respectively. So, the value of MR lies in the range as mentioned above. Thus, frovatriptan can be implemented as a drug molecule (M. K. Chaudhary, Srivastava, et al., 2020).

4.4.11 Molecular docking

Docking is a fundamental tool which explores the binding behavior of drug with protein (Mary et al., 2015; M. K. Chaudhary, Chaudhary, & Joshi, 2021). Frovatriptan is active against the serotonin 1b (5-HT_{1B}) receptor having clinical activity in the treatment of anti-migraine behavior (Ryan et al., 2002; Comer, 2002). The protein target, 5-HT_{1B} receptor, has been predicted from online Swiss target prediction (Daina et al., 2019). The three PDB codes: 4IAQ, 5V54 and 6G79 have been taken into consideration to study the binding activity (Rose et al., 2010) of frovatriptan. The water molecules and the co-crystallized ligand were removed from the protein and the active site has been confined in a grid box of size 60 Å × 60 Å × 60 Å to scrutinize the binding regions.

From the many docked conformations, we have selected only those docked conformations which exhibit good interaction with the ligand. The binding energy, the bond length of conventional hydrogen bond with residues and the binding efficiency of all the docked conformations are tabulated in Table 29. The binding sites of the ligand with the protein is depicted in Figure 39. In frovatriptan, the binding sites are found to be the amine group $N4H_2$ and N3H27. These atoms will take part in the intermolecular hydrogen bonding with the neighboring molecules as explained in Section 4.4.2. Out of the three docked PDB codes, 5V54 shows good binding energy of −9.16 kcal/mol with

four conventional hydrogen bonds (2.10 Å/SER:212, 2.62 Å/THR:209, 1.90 Å/ASP:129, 2.70 Å/TYR:359). Moreover, the docked conformation 4IAQ shows two conventional hydrogen bonds (1.94 Å/SER:66, 2.80 Å/PRO:366), whereas, 6G79 shows four conventional hydrgen bonds (2.23 Å, 2.46 Å/GLY:27, 2.03 Å/SER:98, 2.12 Å/CYS:215) with respective stabilization energies −6.44 kcal/mol and −6.71 kcal/mol (M. K. Chaudhary, Srivastava, et al., 2020). Thus, the computational evaluation of frovatriptan signifies that it has a good clinical use as anti-migraine drug. Out of the three docked conformation, the binding behavior of the ligand increases in the order 5V54 > 6G79 > 4IAQ.

Table 29: Docking parameters of frovatriptan with the predicted targets.

Ligand	Protein	PDB code	Bond length (Å)	Amino acid	Binding energy (kcal/mol)	Ligand efficiency
Frovatriptan	serotonin 1b (5-HT1b) receptor	4IAQ	1.94 2.80	SER:66 PRO:366	−6.44	−0.36
		5V54	2.10 2.62 1.90 2.70	SER:212 THR:209 ASP:129 TYR:359	−9.16	−0.51
		6G79	2.23 2.46 2.03 2.12	GLY:27 GLY:27 SER:98 CYS:215	−6.71	−0.37

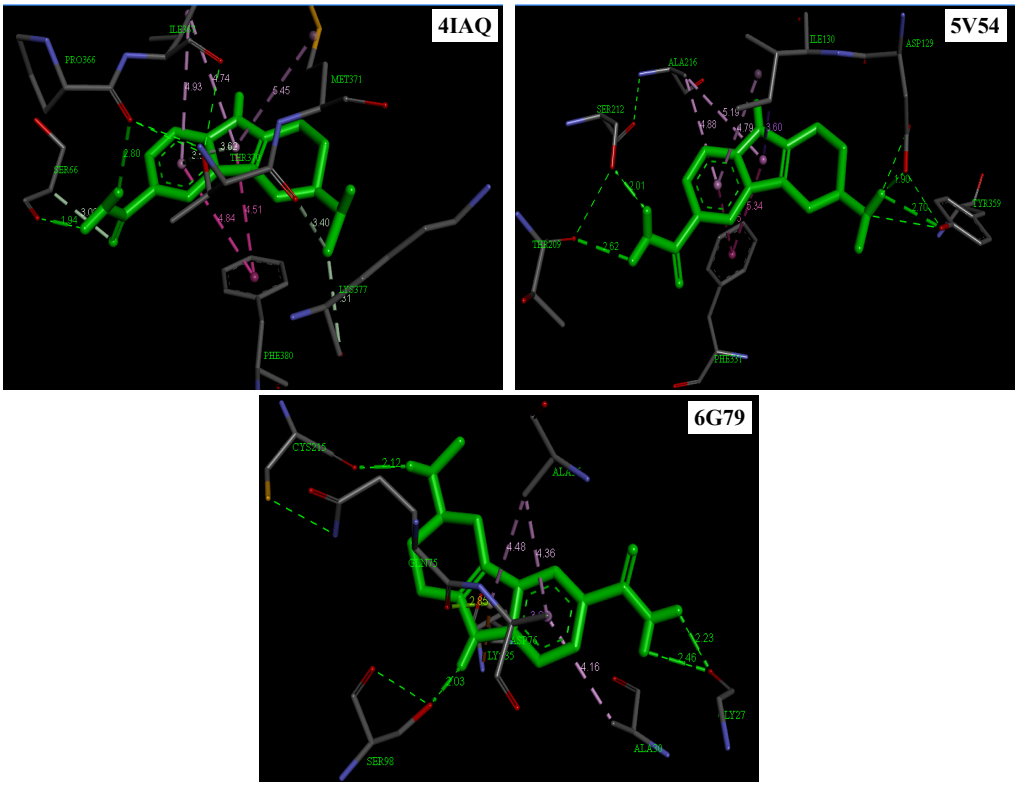

Figure 39: Molecular docking of frovatriptan.

CHAPTER 5

5. CONCLUSIONS AND RECOMMENDATIONS

5.1 Conclusions

The quantum chemical calculation of biological active molecules: RBZ and cefradine has been performed using the DFT approach and the result is compared with the observed vibrational spectroscopic (IR and Raman) data. Furthermore, the DFT calculation of frovatriptan has been conducted.

The conformational analysis of RBZ reveals that the three stable conformers (I–III) can exist at room temperature from one-dimensional PES scan at DFT/B3LYP/6-311++G(d,p) level of calculation. The minimum energy of conformer I is obtained as −787322.8843 kcal/mol. The overlapping of conformers II and III with the conformer I signifies that the benzene and the imidazole ring are coplanar but the side chain containing -CH_2-CH_2-CH_3 in the conformers I and II; and the side chain containing -CH_3 in the conformers I and III are in different planes. While comparing the bond length among the conformers (I-III), the increment in length across S1-C10 in the conformers I and II; and I and III are observed as 0.0059 Å and 0.0050 Å respectively. This is due to the formation of interamolecular hydrogen bond across O2...H22. Moreover, the sulfinyl group has most negative electrostatic potential, so it takes part in intermolecular hydrogen bonding. The comparative study of simulated spectra with the experimental IR and Raman data signifies that they are well matched with each other. The red shift in S-O (sulfinyl group) stretching vibration by 27 cm^{-1} reveals that there is a formation of intermolecular hydrogen bond with the surrounding molecule in the crystal packing, however, our work is based on single molecule in gaseous state, which is also supported by its most negative electrostatic potential. The simulated stretching vibration of (N-H) has been found to be more than the experimental by 98 cm^{-1}. This shifting in wave number is due to the intramolecular hydrogen bond H26...O4 which is also supported by the molecular docking analysis. The donor-acceptor interactions, demonstrated from the NBO analysis, reveal that the interaction LP(1)N7→ π^*(O4-C18) stabilizes the molecular system with the apex value of stabilization energy 61.96 kcal/mol. The MEP surface reveals that the prominent electrophilic and nucleophilic reactive sites are O2 and H26 respectively. The HOMO-LUMO analysis and their energy gap justified that the conformer I is more stable with the highest energy gap 4.9601 eV. Whereas, the least value of the electrophilic index 2.5766 eV and the energy gap 4.9476 eV signifies that the conformer III is the most chemically reactive or less stable among the three. The signifi-

cant high value of the Fukui function of the atoms O2, C12 and S1 infer that these atoms are suitable for the electrophilic, the neuclophilic and the radical attack respectively for further reactions. The QTAIM analysis demonstrated that there were two intramolecular hydrogen bonding interactions of partially covalent in nature. These are C12-H22. . . O2 and N5-H26. . . O4 with energies −3.14671 kcal/mol and −4.37854 kcal/mol at BCP respectively. This is also justified from the vibrational and the docking analysis. The active binding sites in RBZ are predicted as H26, H31, O2, O3 and S1 from the molecular docking. The highest value of the ligand efficiency (−0.42) and the binding energy (−8.07 kcal/mol) of the MAPK protein (3LFB) verified that it is good inhibitor than the other two predicted target proteins.

Furthermore, the variation of the thermodynamic parameters like: H_m°, $C_{p,m}^\circ$ and S_m° with temperature of conformer I of RBZ suggested that their values increases with rise in temperature and their respective values calculated at 298.15 K are 179.085 kcal/mol, 69.573 cal/mol-K and 145.427 cal/mol-K. The study of NLO behavior of RBZ explores that μ_0, $\Delta\alpha_0$, $|\alpha_0|$ and β_0 of RBZ is more than that of the observed value of urea and their respective values are 4.7071 debye, 84.3080×10^{-24} e.s.u, 31.2624×10^{-24} e.s.u and 1.7353×10^{-30} e.s.u. The values of μ_0, $\Delta\alpha_0$ and β_0 for RBZ are 2.7, 8.6 and 1.8 times more than that of the observed values of urea respectively. Moreover, the four favourable conformers (I-IV) of cefradine have been predicted at room temperature from the one-dimensional PES scan. The minimum value of energy −931719.0299 kcal/mol of the conformer I has been computed from the DFT and the quantum chemical calculation. The conformer II overlapped well with the Van de Streek structure and the simulated IR and the Raman spectra of conformer II matches well with the experimental spectra. The significant difference of the bond length of N8-C16 is observed as 0.018 Å in conformer II and IV with respect to the conformer I and III. This increase in bond length is due to the formation of intramolecular hydrogen bonding H27. . . N8. While comparing the bond length of conformers (I-IV) with bond length of Van de Streek structure, the prominent change is found to be 0.083 Å across O4-C18 group in all the conformers and this is due to the formation of intramolecular hydrogen bond O4. . . H31. The QTAIM study assume that the interactions H31. . . O4, H27. . . N8, H33. . . O5 show partial covalent bond with medium nature. It is predicted due to $\nabla^2\rho_{\mathrm{BCP}} > 0$, $H_{\mathrm{BCP}} < 0$ and the bond length acceptor (A) - proton (H) $< (r_{\mathrm{A}} + r_{\mathrm{H}})$. The interaction H35. . . S1 shows weak hydrogen bond as $\nabla^2\rho_{\mathrm{BCP}} > 0$, $H_{\mathrm{BCP}} < 0$ and the bond length acceptor (A) – proton (H) $> (r_{\mathrm{A}} + r_{\mathrm{H}})$. The comparative study of the simulated and the observed vibrational spectra of the cefradine molecule has been visualized about the functional groups appearing in the molecule and they are in good agreement with each other. The stretching wavenumber of C18=O5 is lowered down by 11 cm^{-1}. This change in wavenumber is due to the intermolecular hydrogen bonding with the surrounding

molecule in the solid form. But, our research is concerned with a single-molecule in the gaseous state. The NBO calculation suggested that the charge transfer from LP(1)N7→ π^*(O3–C15) plays a prominent role in the stability of the molecule with the highest stabilization energy 61.87 kcal/mol. The HOMO–LUMO energy gap gives clear picture that conformer III is more stable as it has the highest energy gap (4.7731 eV) and conformer II is more chemically reactive as it has the largest value of softness (0.2129 eV^{-1}) than the remaining three conformers. The MEP surface map proclaim that the carbonyl group (C=O) is the electrophilic region whereas the hydroxyl group (OH) is the nucleophilic region in all the four conformers. These regions are the suitable reactive sites in molecular docking. The Fukui function estimation explained that N8 and C14 are favorable sites for the nucleophilic and the electrophilic attack respectively. The docking analysis demonstrates that the reactive site of cefradine is the amine (NH_2) group. This is also justified by the largest value of the Fukui functions (FF) of N8 atom. The docking simulation reveals that the cefradine has prominent merit as the inhibitors of DPP4, FTase and COX-2.

Besides that, for cefradine (conformer II), the thermodynamic parameters: H°_m, $C^\circ_{p,m}$ and S°_m increase with rise in temperature. Their calculated values at 298.15 K, from B3LYP/6-311++G(d,p) level, are 227.983 kcal/mol, 87.930 cal/mol-K and 169.100 cal/mol-K respectively. The increase in the values of H°_m, $C^\circ_{p,m}$ and S°_m with rise in temperature justify that the atomic vibration in the molecule increases. The NLO behavior of cefradine has been scrutinized and the values of μ_0, $\Delta\alpha$, β_0 and $|\alpha_0|$ from the DFT calculation has been obtained as 5.4587 debye, 84.1207×10^{-24} e.s.u, 2.5307×10^{-30} e.s.u and 36.2435×10^{-24} e.s.u respectively. The values of μ_0, $\Delta\alpha_0$ and β_0 of cefradine are 3.1, 8.6 and 2.7 times greater than that of the experimental values of urea respectively. Thus, the high values of μ_0, $\Delta\alpha_0$ and β_0 motivate that the cefradine can be treated as a good NLO material.

Additionally, the five conformers (I-V) of frovatriptan at room temperature have been scrutinized from the one-dimensional PES graph from DFT/ B3LYP/6-311++G(d,p) level of calculation. The energy of the most stable conformer I is obtained as −491616.9411 kcal/-mol. The superposition of conformer I with conformer (II - V) of frovatriptan demonstrate that the rings R1, R2 and R3 are co-planer. Moreover, the branch chain containing the amine group (-$N4H_2$) also seems to overlap but the chain containing the methyl group (-$C16H_3$) is slightly in different plane. The comparative study of the bond lengths of conformers (II-V) with conformer I reveal that the maximum difference in the bond length is observed as 0.011 Å across the C5-C6 bond. This prominent change in the bond distance is due to the N3 atom attached to the ring R3 which takes part in the intermolecular hydrogen bonding in the crystal structure. But, our research is concerned with a single molecule in the gaseous state. Moreover, the geometry optimization signi-

fies that the atoms O1, N3 and N4 are involved in the intermolecular hydrogen bond in solid. This helps to predict the crystal structure of frovatriptan. The molecular stability has been discussed from hyper conjugative interaction which shows that the transition σ(C15-C18) $\rightarrow \sigma^*$ (C12-C14) stabilizes the molecule with the largest interaction energy 77.48 kcal/mol. The distribution of charge in the MEP surface map justified that the carbonyl group acts as electrophilic center whereas, the amine group behaves as nucleophilic center for further binding with neighboring protein. The highest value of $\Delta E_{\text{L-H}} = 4.8268$ eV and $\eta = 2.4134$ eV infer that the conformer III is more stable. But the highest value of $S = 0.2112$ eV^{-1} and minimal value of $\Delta E_{\text{L-H}} = 4.7345$ eV of conformer I shows that it is more chemical reactive. The high value the FF for the atoms C8, C10 and N3 shows that these atoms are close to the nucleophilic centers, whereas, the atoms C13, O1 and C9 are close to the electrophilic centers. The molecular docking calculation of frovatriptan provoke that it has important healing activity as anti-migraine and the predicted binding sites are $N4H_2$ and N3H27. Furthermore, the molecular docking computer simulation of frovatriptan with the expected target protein reveals the medication activity of the frovatriptan. The thermodynamic parameters: H°_{m}, $C^{\circ}_{p,m}$ and S°_{m} of the conformer I of frovatriptan increase with rise in temperature. Their calculated values at 298.15 K, from B3LYP/6-311++G(d,p) level are: 194.458 kcal/mol, 63.982 cal/mol-K and 127.547 cal/mol-K respectively. The correlation graph of thermodynamic parameters predicts that their values changes with the increase in temperature. This is due to the change in atomic vibration in the molecule. The NLO activity of frovatriptan has been examined and the values of μ_0, $\Delta\alpha$, β_0 and $|\alpha_0|$ from the DFT calculation has been calculated as 5.9568 debye, 73.7370×10^{-24} e.s.u, 6.5775×10^{-30} e.s.u and 29.4537×10^{-24} e.s.u respectively. Moreover, the respective values of μ_0, $\Delta\alpha_0$ and β_0 of frovatriptan are 3.4, 7.5 and 7 times more than that of the experimentally observed values of urea. This motivates that frovatriptan can be used as a good NLO substance.

5.2 Recommendation

The unit cell calculation of the biologically active molecules incorporates all the interactions in solid form like crystal packing and hydrogen bonding. The simulated spectra of unit cell calculation gives good resemblance with the experimental recorded spectra. Moreover, the dimer and the trimer level calculation of the API from the molecular simulation method has great attention towards the crystal structure. The solid state characterization of frovatriptan in terms of spectroscopic method like: IR, Raman and nuclear magnetic resonance (NMR) is still the interest of study. In this regard the following works have been strongly recommended for future studies.

1. The present work is based on the calculation of individual molecule in gaseous form. The unit cell calculation will be performed on the pharmaceutical com-

pounds which provide more accurate informations regarding the crystal structure and packing. The result obtained from simulated spectra of unit cell calculation gives better understanding with the experimental values. Moreover, it helps to identify the intermolecular forces that hold the surrounding molecules present in the crystal.

2. The study on dimmer and trimmer levels of RBZ and cefradine from molecular modeling for their optimization and then compare the simulated spectra with the experimental values.

3. The comparison of simulated spectra (FT-IR, FT-Raman and NMR) of frovatriptan with the experimental data.

4. The solid-state characterization of pharmaceutical compounds (APIs, biological active molecules, co-crystal, salt, etc.) from vibrational spectroscopic technique coupled with quantum chemical calculations.

CHAPTER 6

6. SUMMARY

The geometry optimization of biological active molecules: RBZ, cefradine and frovatriptan have been conducted with Gaussian 09 software from the quantum chemical methods. The minimum energy structures of RBZ, cefradine and frovatriptan have been calculated with the functional B3LYP and the 6-311++G(d,p) basis set. The one-dimensional PES scan has been employed across their flexile bonds. The possible conformers at room temperature from SCF energy have been predicted. Three possible conformers (I-III) for RBZ, four possible conformers (I-IV) for cefradine are obtained. Whereas, five possible conformers (I-V) are obtained for frovatriptan. The optimized parameters like: bond length, bond angle and dihedral angle of all the conformers of RBZ and frovatriptan have been compared with the optimized geometry of their minimum energy structure. Whereas, the optimized geometric parameters of all the conformers of cefradine have been compared with the geometric parameters of Van de Streek structure which shows good agreements. The overlapping of conformers II and III of RBZ with conformer I have been conducted which signify that the branch chain -CH_3 is in different planes, whereas, the benzene and the imidazole rings are in the same plane. Moreover, the optimized parameters of conformers (I-III) match well with each other. The optimized parameters of conformers (I-V) of frovatriptan have been compared with each other and the overlapping of conformers (II-V) have been made with conformer I which signifies that the branch chain containing the methyl group (-C16H_3) are in different planes and the other parts are coplanar. The normal modes of vibration of RBZ and cefradine have been predicted from the relation $(3N - 6)$, where N is the number of atoms in the molecule. So, 96 modes are obtained in the RBZ and 123 modes are obtained in the cefradine by using the Gar2Ped program from Pulay's recommendations. All the modes of vibration are IR and Raman active. The contributions of each mode of vibration in terms of PED have been determined. The experimental IR and Raman spectra of RBZ and cefradine exhibit good resonance with their simulated spectra. The overlapping of conformers (I-IV) of cefradine with the Van de Streek structure shows that conformer II matches well with the Van de Streek structure.

The molecular stability of the molecules: RBZ, cefradine and frovatriptan has been analyzed in terms of NBO analysis and AIM. In the RBZ molecule, the transition LP(1)N7$\rightarrow \pi^*$(O4-C18) stabilizes the molecule with largest stabilization energy. In the cefradine molecule, the transition LP(1)N7$\rightarrow \pi^*$(O3-C15) contributes the stability of molecule with apex value of interaction energy. Similarly, the transition σ(C15-C18)$\rightarrow$

σ^*(C12-C14) plays an important role for the molecular stability in the frovatriptan molecule. The MEP surface analysis of RBZ shows that the sulfinyl group (S1O2) is the most electronegative regions, whereas, the hydrogen atoms in the imidazole ring and N7H31 are most electropositive regions. In the cefradine molecule, O2, O3 and O5 atoms in all the four conformers are the electrophilic regions, whereas the blue color across H43 shows less electron density and it is a nucleophilic region. In frovatriptan molecule, the hydrogens across amine group ($N4H_2$), H26 and H27 atoms show the intense blue regions and have the highest positive potential, whereas the oxygen atom across the carbonyl group (C18=O) has a red region that shows the highest negative potential. The intramolecular hydrogen bonding forms in the RBZ and the cefradine molecules are partially covalent in nature, whereas the intramolecular hydrogen bonding is not seen in the frovatriptan. The HOMO-LUMO analysis signifies that the conformer I of RBZ is the most stable (less chemical reactive) and the conformer III is least stable (more chemical reactive) but in cefradine, conformer III is most stable (less reactive) and the conformer II is least stable (more chemically reactive). Similarly, in frovatriptan, the highest and the least value of $\Delta E_{\text{L-H}}$ for the conformer III and I infer that the former one is more stable, however, the later one is more chemically reactive. While analyzing the local reactivity descriptor of RBZ, suitable reactive sites for the electrophilic, the nucleophilic and the radical attack are O2, C12 and S1 atoms respectively. In cefradine, the prominent sites for the nucleophilic attack are S1 and N8, whereas the significant sites for the electrophilic and the radical attack are C14 and C18 respectively. In the frovatriptan molecule, the sites C8, C10 and N3 are the suitable nucleophilic center, whereas the atoms C13, O1 and C9 are suitable for the electrophilic center.

The ligand-protein interaction of biological active molecules: RBZ, cefradine and frovatriptan have been conducted with the predicted targets. The drug potential of RBZ has been analyzed in terms of molecular docking on the predicted targets: PARP, MAPK and Adenosine A2a receptor and they identify good binding affinity. In cefradine, the docking analysis has been carried out on DPP4, FTase and COX-2 targets and they exhibit good binding interactions. The docking simulation of frovatriptan compound with the receptor, 5-HT_{1B} motivates that it has important healing behavior as anti-migraine. It has the binding sites $N4H_2$ and N3H27.

The variation of thermodynamic parameters: H_m°, $C_{p,m}^\circ$ and S_m° of RBZ, cefradine and frovatriptan with temperature have been studied and their correlation graphs demonstrate that their values increase with rise in temperature due to the increase in atomic vibrations in molecule. Moreover, the NLO behavior of these molecules have been studied and the values of μ_0, $\Delta\alpha$, β_0 and $|\alpha_0|$ obtained from the DFT calculations are more than the experimental value of urea which signify that the studied molecules can also be used as NLO material.

REFERENCES

Abouel-Magd, M. H. (2018). Maternal and fetal toxicity of carisoprodol. *The Egyptian Journal of Hospital Medicine*, *71*(1), 2322–2350.

Ali, K. A., Li, G., & Wang, W. (2020). Comparative Study: The Adsorption Disparity for Tetracycline and Cefradine on Cornstalk Biochar. *Nature Environment and Pollution Technology*, *19*(4), 1379–1390.

Al-Khodir, F., & Refat, M. (2017). Physicochemical, spectroscopic, and anti-tumor studies of cefradine complexes with Ca (II), Zn (II), Fe (III), Au (III), and Pd (II) ions. *Russian Journal of General Chemistry*, *87*(5), 1087–1092.

Allais, G., Chiarle, G., Sinigaglia, S., & Benedetto, C. (2018). Menstrual migraine: a review of current and developing pharmacotherapies for women. *Expert Opinion on Pharmacotherapy*, *19*(2), 123–136.

Alyar, H., Kantarci, Z., Bahat, M., & Kasap, E. (2007). Investigation of torsional barriers and nonlinear optical (NLO) properties of phenyltriazines. *Journal of Molecular Structure*, *834–836*, 516–520.

Amidon, G. L., Lennernäs, H., Shah, V. P., & Crison, J. R. (1995). A theoretical basis for a biopharmaceutic drug classification: the correlation of in vitro drug product dissolution and in vivo bioavailability. *Pharmaceutical Research*, *12*(3), 413–420.

Andersson, M. P., & Uvdal, P. (2005). New scale factors for harmonic vibrational frequencies using the B3LYP density functional method with the triple-ζ basis set 6-311+ G (d,p). *The Journal of Physical Chemistry A*, *109*, 2937–2941.

Aschner, P., Katzeff, H. L., Guo, H., Sunga, S., Williams-Herman, D., Kaufman, K. D., ... Group, S. S. . (2010). Efficacy and safety of monotherapy of sitagliptin compared with metformin in patients with type 2 diabetes. *Diabetes, Obesity and Metabolism*, *12*(3), 252–261.

Atkins, P. (2001). *Physical Chemistry. The Extent of Adsorption.* Oxford University Press, United Kingdom.

Ayers, P. W., & Parr, R. G. (2000). Variational principles for describing chemical reactions: the Fukui function and chemical hardness revisited. *Journal of the American Chemical Society*, *122*(9), 2010–2018.

Bader, R., Anderson, S., & Duke, A. (1979). Quantum topology of molecular charge distributions. 1. *Journal of the American Chemical Society*, *101*(6), 1389–1395.

Bader, R., Slee, T., Cremer, D., & Kraka, E. (1983). Description of conjugation and hyperconjugation in terms of electron distributions. *Journal of the American Chemical Society*, *105*(15), 5061–5068.

Bader, R. F., & MacDougall, P. J. (1985). Toward a theory of chemical reactivity based on the charge density. *Journal of the American Chemical Society*, *107*(24), 6788–6795.

Bader, R. F., & Matta, C. F. (2004). Atomic charges are measurable quantum expectation values: a rebuttal of criticisms of QTAIM charges. *The Journal of Physical Chemistry A*, *108*(40), 8385–8394.

Basha, S. J., Chamundeeswari, S. V., Muthu, S., & Raajaraman, B. (2019). Quantum computational, spectroscopic investigations on 6-aminobenzimidazole by DFT/TD-DFT with different solvents and molecular docking studies. *Journal of Molecular Liquids*, *296*, 111787.

Becke, A. D. (1988). Density-functional exchange-energy approximation with correct asymptotic behavior. *Physical Review A*, *38*(6), 3098.

Becke, A. D. (1993). Density-functional thermochemistry. III. The role of exact exchange. *The Journal of Chemical Physics*, *98*, 5648–5652.

Binkley, J. S., Pople, J. A., & Hehre, W. J. (1980). Self-consistent molecular orbital methods. 21. Small split-valence basis sets for first-row elements. *Journal of the American Chemical Society*, *102*(3), 939–947.

Bolattin, M. B., Nandibewoor, S. T., Joshi, S. D., Dixit, S. R., & Chimatadar, S. A. (2016). Interaction between carisoprodol and bovine serum albumin and effect of β-cyclodextrin on binding: insights from molecular docking and spectroscopic techniques. *Royal Society of Chemistry Advances*, *6*(68), 63463–63471.

Bongioanni, A., Araújo, B. S., de Oliveira, Y. S., Longhi, M. R., Ayala, A., & Garnero, C. (2018). Improving properties of albendazole desmotropes by supramolecular systems with maltodextrin and glutamic acid. *American Association of Pharmaceutical Scientists PharmSciTech*, *19*(3), 1468–1476.

Born, M., & Oppenheimer, R. (1927). Zur quantentheorie der molekeln. *Annalen der Physik*, *389*(20), 457–484.

Brinck, T., Murray, J. S., & Politzer, P. (1993). Molecular surface electrostatic potentials and local ionization energies of Group V–VII hydrides and their anions: Relationships for aqueous and gas-phase acidities. *International Journal of Quantum Chemistry*, *48*(2), 73–88.

Bumbrah, G. S., & Sharma, R. M. (2016). Raman spectroscopy–Basic principle, instrumentation and selected applications for the characterization of drugs of abuse. *Egyptian Journal of Forensic Sciences*, *6*(3), 209–215.

Cao, L., Xu, L., Zhang, D., Zhou, Y., Zheng, Y., Fu, Q., . . . Lu, F. (2017). DA dyad and DAD triad incorporating triphenylamine, benzanthrone and perylene diimide: Synthesis, electrochemical, linear and nonlinear optical properties. *Chemical Physics Letters*, *682*, 133–139.

Carbonaro, T. M., Nguyen, V., Forster, M. J., Gatch, M. B., & Prokai, L. (2020). Carisoprodol pharmacokinetics and distribution in the nucleus accumbens correlates with behavioral effects in rats independent from its metabolism to meprobamate. *Neuropharmacology*, *174*, 108152.

Cassidy, C., Halbout, J., Donaldson, W., & Tang, C. (1979). Nonlinear optical properties of urea. *Optics Communications*, *29*(2), 243–246.

Ceperley, D. M., & Alder, B. J. (1980). Ground state of the electron gas by a stochastic method. *Physical Review Letters*, *45*(7), 566.

Chai, J.-D., & Head-Gordon, M. (2008). Long-range corrected hybrid density functionals with damped atom–atom dispersion corrections. *Physical Chemistry Chemical Physics*, *10*(44), 6615–6620.

Chandran, A., Varghese, H. T., Mary, Y. S., Panicker, C. Y., Manojkumar, T., Van Alsenoy, C., & Rajendran, G. (2012). FT-IR, FT-Raman and computational study of (E)-N-carbamimidoyl-4-((4-methoxybenzylidene) amino) benzenesulfonamide. *Spectrochimica Acta Part A: Molecular and Biomolecular Spectroscopy*, *92*, 84–90.

Chase, D. B., & Rabolt, J. F. (1994). *Fourier transform Raman spectroscopy: from concept to experiment*. Academic Press, Massachusetts.

Chattaraj, P., Nath, S., & Maiti, B. (2003). *Reactivity descriptors*. Marcel Dekker: New York.

Chattaraj, P. K., & Roy, D. R. (2007). Update 1 of: electrophilicity index. *Chemical Reviews*, *107*(9), PR46–PR74.

Chaudhary, M. K., Chaudhary, T., & Joshi, B. D. (2021). Simulated spectra (IR and Raman), NLO, AIM and molecular docking of carisoprodol from DFT approach. *BIBECHANA*, *18*(1), 48–57.

Chaudhary, M. K., Karthick, T., Joshi, B. D., Prajapati, P., de Santana, M. S. A., Ayala, A. P., . . . Tandon, P. (2021). Molecular structure and quantum descriptors of

cefradine by using vibrational spectroscopy (IR and Raman), NBO, AIM, chemical reactivity and molecular docking. *Spectrochimica Acta Part A: Molecular and Biomolecular Spectroscopy*, *246*, 118976.

Chaudhary, M. K., Prajapati, P., & Joshi, B. D. (2020). Quantum Chemical Calculation and DFT Study of Sitagliptin: Insight from Computational Evaluation and Docking Approach. *Journal of Nepal Physical Society*, *6*(1), 73–83.

Chaudhary, M. K., Prajapati, P., Srivastava, K., Silva, K. F., Joshi, B. D., Tandon, P., & Ayala, A. P. (2021). Molecular interactions and vibrational properties of ricobendazole: Insights from quantum chemical calculation and spectroscopic methods. *Journal of Molecular Structure*, *1230*, 129889.

Chaudhary, M. K., Srivastava, A., Singh, K. K., Tandon, P., & Joshi, B. D. (2020). Computational evaluation on molecular stability, reactivity, and drug potential of frovatriptan from DFT and molecular docking approach. *Computational and Theoretical Chemistry*, *1191*, 113031.

Chaudhary, T., Chaudhary, M. K., & Joshi, B. D. (2021). Topological and Reactivity Descriptor of Carisoprodol from DFT and Molecular Docking Approach. *Journal of Institute of Science and Technology*, *26*(1), 74–82.

Chaudhary, T., Chaudhary, M. K., Joshi, B. D., de Santana, M. S. A., & Ayala, A. P. (2021). Spectroscopic (FT-IR, Raman) analysis and computational study on conformational geometry, AIM and biological activity of cephalexin from DFT and molecular docking approach. *Journal of Molecular Structure*, *1240*, 130594.

Chidangil, S., Shukla, M. K., & Mishra, P. C. (1998). A molecular electrostatic potential mapping study of some fluoroquinolone anti-bacterial agents. *Molecular Modeling Annual*, *4*(8), 250–258.

Choudhary, N., Agarwal, P., Gupta, A., & Tandon, P. (2014). Quantum chemical calculations of conformation, vibrational spectroscopic, electronic, NBO and thermodynamic properties of 2, 2-dichloro-N-(2, 3-dichlorophenyl) acetamide and 2, 2-dichloro-N-(2, 3-dichlorophenyl) acetamide. *Computational and Theoretical Chemistry*, *1032*, 27–41.

Choudhary, V., Bhatt, A., Dash, D., & Sharma, N. (2019). DFT calculations on molecular structures, HOMO–LUMO study, reactivity descriptors and spectral analyses of newly synthesized diorganotin (IV) 2-chloridophenylacetohydroxamate complexes. *Journal of Computational Chemistry*, *40*(27), 2354–2363.

Clayden, J. (2000). *Organic chemistry*. Oxford University Press, London.

Colthup, N. B., Daly, L. H., & Wiberley, S. E. (1990). *Introduction to Infrared and Raman Spectroscopy*. Academic Press, New York.

Comer, M. (2002). Pharmacology of the selective 5-HT1B/1D agonist frovatriptan. *Headache: The Journal of Head and Face Pain*, *42*, 47–53.

Connolly, J. D. (1997). Natural products from around the world. *Revista Latinoamer. Quim*, 77–85.

Daina, A., Michielin, O., & Zoete, V. (2019). SwissTargetPrediction: updated data and new features for efficient prediction of protein targets of small molecules. *Nucleic Acids Research*, *47*(W1), W357–W364.

Deepika, D., Dewangan, H. K., Maurya, L., & Singh, S. (2019). Intranasal drug delivery of Frovatriptan succinate–loaded polymeric nanoparticles for brain targeting. *Journal of Pharmaceutical Sciences*, *108*(2), 851–859.

Deleu, D., & Hanssens, Y. (2000). Current and emerging second-generation triptans in acute migraine therapy: A comparative review. *The Journal of Clinical Pharmacology*, *40*(7), 687–700.

Dhillon, S. (2010). Sitagliptin. *Drugs*, *70*(4), 489–512.

Dib, A., Paredes, A. J., Eliópulos, N., Farias, C. E., Suárez, G., Aldrovandi, A., ... Sanchez Bruni, S. F. (2015). Pharmacokinetic Assessment of Novel Controlled Release Formulations of Ricobendazole Intended for Oral Administration in Dogs. *Clinical & Experimental Pharmacology*, *05*(06), 1–8.

Diogo, H. P., Ramos, J. J. M., & Piedade, M. F. M. (2018). Thermal behavior and dynamic fragility in amorphous carisoprodol. Correlation between the dynamic and thermodynamic fragilities. *Thermochimica Acta*, *663*, 99–109.

Dirac, P. A. (1930). Note on exchange phenomena in the Thomas atom. *Mathematical proceedings of the Cambridge philosophical society*, *26*(3), 376–385.

Ditchfield, R., Hehre, W. J., & Pople, J. A. (1971). Self-consistent molecular-orbital methods. IX. An extended Gaussian-type basis for molecular-orbital studies of organic molecules. *The Journal of Chemical Physics*, *54*(2), 724–728.

Du, L., & Luo, W. (2010). Crystallization optimizing of cefradine. *The Open Catalysis Journal*, *3*(1), 19–23.

Dunning, T. H. J. (1989). Gaussian basis sets for use in correlated molecular calculations. I. The atoms boron through neon and hydrogen. *The Journal of Chemical Physics*, *90*, 1007–1023.

Dunning, T. H. J., & Woon, D. E. (1995). Gaussian basis sets for use in correlated molecular calculations. V. Core-valence basis sets for boron through neon. *The Journal of Chemical Physics*, *103*, 4572–4585.

Espinosa, E., Molins, E., & Lecomte, C. (1998). Hydrogen bond strengths revealed by topological analyses of experimentally observed electron densities. *Chemical Physics Letters*, *285*(3-4), 170–173.

Fakhri, A., Rashidi, S., Asif, M., Tyagi, I., Agarwal, S., & Gupta, V. K. (2016). Dynamic adsorption behavior and mechanism of Cefotaxime, Cefradine and Cefazolin antibiotics on CdS-MWCNT nanocomposites. *Journal of Molecular Liquids*, *215*, 269–275.

Fermi, E. (1927). A statistical method for the determination of some priorieta dell'atome. *Rendiconti Lincei. Scienze Fisiche e Naturali*, *6*(602-607), 32.

Fermi, E. (1928). A statistical method for determining some properties of the atoms and its application to the theory of the periodic table of elements. *Zeitschrift für Physik*, *48*(1-2), 73–79.

Ferrari, M. D., Roon, K. I., Lipton, R. B., & Goadsby, P. J. (2001). Oral triptans (serotonin 5-HT1B/1D agonists) in acute migraine treatment: a meta-analysis of 53 trials. *The Lancet*, *358*(9294), 1668–1675.

Fock, V. (1930). Bemerkung zum virialsatz. *Zeitschrift für Physik*, *63*(11-12), 855–858.

Formentini, E., Mestorino, N., & Errecalde, J. (2005). Pharmacokinetics of ricobendazole after its intravenous, intraruminal and subcutaneous administration in sheep. *Veterinary Research Communications*, *29*(7), 595–608.

Formentini, E., Mestorino, O., Marino, E., & Errecalde, J. (2001). Pharmacokinetics of ricobendazole in calves. *Journal of Veterinary Pharmacology and Therapeutics*, *24*(3), 199–202.

Forrester, M. B. (2011). Ingestions of hydrocodone, carisoprodol, and alprazolam in combination reported to Texas poison centers. *Journal of Addictive Diseases*, *30*(2), 110–115.

Foster, J., & Weinhold, F. (1980). Natural hybrid orbitals. *Journal of the American Chemical Society*, *102*(24), 7211–7218.

Frisch, A., Nielson, A., & Holder, A. (2005). *Gauss view user manual. Pittsburgh, PA: Gaussian.* Inc.

Frisch, M. J., Trucks, G. W., Schlegel, H. B., Scuseria, G. E., Robb, M. A., Cheeseman, J. R., ... Fox, D. J. (2009). *Gaussian 09.* (Gaussian Inc. Wallingford CT)

Fukui, K. (1982). Role of frontier orbitals in chemical reactions. *Science*, *218*(4574), 747–754.

Fukui, K., Yonezawa, T., & Shingu, H. (1952). A molecular orbital theory of reactivity in aromatic hydrocarbons. *The Journal of Chemical Physics*, *20*(4), 722–725.

García, A., Barrera, M. G., Piccirilli, G., Vasconi, M. D., Di Masso, R. J., Leonardi, D., ... Lamas, M. C. (2013). Novel albendazole formulations given during the intestinal phase of Trichinella spiralis infection reduce effectively parasitic muscle burden in mice. *Parasitology International*, *62*(6), 568–570.

Geerlings, P., De Proft, F., & Langenaeker, W. (2003). Conceptual density functional theory. *Chemical Reviews*, *103*(5), 1793–1874.

Ghose, A. K., Viswanadhan, V. N., & Wendoloski, J. J. (1999). A knowledge-based approach in designing combinatorial or medicinal chemistry libraries for drug discovery. 1. A qualitative and quantitative characterization of known drug databases. *Journal of Combinatorial Chemistry*, *1*(1), 55–68.

Ghosh, D. C., & Jana, J. (1999). A study of correlation of the order of chemical reactivity of a sequence of binary compounds of nitrogen and oxygen in terms of frontier orbital theory. *Current Science*, *76*(4), 570–573.

Glendening, E. D., Badenhoop, J., & Weinhold, F. (1998). Natural resonance theory: III. Chemical applications. *Journal of Computational Chemistry*, *19*(6), 628–646.

Glendening, E. D., Landis, C. R., & Weinhold, F. (2012). Natural bond orbital methods. *Wiley Interdisciplinary Reviews: Computational Molecular Science*, *2*(1), 1–42.

Gonohe, N., Abe, H., Mikami, N., & Ito, M. (1985). Two-color photoionization of van der Waals complexes of fluorobenzene and hydrogen-bonded complexes of phenol in supersonic jets. *The Journal of Physical Chemistry*, *89*(17), 3642–3648.

Granella, F., Sances, G., Allais, G., Nappi, R., Tirelli, A., Benedetto, C., ... Nappi, G. (2004). Characteristics of menstrual and nonmenstrual attacks in women with menstrually related migraine referred to headache centres. *Cephalalgia*, *24*(9), 707–716.

Green, J., & Feinglos, M. (2008). New combination treatments in the management of diabetes: focus on sitagliptin–metformin. *Vascular Health and Risk Management*, *4*(4), 743–751.

Guirgis, G. A., Klaboe, P., Shen, S., Powell, D. L., Gruodis, A., Aleksa, V., ... Durig, J. R. (2003). Spectra and structure of silicon-containing compounds. XXXVI—Raman and infrared spectra, conformational stability, ab initio calculations and

vibrational assignment of ethyldibromosilane. *Journal of Raman Spectroscopy*, *34*(4), 322–336.

Günter, P. (2012). *Nonlinear optical effects and materials* (Vol. 72). Springer, Germany.

Guo, C., Zhang, F., Wu, X., Yu, X., Wu, X., Shi, D., & Wang, L. (2020). BTH-8, a novel poly (ADP-ribose) polymerase-1 (PARP-1) inhibitor, causes DNA double-strand breaks and exhibits anticancer activities in vitro and in vivo. *International Journal of Biological Macromolecules*, *150*, 238–245.

Guo, L., Guo, Z., & Li, X. (2018). Design and preparation of side chain electro-optic polymeric materials based on novel organic second order nonlinear optical chromophores with double carboxyl groups. *Journal of Materials Science: Materials in Electronics*, *29*(3), 2577–2584.

Gutowski, M., van Duijneveldt-van de Rijdt, J. G., van Lenthe, J. H., & van Duijneveldt, F. B. (1993). Accuracy of the Boys and Bernardi function counterpoise method. *The Journal of Chemical Physics*, *98*(6), 4728–4737.

Haddon, R. C., & Fukunaga, T. (1980). Unified theory of the thermodynamic and kinetic criteria of aromatic character in the [4n+2]annulenes. *Tetrahedron Letters*, *21*(13), 1191–1192.

Hartree, D. R. (1928). The wave mechanics of an atom with a non-Coulomb central field. Part I. Theory and methods. *Mathematical Proceedings of the Cambridge Philosophical Society*, *24*(1), 89–110.

Hehre, W. J. (1976). Ab initio molecular orbital theory. *Accounts of Chemical Research*, *9*(11), 399–406.

Hehre, W. J., Ditchfield, R., & Pople, J. A. (1972). Self—consistent molecular orbital methods. XII. Further extensions of Gaussian—type basis sets for use in molecular orbital studies of organic molecules. *The Journal of Chemical Physics*, *56*(5), 2257–2261.

Heinrich, N., Koch, W., & Frenking, G. (1986). On the use of Koopmans' theorem to estimate negative electron affinities. *Chemical Physics Letters*, *124*(1), 20–25.

Herman, G. A., Stevens, C., Van Dyck, K., Bergman, A., Yi, B., De Smet, M., . . . others (2005). Pharmacokinetics and pharmacodynamics of sitagliptin, an inhibitor of dipeptidyl peptidase IV, in healthy subjects: results from two randomized, double-blind, placebo-controlled studies with single oral doses. *Clinical Pharmacology & Therapeutics*, *78*(6), 675–688.

Hohenberg, P., & Kohn, W. (1964). Inhomogeneous electron gas. *Physical Review*, *136*(3B), B864-B871.

Holt, G. A., & Chandra, A. (2002). Herbs in the modern healthcare environment—an overview of uses, legalities, and the role of the healthcare professional. *Clinical Research and Regulatory Affairs*, *19*(1), 83–107.

Jafari, Z., Baharfar, R., Rad, A. S., & Asghari, S. (2021). Potential of graphene oxide as a drug delivery system for sumatriptan: a detailed density functional theory study. *Journal of Biomolecular Structure and Dynamics*, *39*(5), 1611–1620.

Jiang, Y., Liu, Z., Liu, H., Cui, W., Wang, N., Liu, D., & Ge, X. (2012). DFT study on nonlinear optical properties of lithium-doped corannulene. *Chinese Science Bulletin*, *57*(34), 4448–4452.

Joshi, B. D., Mishra, R., Tandon, P., Oliveira, A. C., & Ayala, A. P. (2014). Quantum chemical studies of structural, vibrational, NBO and hyperpolarizability of ondansetron hydrochloride. *Journal of Molecular Structure*, *1058*, 31–40.

Joshi, B. D., Srivastava, A., Gupta, V., Tandon, P., & Jain, S. (2013). Spectroscopic and quantum chemical study of an alkaloid aristolochic acid i. *Spectrochimica Acta Part A: Molecular and Biomolecular Spectroscopy*, *116*, 258–269.

Joshi, B. D., Srivastava, A., Honorato, S. B., Tandon, P., Pessoa, O. D. L., Fechine, P. B. A., & Ayala, A. P. (2013). Study of molecular structure, vibrational, electronic and NMR spectra of oncocalyxone A using DFT and quantum chemical calculations. *Spectrochimica Acta Part A: Molecular and Biomolecular Spectroscopy*, *113*, 367–377.

Joshi, B. D., Srivastava, A., Tandon, P., & Jain, S. (2011). Molecular structure, vibrational spectra and HOMO, LUMO analysis of yohimbine hydrochloride by density functional theory and ab initio Hartree–Fock calculations. *Spectrochimica Acta Part A: Molecular and Biomolecular Spectroscopy*, *82*(1), 270–278.

Joshi, B. D., Srivastava, A., Tandon, P., Jain, S., & Ayala, A. (2018). A combined experimental (IR, Raman and UV–Vis) and quantum chemical study of canadine. *Spectrochimica Acta Part A: Molecular and Biomolecular Spectroscopy*, *191*, 249–258.

Kalinin, A. A., Smirnov, M. A., Islamova, L. N., Fazleeva, G. M., Vakhonina, T. A., Levitskaya, A. I., ... others (2017). Synthesis and characterization of new second-order NLO chromophores containing the isomeric indolizine moiety for electro-optical materials. *Dyes and Pigments*, *147*, 444–454.

Karabacak, M., Şahin, E., Çınar, M., Erol, I., & Kurt, M. (2008). X-ray, FT-Raman, FT-IR spectra and ab initio HF, DFT calculations of 2-[(5-methylisoxazol-3-yl) amino]-2-oxo-ethyl methacrylate. *Journal of Molecular Structure*, *886*(1-3), 148–157.

Karthick, T., & Tandon, P. (2016). Computational approaches to find the active binding sites of biological targets against busulfan. *Journal of Molecular Modeling*, *22*(6), 1–9.

Kawabata, Y., Wada, K., Nakatani, M., Yamada, S., & Onoue, S. (2011). Formulation design for poorly water-soluble drugs based on biopharmaceutics classification system: basic approaches and practical applications. *International Journal of Pharmaceutics*, *420*(1), 1–10.

Keith, T., & AIMALL, V. (2009). 090201 TK Gristmill Software. *Overland Park, KS, USA*.

Keller, S., Löchte, T., Dippel, B., & Schrader, B. (1993). Quality control of food with near-infrared-excited raman spectroscopy. *Fresenius' Journal of Analytical Chemistry*, *346*(6), 863–867.

Khan, E., Shukla, A., Srivastava, A., Tandon, P., et al. (2015). Molecular structure, spectral analysis and hydrogen bonding analysis of ampicillin trihydrate: a combined DFT and AIM approach. *New Journal of Chemistry*, *39*(12), 9800–9812.

Kitchen, D. B., Decornez, H., Furr, J. R., & Bajorath, J. (2004). Docking and scoring in virtual screening for drug discovery: methods and applications. *Nature Reviews Drug Discovery*, *3*(11), 935–949.

Klastersky, J., Daneau, D., & Weerts, D. (1973). Cephradine. *Chemotherapy*, *18*(3), 191–204.

Koch, U., & Popelier, P. L. (1995). Characterization of CHO hydrogen bonds on the basis of the charge density. *The Journal of Physical Chemistry*, *99*(24), 9747–9754.

Kohn, W., & Sham, L. J. (1965). Self-consistent equations including exchange and correlation effects. *Physical Review*, *140*(4A), A1133–A1138.

Krishnan, R., Binkley, J. S., Seeger, R., & Pople, J. A. (1980). Self-consistent molecular orbital methods. XX. A basis set for correlated wave functions. *The Journal of Chemical Physics*, *72*(1), 650–654.

Kumar, K. A., Lakshmipathi, V., Meenakshi, S., & Balakrishnan, M. H. (2017). Synthesis and Characterization of Potential Impurity of Muscle Relaxant Drug Carisoprodol. *Journal of Chemistry and Chemical Sciences*, *7*(4), 352–360.

Kumru, M., Küçük, V., Kocademir, M., Alfanda, H., Altun, A., & Sarı, L. (2015). Experimental and theoretical studies on IR, Raman, and UV–Vis spectra of quinoline-7-carboxaldehyde. *Spectrochimica Acta Part A: Molecular and Biomolecular Spectroscopy*, *134*, 81–89.

Kurumbail, R. G., Stevens, A. M., Gierse, J. K., McDonald, J. J., Stegeman, R. A., Pak, J. Y., ... others (1996). Structural basis for selective inhibition of cyclooxygenase-2 by anti-inflammatory agents. *Nature*, *384*(6610), 644–648.

Lang, Q., & Wai, C. M. (2001). Supercritical fluid extraction in herbal and natural product studies—a practical review. *Talanta*, *53*(4), 771–782.

Lee, C., Yang, W., & Parr, R. G. (1988, Jan). Development of the Colle-Salvetti correlation-energy formula into a functional of the electron density. *Physical Review B*, *37*, 785–789.

Leonardi, M., Steiner, T. J., Scher, A. T., & Lipton, R. B. (2005). The global burden of migraine: measuring disability in headache disorders with WHO's Classification of Functioning, Disability and Health (ICF). *The Journal of Headache and Pain*, *6*(6), 429–440.

Lewis, D., Ioannides, C., & Parke, D. (1994). Interaction of a series of nitriles with the alcohol-inducible isoform of P450: Computer analysis of structure—activity relationships. *Xenobiotica*, *24*(5), 401–408.

Lipinski, C. A. (2004). Lead-and drug-like compounds: the rule-of-five revolution. *Drug Discovery Today: Technologies*, *1*(4), 337–341.

Lipinski, C. A., Lombardo, F., Dominy, B. W., & Feeney, P. J. (1997). Experimental and computational approaches to estimate solubility and permeability in drug discovery and development settings. *Advanced Drug Delivery Reviews*, *23*(1-3), 3–25.

Lisotto, C., Guidotti, M., Zava, D., & Savi, L. (2013). Frovatriptan and rizatriptan economic EVAluation: the FREEVA study. *The Journal of Headache and Pain*, *14*(1), 1–8.

Liu, X., Schmalz, T., & Klein, D. (1992). Favorable structures for higher fullerenes. *Chemical Physics Letters*, *188*(5-6), 550–554.

Maasumi, K., Tepper, S. J., & Kriegler, J. S. (2017). Menstrual migraine and treatment options. *Headache: The Journal of Head and Face Pain*, *57*(2), 194–208.

MacGregor, E. A., & Hackshaw, A. (2004). Prevalence of migraine on each day of the natural menstrual cycle. *Neurology*, *63*(2), 351–353.

MacGregor, E. A., Pawsey, S. P., Campbell, J. C., & Hu, X. (2010). Safety and tolerability of frovatriptan in the acute treatment of migraine and prevention of menstrual migraine: results of a new analysis of data from five previously published studies. *Gender Medicine*, *7*(2), 88–108.

Manne, R., & Åberg, T. (1970). Koopmans' theorem for inner-shell ionization. *Chemical Physics Letters*, *7*(2), 282–284.

Markus, F., & Mikko, K. (2007). Frovatriptan review. *Expert Opinion on Pharmacotherapy*, *8*(17), 3029–3033.

Martin, J. M. L., & Van Alsenoy, C. (1995). *Gar2ped*. University of Antwerp, Belgium.

Martin, R. M. (2020). *Electronic structure: basic theory and practical methods*. Cambridge University Press, United Kingdom.

Mary, Y. S., Jojo, P., Van Alsenoy, C., Kaur, M., Siddegowda, M., Yathirajan, H., ... Cruz, S. M. (2014). Vibrational spectroscopic studies (FT-IR, FT-Raman, SERS) and quantum chemical calculations on cyclobenzaprinium salicylate. *Spectrochimica Acta Part A: Molecular and Biomolecular Spectroscopy*, *120*, 340–350.

Mary, Y. S., Panicker, C. Y., Thiemann, T., Al-Azani, M., Al-Saadi, A. A., Van Alsenoy, C., ... Srivastava, S. (2015). Molecular conformational analysis, vibrational spectra, NBO, NLO analysis and molecular docking study of bis [(E)-anthranyl-9-acrylic] anhydride based on density functional theory calculations. *Spectrochimica Acta Part A: Molecular and Biomolecular Spectroscopy*, *151*, 350–359.

Maurer-Stroh, S., Washietl, S., & Eisenhaber, F. (2003). Protein prenyltransferases. *Genome Biology*, *4*(4), 1–9.

Mayans, L., & Walling, A. (2018). Acute migraine headache: treatment strategies. *American Family Physician*, *97*(4), 243–251.

McKellar, Q., Scott, E., et al. (1990). The benzimidazole anthelmintic agents-a review. *Journal of Veterinary Pharmacology and Therapeutics*, *13*(3), 223–247.

Meseguer, J. D., Codes, R. B., & Ciriza, S. A. (1994, January 11). *Stable cephradine hydrate.* Google Patents. (US Patent 5,278,157)

Mishra, S., Chaturvedi, D., Srivastava, A., Tandon, P., Ayala, A., & Siesler, H. (2010). Quantum chemical and experimental studies on the structure and vibrational spectra of efavirenz. *Vibrational Spectroscopy*, *53*(1), 112–116.

Mohan, J. (2004). *Organic spectroscopy: principles and applications*. Alpha Science Int'l Ltd., United Kingdom.

Mohan, M. K., Ponnusamy, S., & Muthamizhchelvan, C. (2017). Crystal growth and properties of novel organic nonlinear optical crystals of 4-Nitrophenol urea. *Materials Chemistry and Physics*, *195*, 224–228.

Mohan, V., Yang, W., Son, H.-Y., Xu, L., Noble, L., Langdon, R. B., . . . Kaufman, K. D. (2009). Efficacy and safety of sitagliptin in the treatment of patients with type 2 diabetes in China, India, and Korea. *Diabetes Research and Clinical Practice*, *83*(1), 106–116.

Morris, G., Huey, R., Lindstrom, W., Sanner, M., & Belew, R. (2009). DS Goodsell i AJ Olson. *Journal of Computational Chemistry*, *30*, 2785–2791.

Morris, G. M., Goodsell, D. S., Halliday, R. S., Huey, R., Hart, W. E., Belew, R. K., & Olson, A. J. (1998). Automated docking using a Lamarckian genetic algorithm and an empirical binding free energy function. *Journal of Computational Chemistry*, *19*(14), 1639–1662.

Murray, J. S., Seminario, J. M., Concha, M. C., & Politzer, P. (1992). An analysis of molecular electrostatic potentials obtained by a local density functional approach. *International Journal of Quantum Chemistry*, *44*(2), 113–122.

Muthu, K., Gunasekaran, K., Kala, A., Govindasamy, P., Rajesh, P., & Moorthi, P. (2015). Spectroscopic (FT-IR, FT-Raman & UV-Vis) and density functional theory studies of Cefadroxil. *International Journal of Current Microbiology and Applied Sciences*, *4*, 211–225.

Myneni, S. C., Traina, S. J., Waychunas, G. A., & Logan, T. J. (1998). Vibrational spectroscopy of functional group chemistry and arsenate coordination in ettringite. *Geochimica et Cosmochimica Acta*, *62*(21-22), 3499–3514.

Newman, D. J., & Cragg, G. M. (2007). Natural products as sources of new drugs over the last 25 years. *Journal of Natural Products*, *70*(3), 461–477.

Ott, J. B., & Boerio-Goates, J. (2000). *Chemical Thermodynamics: Advanced Applications: Advanced Applications*. Elsevier, Netherlands.

Padmanabhan, J., Parthasarathi, R., Subramanian, V., & Chattaraj, P. (2007). Electrophilicity-based charge transfer descriptor. *The Journal of Physical Chemistry A*, *111*(7), 1358–1361.

Padron, J., Carrasco, R., & Pellon, R. (2002). Molecular descriptor based on a molar refractivity partition using Randic-type graph-theoretical invariant. *Journal of Pharmacy & Pharmaceutical Sciences*, *5*(3), 258–266.

Palomo-Coll, A., & Palomo-Coll, A. L. (1983, September 20). *Process for the preparation of solutions of 7-aminocephalosporanic acids.* Google Patents. (US Patent 4,405,782)

Parr, R. G., & Pearson, R. G. (1983). Absolute hardness: companion parameter to absolute electronegativity. *Journal of the American Chemical Society*, *105*(26), 7512–7516.

Parr, R. G., Szentpály, L. v., & Liu, S. (1999). Electrophilicity index. *Journal of the American Chemical Society*, *121*(9), 1922–1924.

Parr, R. G., & Yang, W. (1984). Density functional approach to the frontier-electron theory of chemical reactivity. *Journal of the American Chemical Society*, *106*(14), 4049–4050.

Parr, R. G., & Yang, W. (1989a). *Density-Functional Theory of Atoms and Molecules*. Oxford University Press, United Kingdom.

Parr, R. G., & Yang, W. (1989b). *Fourier transform Raman spectroscopy: from concept to experiment*. Oxford University Press, England.

Patwardhan, B., Vaidya, A. D., & Chorghade, M. (2004). Ayurveda and natural products drug discovery. *Current Science*, *86*(6), 789–799.

Pearson, R. G. (1989). Absolute electronegativity and hardness: applications to organic chemistry. *The Journal of Organic Chemistry*, *54*(6), 1423–1430.

Perdew, J. P. (1986). Density-functional approximation for the correlation energy of the inhomogeneous electron gas. *Physical Review B*, *33*(12), 8822–8824.

Perdew, J. P., Burke, K., & Ernzerhof, M. (1996). Generalized gradient approximation made simple. *Physical Review Letters*, *77*(18), 3865–3868.

Perdew, J. P., & Wang, Y. (1992). Accurate and simple analytic representation of the electron-gas correlation energy. *Physical Review B*, *45*(23), 13244–13249.

Peterson, K. A., Woon, D. E., & Dunning Jr, T. H. (1994). Benchmark calculations with correlated molecular wave functions. IV. The classical barrier height of the H+ H2→ H2+ H reaction. *The Journal of Chemical Physics*, *100*(10), 7410–7415.

Pettersen, E. F., Goddard, T. D., Huang, C. C., Couch, G. S., Greenblatt, D. M., Meng, E. C., & Ferrin, T. E. (2004). UCSF Chimera—a visualization system for exploratory research and analysis. *Journal of Computational Chemistry*, *25*(13), 1605–1612.

Pinna, A., Wardas, J., Domenici, M. R., Popoli, P., Cossu, G., & Morelli, M. (2017). Control of Motor Function by Adenosine A2A Receptors in Parkinson's and

Huntington's Disease. In *Adenosine Receptors in Neurodegenerative Diseases* (pp. 187–213). Elsevier, Netherlands.

Polavarapu, P. L. (1990). Ab initio vibrational Raman and Raman optical activity spectra. *Journal of Physical Chemistry*, *94*, 8106–8112.

Pople, J. A., Head-Gordon, M., Fox, D. J., Raghavachari, K., & Curtiss, L. A. (1989). Gaussian-1 theory: A general procedure for prediction of molecular energies. *The Journal of Chemical Physics*, *90*(10), 5622–5629.

Pople, J. A., & Hehre, W. J. (1978). Computation of electron repulsion integrals involving contracted Gaussian basis functions. *Journal of Computational Physics*, *27*(2), 161–168.

Prajapati, P., Pandey, J., Shimpi, M. R., Srivastava, A., Tandon, P., Velaga, S. P., & Sinha, K. (2016). Combined spectroscopic and quantum chemical studies of ezetimibe. *Journal of Molecular Structure*, *1125*, 193–203.

Priotti, J., Baglioni, M. V., García, A., Rico, M. J., Leonardi, D., Lamas, M. C., & Márquez, M. M. (2018). Repositioning of anti-parasitic drugs in cyclodextrin inclusion complexes for treatment of triple-negative breast cancer. *American Association of Pharmaceutical Scientists PharmSciTech*, *19*(8), 3734–3741.

Priotti, J., Leonardi, D., Pico, G., & Lamas, M. C. (2018). Application of fluorescence emission for characterization of albendazole and ricobendazole micellar systems: elucidation of the molecular mechanism of drug solubilization process. *American Association of Pharmaceutical Scientists*, *19*(3), 1152–1159.

PubChem Compound Database. (2019a). *Albendazole oxide.* U.S. National Library of Medicine, USA.

PubChem Compound Database. (2019b). *Cefradine.* U.S. National Library of Medicine, USA.

PubChem Compound Database. (2019c). *Frovatriptan.* U.S. National Library of Medicine, USA.

Pulay, P., Fogarasi, G., Pang, F., & Boggs, J. E. (1979). Systematic ab initio gradient calculation of molecular geometries, force constants, and dipole moment derivatives. *Journal of the American Chemical Society*, *101*(10), 2550–2560.

Raafat, M., Mohamed, K., & Faten, M. (2008). Quantum chemical studies on the inhibition of corrosion of copper surface by substituted uracils. *Applied Surface Science*, *255*(5), 2433–2441.

Rajesh, S., Gunasekaran, S., & Rajesh, P. (2018). HOMO-LUMO, NBO and Vibrational analysis of Sitagliptin by using DFT calculations and Experimental Study (FT-IR, FT-Raman and UV-Visible Spectroscopies). *International Journal of ChemTech Research*, *11*(7), 107–122.

Raman, C. V., & Krishnan, K. S. (1928). A new type of secondary radiation. *Nature*, *121*(3048), 501–502.

Raz, I., Chen, Y., Wu, M., Hussain, S., Kaufman, K. D., Amatruda, J. M., . . . Alba, M. (2008). Efficacy and safety of sitagliptin added to ongoing metformin therapy in patients with type 2 diabetes. *Current Medical Research and Opinion*, *24*(2), 537–550.

Reed, A. E., Curtiss, L. A., & Weinhold, F. (1988). Intermolecular interactions from a natural bond orbital, donor-acceptor viewpoint. *Chemical Reviews*, *88*(6), 899–926.

Reed, A. E., & Weinhold, F. (1983). Natural bond orbital analysis of near-Hartree–Fock water dimer. *The Journal of Chemical Physics*, *78*(6), 4066–4073.

Reeves, R. R., & Burke, R. S. (2010). Carisoprodol: abuse potential and withdrawal syndrome. *Current Drug Abuse Reviews*, *3*(1), 33–38.

Riviere, J. E., & Papich, M. G. (2018). *Veterinary pharmacology and therapeutics*. John Wiley & Sons, USA.

Robertson, M., & Marinetti, L. (2003). Carisoprodol-effects on human performance and behavior. *Forensic Science Review*, *15*(1), 3–9.

Rose, P. W., Beran, B., Bi, C., Bluhm, W. F., Dimitropoulos, D., Goodsell, D. S., . . . others (2010). The RCSB Protein Data Bank: redesigned web site and web services. *Nucleic Acids Research*, *39*(suppl_1), D392–D401.

Rozas, I., Alkorta, I., & Elguero, J. (2000). Behavior of ylides containing N, O, and C atoms as hydrogen bond acceptors. *Journal of the American Chemical Society*, *122*(45), 11154–11161.

Rubio-Beltrán, E., Labastida-Ramírez, A., Villalón, C. M., & MaassenVanDenBrink, A. (2018). Is selective 5-HT1F receptor agonism an entity apart from that of the triptans in antimigraine therapy? *Pharmacology & Therapeutics*, *186*, 88–97.

Ryan, R., Geraud, G., Goldstein, J., Cady, R., & Keywood, C. (2002). Clinical efficacy of frovatriptan: Placebo-controlled studies. *Headache: The Journal of Head and Face Pain*, *42*(s2), 84–92.

Sanford, M. (2012). Frovatriptan. *CNS Drugs*, *26*(9), 791–811.

Saracheva, K., Vasileva, L., & Getova, D. (2019). Effects of frovatriptan and almotriptan on locomotor activity in female rats with experimental model of migraine. *Euro. Neuropsychopharmacol*, *29*, S266–S267.

Sayed, M., Aboubakr, M., & Rabea, S. (2016). Pharmacokinetics and tissue residues of cephradine in healthy and experimentally Salmonella Entretidis infected broiler chickens. *World Journal of Pharmacy and Pharmaceutical Sciences*, *5*(6), 61–74.

Schmalz, T. G., Seitz, W. A., Klein, D. J., & Hite, G. (1988). Elemental carbon cages. *Journal of the American Chemical Society*, *110*(4), 1113–1127.

Schwenke, D. W., & Truhlar, D. G. (1985). Systematic study of basis set superposition errors in the calculated interaction energy of two HF molecules. *The Journal of Chemical Physics*, *82*(5), 2418–2426.

Scott, R., Loeys, T., Davies, M., Engel, S., & Group, S. S. . (2008). Efficacy and safety of sitagliptin when added to ongoing metformin therapy in patients with type 2 diabetes. *Diabetes, Obesity and Metabolism*, *10*(10), 959–969.

Segalés Dalmau, J., Perdiguero, E., & Muñoz Cánoves, P. (2016). Regulation of muscle stem cell functions: a focus on the p38 MAPK signaling pathway. *Frontiers in Cell and Developmental Biology*, *4*, 1–15.

Settle, F. A. (1997). *Handbook of instrumental techniques for analytical chemistry*. Upper Saddle River, United States.

Shawky, L. M., Morsi, A. A., El Bana, E., & Hanafy, S. M. (2020). The Biological Impacts of Sitagliptin on the Pancreas of a Rat Model of Type 2 Diabetes Mellitus: Drug Interactions with Metformin. *Biology*, *9*(1), 6.

Shweta, Khan, E., Tandon, P., Bharti, P., Kumar, P., & Maurya, R. (2017). Experimental and quantum chemical studies on the structure and vibrational spectra of cearoin (a neoflavonoid). *Canadian Journal of Physics*, *95*(10), 905–915.

Silberstein, S. D., Elkind, A. H., Schreiber, C., & Keywood, C. (2004). A randomized trial of frovatriptan for the intermittent prevention of menstrual migraine. *Neurology*, *63*(2), 261–269.

Silverstein, R. M., G. C., Bassler, & Morrill, T. C. (1981). *Spectrometric identification of organic compounds 4th ed.* John Wiley and Sons, United States.

Silverstein, R. M., & Bassler, G. C. (1962). Spectrometric identification of organic compounds. *Journal of Chemical Education*, *39*(11), 546.

Singh, A. K., Singh, A. K., & Ebenso, E. E. (2014). Inhibition effect of cefradine on corrosion of mild steel in HCl solution. *International Journal of Electrochemical Science*, *9*, 352–364.

Singh, R., Kaur, P., Sachdeva, R., Grewal, J. S., Sathe, V., & Saini, G. (2018). Computational study of effect of solvents on vibrational spectra of coumarin 500. *Computational and Theoretical Chemistry*, *1130*, 46–57.

Sjoberg, P., Murray, J. S., Brinck, T., & Politzer, P. (1990). Average local ionization energies on the molecular surfaces of aromatic systems as guides to chemical reactivity. *Canadian Journal of Chemistry*, *68*(8), 1440–1443.

Skoog, D. A., Holler, F. J., & Crouch, S. R. (2017). *Principles of instrumental analysis*. Cengage Learning, United States.

Slater, J. C. (1937). Wave functions in a periodic potential. *Physical Review*, *51*(10), 846–851.

Smith, T. R., Sunshine, A., Stark, S. R., Littlefield, D. E., Spruill, S. E., & Alexander, W. J. (2005). Sumatriptan and naproxen sodium for the acute treatment of migraine. *Headache: The Journal of Head and Face Pain*, *45*(8), 983–991.

Song, G., Guo, Y., Li, G., Zhao, W., & Yu, Y. (2019). Comparison for adsorption of tetracycline and cefradine using biochar derived from seaweed Sargassum sp. *Desalination and Water Treatment*, *160*, 316–324.

Srivastava, A., Joshi, B., Tandon, P., Ayala, A., Bansal, A., & Grillo, D. (2013). Study of polymorphism in imatinib mesylate: A quantum chemical approach using electronic and vibrational spectra. *Spectrochimica Acta Part A: Molecular and Biomolecular Spectroscopy*, *103*, 325–332.

Srivastava, A., Mishra, S., Tandon, P., Patel, S., Ayala, A., Bansal, A., & Siesler, H. (2010). Molecular structure and vibrational spectroscopic analysis of an antiplatelet drug; clopidogrel hydrogen sulphate (form 2)–A combined experimental and quantum chemical approach. *Journal of Molecular Structure*, *964*(1-3), 88–96.

Srivastava, A., Rawat, P., Tandon, P., & Singh, R. (2012). A computational study on conformational geometries, chemical reactivity and inhibitor property of an alkaloid bicuculline with γ-aminobutyric acid (GABA) by DFT. *Computational and Theoretical Chemistry*, *993*, 80–89.

Srivastava, K. (2019). *Study of Structural Properties of Pharmaceutical Cocrystals using Vibrational Spectroscopy and Quantum Chemical Calculations* (Ph.D. thesis). University of Lucknow, Department of Physics, India.

Srivastava, K., Srivastava, A., Tandon, P., Sinha, K., & Wang, J. (2016). Spectroscopic, quantum chemical calculation and molecular docking of dipfluzine. *Journal of Molecular Structure*, *1125*, 751–762.

Stuchlíková, L. R., Matoušková, P., Vokřál, I., Lamka, J., Szotáková, B., Sečkařová, A., ... Skálová, L. (2018). Metabolism of albendazole, ricobendazole and flubendazole in Haemonchus contortus adults: sex differences, resistance-related differences and the identification of new metabolites. *International Journal for Parasitology: Drugs and Drug Resistance*, *8*(1), 50–58.

Studio, D. (2009). *2.5 Guide, Accelrys Inc., San Diego, 2009.*

Sundaraganesan, N., Ilakiamani, S., Subramani, P., & Joshua, B. D. (2007). Comparison of experimental and ab initio HF and DFT vibrational spectra of benzimidazole. *Spectrochimica Acta Part A: Molecular and Biomolecular Spectroscopy*, *67*(3-4), 628–635.

Suresh, T., Vetrivel, S., Gopinath, S., & Mullai, R. (2018). A new metal-organic nonlinear optical material: L-Asparagine Indium chloride (LAIn) for photonics application. *Chinese Journal of Physics*, *56*(6), 2773–2781.

Thamarai, A., Vadamalar, R., Raja, M., Muthu, S., Narayana, B., Ramesh, P., ... Aayisha, S. (2020). Molecular structure interpretation, spectroscopic (FT-IR, FT-Raman), electronic solvation (UV–Vis, HOMO-LUMO and NLO) properties and biological evaluation of (2E)-3-(biphenyl-4-yl)-1-(4-bromophenyl) prop-2-en-1-one: Experimental and computational modeling approach. *Spectrochimica Acta Part A: Molecular and Biomolecular Spectroscopy*, *226*, 117609.

Thomas, L. H. (1927). The calculation of atomic fields. *Mathematical Proceedings of the Cambridge Philosophical Society*, *23*(5), 542–548.

Thulluru, A., Srikanth, G., Firoz, S., Chowdary, V. E., Aruna, K., & Geetha, K. (2016). Formulation and in vitro Evaluation of Frovatriptan Succinate Oral Disintegrating Tablets by Direct Compression Technique. *Journal of PharmaSciTech*, *6*(2).

Tortorella, S., Talamo, M. M., Cardone, A., Pastore, M., & De Angelis, F. (2016). Benchmarking DFT and semi-empirical methods for a reliable and cost-efficient computational screening of benzofulvene derivatives as donor materials for small-molecule organic solar cells. *Journal of Physics: Condensed Matter*, *28*(7), 074005.

Trott, O., & Olson, A. J. (2010). AutoDock Vina: improving the speed and accuracy of docking with a new scoring function, efficient optimization, and multithreading. *Journal of Computational Chemistry*, *31*(2), 455–461.

Van de Streek, J., Rantanen, J., & Bond, A. D. (2013). Structures of cefradine dihydrate and cefaclor dihydrate from DFT-D calculations. *Acta Crystallographica Section C: Crystal Structure Communications*, *69*(11), 1229–1233.

Varsányi, G., Kovner, M. A., & Láng, L. (1973). *Assignments for vibrational spectra of 700 benzene derivatives*. Akademiai Kiado, Budapest.

Verma, R. P., & Hansch, C. (2005). A comparison between two polarizability parameters in chemical–biological interactions. *Bioorganic & Medicinal Chemistry*, *13*(7), 2355–2372.

Verma, R. P., Kurup, A., & Hansch, C. (2005). On the role of polarizability in QSAR. *Bioorganic & Medicinal Chemistry*, *13*(1), 237–255.

Vidya, S., Ravikumar, C., Hubert Joe, I., Kumaradhas, P., Devipriya, B., & Raju, K. (2011). Vibrational spectra and structural studies of nonlinear optical crystal ammonium D, L-tartrate: a density functional theoretical approach. *Journal of Raman Spectroscopy*, *42*(4), 676–684.

Vilsbøll, T., Rosenstock, J., Yki-Järvinen, H., Cefalu, W., Chen, Y., Luo, E., ... others (2010). Efficacy and safety of sitagliptin when added to insulin therapy in patients with type 2 diabetes. *Diabetes, Obesity and Metabolism*, *12*(2), 167–177.

Voet, D., & Voet, J. G. (2004). *Biochemistry* (3rd ed.). Wiley, USA.

Walter, H. S., & Ahmed, S. (2018). Targeted therapies in cancer. *Surgery*, *36*(3), 122–127.

Weiner, P. K., Langridge, R., Blaney, J. M., Schaefer, R., & Kollman, P. A. (1982). Electrostatic potential molecular surfaces. *Proceedings of the National Academy of Sciences*, *79*(12), 3754–3758.

Weinhold, F., & Landis, C. R. (2005). *Valency and bonding: a natural bond orbital donor-acceptor perspective*. Cambridge University Press, United Kingdom.

Weliky, I., Gadebusch, H., Kripalani, K., Arnow, P., & Schreiber, E. (1974). Cephradine: absorption, excretion, and tissue distribution in animals of a new cephalosporin antibiotic. *Antimicrobial Agents and Chemotherapy*, *5*(1), 49–54.

Wesley, U. V., McGroarty, M., & Homoyouni, A. (2005). Dipeptidyl peptidase inhibits malignant phenotype of prostate cancer cells by blocking basic fibroblast growth factor signaling pathway. *Cancer Research*, *65*(4), 1325–1334.

Willard, H. H., Merritt, J. L. L., Dean, J. A., & Settle, J. F. A. (1989). *Instrumental methods of analysis*. Wadsworth Publishing Company, USA.

Williams, D. J. (1984). Organic polymeric and non-polymeric materials with large optical nonlinearities. *Angewandte Chemie International Edition in English*, *23*(9), 690–703.

Williams, T. R. (1963). Infrared absorption spectroscopy (Nakanishi, Koji). *Journal of Chemical Education*, *40*(11), 616.

Williams-Herman, D., Engel, S. S., Round, E., Johnson, J., Golm, G. T., Guo, H., ... Goldstein, B. J. (2010). Safety and tolerability of sitagliptin in clinical studies: a pooled analysis of data from 10,246 patients with type 2 diabetes. *BMC Endocrine Disorders*, *10*(1), 1–21.

Woodgate, R. G., Cornell, A. J., & Sangster, N. C. (2017). Occurrence, measurement and clinical perspectives of drug resistance in important parasitic helminths of livestock. In D. L. Mayers, J. D. Sobel, M. Ouellette, K. S. Kaye, & D. Marchaim (Eds.), *Antimicrobial Drug Resistance: Clinical and Epidemiological Aspects* (Vol. 2, pp. 1305–1326). Cham: Springer International Publishing.

Wortmann, R., Krämer, P., Glania, C., Lebus, S., & Detzer, N. (1993). Deviations from Kleinman symmetry of the second-order polarizability tensor in molecules with low-lying perpendicular electronic bands. *Chemical Physics*, *173*(1), 99–108.

Wu, C.-Y., & Benet, L. Z. (2005). Predicting drug disposition via application of BCS: transport/absorption/elimination interplay and development of a biopharmaceutics drug disposition classification system. *Pharmaceutical Research*, *22*(1), 11–23.

Wu, Z., Razzak, M., Tucker, I. G., & Medlicott, N. J. (2005). Physicochemical characterization of ricobendazole: I. Solubility, lipophilicity, and ionization characteristics. *Journal of Pharmaceutical Sciences*, *94*(5), 983–993.

Wu, Z., Tucker, I. G., Razzak, M., Yang, L., McSporran, K., & Medlicott, N. J. (2010). Absorption and tissue tolerance of ricobendazole in the presence of hydroxypropyl-β-cyclodextrin following subcutaneous injection in sheep. *International Journal of Pharmaceutics*, *397*(1-2), 96–102.

Yang, W., & Mortier, W. J. (1986). The use of global and local molecular parameters for the analysis of the gas-phase basicity of amines. *Journal of the American Chemical Society*, *108*(19), 5708–5711.

Zhang, R., Du, B., Sun, G., & Sun, Y. (2010). Experimental and theoretical studies on o-, m-and p-chlorobenzylideneaminoantipyrines. *Spectrochimica Acta Part A: Molecular and Biomolecular Spectroscopy*, *75*(3), 1115–1124.

Zhao, Y., Hou, S., Liu, D., & Zhong, C. (2018). Effective adsorption of cefradine from wastewater with a stable zirconium metal–organic framework. *Industrial & Engineering Chemistry Research*, *57*(44), 15132–15137.

Zhong, J., Shen, Z., Yang, Y., & Chen, J. (2005). Preparation and characterization of uniform nanosized cephradine by combination of reactive precipitation and liquid anti-solvent precipitation under high gravity environment. *International Journal of Pharmaceutics*, *301*(1-2), 286–293.

APPENDIX

A. Optimized parameters of conformers I, II and III of ricobendazole with B3LYP/6-311++G (d,p)

Table 30: Optimized parameters of conformers I, II and III of ricobendazole with B3LYP/6-311++G (d,p).

Parameters	**Conformer I**	**Conformer II**	**Conformer III**
Bond length	(Å)	(Å)	(Å)
R(S1-O2)	1.5193	1.5193	1.520
R(S1-C9)	1.8241	1.8265	1.823
R(S1-C10)	1.8545	1.8604	1.860
R(O3-C18)	1.3443	1.3443	1.344
R(O3-C19)	1.4420	1.4419	1.442
R(O4-C18)	1.2146	1.2145	1.215
R(N5-C8)	1.3881	1.3882	1.388
R(N5-C16)	1.3675	1.3675	1.368
R(N5-H26)	1.0113	1.0113	1.011
R(N6-C11)	1.3873	1.3872	1.387
R(N6-C16)	1.3080	1.3081	1.308
R(N7-C16)	1.3859	1.3859	1.386
R(N7-C18)	1.3722	1.3721	1.372
R(N7-H31)	1.0102	1.0102	1.010
R(C8-C11)	1.4156	1.4154	1.416
R(C8-C12)	1.3896	1.3899	1.390
R(C9-C12)	1.3890	1.3889	1.389
R(C9-C14)	1.4047	1.4050	1.405
R(C10-C13)	1.5264	1.5233	1.528
R(C10-H20)	1.0939	1.0941	1.094
R(C10-H21)	1.0932	1.0938	1.092
R(C11-C15)	1.3978	1.3979	1.398
R(C12-H22)	1.0845	1.0843	1.085
R(C13-C17)	1.5329	1.5333	1.532
R(C13-H23)	1.0936	1.0938	1.096
R(C13-H24)	1.0958	1.0934	1.094
R(C14-C15)	1.3901	1.3900	1.390
R(C14-H25)	1.0850	1.0850	1.085
R(C15-H27)	1.0831	1.0831	1.083
R(C17-H28)	1.0931	1.0932	1.093
R(C17-H29)	1.0943	1.0942	1.093
R(C17-H30)	1.0940	1.0944	1.095
R(C19-H32)	1.0902	1.0902	1.090
R(C19-H33)	1.0872	1.0872	1.087
R(C19-H34)	1.0902	1.0902	1.090
Bond angle	(°)	(°)	(°)
A(O2-S1-C9)	106.7487	106.3707	106.8809

A(O2-S1-C10)	106.0922	106.6481	105.6795
A(C9-S1-C10)	97.1479	98.5855	96.8624
A(C18-O3-C19)	115.6833	115.7019	115.6778
A(C8-N5-C16)	106.0386	106.0338	106.0371
A(C8-N5-H26)	130.0300	129.9961	130.0071
A(C16-N5-H26)	123.9311	123.9693	123.9555
A(C11-N6-C16)	104.2224	104.2222	104.2260
A(C16-N7-C18)	125.4374	125.4641	125.4565
A(C16-N7-H31)	115.6320	115.6193	115.6186
A(C18-N7-H31)	118.9297	118.9121	118.9238
A(N5-C8-C11)	104.7781	104.7794	104.7793
A(N5-C8-C12)	132.3660	132.3745	132.3791
A(C11-C8-C12)	122.8543	122.8447	122.8401
A(S1-C9-C12)	117.1465	117.1286	117.0970
A(S1-C9-C14)	119.9866	120.0225	120.0269
A(C12-C9-C14)	122.7932	122.7061	122.8029
A(S1-C10-C13)	110.6042	114.0429	111.1669
A(S1-C10-H20)	106.4998	103.3931	106.5559
A(S1-C10-H21)	106.0714	106.0346	105.3628
A(C13-C10-H20)	112.1699	111.3234	112.3162
A(C13-C10-H21)	111.9763	113.1062	111.7738
A(H20-C10-H21)	109.1969	108.2990	109.3061
A(N6-C11-C8)	110.3305	110.3397	110.3333
A(N6-C11-C15)	129.8641	129.8729	129.8547
A(C8-C11-C15)	119.7995	119.7816	119.8060
A(C8-C12-C9)	115.8411	115.8993	115.8481
A(C8-C12-H22)	124.2882	124.3134	124.3122
A(C9-C12-H22)	119.8649	119.7848	119.8348
A(C10-C13-C17)	111.9963	111.9577	114.3548
A(C10-C13-H23)	108.8095	109.4943	107.3340
A(C10-C13-H24)	109.5485	108.4755	108.5767
A(C17-C13-H23)	109.8512	109.8160	109.5871
A(C17-C13-H24)	109.6950	110.0800	110.3826
A(H23-C13-H24)	106.7987	106.8765	106.2529
A(C9-C14-C15)	120.5811	120.6296	120.5580
A(C9-C14-H25)	119.8036	119.8761	119.8320
A(C15-C14-H25)	119.6115	119.4911	119.6061
A(C11-C15-C14)	118.1156	118.1207	118.1315
A(C11-C15-H27)	120.4907	120.4881	120.4825
A(C14-C15-H27)	121.3900	121.3863	121.3820
A(N5-C16-N6)	114.6304	114.6248	114.6244
A(N5-C16-N7)	122.7503	122.7807	122.7687
A(N6-C16-N7)	122.6193	122.5944	122.6068
A(C13-C17-H28)	110.7641	110.6715	110.7323
A(C13-C17-H29)	111.5206	111.3227	111.7212
A(C13-C17-H30)	111.1856	111.5883	111.2530
A(H28-C17-H29)	107.7401	107.6281	107.4721

A(H28-C17-H30)	107.6928	107.6786	107.7409
A(H29-C17-H30)	107.7687	107.7748	107.7374
A(O3-C18-O4)	125.0786	125.0896	125.0805
A(O3-C18-N7)	109.8413	109.8270	109.8354
A(O4-C18-N7)	125.0801	125.0833	125.0841
A(O3-C19-H32)	110.3627	110.3517	110.3550
A(O3-C19-H33)	105.1021	105.1022	105.1043
A(O3-C19-H34)	110.3585	110.3803	110.3557
A(H32-C19-H33)	110.6730	110.6599	110.6704
A(H32-C19-H34)	109.6110	109.6052	109.6105
A(H33-C19-H34)	110.6653	110.6737	110.6767
Dihedral angle	(°)	(°)	(°)
D(O2-S1-C9-C12)	4.0022	-0.2963	3.4854
D(O2-S1-C9-C14)	-172.9637	-176.0687	-173.4907
D(C10-S1-C9-C12)	-105.2344	-110.5595	-105.2370
D(C10-S1-C9-C14)	77.7997	73.6680	77.7869
D(O2-S1-C10-C13)	67.9003	-43.3868	65.8408
D(O2-S1-C10-H20)	-169.9712	77.6464	-171.4818
D(O2-S1-C10-H21)	-53.7255	-168.5096	-55.4180
D(C9-S1-C10-C13)	177.6831	66.6523	175.5694
D(C9-S1-C10-H20)	-60.1885	-172.3145	-61.7532
D(C9-S1-C10-H21)	56.0573	-58.4704	54.3105
D(C19-O3-C18-O4)	-0.0724	-0.2218	-0.0683
D(C19-O3-C18-N7)	179.9219	179.8005	179.9724
D(C18-O3-C19-H32)	-60.4587	-60.7804	-60.7445
D(C18-O3-C19-H33)	-179.8121	179.8873	179.9078
D(C18-O3-C19-H34)	60.8457	60.5238	60.5522
D(C16-N5-C8-C11)	-0.0627	0.0147	-0.0444
D(C16-N5-C8-C12)	-179.5925	-179.5597	-179.5868
D(H26-N5-C8-C11)	179.7434	179.7083	179.7496
D(H26-N5-C8-C12)	0.2136	0.1339	0.2072
D(C8-N5-C16-N6)	0.0504	-0.0364	0.0330
D(C8-N5-C16-N7)	-179.9216	179.9332	-179.9252
D(H26-N5-C16-N6)	-179.7706	-179.7534	-179.7768
D(H26-N5-C16-N7)	0.2574	0.2162	0.2650
D(C16-N6-C11-C8)	-0.0290	-0.0293	-0.0246
D(C16-N6-C11-C15)	179.0672	179.0787	179.0618
D(C11-N6-C16-N5)	-0.0134	0.0407	-0.0053
D(C11-N6-C16-N7)	179.9587	-179.9289	179.9529
D(C18-N7-C16-N5)	-0.1002	-0.4001	-0.2540
D(C18-N7-C16-N6)	179.9300	179.5670	179.7912
D(H31-N7-C16-N5)	-179.7514	-179.6224	-179.8525
D(H31-N7-C16-N6)	0.2788	0.3447	0.1927
D(C16-N7-C18-O3)	-179.7717	-179.4288	-179.7379
D(C16-N7-C18-O4)	0.2227	0.5935	0.3028
D(H31-N7-C18-O3)	-0.1309	-0.2299	-0.1515
D(H31-N7-C18-O4)	179.8634	179.7924	179.8892

D(N5-C8-C11-N6)	0.0583	0.0087	0.0438
D(N5-C8-C11-C15)	-179.1422	-179.2025	-179.1479
D(C12-C8-C11-N6)	179.6448	179.6346	179.6415
D(C12-C8-C11-C15)	0.4442	0.4233	0.4498
D(N5-C8-C12-C9)	179.7355	179.7877	179.6929
D(N5-C8-C12-H22)	0.6142	0.3694	0.5062
D(C11-C8-C12-C9)	0.2767	0.2775	0.2196
D(C11-C8-C12-H22)	-178.8446	-179.1408	-178.9672
D(S1-C9-C12-C8)	-178.1150	-176.9666	-178.0329
D(S1-C9-C12-H22)	1.0478	2.4799	1.1927
D(C14-C9-C12-C8)	-1.2413	-1.3168	-1.1478
D(C14-C9-C12-H22)	177.9215	178.1296	178.0778
D(S1-C9-C14-C15)	178.2896	177.2042	178.2192
D(S1-C9-C14-H25)	-1.0032	-2.1473	-1.0555
D(C12-C9-C14-C15)	1.5015	1.6760	1.4221
D(C12-C9-C14-H25)	-177.7913	-177.6754	-177.8526
D(S1-C10-C13-C17)	-178.1576	172.0703	69.1105
D(S1-C10-C13-H23)	-56.5236	-65.8927	-169.1013
D(S1-C10-C13-H24)	59.8954	50.4015	-54.6318
D(H20-C10-C13-C17)	63.1022	55.5559	-50.1801
D(H20-C10-C13-H23)	-175.2638	177.5930	71.6081
D(H20-C10-C13-H24)	-58.8448	-66.1129	-173.9225
D(H21-C10-C13-C17)	-60.0815	-66.6521	-173.4643
D(H21-C10-C13-H23)	61.5525	55.3849	-51.6761
D(H21-C10-C13-H24)	177.9715	171.6791	62.7933
D(N6-C11-C15-C14)	-179.2469	-179.1463	-179.2232
D(N6-C11-C15-H27)	0.0627	0.0590	0.0679
D(C8-C11-C15-C14)	-0.2236	-0.1099	-0.2105
D(C8-C11-C15-H27)	179.0860	179.0954	179.0806
D(C10-C13-C17-H28)	179.7213	-179.8731	178.2982
D(C10-C13-C17-H29)	-60.2924	-60.2208	-61.9426
D(C10-C13-C17-H30)	60.0163	60.2358	58.5093
D(H23-C13-C17-H28)	58.6875	58.2742	57.7537
D(H23-C13-C17-H29)	178.6738	177.9265	177.5129
D(H23-C13-C17-H30)	-61.0175	-61.6169	-62.0352
D(H24-C13-C17-H28)	-58.4156	-59.1307	-58.9336
D(H24-C13-C17-H29)	61.5707	60.5216	60.8256
D(H24-C13-C17-H30)	-178.1207	-179.0218	-178.7225
D(C9-C14-C15-C11)	-0.7022	-0.8906	-0.6800
D(C9-C14-C15-H27)	179.9948	179.9116	-179.9644
D(H25-C14-C15-C11)	178.5920	178.4634	178.5963
D(H25-C14-C15-H27)	-0.7110	-0.7344	-0.6881

B. Theoretical and experimental vibrational wavenumber (cm^{-1}) for conformers (I-III) of ricobendazole with potential energy distribution (PED)

Table 31: Theoretical and experimental vibrational wavenumber (cm^{-1}) for conformers (I-III) of ricobendazole with potential energy distribution (PED).

Unscaled DFT	Scaled DFT			Experimental		PED Assignment
	I	II	III	IR	Raman	
3624	3508	3509	3508	–	–	ν(N7H)(99)
3602	3487	3488	3486	3390	–	R2[ν(NH)](99)
3196	3093	3093	3092	3167	–	R1[ν_s(CH)](99)
3181	3079	3081	3078	–	–	R1[ν(CH)](99)
3166	3064	3064	3064	–	3065	$\nu_a(C19H_3)$(99)
3163	3061	3062	3061	3065	–	R1[ν_s(CH)](99)
3134	3033	3033	3033	3020	3020	$\nu_a(C19H_3)$(100)
3104	3005	3001	3007	–	–	$\nu_a(C10H_2)$(81) + $\nu(C13H_2)$(9)
3090	2991	2989	2996	2995	2996	$\nu_a(C17H_3)$(98)
3086	2987	2986	2988	–	–	$\nu_a(C17H_3)$(66) + $\nu(C13H_2)$(14) + $\nu_a(C10H_2)$(14)
3064	2965	2968	2963	2969	2971	$\nu_a(C13H_2)$(67) + $\nu_a(C17H_3)$(26)
3057	2959	2959	2959	–	–	$\nu_s(C19H_3)$(100)
3039	2942	2947	2944	2949	2948	$\nu_s(C10H_2)$(93) + $\nu(C13H_2)$(5)
3024	2927	2939	2928	2872	–	$\nu_s(C13H_2)$(83) + $\nu_s(C17H_3)$(11)
3022	2925	2923	2927	–	2923	$\nu_s(C17H_3)$(89) + $\nu(C13H_2)$(9)
1772	1716	1716	1716	1729	1720	ν(C=O)(67) + ρ(N7C18)(13) + ν(N7C18)(7) + ν(O3C18)(6)
1672	1618	1618	1618	1631	1635	R2[ν(C=N)(14) + ν(N7C16)(9) + ν(N5C8)(6) + δ_{sci}(N7C16)(5)] + R1[ν(CC)(29) + δ_{asym}(5)]
1615	1563	1563	1564	1587	1588	R1[ν(CC)](61) + δ(CH)(6)] + R2[ν(N7C16)](6)
1602	1551	1551	1551	1575	–	R1[ν(CC)](25) + R2[ν(N7C16)(14) + ν(C=N)(11) + δ_{sci}(N7C16)(6) + δ(6)]
1526	1477	1477	1477	1516	1524	R2[ν(N5C16)(23) + δ_{sci}(N7C16)(15) + ρ(N7C16)(14) + δ(NH)(9) + δ'(6)] + ν(N7C18)(7)
1510	1461	1461	1456	1466	1466	$C13H_2$ [δ'_{asym}(31) + δ_{sym}(14) + δ_{asym} (12)] + $C17H_3$[δ'_{asym}(24) + δ_{asym}(11)]
1501	1452	1452	1453	–	–	$C19H_3$[δ'_{asym}(49) + δ_{asym}(16) + δ_{sym} (15) + ρ'(7)]
1499	1451	1451	1452	1447	–	$C17H_3$[δ_{asym}(62) + δ'_{asym}(30) + ρ'(8)]
1496	1448	1448	1443	–	–	$C17H_3$[δ'_{asym}(34) + δ_{asym}(17)] + $C13H_2$[δ'_{asym}(28) + δ_{asym}(11) + δ_{sym}(5)]
1490	1442	1443	1441	–	–	$C19H_3$[δ_{sym}(14) + δ'_{asym}(11)] + R2[ν(C=N)(11) + δ(8)] + R1[δ(CH)(9) + ν(CC)(13] + ν(N7C18)(6)

1484	1437	1437	1436	–	–	$C19H_3[\delta_{asym}(70) + \delta'_{asym}(22) + \rho(6)]$
1478	1431	1431	1431	1429	1430	$R1[\nu(CC)](21) + \delta(CH)(28)] + R2[\nu(N5C16)(10) + \nu(N6C11)(5) + \nu(N7C16)(5)] + \delta_{sym}(C19H_3)(7)$
1468	1421	1421	1421	1415	1413	$\delta_{sym}(C19H_3)(28) + R1[\nu(CC)(26) + \delta(CH)(11)] + R2[\nu(N5C8)(9)]$
1449	1403	1409	1399	–	1401	$C10H_2[\delta'_{asym}(65) + \delta_{asym}(22) + \delta_{sym}(7)]$
1445	1399	1399	1399	–	–	$\delta_{sym}(C19H_3)(20) + R2[\nu(C=N)(20) + \delta_{sci}(N7C16)(14) + \nu(N5C16)(7)] + \nu(N7C18)(10)$
1413	1367	1367	1372	1368	1365	$\delta_{sym}(C17H_3)(92) + \nu(C13C17)(7)$
1373	1329	1328	1334	–	–	$C13H_2[\delta_{sym}(44) + \rho(14) + \delta'_{asym}(10)] + \delta_{sym}(C10H_2)(10) + \nu(C10C13)(6) + \nu(C13C17)(5)$
1371	1327	1327	1327	1303	1303	$R1[\nu(CC)](72)]$
1328	1285	1284	1282	–	–	$C13H_2[\rho'(47) + \delta_{asym}(22) + \delta'_{asym}(9)] + \delta_{asym}(C10H_2)(11)$
1310	1268	1269	1267	–	–	$R1[\delta(CH)(35) + \delta_{tri}(5)] + R2[\delta(NH)(18) + \nu(N5C8)(13) + \nu(N7C16)(6)]$
1294	1253	1253	1253	1253	1246	$R2[\nu(N6C11)(27) + \nu(N5C8)(10)] + R1[\nu(CC)(35) + \delta(CH)(9)]$
1254	1214	1227	1222	1228	1224	$C10H_2[\delta_{sym}(57) + \rho(14) + \delta'_{asym}(8)] + \delta_{sym}(C13H_2)(7)$
1242	1202	1203	1201	–	–	$R1[\delta(CH)](37) + \nu(CC)(8) + (\delta_{tri})(7)] + R2[\nu(N6C11)](19)$
1240	1200	1197	1197	1193	1191	$C10H_2[\delta_{asym}(25) + \rho'(9) + \delta_{sym}(5)] + \rho'(C17H_3)(21) + \delta_{asym}(C13H_2)(15)$
1236	1197	1197	1185	–	–	$\nu(O3C18)(33) + R2[\delta_{sci}(N7C16)](17) + \rho(N7C16)(11)] + N7C18[\nu(14) + \rho(6)] + \nu(O3C19)(6)$
1215	1176	1176	1176	–	–	$C19H_3[\rho'(47) + \rho(16) + \delta'_{asym}(6)] + \nu(O3C18)(7)$
1209	1170	1171	1170	–	1158	$R2[\delta(NH)(32) + \nu(N5C8)(12) + \nu(N7C16)(8)] + R1[\delta_{tri}(12)] + \rho'(C19H_3)(6)$
1175	1137	1137	1137	1127	1123	$C19H_3[\rho(69) + \rho'(24) + \delta_{asym}(5)]$
1143	1107	1108	1107	1092	1089	$R1[\delta(CH)(56) + \nu(CC)(17) + \delta_{tri}(6)]$
1105	1070	1071	1067	–	–	$\rho(C17H_3)(35) + \nu(C10C13)(33) + \rho(C13H_2)(13) + \rho(C10H_2)(7)$
1103	1067	1068	1056	1043	–	$\nu(O3C19)(25) + \nu(N7C18)(15) + R2[\nu(N5C16)(11) + \delta_{sci}(N7C16)(11)] + \nu(O3C18)(6)$
1075	1040	1038	1036	–	1045	$\rho'(C10H_2)(40) + \rho'(C13H_2)(19) + \rho'(C17H_3)(12) + \nu(SO)(9)$
1054	1021	1022	1024	1026	–	$R1[\nu(CC)(39) + \delta(CH)(21) + \nu(SC)(10)] + \rho'(C10H_2)(6)$
1038	1005	1005	1010	1006	1008	$\nu(C13C17)(64) + \nu(C10C13)(21)$
1023	990	990	989	–	–	$R2[\nu(N5C16)(24) + \delta'(20) + \nu(N7C16)(8) + \nu(C=N)(5)] + \nu(O3C19)(16)$
1011	979	981	975	–	962	$\nu(SO)(82)$
976	945	945	944	957	–	$\nu(O3C19)(32) + \rho(N7C18)(19) + \nu(O3C18)(14) + R2[\rho(N7C16)(9)]$
952	922	923	921	927	922	$R1[oop(CH)](86) + puck(6) + \tau'_a(5)]$
929	899	899	899	–	–	$R1[\delta_{tri}(42) + \nu(SC)(10) + \delta_{asym}(8)] + R2[\nu(N5C8)(10) + \delta(5)]$
912	883	883	878	883	882	$R1[oop(CH)(65) + puck(7)] + \rho(C17H_3)(7) + \nu(C10C13)(6)$
906	877	879	868	860	860	$R1[oop(CH)](30) + \nu(C10C13)(22) + \rho(C17H_3)(20) + \nu(C13C17)(13)$
863	836	836	835	840	–	$R1[\nu(CC)(20)] + \rho'(C17H_3)(12) + R2[\delta'(12) + \nu(N6C11)(6)] + \delta_{asym}(C13H_2)(6) + C10H_2[\rho'(5) + \delta_{asym}(5)]$
862	835	831	820	818	–	$\rho'(C17H_3)(26) + C13H_2[\delta_{asym}(12) + \delta'_{asym}(5)] + C10H_2[\rho'(11) + \delta_{asym}(9)] + R1[\nu(CC)](7) + R2(\delta')(5)$

822	796	795	795	799	–	R1[oop(CH)(68) + τ_a(12)] + R2(τ')(6)
770	745	745	767	764	749	ω(N7C18)(58) + R1[puck(18) + oop(CH)(5)] + R2(τ')(7)
769	744	744	745	–	–	δ_{sym}(N7C18)(15) + ν(O3C18)(14) + R2[ρ(N7C16)(12) + δ'(11) + δ(N7C16)(5)] + R1(δ'$_{asym}$)(8) + ν(O3C19)(6) + δ(C19O3C18)(5)
759	735	736	744	–	735	R1[puck(48) + oop(CH)(7)] + R2(τ')(20) + ω(N7C18)(13)
750	726	721	734	–	–	$C13H_2$[ρ'(27) + δ_{asym}(14) + δ'$_{asym}$(5)] + $C10H_2$[δ_{asym}(17) + ρ'(5) + δ'$_{asym}$(5)] + ρ'($C17H_3$)(12) + τ(C10C13)(5)
733	710	710	710	–	710	δ_{sym}(N7C18)(41) + δ(C19O3C18)(10) + R2[δ'(9)] + R1[δ_{asym}(6) + δ'$_{asym}$(6)] + ν(O3C18)(6)
716	693	694	693	–	694	R2[τ(49) + oop(N7C16)(41) + τ'(6)]
706	683	681	683	–	–	R2(δ)(33) + R1[δ_{asym}(20) + ν(SC)(17)+ ν(CC)(6)]
683	661	632	609	647	645	ν(SC10)(59) + ρ($C10H_2$)(6) + ρ($C13H_2$)(6)
619	599	608	581	612	613	R1[puck(24) + oop(CS)(22) + τ_a(21) + τ'$_a$(5)] + R2[τ'(6) + oop(NH)(5)]
599	580	579	578	585	584	R1[δ'$_{asym}$(39) + ν(CC)(8) + ν(SC)(7)] + R2[δ(9)] + δ_{sym}(N7C18)(8)
590	571	577	567	–	–	R2[oop(NH)(62) + τ'(13) + oop(N7C16)(6)] + R1[τ_a(6)]
560	542	545	545	530	528	τ(N7C18)(38) + R2[ω(N7C16)(32) + τ(N7C16)(25)]
513	496	498	496	–	–	R1[δ_{asym}(20) + δ'$_{asym}$(20)+ ω(SC9)(10)] + R2[δ(N7C16)(17)] + δ_{sym}(N7C18)(5)
462	447	471	459	459	451	R1[ω(SC9)(32) + δ_{sci}(SC9)(13) + ν(SC)(8)] + ρ(N7C18)(7)
446	432	430	430	438	438	R1[τ'$_a$(42) + τ_a (13) + oop(CS)(5)] + τ(N5C8C11C15)(25)
411	398	413	403	–	410	R1[δ_{sci}(SC9)(13) + ω(SC9)(11) + puck(10)] + $C10H_2$[ρ'(10) + ρ(5)] + ρ($C13H_2$)(8) + R2[oop(N7C16)(6)]
382	370	365	379	–	397	R1[ρ(C9S)(11) + δ_{sci}(SC9)(9) + δ(CS)(6) + puck(5) + oop(CS)(5)] + ρ(N7C18)(6) + R2[δ(N7C16)(6) + oop(N7C16)(6)] + δ(C19O3C18)(5)
368	356	354	359	–	349	δ(C19O3C18)(31) + ρ(N7C18)(14) + R1[ω(SC9)(9) + ρ(C9S)(6)] + R2[ν(N7C16)(8)]
350	339	347	353	–	341	R1[ν(SC)(10) + τ_a(6) + τ'$_a$(5) + δ(CS)(5) + ρ(C9S)(5)] + ρ($C13H_2$)(7) + δ_{sym}(N7C18)(7) + R2[δ(N7C16)(5) + oop(N7C16)(5)]
312	302	296	330	–	312	R1[δ_{sci}(SC9)(14) + ρ(C9S)(7) + τ'$_a$(6)] + R2[τ'(9) + oop(NH)(6)] + ρ($C13H_2$)(8) + τ(N5C8C11C15)(7) + δ_{sym}(N7C18)(6)
285	276	282	289	–	–	R1[δ_{sci}(SC9)(20)] + ρ($C13H_2$)(15) + ν(SC10)(13) R2(τ')(8) + τ(N5C8C11C15)(6)
270	261	261	258	–	–	τ(N5C8C11C15)(16) + R2[τ'(14) + oop(NH)(7)] R1[τ_a(12) + τ'$_a$(6) + oop(CS)(6)] + δ(C19O3C18)(5)
252	244	244	243	–	–	δ(C19O3C18)(16) + R2[δ(N7C16)](12) + ρ(N7C18)(10) + R1[ρ(C9S)(9) + δ_{asym}(8) + ω(SC9)(7) + δ_{sci}(SC9)(6)]
245	237	238	241	–	227	τ(C13C17)(85)

222	215	215	212	–	–	τ(N5C8C11C15)(26) + R1[τ_a(18) + ν(SC)(7) + τ' $_a$(5)]
200	193	192	176	–	–	ρ(C10H$_2$)(15) + τ(N5C8C11C15)(15) + τ(O3C18)(9) + R1[oop(CS)(6) + ν(SC)(5)] + R2[ω(N7C16)](6) + τ(N7C18)(6) + ρ(C13H$_2$)(5)
162	157	160	161	–	164	τ(O3C18)(37) + τ(O3C19)(17) + R1[τ_a(9)] + τ(N7C18)(8) + ρ(C10H$_2$)(6)
156	151	151	149	–	–	R1[δ(CS)(38) + ω(SC9)(14) + ρ(C9S)(5)] + ρ(N7C18)(7) + R2[ρ(N7C16)(6)] + τ(SC10)(6)
121	117	134	124	–	–	τ(O3C19)(34) + R1[τ_a(11) + ρ(C9S)(7)] + ρ(C10H$_2$)(6) + R2[ω(N7C16)(5)]
107	104	109	106	–	–	τ(O3C18)(36) + τ(O3C19)(32) + R2[oop(NH)(8) + τ(N7C16)(6)]
95.1	92	101	103	–	–	τ(C10C13)(49) + R1[τ(SC9)(20)] + R2[τ(N7C16)(5)]
84.3	81.6	76.5	82.2	–	–	τ(SC10)(45) + R2[δ(N7C16)(13) + ρ(N7C16)(10)] + τ(C10C13)(5)
77.7	75.2	70.2	73.9	–	–	R2[τ(N7C16)(33) + oop(NH)(14)] + τ(C10C13)(11) + τ(N7C18)(10) + R1[δ_{sci}(SC9)(5)]
66.8	64.6	62.9	57.1	–	–	τ(SC10)(28) + R1[δ(CS)(17) + τ(SC9)(7)] + R2[τ(N7C16)(7) + δ(N7C16)(7)]
48.8	47.2	48.8	46.3	–	–	R2[τ(N7C16)(19) + ω(N7C16)(15) + oop(NH)(10)] + R1[oop(CS)(17) + ρ(C9S)(10) + δ_{sci}(SC9)(5) + ω(SC9)(5)] + ρ(C10H$_2$)(5)
45.3	43.8	38.9	35.3	–	–	R1[τ(SC9)(21)] + R2[ω(N7C16)(18) + oop(NH)(6)] + τ(N7C18)(14) + τ(SC10)(5)
22.2	21.4	24.7	21.3	–	–	R1[τ(SC9)(38) + oop(CS)(9)] + R2[τ(N7C16)(10) + oop(NH)(9) + ω(N7C16)(9)] + τ(SC10)(5)

C. Optimized geometrical parameters (bond length, bond angle and dihedral angle) of cefradine at B3LYP/6-311++G(d,p) level

Table 32: Optimized geometrical parameters (bond length, bond angle and dihedral angle) of cefradine at B3LYP/6-311++G(d,p) level.

Parameters	DFT-D*	B3LYP			
		Conformer I	Conformer II	Conformer III	Conformer IV
Bond length		(Å)	(Å)	(Å)	(Å)
R(S1-C9)	1.805	1.832	1.831	1.832	1.831
R(S1-C13)	1.828	1.838	1.838	1.838	1.837
R(O2-C11)	1.234	1.197	1.198	1.197	1.197
R(O3-C15)	1.250	1.218	1.219	1.219	1.219
R(O4-C18)	1.271	1.354	1.350	1.354	1.354
R(O4-H43)	-	0.970	0.969	0.970	0.970
R(O5-C18)	1.275	1.204	1.208	1.204	1.204
R(N6-C9)	1.468	1.458	1.460	1.458	1.459
R(N6-C11)	1.372	1.399	1.398	1.399	1.397
R(N6-C12)	1.400	1.406	1.409	1.406	1.407
R(N7-C10)	1.438	1.426	1.429	1.426	1.429
R(N7-C15)	1.350	1.368	1.370	1.367	1.367
R(N7-H27)	1.055	1.014	1.010	1.014	1.011
R(N8-C16)	1.499	1.477	1.459	1.477	1.460
R(N8-H37)	1.068	1.015	1.015	1.016	1.013
R(N8-H38)	1.054	1.016	1.013	1.014	1.016
R(C9-C10)	1.568	1.569	1.569	1.569	1.569
R(C9-H25)	1.101	1.091	1.091	1.091	1.091
R(C10-C11)	1.543	1.551	1.550	1.551	1.551
R(C10-H26)	1.098	1.091	1.091	1.091	1.091
R(C12-C14)	1.349	1.350	1.352	1.350	1.350
R(C12-C18)	1.517	1.499	1.494	1.498	1.498
R(C13-C14)	1.508	1.516	1.515	1.516	1.516
R(C13-H28)	1.101	1.093	1.093	1.093	1.093
R(C13-H29)	1.103	1.096	1.096	1.096	1.096
R(C14-C17)	1.499	1.506	1.505	1.506	1.506
R(C15-C16)	1.534	1.545	1.541	1.546	1.547
R(C16-C19)	1.503	1.520	1.526	1.519	1.520
R(C16-H30)	1.101	1.096	1.098	1.096	1.103
R(C17-H31)	1.101	1.086	1.096	1.086	1.086
R(C17-H32)	1.105	1.096	1.095	1.096	1.096
R(C17-H33)	1.098	1.096	1.086	1.096	1.095
R(C19-C20)	1.502	1.513	1.512	1.512	1.510
R(C19-C21)	1.340	1.335	1.337	1.335	1.338
R(C20-C23)	1.498	1.504	1.504	1.504	1.503
R(C20-H34)	1.105	1.098	1.099	1.101	1.097
R(C20-H35)	1.109	1.099	1.100	1.099	1.100
R(C21-C22)	1.493	1.503	1.503	1.503	1.504

R(C21-H36)	1.093	1.087	1.088	1.088	1.089
R(C22-C24)	1.497	1.503	1.503	1.503	1.504
R(C22-H39)	1.109	1.100	1.100	1.100	1.100
R(C22-H40)	1.106	1.100	1.100	1.100	1.100
R(C23-C24)	1.335	1.331	1.331	1.331	1.332
R(C23-H41)	1.091	1.086	1.087	1.087	1.087
R(C24-H42)	10.91	1.086	1.086	1.086	1.086
Bond angle		(°)	(°)	(°)	(°)
A(C9-S1-C13)	95.06	93.99	93.99	93.93	94.04
A(C18-O4-H43)	-	106.52	107.03	106.50	106.53
A(C9-N6-C11)	95.38	94.90	94.75	94.89	94.89
A(C9-N6-C12)	126.12	126.39	126.02	126.32	126.32
A(C11-N6-C12)	135.78	131.58	131.86	131.58	131.51
A(C10-N7-C15)	120.49	122.11	122.03	122.03	121.99
A(C10-N7-H27)	117.03	121.41	119.17	121.65	119.73
A(C15-N7-H27)	122.05	116.19	118.78	116.19	118.12
A(C16-N8-H37)	105.51	110.12	110.52	111.03	111.05
A(C16-N8-H38)	113.35	110.87	111.64	109.97	109.56
A(H37-N8-H38)	104.70	107.26	110.02	106.82	109.18
A(S1-C9-N6)	111.24	110.66	110.67	110.60	110.60
A(S1-C9-C10)	118.25	115.80	115.49	115.69	115.59
A(S1-C9-H25)	111.88	110.22	110.44	110.32	110.45
A(N6-C9-C10)	90.05	88.01	87.91	87.98	87.91
A(N6-C9-H25)	111.23	113.75	113.82	113.78	113.81
A(C10-C9-H25)	114.25	116.67	116.72	116.72	116.69
A(N7-C10-C9)	119.18	120.92	121.32	120.96	121.08
A(N7-C10-C11)	114.71	116.98	116.76	117.29	116.77
A(N7-C10-H26)	109.70	108.55	108.62	108.42	108.63
A(C9-C10-C11)	85.00	84.83	84.81	84.82	84.82
A(C9-C10-H26)	112.78	110.93	110.73	110.91	110.87
A(C11-C10-H26)	113.69	113.08	113.01	112.89	113.11
A(O2-C11-N6)	132.65	132.78	133.03	132.76	132.91
A(O2-C11-C10)	135.29	136.22	135.94	136.28	136.08
A(N6-C11-C10)	92.06	90.89	90.93	90.85	90.88
A(N6-C12-C14)	120.40	121.05	120.94	121.03	120.97
A(N6-C12-C18)	113.90	112.51	115.64	112.51	112.46
A(C14-C12-C18)	125.70	126.21	123.36	126.23	126.34
A(S1-C13-C14)	117.07	117.75	117.81	117.79	117.86
A(S1-C13-H28)	104.56	104.91	104.92	104.89	104.87
A(S1-C13-H29)	109.36	109.00	109.13	109.03	109.07
A(C14-C13-H28)	110.29	108.76	108.74	108.72	108.70
A(C14-C13-H29)	110.00	109.35	109.22	109.33	109.28
A(H28-C13-H29)	104.77	106.45	106.40	106.46	106.43
A(C12-C14-C13)	123.63	122.62	122.77	122.61	122.67
A(C12-C14-H17)	121.60	124.97	124.61	124.96	124.98
A(C13-C14-H17)	117.07	112.33	112.57	112.35	112.27
A(O3-C15-N7)	123.16	123.74	122.56	123.61	122.84

A(O3-C15-C16)	120.60	121.62	122.83	122.09	121.78
A(N7-C15-C16)	116.22	114.64	114.60	114.26	115.29
A(N8-C16-C15)	105.48	110.69	108.15	110.58	108.00
A(N8-C16-C19)	111.82	110.37	115.12	115.20	111.69
A(N8-C16-H30)	106.38	112.88	108.85	106.41	112.63
A(C15-C16-C19)	116.10	110.26	110.51	111.92	113.67
A(C15-C16-H30)	107.52	104.81	106.79	104.18	103.35
A(C19-C16-H30)	108.67	107.66	107.09	107.75	107.30
A(C14-C17-H31)	112.22	113.40	109.78	113.38	113.40
A(C14-C17-H32)	110.08	110.08	109.80	110.11	110.08
A(C14-C17-H33)	111.14	109.78	113.16	109.76	109.73
A(H31-C17-H32)	107.97	107.76	107.03	107.77	107.77
A(H31-C17-H33)	108.52	108.65	107.37	108.66	108.68
A(H32-C17-H33)	106.71	106.94	109.48	106.94	106.96
A(O4-C18-O5)	126.57	122.83	122.83	122.80	122.82
A(O4-C18-C12)	117.61	113.53	111.59	113.53	113.55
A(O5-C18-C12)	115.75	123.64	125.58	123.67	123.63
A(C16-C19-C20)	118.26	117.80	117.74	117.47	117.06
A(C16-C19-C21)	118.81	120.03	120.18	120.51	120.73
A(C20-C19-C21)	122.88	122.17	122.06	122.01	122.21
A(C19-C20-C23)	112.80	113.36	113.49	113.53	113.42
A(C19-C20-H34)	110.41	110.07	109.69	110.46	108.66
A(C19-C20-H35)	109.35	109.63	109.80	108.97	109.82
A(C23-C20-H34)	109.64	109.84	109.75	109.03	110.69
A(C23-C20-H35)	110.22	109.27	109.43	109.53	109.70
A(H34-C20-H35)	104.06	104.27	104.28	104.96	104.15
A(C19-C21-C22)	123.77	124.35	124.45	124.47	124.35
A(C19-C21-H36)	119.33	119.15	119.09	119.16	119.15
A(C22-C21-H36)	116.88	116.49	116.46	116.36	116.50
A(C21-C22-C24)	112.98	113.04	113.01	113.02	112.99
A(C21-C22-H39)	110.14	109.42	109.69	109.55	109.76
A(C21-C22-H40)	108.65	109.60	109.53	109.70	109.42
A(C24-C22-H39)	110.29	109.93	109.92	109.79	110.05
A(C24-C22-H40)	110.36	110.00	109.91	109.93	109.90
A(H39-C22-H40)	104.03	104.49	104.43	104.52	104.38
A(C20-C23-C24)	123.69	123.80	123.78	123.69	123.87
A(C20-C23-H41)	116.69	116.43	116.51	116.55	116.53
A(C24-C23-H41)	119.31	119.77	119.70	119.76	119.60
A(C22-C24-C23)	123.20	123.10	123.16	123.13	123.14
A(C22-C24-H42)	117.05	117.08	117.04	117.08	116.98
A(C23-C24-H42)	119.74	119.83	119.80	119.79	119.88
Dihedral angle		(°)	(°)	(°)	(°)
D(C13-S1-C9-N6)	52.25	53.54	53.88	53.75	53.61
D(C13-S1-C9-C10)	151.26	151.65	151.74	151.74	151.48
D(C13-S1-C9-H25)	-72.82	-73.17	-73.09	-73.01	-73.28
D(C9-S1-C13-C14)	-45.24	-45.71	-45.51	-45.66	-45.36
D(C9-S1-C13-H28)	-167.59	-166.78	-166.60	-166.69	-166.39

D(C9-S1-C13-H29)	80.67	79.53	79.72	79.61	79.94
D(H43-O4-C18-O5)	-	-0.04	5.02	-0.03	0.08
D(H43-O4-C18-C12)	-	179.42	-175.68	179.37	179.45
D(C11-N6-C9-S1)	118.39	107.71	106.60	107.27	107.01
D(C11-N6-C9-C10)	-1.05	-9.19	-9.93	-9.48	-9.60
D(C11-N6-C9-H25)	-116.16	-127.58	-128.33	-127.92	-127.98
D(C12-N6-C9-S1)	-45.35	-45.24	-46.08	-45.56	-45.68
D(C12-N6-C9-C10)	-164.79	-162.13	-162.60	-162.31	-162.30
D(C12-N6-C9-H25)	80.10	79.48	79.00	79.26	79.33
D(C9-N6-C11-O2)	-178.66	-167.25	-166.60	-167.02	-166.59
D(C9-N6-C11-C10)	1.07	9.29	10.04	9.59	9.72
D(C12-N6-C11-O2)	-17.58	-16.57	-16.51	-16.48	-16.17
D(C12-N6-C11-C10)	162.12	159.98	160.14	160.12	160.14
D(C9-N6-C12-C14)	14.65	11.10	11.98	11.19	11.43
D(C9-N6-C12-C18)	-165.24	-163.68	-165.44	-163.62	-163.38
D(C11-N6-C12-C14)	-141.73	-131.61	-130.12	-131.34	-130.95
D(C11-N6-C12-C18)	38.32	53.61	52.46	53.85	54.24
D(C15-N7-C10-C9)	124.60	115.86	107.73	115.69	112.38
D(C15-N7-C10-C11)	-136.94	-143.36	-151.42	-143.30	-146.91
D(C15-N7-C10-H26)	-7.56	-13.95	-22.23	-14.00	-17.57
D(H27-N7-C10-C9)	-62.73	-70.47	-73.79	-68.65	-72.31
D(H27-N7-C10-C11)	35.73	30.32	27.07	32.36	28.40
D(H27-N7-C10-H26)	165.11	159.72	156.25	161.66	157.74
D(C10-N7-C15-O3)	-4.72	-4.91	-3.40	-3.09	-5.36
D(C10-N7-C15-C16)	173.93	174.35	177.51	179.16	171.16
D(H27-N7-C15-O3)	-177.01	-178.89	178.12	-178.97	179.26
D(H27-N7-C15-C16)	1.64	0.37	-0.97	3.28	-4.23
D(H37-N8-C16-C15)	-177.50	-162.78	-28.46	-82.10	149.91
D(H37-N8-C16-C19)	-50.18	-40.43	95.67	46.02	-84.40
D(H37-N8-C16-H30)	68.32	80.10	-144.13	165.35	36.43
D(H38-N8-C16-C15)	68.51	78.67	-151.26	159.89	29.22
D(H38-N8-C16-C19)	-164.17	-158.98	-27.14	-71.99	154.91
D(H38-N8-C16-H30)	-45.68	-38.45	93.07	47.34	-84.25
D(S1-C9-C10-N7)	3.64	14.72	15.29	15.46	15.01
D(S1-C9-C10-C11)	-111.94	-103.77	-103.01	-103.39	-103.24
D(S1-C9-C10-H26)	134.45	143.48	144.33	144.06	143.98
D(N6-C9-C10-N7)	116.51	126.77	127.25	127.40	126.90
D(N6-C9-C10-C11)	0.94	8.28	8.95	8.55	8.65
D(N6-C9-C10-H26)	-112.68	-104.47	-103.71	-104.00	-104.13
D(H25-C9-C10-N7)	-131.27	-117.54	-117.03	-116.88	-117.39
D(H25-C9-C10-C11)	113.15	123.98	124.67	124.26	124.36
D(H25-C9-C10-H26)	-0.47	11.22	12.01	11.71	11.58
D(N7-C10-C11-O2)	58.81	45.50	44.53	45.18	44.74
D(N7-C10-C11-N6)	-120.91	-130.84	-131.95	-131.22	-131.36
D(C9-C10-C11-O2)	178.72	167.71	167.13	167.49	167.07
D(C9-C10-C11-N6)	-1.00	-8.63	-9.35	-8.91	-9.03
D(H26-C10-C11-O2)	-68.57	-81.73	-82.53	-81.98	-82.43

D(H26-C10-C11-N6)	111.71	101.93	100.99	101.63	101.47
D(N6-C12-C14-C13)	-2.73	2.40	2.08	2.65	2.64
D(N6-C12-C14-C17)	176.86	-174.04	-175.25	-173.81	-173.85
D(C18-C12-C14-C13)	177.15	176.42	179.29	176.70	176.68
D(C18-C12-C14-C17)	-3.27	-0.02	1.96	0.23	0.19
D(N6-C12-C18-O4)	-90.09	-145.19	26.44	-145.42	-146.31
D(N6-C12-C18-O5)	87.26	34.26	-154.28	33.98	33.06
D(C14-C12-C18-O4)	142.36	40.35	-150.91	40.11	39.22
D(C14-C12-C18-O5)	90.03	-140.20	28.37	-140.49	-141.41
D(S1-C13-C14-C12)	24.72	22.15	21.92	21.86	21.56
D(S1-C13-C14-C17)	-154.89	-161.01	-160.46	-161.28	-161.55
D(H28-C13-C14-C12)	144.05	141.20	141.01	140.89	140.60
D(H28-C13-C14-C17)	-35.56	-41.95	-41.37	-42.24	-42.51
D(H29-C13-C14-C12)	-100.88	-102.93	-103.26	-103.27	-103.64
D(H29-C13-C14-C17)	79.51	73.92	74.36	73.59	73.26
D(C12-C14-C17-H31)	18.63	11.92	-105.11	11.91	12.76
D(C12-C14-C17-H32)	-101.65	-108.89	137.49	-108.92	-108.06
D(C12-C14-C17-H33)	140.35	133.65	14.83	133.62	134.49
D(C13-C14-C17-H31)	-161.75	-164.85	77.32	-164.87	-164.05
D(C13-C14-C17-H32)	77.97	74.35	-40.08	74.31	75.13
D(C13-C14-C17-H33)	-40.03	-43.11	-162.74	-43.16	-42.32
D(O3-C15-C16-N8)	1.78	-162.55	17.04	163.63	-23.18
D(O3-C15-C16-C19)	-122.91	75.03	-109.81	33.74	-147.69
D(O3-C15-C16-H30)	115.18	-40.56	134.05	-82.41	96.35
D(N7-C15-C16-N8)	176.91	18.17	-163.88	-18.58	160.27
D(N7-C15-C16-C19)	85.40	-104.25	69.28	-148.47	35.75
D(N7-C15-C16-H30)	-63.51	140.16	-46.87	95.38	-80.21
D(N8-C16-C19-C20)	-72.64	-61.63	-64.11	-68.55	-51.17
D(N8-C16-C19-C21)	104.82	118.23	114.21	110.24	128.05
D(C15-C16-C19-C20)	48.94	60.97	58.76	58.91	71.34
D(C15-C16-C19-C21)	-133.61	-119.17	-122.92	-122.31	-109.44
D(H30-C16-C19-C20)	170.24	174.76	174.72	172.86	-175.05
D(H30-C16-C19-C21)	-12.31	-5.38	-6.96	-8.35	4.17
D(C16-C19-C20-C23)	169.73	176.21	176.40	175.13	-179.42
D(C16-C19-C20-H34)	46.68	52.74	53.26	52.31	57.03
D(C16-C19-C20-H35)	-67.24	-61.40	-60.78	-62.50	-56.29
D(C21-C19-C20-C23)	-7.61	-3.65	-1.88	-3.64	1.37
D(C21-C19-C20-H34)	-130.66	-127.12	-125.03	-126.46	-122.18
D(C21-C19-C20-H35)	115.42	118.75	120.93	118.73	124.50
D(C16-C19-C21-C22)	-175.42	-179.52	-178.28	-177.98	179.85
D(C16-C19-C21-H36)	2.95	1.22	0.99	2.66	-0.74
D(C20-C19-C21-C22)	1.91	0.34	-0.03	0.75	-0.98
D(C20-C19-C21-H36)	-179.72	-178.93	179.24	-178.61	178.43
D(C19-C20-C23-C24)	6.51	3.63	2.03	3.47	-0.89
D(C19-C20-C23-H41)	-171.79	-176.99	-178.27	-177.30	179.29
D(H34-C20-C23-C24)	129.99	127.22	125.15	127.07	121.54
D(H34-C20-C23-H41)	-48.31	-53.40	-55.15	-53.70	-58.28

D(H35-C20-C23-C24)	-110.04	-118.97	-120.99	-118.59	-124.08
D(H35-C20-C23-H41)	65.68	60.41	58.71	60.64	56.10
D(C19-C21-C22-C24)	5.09	3.09	1.83	2.45	-0.01
D(C19-C21-C22-H39)	-118.74	-119.78	-121.21	-120.32	-123.24
D(C19-C21-C22-H40)	127.91	126.19	124.73	125.50	122.79
D(H36-C21-C22-C24)	-173.32	-177.63	-177.46	-178.18	-179.43
D(H36-C21-C22-H39)	62.85	59.50	59.51	59.05	57.34
D(H36-C21-C22-H40)	-50.50	-54.53	-54.56	-55.13	-56.64
D(C21-C22-C24-C23)	-6.22	-3.13	-1.69	-2.65	0.51
D(C21-C22-C24-H42)	172.88	177.16	178.25	177.69	-179.75
D(H39-C22-C24-C23)	117.52	119.46	121.22	119.98	123.58
D(H39-C22-C24-H42)	-63.37	-60.26	-58.84	-59.68	-56.68
D(H40-C22-C24-C23)	-128.09	-126.01	-124.37	-125.58	-122.01
D(H40-C22-C24-H42)	51.02	54.28	55.57	54.76	57.72
D(C20-C23-C24-C22)	0.35	-0.23	-0.24	-0.33	-0.02
D(C20-C23-C24-H42)	-178.74	179.47	179.83	179.32	-179.75
D(H41-C23-C24-C22)	178.61	-179.59	-179.93	-179.54	179.79
D(H41-C23-C24-H42)	-0.47	0.12	0.13	0.11	0.06

D. Experimental and theoretical vibrational wavenumber (cm^{-1}) of conformers (I-IV) cefradine with potential energy distribution (PED)

Table 33: Experimental and theoretical vibrational wavenumber (cm^{-1}) of conformers (I-IV) cefradine with potential energy distribution (PED).

Unscaled DFT	Scaled DFT				Experimental		Contributions
	I	II	III	IV	IR	Raman	
3753	3556	3570	3556	3557	3557	3557	ν(O4H)(100)
3578	3401	3434	3402	3415	3435	3433	ν_a(N8H$_2$)(100)
3548	3373	3424	3373	3412	–	–	ν(N7H)(99)
3500	3330	3337	3331	3333	–	–	ν_s(N8H$_2$)(100)
3161	3025	3026	3026	3026	3024	3024	ν_a(C17H$_3$)(100)
3160	3025	3024	3024	3023	–	–	R3[ν_s(CH)(99)]
3137	3004	3003	3003	3002	3003	3003	R3[ν_a(CH)(99)]
3137	3004	2992	2994	2992	2992	2992	R3[ν(CH)(99)]
3098	2968	2974	2968	2974	2974	2974	R2[ν(C10H)(94)] + R1[ν(C9H)(5)]
3082	2954	2955	2953	2955	2956	2956	R1[ν(C9H)(93)] + R2[ν(C10H)(5)]
3076	2948	2950	2948	2948	2948	2947	R1[ν_a(C13H$_2$)(99)]
3059	2933	2934	2933	2934	2934	2934	ν_a(C17H$_3$)(99)
3025	2902	2901	2915	2906	–	–	ν(C16H)(99)
3023	2900	2895	2900	2901	2900	2900	R1[ν_s(C13H$_2$)(78)] + ν_s(C17H$_3$)(21)
3017	2895	2881	2895	2895	–	–	ν_s(C17H$_3$)(77) + R1[ν_s(C13H$_2$)(22)]
3008	2886	2879	2885	2865	2881	2881	R3[ν_a(CH$_2$)(100)]
2992	2872	2866	2864	2863	–	–	R3[ν_s(CH$_2$)(99)]
2985	2865	2865	2859	2860	2865	2865	R3[ν_a(CH$_2$)(99)]
2978	2859	2860	2849	2824	2859	2859	R3[ν_s(CH$_2$)(98)]
1860	1819	1818	1820	1819	1821	1821	R2[ν(C=O)(81) + ν(N6C11)(6) + ν(CC)(5) + δ(5)]
1799	1762	1751	1761	1761	1762	1762	ν(C18=O)(78) + R1[ν(C12C18)(5)]
1752	1717	1719	1714	1715	1719	1719	ν(C15=O)(61) + R3[ν(CC)(14)]
1746	1711	1706	1712	1706	1706	1706	R3[ν(CC)(60) + δ(CH)(8)] + ν(C15=O)(17)
1703	1671	1666	1672	1667	–	–	R3[ν(CC)(82) + δ(CH)(9)]
1679	1648	1641	1647	1647	1647	1647	R1[ν(CC)(71) + ν(N6C12)(5)]
1655	1625	1597	1631	1600	1597	1597	δ_{sci}(N8H$_2$)(95)

1531	1506	1515	1504	1514	–	–	δ(C10N7C15)(49) + ν(N7C15)(23) + R2[ν(N7C10)(11) + oop(C10NH)(7)]
1489	1466	1461	1465	1465	–	–	R1[δ'$_{asym}$(CH_3)(82) + δ_{sym}(CH_3)(6) + ρ(CH_3)(5)]
1484	1461	1456	1461	1461	1462	1464	R1[δ_{asym}(CH_3)(88) + ρ'(CH_3)(7)]
1474	1452	1451	1450	1453	1452	–	R3[oop(CH_2)(97)]
1469	1447	1447	1446	1448	–	1446	R3[oop(CH_2)](94)
1451	1430	1429	1430	1431	1430	1430	R1[oop($C13H_2$)(93)]
1425	1404	1405	1404	1405	–	–	R3[δ(CH)(71) + ν(CC)(15)]
1421	1400	1397	1400	1401	1399	1400	R1[δ_{sym}(CH_3)(78) + δ'$_{asym}$(CH_3)(7)]
1405	1385	1386	1385	1387	–	1385	R3[ν(CC)(34) + ω(CH_2)(32) + δ(CH)(15) + δ_{asym}(6)]
1398	1379	1381	1378	1379	1380	1380	R1[ν(N6C12)(21) + ν(C12C18)(12) + δ_{sym}(CH_3)(7) + δ_{asym}(5)] + R2[oop(C10NH)(5)] + ν(C18O4)(5)
1379	1360	1367	1369	1359	1367	1367	R3[ω(CH_2)(55) + δ(CH)(19) + ν(CC)(19)]
1368	1349	1359	1358	1353	1345	1358	R2[oop(C10NH)(30) + ρ(C10NH)(8)] + δ(C18O4H)(7) + ν(C18O4)(5) + R1[ν(C12C18)(5)]
1360	1342	1341	1346	1338	1335	1346	ω(C16N8H30)(19) + R3[ω(CH_2)(18) + δ(CH)(11) + ν(CC)(9) + ν(C16C19)(5)] + δ_{sci}(C16N8H30)(10) + Υ(C16N8H30)(7) + ρ(NH_2)(6)
1341	1324	1335	1329	1336	1323	1323	R2[δ(C9H)(17) + oop(C10NH)(14) + ν(N6C11)(11)] + R1[ν(N6C12)(12)] + δ(C18O4H)(7)
1329	1312	1320	1321	1322	–	–	δ_{sci}(C16N8H30)(50) + ρ(C16N8H30)(15) + ω(C16N8H30)(14) + Υ(C16N8H30)(6)
1322	1305	1286	1283	1291	–	–	R3[δ(CH)(28) + ω(CH_2)(14) + ν(C16C19)(8)] + ρ(NH_2)(19) + ω(C16N8H30)(11)
1298	1282	1278	1278	1283	1281	1281	R1[ω($C13H_2$)(35) + ν(CC)(9) + δ_{tri}(5)] + R2[δ(C9H)(12)] + δ(C18O4H)(10)
1296	1280	1275	1263	1279	–	1274	R2[oop(C9H)(48) + δ(C9H)(17)] + R1[τ(N6C9)(20)]
1265	1250	1246	1247	1246	–	1247	R1[τ(N6C9)(46)] + R2[oop(C9H)(21) + δ(C9H)(12)]
1255	1240	1233	1226	1226	1233	1233	R1[τ(N6C9)(32)] + R2[oop(C9H)(16)] + δ(C10N7C15)(9) + ν(N7C15)(7) + Υ(C16N8H30)(6) + ρ(NH_2)(5)
1236	1222	1218	1210	1210	–	1219	R3[Υ(CH_2)(90)]
1223	1209	1208	1208	1210	1210	1210	R2[oop(C9H)(16) + ν(N7C10)(10) + puck(5)] + R1[ω($C13H_2$)(16) + ν(C14C17)(6)] + δ(C18O4H)(6)

1221	1208	1207	1206	1207	–	–	R3[ϒ(CH_2)(92) + oop(CH)(5)]
1210	1196	1196	1193	1203	–	1197	R2[δ(C9H)(13) + ν(N7C10)(12)] + R3[δ(CH)(11) + δ(CH)(8) + ν(C16C19)(5)] + ϒ(C16N8H30)(5)
1207	1193	1190	1191	1193	–	–	R1[ϒ($C13H_2$)(52)] + R2[ω(C10NH)(12)] + R3[τ'$_a$(8) + ϒ(C10NH)(6)]
1200	1187	1188	1182	1186	–	1188	R3[δ(CH)(44) + ω(CH_2)(9)] + R2[δ(C9H)(12) + ν(N7C10)(10)]
1187	1174	1181	1173	1172	1172	1172	R1[τ(N6C9)(18) + ν(N6C9)(9) + ϒ($C13H_2$)(6)] + R2[oop(C9H)(13) + δ(C9H)(11) + ω(C10NH)(6)] + R3[puck(6)]
1180	1167	1161	1165	1170	–	1161	R2[ν(N7C10)(11) + δ(C9H)(11)] + ν(N7C15)(7) + R3[ν(C16C19)(7) + δ(CH)(9)] + ν(C15C16)(5)
1167	1155	1149	1155	1155	1154	1155	ν(C18O4)(26) + δ(C18O4H)(24) + R1[ν(C12C18)(10) + ν(CC)(9) + ρ($C17H_3$)(9) + ν(C14C17)(6)]
1135	1124	1132	1141	1140	1122	1122	R1[τ(N6C9)(32) + ν(N6C9)(9)] + R2[δ(C9H)(23) + ω(C10NH)(7)] + R3[ϒ(C10NH)(5)]
1124	1113	1116	1123	1121	1113	1113	R3[ν(C16C19)(22) + δ_{tri}(9) + ν(CC)(6)] + ρ($N8H_2$)(20) + ν(N8C16)(12) + ν(N7C15)(7)
1073	1064	1107	1075	1088	–	–	R3[ν(CC)(25) + ω(CH_2)(13) + δ(CH)(6)] + ν(N8C16)(17)
1063	1054	1057	1054	1055	1054	1054	R1[τ(N6C9)(15) + ν(C14C17)(13)] + R2[ν(N6C11)(12) + δ(C9H)(8) + δ(C=O)(8) + ν(CC)(7)]
1046	1037	1048	1052	1044	–	1048	R1[ρ'($C17H_3$)(46) + oop(C14C17)(6)] + R3[puck(20) + τ'$_a$(8)]
1044	1035	1040	1037	1037	1036	1036	R1[ρ($C17H_3$)(19) + ν(N6C9)(15) + ν(C12C18)(5)] + ν(C18O4)(14) + R3[τ'$_a$(7)]
1043	1034	1034	1035	1035	–	–	ν(N8C16)(29) + R3[δ_{tri}(11) + ν(CC)(14)] + ν(C15C16)(5) + ρ($N8H_2$)(5)
1015	1007	1007	1005	1006	–	1007	R3[oop(CH)(65) + puck(16) + ρ(CH_2)(14)]
995	987	986	982	984	–	–	R2[puck(23) + ρ(C10NH)(7)] + R1[τ(N6C9)(19)] + ρ(N7H)(7)
990	982	981	980	982	984	984	R3[oop(CH)(50) + ρ(CH_2)(41)]
978	971	969	972	968	969	969	R3[ρ(CH_2)(17) + ν(CC)(11) + oop(CH)(6)] + R1[τ(N6C9)(12)] + R2[puck(9)]
972	965	961	959	959	–	–	R3[ρ(CH_2)(26) + ν(CC)(10) + puck(7) + oop(CH)(5)] + R1[τ(N6C9)(6)] + ω($N8H_2$)(5)

957	950	951	951	950	960	–	R1[ν(CC)(16) + ρ(C17H$_3$)(9) + τ(N6C9)(5)] + R3[ν(CC)(19) + δ_{tri}(6)] + R2[puck(5)]
953	946	943	944	945	948	948	R3[δ_{tri}(24) + ν(CC)(14)] + R1[τ(N6C9)(12) + ν(CC)(5)] + R2[ν(CC)(8) + puck(5)]
936	930	926	931	924	924	924	R1[τ(N6C9)(20)] + R2[ν(CC)(19) + δ(C9H)(6)] + R3[δ_{tri}(10) + ν(CC)(12)]
910	904	899	911	898	899	899	ω(N8H$_2$)(11) + R2[δ(8) + ν(CC)(12)] + R1[ν(CC)(6) + ν(C14C17)(6) + δ(C12C18)(5)] + R3[τ'$_a$(5) + ν(CC)(5)]
895	890	882	880	880	–	–	R3[ν(CC)(66)] + ω(N8H$_2$)(13)
879	874	863	876	864	881	883	ω(N8H$_2$)(31) + R3[oop(CH)(12) + puck(6) + ν(C15C16)(5) + ν(CC)(8)] + R2[puck(5)]
868	863	852	863	862	–	864	R3[puck(41) + τ'$_a$(14)] + R1[ρ(C13H2)(25) + τ(N6C9)(9)]
854	849	826	849	853	–	851	R3[oop(CH)(47) + ρ(CH$_2$)(9)] + ω(N8H$_2$)(6) + ρ(C15C16)(4)
823	819	823	818	821	824	826	R2[puck(26) + δ(20) + ν(CC)(7)] + R3[τ'$_a$(8)] + R1[τ(N6C9)(6)]
795	792	793	794	786	794	794	ω(C15C16)(36) + R3[ν(CC)(15) + δ_{sci}(C15C16C19)(10) + oop(CH)(7)] + ω(N8H$_2$)(9)
784	781	782	780	782	779	779	R3[puck(31)] + R1[ω(C18O4)(17) + τ(N6C9)(11) + oop(C12C18)(7)] + R2[puck(17)]
759	756	759	757	763	758	758	R2[puck(28)] + R1[ν(S1C13)(21)] + R3[τ'$_a$(4)]
754	751	748	755	753	747	747	R2[puck(21) + oop(C9H)(5)] + R3[τ'$_a$(16)] + R1[ν(S1C9)(8) + ν(S1C13)(6)] + ρ(C15C16)(5)
736	733	740	735	741	740	740	R3[puck(18) + ν(CC)(5)] + R1[τ(N6C9)(15) + ν(S1C13)(11)]
696	695	700	694	700	697	697	R1[τ(N6C9(53)] + R3[puck(12) + τ'$_a$(8)]
693	692	692	686	684	684	684	R1[δ(O5C18C12)(19) + τ(N6C9)(7) + δ_{tri}(6)] + τ(N7C15)(11) + R2[puck(7)] + R3[oop(CH)(10)] + ω(N7H)(5)
685	683	679	683	676	679	679	R3[oop(CH)(35) + ρ(CH$_2$)(6)] + R1[δ(O5C18C12)(12) + τ(N6C9)(6)] + ω(N7H)(5) + τ(N7C15)(5)
673	671	656	674	645	656	656	R3[oop(CH)(34) + ρ(CH$_2$)(10)] + ω(N7H)(16) + τ(N7C15)(16)
646	645	631	643	623	643	642	R3[puck(38) + τ_a(5)] + τ(O4C18)(13) + R1[oop(C12C18)(9) + τ(N6C9)(6)]
633	632	604	612	606	605	605	R1[τ(N6C9)(45)] + R3[puck(21)] + τ(O4C18)(5)
596	596	582	597	575	582	582	R3[δ_{asym}(11) + δ'$_{asym}$(9) + oop(C16C19)(7) + ρ(CH$_2$)(5)] + δ(O3N7C15)(7) + R1[τ(N6C9)(6)] + ρ(C16N8H30)(5) + ν(N8C16)(5)
583	583	558	565	564	–	–	R1[τ(N6C9)(13)] + R2[oop(C=O)(12) + puck(11)] + ρ(C16N8H30)(7)
563	563	549	560	561	562	562	R3[puck(33)] + R1[τ(N6C9)(29)] + τ(O4C18)(12)

557	557	518	544	554	–	557	R3[δ'$_{asym}$(49) + puck(6)] + R1[τ(N6C9)(12)]
523	523	501	539	526	526	526	R3[puck(22)] + R1[δ(O5C18C12)(10) + δasym(10) + ν(C12C18)(5)] + R2[puck(7)]
505	506	495	518	512	–	507	R3[puck(38)] + R1[τ(N6C9)(9) + δtri(7)]
492	493	464	500	491	496	496	R3[oop(C16C19)(26) + puck(21) + τ_a(11) + δ_{asym}(5)] + R1[τ(N6C9)(6)]
476	476	457	466	451	462	462	δ(O3N7C15)(14) + R3[δ_{asym}(11) + τ'$_a$(10)] + ν(C15C16)(9) + ω(C16N8H30)(6)
447	448	437	449	443	435	435	R3[τ'$_a$(54) + puck(6)] + R1[τ(N6C9)(10) + oop(C14C17)(8)] + R2[puck(7)]
407	408	413	410	404	401	403	R3[puck(37)] + R1[δ'$_{asym}$(16) + ν(S1C9)(6)] + R2[puck(9)]
398	399	400	398	400	–	–	R3[puck(48) + oop(CH)(25) + τ_a(18) + ρ(CH$_2$)(5)]
385	386	377	388	377	–	372	R1[τ(N6C9)(52) + ρ(C18 O4)(4)] + R3[puck(27) + τ'$_a$(3)]
363	364	366	363	365	–	363	R1[τ(N6C9)(42) + δ(C14C17)(11) + oop(C14C17)(5)] + R3[τ'$_a$(32)]
329	330	327	330	344	–	326	R3[τ_a(13) + puck(12) + oop(C16C19)(8) + oop(CH)(6) + τ'$_a$(8)] + R1[τ(N6C9)(12)] + Υ(C16N8H30)(9) + ω(C16N8H30)(6)
300	301	315	301	322	–	311	R1[τ(N6C9)(44)] + R3[τ'$_a$(33)]
295	296	304	299	301	–	300	R3[τ'$_a$(37)] + R1[δ_{asym}(26) + oop(C14C17)(5)]
284	286	292	286	293	–	293	τ(N8C16)(38) + R3[τ'$_a$(11) + oop(CH)(7) + puck(6) + τ_a(5)]
273	274	261	281	273	–	263	R1[τ(N6C9)(17) + δ_{asym}(10)] + δ(O3N7C15)(7) + R3[Υ(C10NH)(6) + puck(5)]
259	260	252	262	257	–	252	τ(N8C16)(14) + R3[δ(C16C19)(10) + τ'$_a$(9)] + R1[τ(N6C9)(6) + δ(C12C18)(5)] + ω(N7H)(5)
245	246	240	238	242	–	240	R1[τ(N6C9)(21)] + τ(N8C16)(12) + τ(N7C15)(6) + R3[puck(6) + τ'$_a$(6)] + R2[ν(CC)(5)]
204	205	209	212	209	–	209	R3[δ(C16C19)(29) + τ'$_a$(6) + puck(5)] + τ(N8C16)(7) + ρ(C16N8H30)(6) + R1[τ(N6C9)(5)] + τ(C15C16)(5)
197	198	196	199	197	–	196	R3[puck(15) + τ'$_a$(14) + oop(C16C19)(7)] + R1[τ(N6C9)(12)] + ρ(N7H)(9)
176	177	184	178	195	–	182	R3[puck(36) + τ'$_a$(19)] + R1[τ(C14C17)(14) + τ(N6C9)(9)]
150	151	152	151	151	–	141	R3[τ'$_a$(41) + puck(37)] + R1[τ(N6C9)(7)] + R2[puck(5)]
128	129	142	131	143	–	–	R1[τ(N6C9)(36) + τ(C14C17)(11) + δ(C12C18)(5)] + R3[τ'$_a$(35)]
124	124	123	125	119	–	117	R3[τ'$_a$(46) + puck(13) + τ'$_a$(5) + τ_a(5)] + R1[τ(N6C9)(17)]
117	118	120	114	116	–	–	R1[τ(N6C9)(41)] + R3[τ'$_a$(36) + puck(5)] + R2[puck(8)]
113	114	110	114	108	–	109	R3[τ'$_a$](50) + R2[puck(40)]
79	79	83	80	80	–	81	R3[τ_a(36) + τ'$_a$(34)] + R2[puck(12)]

73	74	76	73	71	–	–	R3[τ_a47) + τ'$_a$(28)] + R2[puck(6)]
66	66	73	62	68	–	–	R1[τ(C12C18)(32) + τ(N6C9)(25)] + τ(C15C16)(8) + R2[puck(8)]
52	53	53	46	58	–	–	R1[τ(N6C9)(38) + τ(C12C18)(7)] + R3[τ'$_a$(30)] + τ(C15C16)(12)
39	40	39	45	50	–	–	R1[τ(N6C9)(62)] + R3[τ'$_a$(20)] + R2[puck(10)]
30	30	33	30	32	–	–	R1[τ(N6C9)(65)] + R3[τ'$_a$(21)] + R2[puck(9)]
26	26	24	27	25	–	–	ω(N7H)(22) + τ(N7C15)(22) + R3[τ'$_a$(16) + δ_{sci}(C15C16C19)(6) + Υ(C10NH)(6) + τ_a(7)]
14	14	11	15	17	–	–	R1[τ(N6C9)(33)] + R2[τ(N7C10)(30)] + τ(C15C16)(13)

E. Optimized parameters (bond distance, bond angle and torsion angle) of frovatriptan by using the functional B3LYP/6-311++G(d,p)

Table 34: Optimized parameters (bond distance, bond angle and torsion angle) of frovatriptan by using the functional B3LYP/6-311++G(d,p).

	B3LYP				
Parameters	Conformer I	Conformer II	Conformer III	Conformer IV	Conformer V
Bond Distance	(Å)	(Å)	(Å)	(Å)	(Å)
R(O1-C18)	1.222	1.222	1.222	1.222	1.222
R(N2-C10)	1.388	1.388	1.389	1.388	1.388
R(N2-C12)	1.378	1.378	1.378	1.378	1.378
R(N2-H26)	1.007	1.007	1.007	1.007	1.007
R(N3-C5)	1.465	1.465	1.464	1.464	1.464
R(N3-C16)	1.460	1.461	1.461	1.460	1.460
R(N3-H27)	1.014	1.014	1.016	1.016	1.016
R(N4-C18)	1.378	1.377	1.377	1.378	1.378
R(N4-H34)	1.007	1.007	1.007	1.007	1.007
R(N4-H35)	1.009	1.009	1.009	1.009	1.009
R(C5-C6)	1.540	1.543	1.551	1.551	1.551
R(C5-C7)	1.540	1.537	1.539	1.538	1.538
R(C5-H19)	1.107	1.108	1.099	1.099	1.099
R(C6-C8)	1.500	1.501	1.501	1.501	1.501
R(C6-H20)	1.098	1.098	1.100	1.100	1.100
R(C6-H21)	1.098	1.095	1.095	1.095	1.095
R(C7-C9)	1.540	1.540	1.540	1.540	1.540
R(C7-H22)	1.093	1.096	1.092	1.092	1.092
R(C7-H23)	1.095	1.095	1.098	1.098	1.098
R(C8-C10)	1.369	1.368	1.368	1.369	1.369
R(C8-C11)	1.440	1.441	1.441	1.441	1.441
R(C9-C10)	1.494	1.494	1.494	1.494	1.494
R(C9-H24)	1.099	1.099	1.099	1.099	1.099
R(C9-H25)	1.096	1.096	1.097	1.096	1.096
R(C11-C12)	1.423	1.423	1.424	1.423	1.423
R(C11-C13)	1.400	1.400	1.397	1.400	1.400
R(C12-C14)	1.396	1.396	1.395	1.396	1.396
R(C13-C15)	1.396	1.396	1.395	1.396	1.396
R(C13-H28)	1.084	1.084	1.083	1.084	1.084
R(C14-C17)	1.385	1.385	1.388	1.385	1.385
R(C14-H29)	1.085	1.085	1.085	1.085	1.085
R(C15-C17)	1.412	1.412	1.414	1.412	1.412
R(C15-C18)	1.498	1.498	1.498	1.498	1.498
R(C16-H30)	1.104	1.093	1.101	1.094	1.101
R(C16-H31)	1.092	1.092	1.093	1.101	1.093
R(C16-H32)	1.093	1.104	1.094	1.093	1.094
R(C17-H33)	1.083	1.083	1.084	1.083	1.083

Bond angle	(°)	(°)	(°)	(°)	(°)
A(C10-N2-C12)	109.28	109.23	109.23	109.28	109.29
A(C10-N2-H26)	125.26	125.32	125.24	125.27	125.29
A(C12-N2-H26)	125.41	125.41	125.52	125.41	125.42
A(C5-N3-C16)	115.19	115.17	115.79	115.90	115.89
A(C5-N3-H27)	109.22	108.96	109.80	109.90	109.90
A(C16-N3-H27)	109.30	109.20	110.15	110.25	110.26
A(C18-N4-H34)	120.45	120.48	120.65	120.39	120.45
A(C18-N4-H35)	115.60	115.62	115.63	115.56	115.58
A(34-N4-H35)	117.01	117.03	117.05	116.97	116.99
A(N3-C5-C6)	109.38	110.90	114.91	114.93	114.92
A(N3-C5-C7)	110.87	109.16	109.08	109.11	109.09
A(N3-C5-H19)	110.69	110.91	106.33	106.35	106.35
A(C6-C5-C7)	110.56	110.58	110.69	110.65	110.67
A(C6-C5-H19)	107.66	107.36	107.75	107.72	107.70
A(C7-C5-H19)	107.62	107.88	107.77	107.77	107.79
A(C5-C6-C8)	111.05	110.75	111.01	111.03	111.02
A(C5-C6-H20)	108.50	108.28	108.79	108.72	108.67
A(C5-C6-H21)	109.25	109.92	110.05	109.89	109.89
A(C8-C6-H20)	110.86	111.17	110.46	110.56	110.60
A(C8-C6-H21)	110.53	110.11	110.29	110.37	110.34
A(H20-C6-H21)	106.51	106.50	106.11	106.14	106.19
A(C5-C7-C9)	111.99	112.38	112.65	112.62	112.64
A(C5-C7-H22)	110.27	109.65	108.73	108.72	108.71
A(C5-C7-H23)	108.11	108.41	108.77	108.78	108.78
A(C9-C7-H22)	109.36	109.39	110.28	110.28	110.29
A(C9-C7-H23)	109.97	109.85	109.16	109.19	109.17
A(H22-C7-H23)	107.01	107.00	107.09	107.09	107.09
A(C6-C8-C10)	122.78	122.97	122.85	122.79	122.81
A(C6-C8-C11)	130.18	130.07	130.15	130.23	130.21
A(C10-C8-C11)	107.05	106.96	107.00	106.98	106.98
A(C7-C9-C10)	109.30	109.27	109.61	109.62	109.63
A(C7-C9-H24)	110.16	110.17	109.89	109.88	109.88
A(C7-C9-H25)	109.95	109.88	110.04	110.03	110.03
A(C10-C9-H24)	110.13	110.14	110.05	110.05	110.05
A(C10-C9-H25)	110.97	111.01	110.96	110.97	110.97
A(H24-C9-H25)	106.30	106.34	106.25	106.24	106.24
A(N2-C10-C8)	109.51	109.60	109.58	109.55	109.54
A(N2-C10-C9)	124.87	124.76	124.63	124.66	124.66
A(C8-C10-C9)	125.62	125.64	125.78	125.79	125.79
A(C8-C11-C12)	106.91	106.97	106.91	106.95	106.95
A(C8-C11-C13)	134.20	134.16	134.10	134.18	134.17
A(C12-C11-C13)	118.89	118.88	118.98	118.87	118.88
A(N2-C12-C11)	107.25	107.25	107.27	107.24	107.23
A(N2-C12-C14)	130.73	130.72	130.77	130.72	130.73
A(C11-C12-C14)	122.01	122.03	121.96	122.04	122.03

A(C11-C13-C15)	119.52	119.53	119.63	119.53	119.53
A(C11-C13-H28)	119.68	119.64	121.77	119.67	119.66
A(C15-C13-H28)	120.75	120.78	118.60	120.76	120.76
A(C12-C14-C17)	117.81	117.80	117.77	117.80	117.80
A(C12-C14-H29)	121.42	121.43	121.51	121.43	121.43
A(C17-C14-H29)	120.77	120.77	120.72	120.77	120.76
A(C13-C15-C17)	120.23	120.23	120.15	120.24	120.23
A(C13-C15-C18)	122.70	122.72	117.20	122.70	122.70
A(C17-C15-C18)	117.05	117.04	122.65	117.06	117.06
A(N3-C16-H30)	113.67	110.44	115.14	109.18	115.16
A(N3-C16-H31)	109.23	109.12	109.09	115.16	109.11
A(N3-C16-H32)	110.43	113.68	109.16	109.11	109.18
A(H30-C16-H31)	108.36	107.21	107.94	107.78	107.92
A(H30-C16-H32)	107.77	107.86	107.80	107.44	107.76
A(H31-C16-H32)	107.16	108.30	107.45	107.90	107.45
A(C14-C17-C15)	121.53	121.53	121.50	121.52	121.52
A(C14-C17-H33)	120.60	120.61	118.44	120.60	120.60
A(C15-C17-H33)	117.88	117.87	120.01	117.88	117.88
A(O1-C18-N4)	121.08	121.08	121.01	121.10	121.08
A(O1-C18-C15)	122.42	122.42	122.45	122.43	122.42
A(N4-C18-C15)	116.48	116.49	116.53	116.47	116.48
Dihedral angle	(°)	(°)	(°)	(°)	(°)
D(C12-N2-C10-C8)	0.42	0.37	0.28	0.36	0.09
D(C12-N2-C10-C9)	179.69	179.49	179.49	179.40	179.27
D(H26-N2-C10-C8)	178.07	178.15	179.21	178.47	-179.51
D(H26-N2-C10-C9)	-2.66	-2.72	-1.57	-2.49	-0.33
D(C10-N2-C12-C11)	-0.47	-0.48	-0.22	-0.46	0.10
D(C10-N2-C12-C14)	178.69	178.68	179.06	178.65	-179.34
D(H26-N2-C12-C11)	-178.12	-178.26	-179.15	-178.57	179.70
D(H26-N2-C12-C14)	1.04	0.90	0.12	0.54	0.26
D(C16-N3-C5-C6)	160.49	68.32	63.56	63.40	63.46
D(C16-N3-C5-C7)	-77.34	-169.60	-171.50	-171.67	-171.60
D(C16-N3-C5-H19)	42.02	-50.88	-55.54	-55.69	-55.60
D(H27-N3-C5-C6)	37.07	-168.60	-61.94	-62.40	-62.34
D(H27-N3-C5-C7)	159.24	-46.53	63.00	62.53	62.59
D(H27-N3-C5-H19)	-81.40	72.20	178.96	178.51	178.60
D(C5-N3-C16-H30)	-52.36	-71.11	-61.32	59.93	-61.46
D(C5-N3-C16-H31)	-173.49	171.28	177.19	-61.44	177.05
D(C5-N3-C16-H32)	68.90	50.28	60.05	177.08	59.89
D(H27-N3-C16-H30)	71.02	165.94	64.01	-174.45	64.17
D(H27-N3-C16-H31)	-50.12	48.33	-57.48	64.18	-57.33
D(H27-N3-C16-H32)	-167.72	-72.67	-174.63	-57.30	-174.49
D(H34-N4-C18-O1)	158.24	158.36	-158.95	158.07	-158.22
D(H34-N4-C18-C15)	-22.84	-22.70	22.03	-23.02	22.87
D(H35-N4-C18-O1)	8.28	8.24	-8.42	8.38	-8.33
D(H35-N4-C18-C15)	-172.80	-172.82	172.55	-172.71	172.76
D(N3-C5-C6-C8)	167.81	166.87	169.18	169.31	169.25

D(N3-C5-C6-H20)	45.73	44.74	47.43	47.47	47.40
D(N3-C5-C6-H21)	-70.02	-71.23	-68.43	-68.30	-68.39
D(C7-C5-C6-C8)	45.45	45.63	45.08	45.19	45.15
D(C7-C5-C6-H20)	-76.63	-76.50	-76.67	-76.65	-76.70
D(C7-C5-C6-H21)	167.62	167.53	167.47	167.58	167.50
D(H19-C5-C6-C8)	-71.85	-71.82	-72.52	-72.38	-72.45
D(H19-C5-C6-H20)	166.06	166.05	165.73	165.79	165.70
D(H19-C5-C6-H21)	50.32	50.08	49.87	50.02	49.91
D(N3-C5-C7-C9)	175.54	174.97	171.03	170.93	170.99
D(N3-C5-C7-H22)	53.51	53.08	48.49	48.41	48.44
D(N3-C5-C7-H23)	-63.16	-63.42	-67.81	-67.89	-67.84
D(C6-C5-C7-C9)	-62.98	-62.77	-61.60	-61.68	-61.63
D(C6-C5-C7-H22)	175.00	175.34	175.86	175.80	175.82
D(C6-C5-C7-H23)	58.33	58.84	59.56	59.50	59.54
D(H19-C5-C7-C9)	54.35	54.37	56.00	55.85	55.91
D(H19-C5-C7-H22)	-67.67	-67.52	-66.55	-66.67	-66.63
D(H19-C5-C7-H23)	175.65	175.98	177.16	177.04	177.08
D(C5-C6-C8-C10)	-15.81	-16.29	-16.30	-16.37	-16.34
D(C5-C6-C8-C11)	164.10	163.50	163.87	163.46	163.79
D(H20-C6-C8-C10)	104.89	104.13	104.47	104.39	104.37
D(H20-C6-C8-C11)	-75.20	-76.08	-75.36	-75.78	-75.50
D(H21-C6-C8-C10)	-137.23	-138.08	-138.55	-138.47	-138.43
D(H21-C6-C8-C11)	42.68	41.72	41.62	41.35	41.70
D(C5-C7-C9-C10)	45.40	44.80	43.99	44.03	43.98
D(C5-C7-C9-H24)	-75.72	-76.33	-77.07	-77.03	-77.07
D(C5-C7-C9-H25)	167.44	166.83	166.28	166.33	166.29
D(H22-C7-C9-C10)	167.94	166.84	165.66	165.67	165.64
D(H22-C7-C9-H24)	46.82	45.71	44.60	44.61	44.58
D(H22-C7-C9-H25)	-70.02	-71.13	-72.05	-72.03	-72.06
D(H23-C7-C9-C10)	-74.83	-75.98	-76.95	-76.92	-76.97
D(H23-C7-C9-H24)	164.05	162.88	161.99	162.02	161.98
D(H23-C7-C9-H25)	47.21	46.05	45.34	45.38	45.34
D(C6-C8-C10-N2)	179.73	179.73	179.92	179.76	179.87
D(C6-C8-C10-C9)	0.47	0.62	0.71	0.73	0.70
D(C11-C8-C10-N2)	-0.19	-0.11	-0.22	-0.10	-0.23
D(C11-C8-C10-C9)	-179.45	-179.22	-179.42	-179.13	-179.40
D(C6-C8-C11-C12)	179.99	180.00	179.93	179.98	-179.82
D(C6-C8-C11-C13)	0.47	0.52	0.36	0.50	-0.11
D(C10-C8-C11-C12)	-0.09	-0.18	0.08	-0.17	0.29
D(C10-C8-C11-C13)	-179.61	-179.67	-179.49	-179.65	-179.99
D(C7-C9-C10-N2)	165.66	166.38	166.62	166.82	166.70
D(C7-C9-C10-C8)	-15.18	-14.64	-14.29	-14.29	-14.25
D(H24-C9-C10-N2)	-73.19	-72.47	-72.42	-72.22	-72.34
D(H24-C9-C10-C8)	105.96	106.51	106.67	106.67	106.71
D(H25-C9-C10-N2)	44.24	45.03	44.89	45.09	44.96
D(H25-C9-C10-C8)	-136.61	-135.99	-136.02	-136.03	-135.99
D(C8-C11-C12-N2)	0.34	0.40	0.08	0.39	-0.24

D(C8-C11-C12-C14)	-178.91	-178.85	-179.27	-178.81	179.26
D(C13-C11-C12-N2)	179.95	179.98	179.73	179.96	179.99
D(C13-C11-C12-C14)	0.70	0.73	0.38	0.76	-0.51
D(C8-C11-C13-C15)	179.28	179.27	-179.91	179.20	-179.57
D(C8-C11-C13-H28)	1.76	1.72	0.29	1.64	-1.85
D(C12-C11-C13-C15)	-0.19	-0.17	0.55	-0.22	0.12
D(C12-C11-C13-H28)	-177.71	-177.72	-179.24	-177.79	177.84
D(N2-C12-C14-C17)	-179.32	-179.38	-179.93	-179.30	179.51
D(N2-C12-C14-H29)	0.40	0.37	-0.71	0.44	-0.19
D(C11-C12-C14-C17)	-0.27	-0.32	-0.75	-0.31	0.13
D(C11-C12-C14-H29)	179.45	179.42	178.47	179.44	-179.56
D(C11-C13-C15-C17)	-0.71	-0.77	-1.09	-0.72	0.62
D(C11-C13-C15-C18)	-179.48	-179.57	179.64	-179.51	179.49
D(H28-C13-C15-C17)	176.78	176.75	178.71	176.82	-177.08
D(H28-C13-C15-C18)	-1.98	-2.04	-0.56	-1.97	1.78
D(C12-C14-C17-C15)	-0.67	-0.65	0.19	-0.66	0.63
D(C12-C14-C17-H33)	179.12	179.16	177.64	179.14	-179.13
D(H29-C14-C17-C15)	179.61	179.61	-179.03	179.59	-179.68
D(H29-C14-C17-H33)	-0.60	-0.59	-1.59	-0.61	0.57
D(C13-C15-C17-C14)	1.17	1.21	0.73	1.20	-1.02
D(C13-C15-C17-H33)	-178.62	-178.60	-176.68	-178.61	178.74
D(C18-C15-C17-C14)	-179.99	-179.93	179.95	-179.95	-179.95
D(C18-C15-C17-H33)	0.21	0.26	2.55	0.24	-0.19
D(C13-C15-C18-O1)	158.87	159.02	18.71	158.71	-158.83
D(C13-C15-C18-N4)	-20.03	-19.91	-162.28	-20.19	20.06
D(C17-C15-C18-O1)	-19.93	-19.81	-160.54	-20.12	20.07
D(C17-C15-C18-N4)	161.17	161.26	18.47	160.99	-161.04

F. Papers published in international journals

Chaudhary, M. K., Karthick, T., Joshi, B. D., Prajapati, P., de Santana, M. S. A., Ayala, A. P., . . . Tandon, P. (2021). Molecular structure and quantum descriptors of cefradine by using vibrational spectroscopy (IR and Raman), NBO, AIM, chemical reactivity and molecular docking. *Spectrochimica Acta Part A: Molecular and Biomolecular Spectroscopy*, *246*, 118976.

Chaudhary, M. K., Prajapati, P., Srivastava, K., Silva, K. F., Joshi, B. D., Tandon, P., & Ayala, A. P. (2021). Molecular interactions and vibrational properties of ricobendazole: Insights from quantum chemical calculation and spectroscopic methods. *Journal of Molecular Structure*, *1230*, 129889.

Chaudhary, M. K., Srivastava, A., Singh, K. K., Tandon, P., & Joshi, B. D. (2020). Computational evaluation on molecular stability, reactivity, and drug potential of frovatriptan from DFT and molecular docking approach. *Computational and Theoretical Chemistry*, *1191*, 113031.

Chaudhary, T., Chaudhary, M. K., Joshi, B. D., de Santana, M. S. A., & Ayala, A. P. (2021). Spectroscopic (FT-IR, Raman) analysis and computational study on conformational geometry, AIM and biological activity of cephalexin from DFT and molecular docking approach. *Journal of Molecular Structure*, *1240*, 130594.

Singh, K. K., Tandon, P., Kumar, R., Misra, A., Yadav, M., Ahmad, A., & Chaudhary, M. K. (2021). Formation of aminomethanol in ammonia-water interstellar ice. *Monthly Notices of the Royal Astronomical Society*, *506*(2), 2059–2065.

G. Papers published in national journals

Chaudhary, M. K., Chaudhary, T., & Joshi, B. D. (2021). Simulated spectra (IR and Raman), NLO, AIM and molecular docking of carisoprodol from DFT approach. *BIBECHANA*, *18*(1), 48–57.

Chaudhary, M. K., Prajapati, P., & Joshi, B. D. (2020). Quantum Chemical Calculation and DFT Study of Sitagliptin: Insight from Computational Evaluation and Docking Approach. *Journal of Nepal Physical Society*, *6*(1), 73–83.

Chaudhary, T., Chaudhary, M. K., & Joshi, B. D. (2021). Topological and Reactivity Descriptor of Carisoprodol from DFT and Molecular Docking Approach. *Journal of Institute of Science and Technology*, *26*(1), 74–82.

Joshi, B. D., & Chaudhary, M. K. (2018). NBO, nonlinear optical and thermodynamic properties of 10-Acetyl-10H-phenothiazine 5-oxide. *BIBECHANA*, *15*, 131–139.

Joshi, B. D., Thakur, G., & Chaudhary, M. K. (2021). Molecular Structure, HOMO-LUMO and Vibrational Analysis of Ergoline by Density Functional Theory. *Scientific World*, *14*(14), 21–30.

H. Participation in conferences, seminars, workshops and lecture series

- "Scientific secession of NPS 37th Annual Convention" organized by Nepal Physical Society, Febuary-6 2021.
  Oral presentation: "Structural properties of ricobendazole from quantum chemical calculation and spectroscopic methods"
- "International Seminar on Applications of Vibrational Spectroscopy" organized by The Department of Physics, SRM Institute of Science & Technology, Ramapuram Campus, Chennai, India on 29th August 2020.
- "Workshop on Computer Aided Drug Design using BIOVIA Discovery Studio" organized by Department of Physics, Deen Dayal Upadhyaya Gorakhpur University, Gorakhpur, India, 13-14 August 2020.
- "ANPA conference-2020" organized by ANPA, 17-19 July 2020.
  Oral presentation: "Structural, spectroscopic (IR and Raman) and physicochemical properties of Ricobendazole, from experimental and computational approach"
- "Lecture Series on Experimental Techniques in Advanced Materials (CETAM-2020)" organized by Periyar University Post Graduate Extension Center Dharmapuri-636701, India in association with Indian Science and Technology Association and Elavenial Organisation, 1-3 June 2020.
- "National E-Conference on Interdisciplinary Research in Science and Technology (NCIRST-20)" organized by Amiruddaula Islamia Degree College, Lucknow, India, 30-31 May 2020.
  Poster presentation: "Simulated spectra (IR and Raman), NLO, AIM and molecular docking of carisoprodol from DFT approach"
- "Webinar on Biomedical Applications of Raman Spectroscopy" organized by University of Lucknow, India on 11th May 2020.
- "Indo-Brazilian e-Symposium on Solid-State Properties of Pharmaceuticals" organized by University of Lucknow, India and Federal University of Ceará, Brazil, 29-30 April 2020.
  Poster presentation: "Computational evaluation on molecular stability, reactivity and drug potential of Frovatriptan: Insights from DFT and molecular docking approach"
- "8th International Conference on Perspectives in Vibrational Spectroscopy (ICOPVS-2020)" organized by JNCASR, Bengaluru, India, 24-28 February 2020.
  Oral presentation: "Study on Vibrational Spectroscopy and Quantum Chemical Calculation Method of Cefradine"

- "International Conference on Ultrasonics and Materials Science for Advanced Technology 2019 (ICUMSAT-2019)" organized by Department of Physics Prof. Rajendra Singh (Rajju Bhaia) Institute of Physical Sciences for Study and research VBS Purvanchal University, Jaunpur-2220003 (U. P.), India, 16-18 November 2019.
  Oral presentation: "Study on Vibrational Spectroscopy and Quantum Chemical Calculation Method of Ricobendazole"

- "International Symposium on Advances in Functional and Biological Materials (ISAFBM-2019)" organized by Humboldt Academy Lucknow and Physics Department, University of Lucknow, 28^{th} Febuary 2019.
  Poster presentation: "Study on Vibrational Spectroscopy and Quantum chemical calculation of Ricobendazole"

- "International Conference on Nanosciences and High Energy Physics" organized by the central department of physics, Tribhuvan University, Kirtipur, Kathmandu, Nepal, 4-6 February 2019.
  Poster presentation: "NBO and HOMO-LUMO analysis of Ricobendazole"

- "International Conference on Explorations in Physics (ICEP-2018)" organized by Amrit Campus, Thamel, Kathmandu, Nepal, 29-31 May 2018.
  Oral presentation: "Study on Vibrational Spectroscopy and Quantum Chemical Calculation of Ricobendazole"

- "International Chemical Congress" organized by Nepal Chemical Society, 8-10 March 2018.
  Oral presentation: "NBO and HOMO-LUMO Properties of Ricobendazole Using Vibrational Spectroscopy and Quantum Chemical Methods"

- "International Conference on Physics of Space and Materials" organized by St. Xavier's College, Kathmandu, Nepal, 2-3 September 2017.
  Poster presentation: "Quantum Chemical Study of Benzimidazolic Drug: Ricobendazole"

- "Lecture Series on Research Methodology" organized by Central Department of Physics, Tribhuvan University, Kirtipur, Kathmandu, Nepal, 6 November–22 December 2017.

Nepal Physical Society

Ghantaghar, Kathmandu

Certificate of Participation

This certificate is awarded to

Mr. Manoj Kumar Chaudhary **from**

Central Department of Physics, TU, Nepal, for his presentation entitled

Structural properties of ricobendazole from quantum chemical calculation and spectroscopic methods

On Scientific Session of 37th Annual Convention, February 6, 2021.

Prof. Dr. Narayan Prasad Chapagain	**Dr. Sunil Babu Shrestha**	**Prof. Dr. Leela Pradhan Joshi**
President	Chief Guest	Chair, Scientific Committee
Nepal Physical Society	Vice – Chancellor, NAST	37th Annual Convention, NPS

February 6, 2021

Certificate of Appreciation

THIS CERTIFICATE IS PRESENTED TO

MR. MANOJ K. CHAUDHARY

Tribhuvan University, Nepal

FOR YOUR PRESENTATION DURING THE ANPA CONFERENCE 2020

DR. CHET R. BHATT
CHAIR, ANPA CONFERENCE 2020

DR. SHREE K. BHATTARAI
PRESIDENT, ANPA

National E-Conference on

Interdisciplinary Research in Science and Technology

(NCIRST-20)

AIDC/NCIRST/P/022

30 & 31 May 2020

Certificate

This is to certify that Prof./Dr./Mr./Ms.

Manoj Kumar Chaudhary

Central Department of Physics, Tribhuvan University, Kirtipur, Kathmandu, Nepal

has participated and presented a paper (Poster) in the "National E-Conference on Interdisciplinary Research in Science and Technology" organized by Amiruddaula Islamia Degree College, Lucknow (U.P.) India.

Title of Paper: **Simulated spectra (IR and Raman), NLO, AIM and molecular docking of carisoprodol from DFT approach**

Dr. Abdul Quayoum
Principal

Dr. Nishant Kumar
Convener

Webinar

on

Biomedical Applications of Raman Spectroscopy

May 11 , 2020

Certificate

This is to certify that

Manoj Kumar Chaudhary

Tribhuvan University, Kirtipur, Kathmandu, Nepal

has actively Participated
in the Webnar on
Biomedical Applications of Raman Spectroscopy
Organized by University of Lucknow, India

Place : Lucknow
Date : 11 May, 2020

Tandon

Poonam Tandon
Convenor
Head, Physics Department
University of Lucknow, India

CERTIFICATE OF PARTICIPATION

8th ICOPVS
International Conference on Perspectives in Vibrational Spectroscopy

This certificate is awarded to

Mr. Manoj Kumar Chaudhary

Central Dept of Physics, Tribhuvan University, Kirtipur, Kathmandu, Nepal

In appreciation of participation as an Oral Presenter for the talk entitled,

"Study on vibrational spectroscopy and quantum chemical calculation of cefradine"

in the 8th International Conference on Perspectives in Vibrational Spectroscopy held during 24-28th February, 2020 at JNCASR, Bengaluru.

Prof. A Sundaresan
Co-Chair

Prof. Chandrabhas Narayana
Conference Chair

Prof. Umesh V Waghmare
Co-Chair

TEQIP

ULTRASONICS SOCIETY OF INDIA • Founded 1974 •

International Conference on
Ultrasonics and Materials Science for Advanced Technology 2019 (ICUMSAT-2019)
Theme: Ultrasonics in Materials Science
November 16-18, 2019

CERTIFICATE

Certified that Prof. / Dr. / Mr. / Ms. Monoj Kumar Chaudhary

from Tribhuvan University, Kirtipur, Kathmandu, Nepal

participated as Chairperson of a Session / Plenary Speaker / Invited Speaker / Contributor of a Research Paper for Oral / Poster Presentation.

Title of the Talk / Paper Studyon Vibrational - - - - - - - - - - - - - RicBbendazole

(Dr. Punit K. Dhawan)
Organizing Secretary

(Dr. Giridhar Mishra)
Convener

In collaboration with :
Ultrasonics Society of India
National Physical Laboratory
New Delhi – 110012, India

Organized by :
Department of Physics
Prof. Rajendra Singh (Rajju Bhaiya) Institute of Physical Sciences for Study and Research
VBS Purvanchal University, Jaunpur-222003 (U.P.) India

ISAFBM - 2019
International Symposium
on Advances in Functional & Biological Materials

Certificate

This is to certify that

Manoj Kumar Chaudhary

Tribhuvan University, Kathmandu

delivered Keynote Lecture / Invited Lecture / Oral Presentation / Chaired Session / Presented Poster/ Participated in ISAFBM - 2019

Organized by

Humboldt Academy Lucknow & Physics Department, University of Lucknow

Date : February 28, 2019
Place : Lucknow

Prof. PoonamTandon
Organizing Secretary
ISAFBM-2019

International Conference on
Nanosciences and High Energy Physics
(ICNHEP-2019)
February 4-6, 2019
Central Department of Physics
Tribhuvan University, Kirtipur, Nepal

Certificate

This is to Certify that ~~Dr./Mr./Ms~~ Manoj Kumar Chaudhary has actively participated in International Conference in Nanosciences and High Energy Physics "ICNHEP-2019" organized by Central Department of Physics, Tribhuvan University, Kirtipur Kathmandu, Nepal on 4-6 February, 2019.

Prof. Dr. Ram Pd. Khatiwada
Dean, IoST, TU, Kirtipur

Dr. Gopi Chandra Kaphle
Convener, ICNHEP-2019

Prof. Dr. Binil Aryal
Head CDP, TU, Kirtipur

INTERNATIONAL CONFERENCE ON
EXPLORATIONS IN PHYSICS (ICEP-2018)

29-31 May, 2018, Kathmandu, Nepal

Manoj Kumar Chaudhary

Department of Physics, Amrit Campus, Tribhuvan University, Kathmandu, Nepal

Contributed an oral presentation entitled

NBO, DIPOLE MOMENT, PLARISIBILITY and HOMO-LUMO Properties of Ricobendazole Using Vibrational Spectroscopy and Quantum Chemical Methods

during the conference

Chief Guest
Prof. Dr. Jiba Raj Pokharel
Vice Chancellor, NAST

Campus Chief
Rajesh Mahaju
Amrit Campus

SOC Chair
Assoc. Prof. Dr. Leela Pradhan Joshi
Amrit Campus

ICC-2018

International Chemical Congress

- Chemistry for Sustainable Development-

Organized by

Nepal Chemical Society

In co-operation with

Department of Chemistry

Birendra M. Campus, Bharatpur, Tribhuvan University
Chitwan, Nepal

Certificate of Participation

This is to certify that

Mr. Manoj Kumar Chaudhary

participated as Plenary/Keynote/Invited/Oral Lecture/Poster /Delegate in the International Chemical Congress Chemistry for Sustainable Development

March 8-10, 2018, Sauraha, Chitwan, Nepal

Dr. Surya Kant Kalauni General Secretary Nepal Chemical Society	**Govind Sapkota** Co-patron ICC-2018 Campus Chief, Birendra M. Campus	Chief Guest	**Prof. Dr. Amar Prasad Yadav** Convener ICC-2018 President Nepal Chemical Society

International Conference on Physics
of
Space and Materials
(ICPSM - 2017)

This certificate is awarded to Mr Manoj Kumar Chaudhary
for poster presentation on the title
Quantum chemical study of a benzimidazolic drug: Ricobendazole
in
the International Conference on Physics of Space and Materials
held on September 2-3, 2017
Organized by
St. Xavier's College, Kathmandu, Nepal.

MR. DRABINDRA PANDIT
HEAD OF DEPARTMENT
PHYSICS

PROF. DR. JIBA RAJ POKHAREL
VICE CHANCELLOR
NAST
CHIEF GUEST

FR. JIJU VARGHESE S. J.
PRINCIPAL

Lecture Series on

Research Methodology

6 November – 22 December 2017

Central Department of Physics
Tribhuvan University, Kirtipur, Nepal

Participation Certificate

Manoj Kumar Chaudhary

Central Department of physics T.U.

participated in **21 hours lecture series** on **Research Methodology** delivered by **Prof. Dr. Subodh R. Shenoy**, TIFR, India during 6 November to 22 December 2017.

Subodh R. Shenoy

Prof. Dr. Subodh R. Shenoy
Guest Speaker
Tata Institute of Fundamental Research, India

Prof. Dr. Binil Aryal
Head
CDP, TU, Kirtipur

Journal of Molecular Structure 1230 (2021) 129889

Contents lists available at ScienceDirect

Journal of Molecular Structure

journal homepage: www.elsevier.com/locate/molstr

Molecular interactions and vibrational properties of ricobendazole: Insights from quantum chemical calculation and spectroscopic methods

Manoj Kumar Chaudhary[a,b], Preeti Prajapati[b], Karnica Srivastava[b], Keilla Façanha Silva[c], Bhawani Datt Joshi[d,*], Poonam Tandon[b,*], Alejandro Pedro Ayala[c]

[a] Central Department of Physics, Tribhuvan University, Kirtipur, Kathmandu, Nepal
[b] Department of Physics, University of Lucknow, Lucknow 226007, India
[c] Departamento de Fisica, Universidade Federal do Ceará, C.P. 6030, 60.455-900, Fortaleza, CE, Brazil
[d] Department of Physics, Tribhuvan University, Siddhanath Science Campus, Mahendranagar, 10406, Nepal

ARTICLE INFO

Article history:
Received 10 February 2020
Revised 29 September 2020
Accepted 5 January 2021
Available online 7 January 2021

Keywords:
Ricobendazole
Vibrational spectroscopy
Natural bond orbital
Chemical reactivity
Molecular docking

ABSTRACT

The structural, spectroscopic (FT-IR and FT-Raman), and physicochemical properties of ricobendazole (RBZ) has been presented with the help of combined experimental and computational approaches. A comparison between the observed and simulated spectra show good agreement with each other. The conformational analysis was performed around eight flexible bonds to predict the most stable conformers, by employing density functional theory (DFT) at B3LYP/6–311++*G*(d,p) level. The chemical reactivity has been demonstrated in terms of frontier molecular orbitals (HOMO-LUMO) energy gap, molecular electrostatic potential (MEP) surface, and global reactivity. The local reactivity descriptors explored an idea about the donor/acceptor/free radical reactive sites present in the molecule. Natural bond orbital (NBO) analysis was performed to study the interactions between bonding and antibonding orbitals. The intramolecular hydrogen bonding interactions were demonstrated using QTAIM theory. Binding sites against three targets such as Poly [ADP-ribose] polymerase-1, MAP kinase p38 alpha, and Adenosine A2a receptor were identified by molecular docking analysis as RBZ is believed to inhibit against them.

1. Introduction

Benzimidazoles are the most widely used anthelmintics in the world [1]. Low toxicity and broad-spectrum activity have contributed to its success as an anthelmintic agent. sulfur-containing derivatives such as fenbendazole, oxfendazole, and albendazole are essential drugs in this class [2-6]. Ricobendazole (RBZ) belongs to the benzimidazole group of compounds (BZDS). It is an active metabolite of albendazole and also known as albendazole sulfoxide. Metabolism is understood as a process through which biochemical reactions occur in the body alters the drug [3].

Ricobendazole (RBZ), $C_{12}H_{15}N_3O_3S$, is denominated by IUPAC as methyl N-(6-propylsulfinyl-1H-benzimidazol-2-yl)carbamate. Its chemical structure is presented in Fig. 1. The benzimidazole drug is prescribed for the treatment of worms. It is widely used in veterinary medicine to prevent and treat parasitic diseases, being the most effective anthelmintic agents [7]. The pharmacological activities of RBZ are focused on the inhibition of tubulin polymerization and blockage of glucose uptake which produce depletion of glycogen stores and decrease the adenosine triphosphate (ATP) formation in the larval and adult stages of parasites [8-16]. Due to low solubility, and high permeability, RBZ belongs to class II of the Biopharmaceutical Classification Systems (BCS) [6,17]. The speed of absorption is greater than that of dissolution, where the dissolution controls the speed of absorption. Thus, absorption and bioavailability are limited by the rate of dissolution of the drug [18]. BCS was developed to guide the correlation between drug dissolution *in vitro* and bioavailability *in vivo* [19]. Using these two criteria to characterize the drugs oral absorption, BCS classifies them into four categories, as shown in Fig. 2. It is estimated that about 30% of commercially developed drugs belong to class II. So, they exhibit limitations for oral administration due to their low solubility [20].

The present motive is to study the structural, conformational, intramolecular hydrogen bonding, global reactivity, and local reactivity descriptors that predict the reactive sites of RBZ. Chem-

* Corresponding author.
E-mail addresses: pbdjoshi@gmail.com (B.D. Joshi), poonam_tandon@yahoo.co.uk (P. Tandon).

https://doi.org/10.1016/j.molstruc.2021.129889
0022-2860/

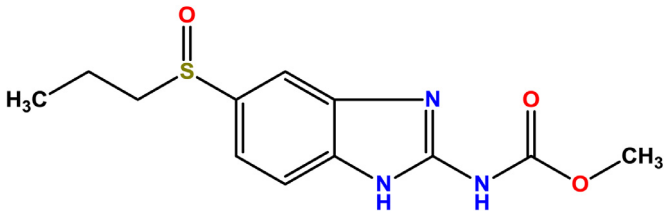

Fig. 1. Chemical structure of RBZ.

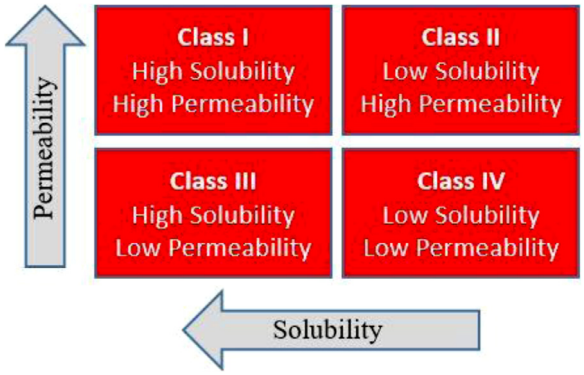

Fig. 2. Graphical representation of the four categories of the Biopharmaceutical Classification System (BCS).

ical reactivity has been studied in terms of molecular electrostatic potential (MEP) surface, frontier molecular orbitals (FMOs), and Hirshfeld charges. The hyperconjugative interaction of the title molecule has been scrutinized with NBO analysis. The geometrical and topological parameters along with the interaction energy of intramolecular hydrogen bonds at bond critical point (BCP) have been discussed by implementing quantum theory of atoms in molecule (QTAIM). Moreover, the drug-likeness and molecular docking of RBZ has been carried out. The above-mentioned atomic-level properties have been investigated by using vibrational spectroscopy and quantum chemical calculation approach by using density functional theory (DFT) [21].

2. Experimental details

The compound, RBZ, in solid form of purity level more than 98% was purchased from the Merck & Co., multinational pharmaceutical company, USA. The spectra (Infrared and Raman) were recorded without making any further purification. Using Bruker Vertex 70 FT-IR spectrometer the infra-red spectrum (IR) was recorded in the range of 400–4000 cm^{-1} with a resolution of 4 cm^{-1}. KBr was used as a binding material during the pellet formation with the sample in the ratio 200:1. OPUS software was used for the baseline corrections. Raman spectrum of the sample was recorded in the range 100–3600 cm^{-1} by implementing the RAM II module with the help of diode-pumped Nd: YAG laser with an excitation wavelength of 1064 nm at a laser power lower than 100 mW.

3. Computational details

Initially, the 3D electronic structure of RBZ was taken from PubChem data [22]. The geometry optimization was performed using density functional theory (DFT) with the implementation of B3LYP/6–311++*G*(d,p) [23-25] basis set using Gaussian 09 software [26]. The B3LYP functional is composed of Becke's three parameters (local, nonlocal, Hartree-Fock) hybrid exchange and Lee-Yang-Parr correlation functional [27,28]. The optimized geometry was subjected to conformational analysis. It was found that there exist three conformers having energy difference less than the value of kT (0.56 kcal/mol) with respect to the lowest energy conformer. Analytical frequency calculations were performed at the same level, which infers about calculated IR and Raman spectra. GaussView 05 program was used for visualization of the simulated data [29]. Hyperconjugative interaction of intramolecular charge transfer was analyzed with the NBO program as implemented in Gaussian 09 program packages [30]. The normal modes of vibration were assigned using the program Gar2Ped [31]. A complete set of 96 internal coordinates were defined by using Pulay's recommendations [32]. The topological properties of the title molecule were studied within the framework of QTAIM [33-35] using AIM2000 and AIMALL software [36]. Molecular docking simulations have also been made to examine the ligand-protein interaction using AutoDock [37] and Discovery studio for visualization [38].

4. Results and discussion

4.1. Conformational studies

To obtain the most stable conformer, one-dimensional potential energy surface (PES) scan has been performed across the eight rotatable bonds with corresponding dihedral angles: ϕ1(H33-C19-O3-C18), ϕ2(C19-O3-C18-N7), ϕ3(O3-C18-N7-C16), ϕ4(C18-N7-C16-N5), ϕ5(C14-C9-S1-O2), ϕ6(C9-S1-C10-C13), ϕ7(S1-C10-C13-C17) and ϕ8(C10-C13-C17-H29) on the initially optimized structure shown in Fig. 3. The torsion angle was varied in a regular interval of 10º around the flexible bonds in the range of 0–360º. All the potential energy surface (PES) scan curves are presented in Fig. S1 (Supplementary Material). Eight conformers were obtained as suggested by the PES scan graph based on global and local minima. The optimized energy of all these conformers relative to the most stable conformer (conformer I) is presented in Table S1 (Supplementary Material). The optimized structure of eight conformers along with relative energy is presented in Fig. S2 (Supplementary Material). Only three conformers: conformer I, conformer II and conformer III have energy less than 0.56 kcal/mol (equivalent to kT), and they are considered as the most stable conformers which may exist at room temperature. The optimized energy values of conformer I, II, and III are –787,322.8843, –787,322.7170, and –787,322.5046 kcal/mol, respectively. The present work is based on these three stable conformers.

4.2. Geometry optimization

The optimized molecular structures of conformers II & III have been compared by overlapping them with the most stable conformer I by using a least-squares algorithm, which minimizes the distances of the corresponding non-hydrogen atoms. The overlapped structure of conformers II & III with conformer I is shown in Fig. S3 (Supplementary Material). The conformers I & II overlapped well with each other except the side chain -CH_2–CH_2–CH_3, while in case of the conformers I & III, only -CH_3 side chain is slightly tilted.

The optimized geometrical parameters, the bond length, bond angle, and dihedral angle of the conformers (I–III) are listed in Table S2 (Supplementary Material), based on the atom-numbering scheme presented in Fig. 3. The significant difference in the bond length is observed as 0.0059 Å and 0.0050 Å across the bond S1-C10 in conformers I & II, and I & III, respectively. This increase in bond length is due to the formation of an intramolecular hydrogen bond across O2**...**H22 as explained in Section 4.8. The bond angles of S1-C10-H20, S1-C10-C13, and C9-S1-C10 showed a difference of 3.1067º, 3.4387º, and 1.4376º between conformers I & II, whereas the bond angles of C10-C13-H23 and C10-C13-C17 showed a difference of 1.4755º and 2.3585º in conformers I & III, respectively. Due to different orientations of the plane of the side-chain

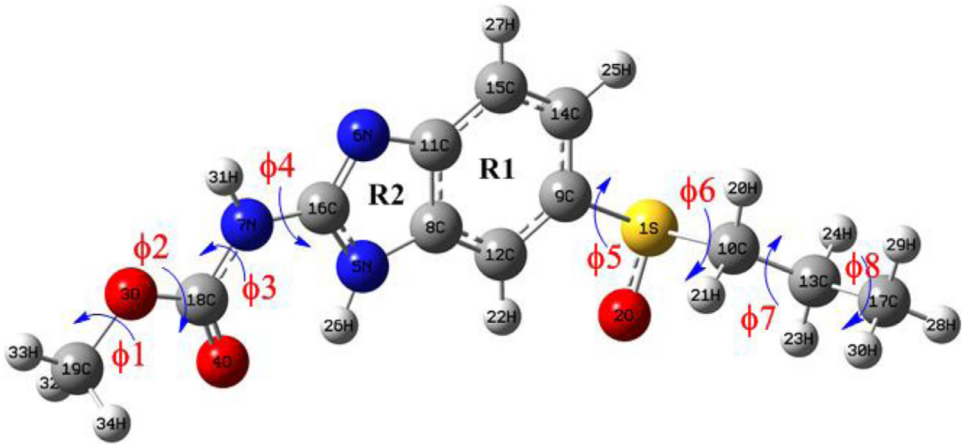

Fig. 3. Stable conformer of RBZ with atom numbering scheme.

$-CH_2-CH_2-CH_3$ in conformers I & II, certain dihedral angles do not match with each other. Similarly, the side chain $-CH_3$ in conformers I & III do not overlap with each other so certain dihedral angles showed a significant difference due to the orientation of plane.

4.3. Vibrational spectra

RBZ molecule has 34 atoms and hence gives 96 (3N–6) normal modes of vibration. All these modes are both IR and Raman active. Table S3 (Supplementary Material) shows the assigned wavenumbers of the normal modes with their respective potential energy distributions (PED) values. As the quantum chemical calculation produces Raman amplitudes, not Raman intensities, so Raman intensities were determined for each normal mode of vibration in terms of Raman scattering cross-section, $\frac{\partial\sigma_j}{\partial\Omega}$, and is given by the relation [39,40]

$$\frac{\partial\sigma_j}{\partial\Omega} = \left(\frac{2^4\pi^4}{45}\right)\left(\frac{\left(\nu_0-\nu_j\right)^4}{1-exp\left[\frac{-hc\nu_j}{kT}\right]}\right)\left(\frac{h}{8\pi^2 c\nu_j}\right)S_j$$

where, Sj = scattering activities, ν_j = predicted wavenumbers for j^{th} normal mode, ν_0 = wave number of Raman excited state, and h, c, and k are universal constants. A Lorentzian line shape (FWHM = 8 cm^{-1}) is used to produce simulated spectra from the calculated Raman and IR intensities by convoluting the predicted vibrational mode.

4.3.1. Scaling of vibrational wavenumbers

In the calculated spectra, there was some overestimation of the wavenumber due to the anharmonicity present in a real system. To compensate this deficiency, the calculated wavenumbers were scaled down by a scaling factor 0.9679 [41] and listed in Table S3 (Supplementary Material). Comparison between observed and calculated spectra (IR and Raman) for the three conformers was made and presented in Figs. 4 and 5 which shows a good agreement.

4.3.2. C = O and S-O vibration

Strong stretching vibration absorption band of the carbonyl group ($C=O$) lies in the range 1670–1820 cm^{-1} [42-44]. A strong IR stretching vibration was observed at 1729 cm^{-1} and its Raman counterpart at 1720 cm^{-1}, their corresponding calculated values lie at 1716 cm^{-1} in all the three conformers. The S-O stretching is generally found at 989 cm^{-1} [45]. In the present work, ν(S-O) was calculated at 979/981/975 cm^{-1} in conformers I/II/III and observed in the Raman spectrum at 962 cm^{-1}. This shifting of wavenumber is due to intramolecular H-bond between O2 and H22 as explained in Section 4.8.

4.3.3. Benzene ring vibration

The C–H stretching vibrations in aromatic compounds are generally observed in the range of 3000–3100 cm^{-1} [42,46,47]. Small peaks of C–H stretching were calculated at 3093 and 3061 cm^{-1} and observed in the IR spectra at 3167 and 3065 cm^{-1}. The ν(CC) ring stretching was observed at 1303 cm^{-1} with a distinct peak in both the IR and Raman spectra and calculated at 1327 cm^{-1} in all the conformers.

4.3.4. N–H, C–N, C = N, and C-S vibration

The N–H stretching vibrations were calculated at 3487/3488/3486 cm^{-1} in conformers I/II/III respectively and it was observed at 3390 cm^{-1} in IR spectra. This shifting of wavenumber is due to the formation of intramolecular H-bond between H26 and O4 as explained in Section 4.8. Karabacak etal. [48] assigned C=N and C–N stretching at 1689 and 1302 cm^{-1} in the IR spectrum, respectively. Sundaraganesan et al. [49] assigned C–N stretching vibration at 1281 cm^{-1} for benzimidazole. In the present work, C=N stretching vibration was observed at 1631/1635 cm^{-1} in IR/ Raman spectra and computed at 1618 cm^{-1} in all the conformers. C–N stretching vibration was calculated at 1477 cm^{-1}, and it was observed at 1516/1524 cm^{-1} in IR/Raman spectrum with distinct peaks. In this study, the C-S stretching mode was observed at 647/645 cm^{-1} in IR/Raman spectrum and calculated at 661/632/609 cm^{-1} in conformers I/II/III respectively.

4.3.5. CH_3 and CH_2 vibration

The stretching vibrations of CH_3 group were obtained in the higher wavenumber region. $\nu_a(C19H_3)$ vibration was calculated at 3064 cm^{-1} in all the three conformers and observed at 3065 cm^{-1} in Raman spectrum. $\nu_a(C17H_3)$ were calculated at 2991/2989/2996 cm^{-1} for conformers I/II/III respectively and observed at 3020 cm^{-1} in both IR and Raman spectra. The symmetric deformation and rocking vibrations of $C19H_3$ were calculated at 1421 and 1137 cm^{-1} and observed at 1415/1413 and 1127/1123 cm^{-1} in IR/Raman spectra, respectively.

One can expect five modes of vibrations related to each ethyl group $C10H_2$ and $C13H_2$ attached in this molecule. The symmetric deformation $\delta_{sym}(C10H_2)$ was calculated at 1214/1227/1222 cm^{-1} in conformers I/II/III and observed at 1228/1224 cm^{-1} in IR/Raman spectrum. Asymmetric deformation δ_{asym} $(C10H_2)$ was calculated at 1200/1197/1197 cm^{-1} in conformers I/II/III, respectively, and observed at 1193/1191 cm^{-1} in IR/Raman spectrum. The δ'_{asym} $(C13H_2)$ vibration was calculated at 1461/1461/1456 cm^{-1} in conformers I/II/III and observed at 1466 cm^{-1} in both IR and Raman spectra.

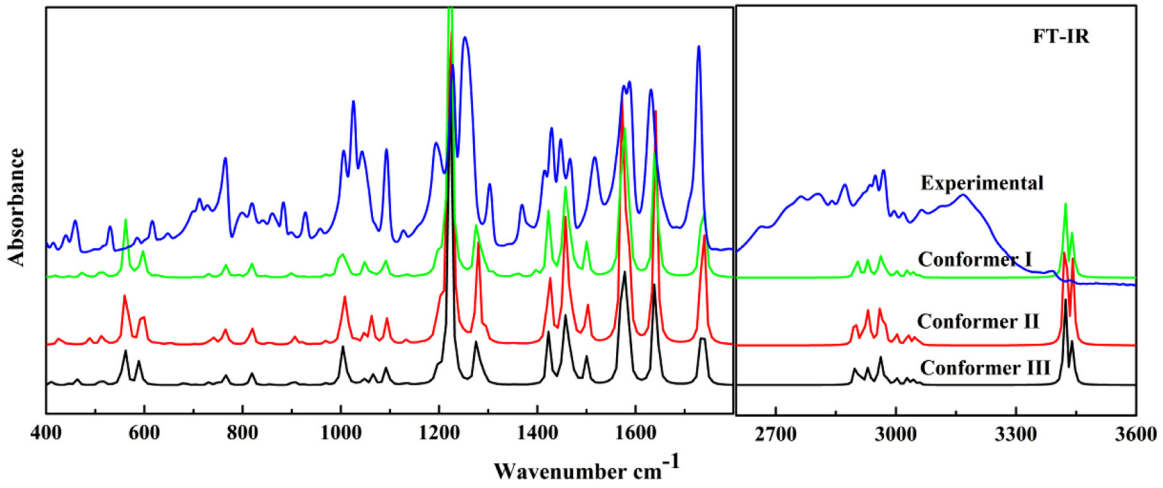

Fig. 4. Calculated and observed infrared spectra of RBZ in the region 400–1800 cm^{-1} and 2601–3600 cm^{-1}.

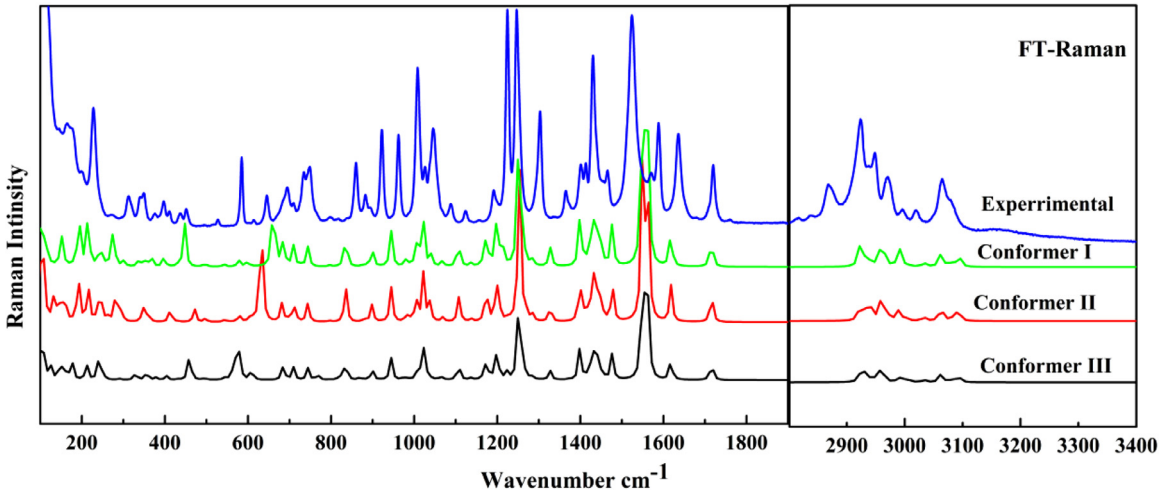

Fig. 5. Calculated and observed Raman spectra of RBZ in the region 100–1900 cm^{-1} and 2801–3400 cm^{-1}.

4.4. Natural bond orbital (NBO)

NBO analysis has been performed *via* second-order perturbation theory to reveal all the possible interaction between filled donor Lewis type and virtual acceptor Lewis type NBOs orbital and their stabilization energy $E^{(2)}$ have been analyzed [50-53]. The interaction energy E(i,j) between i (donor) and j (acceptor) NBOs is numerically described which gives the stabilization energy among bonding and antibonding interaction. It is mathematically obtained from the off-diagonal Fock matrix element [54,55]

$$E^{(2)} = E(i,j) = -q_i \frac{(F_{ij})^2}{E_j - E_i}$$

where q_i is referred to as the donor orbital occupancy, E_i and E_j are the respective energy of donor and acceptor orbitals and F_{ij} are the off-diagonal Fock matrix elements. The larger value of $E^{(2)}$ implies the more intensive donor-acceptor interactions. The π orbitals have lower occupancies, which show more electron-donor ability in comparison to the σ orbital [56,57]. The different types of donor-acceptor interactions and their equilibrium energies are determined by second-order perturbation analysis of the Fock matrix for conformer I of RBZ are tabulated in Table 1. The interaction of π(C11-C15) $\rightarrow$ π^*(C8-C12) produces resonance in the molecule, leading to a stabilization energy of 23.08 kcal/mol. A very strong interaction has been identified between the lone pair LP(1)N7 $\rightarrow$ π^*(O4-C18)/π^*(N6-C16) which stabilizes the molecule with stabilization energy 61.96/43.39 kcal/mol. The lone pair LP (1) N5 participates in charge transfer from LP(1)N5 $\rightarrow$ π^*(N6-C16)/π^*(C8-C12) with energies of 55.06/36.74 kcal/mol. The interactions LP(2)O3 $\rightarrow$ π^*(O4-C18) leads to a stabilization energy of 45.67 kcal/mol. The stabilization energy values for conformers II & III were very similar to conformer I and their values are presented in Table S4 and S5 (Supplementary Material).

4.5. Molar refractivity

Molar refractivity (MR) is a useful property that measures the binding property and lipophilicity that helps to predict drug-likeness of the studied system for oral administration in human [58]. To deduce the drug-likeness of a particular molecular system, Lipinski proposed several rules. According to these improved rules, a molecule should have: (i) MR value from 40 to 130 e.s.u. (ii) molecular weight from 180 to 500 g/mol, and (iii) number of atoms in the molecular system between 20 and 70. MR is a constitutive–additive property and may be calculated using the Lorenz–Lorentz formula [59-61]

$$MR = \left[\frac{n^2-1}{n^2+2}\right]\left(\frac{MW}{\rho}\right) = 1.333\pi\alpha N$$

Table 1
Second-order perturbation theory analysis of Fock matrix in NBO basis for conformer I of RBZ.

Donor NBO(i)	ED(i)/e	Acceptor NBO (j)	ED(j)/e	$E^{(2)}$[a] kcal/mol	E(j) - E(i)[b] a.u	F(i,j)[c] a.u
σ(N6-C11)	1.97364	σ^*(N7-C16)	0.03667	8.42	1.18	0.089
σ(N6-C16)	1.98110	σ^*(C11-C15)	0.02215	5.34	1.44	0.078
π(N6-C16)	1.86010	π^*(C11-C15)	0.42074	20.84	0.35	0.083
π(C8-C12)	1.63923	π^*(C9-C14)	0.45257	20.62	0.28	0.069
π(C8-C12)	1.63923	π^*(C11-C15)	0.42074	18.19	0.29	0.066
σ(C9-C12)	1.97236	σ^*(N5-C8)	0.02573	6.31	1.15	0.076
π(C9-C14)	1.68041	π^*(C11-C15)	0.42074	17.39	0.29	0.065
π(C11-C15)	1.60403	π^*(N6-C16)	0.40469	13.19	0.25	0.051
π(C11-C15)	1.60403	π^*(C8-C12)	0.40965	20.36	0.28	0.067
π(C11-C15)	1.60403	π^*(C9-C14)	0.45257	23.08	0.27	0.071
σ(C14-C15)	1.97130	σ^*(N6-C11)	0.01787	5.19	1.17	0.070
σ(C19-H32)	1.99540	σ^*(C19-H33)	0.00824	7.49	1.18	0.084
σ(C19-H32)	1.99540	σ^*(C19-H34)	0.01270	18.63	4.20	0.250
σ(C19-H34)	1.99539	σ^*(C19-H33)	0.00824	8.11	1.17	0.087
σ(C19-H34)	1.99539	σ^*(C19-H34)	0.01270	21.60	4.19	0.269
LP(2)O2	1.89048	σ^*(S1-C9)	0.12617	5.38	0.42	0.042
LP(2)O2	1.89048	σ^*(S1-C10)	0.11846	8.36	0.39	0.051
LP(3)O2	1.82449	σ^*(S1-C9)	0.12617	12.88	0.41	0.066
LP(3)O2	1.82449	σ^*(S1-C10)	0.11846	9.73	0.38	0.055
LP(1)O3	1.96206	σ^*(O4-C18)	0.02150	8.24	1.17	0.088
LP(2)O3	1.81638	π^*(O4-C18)	0.35949	45.67	0.33	0.114
LP(2)O4	1.83842	σ^*(O3-C18)	0.09322	29.73	0.63	0.124
LP(2)O4	1.83842	σ^*(N7-C18)	0.07071	22.69	0.70	0.115
LP(1)N5	1.62366	π^*(N6-C16)	0.40469	55.06	0.27	0.110
LP(1)N5	1.62366	π^*(C8-C12)	0.40965	36.74	0.30	0.095
LP(1)N6	1.92046	σ^*(N5-C16)	0.04216	9.41	0.81	0.078
LP(1)N6	1.92046	σ^*(C8-C11)	0.03710	5.47	0.91	0.063
LP(1)N7	1.68641	π^*(O4-C18)	0.35949	61.96	0.27	0.117
LP(1)N7	1.68641	π^*(N6-C16)	0.40469	43.39	0.29	0.103

[a] $E^{(2)}$ means the energy of hyper conjugative interaction (stabilization energy).
[b] Energy difference between donor (i) and acceptor (j) NBO orbitals.
[c] F(i,j) is the Fock matrix element between i and j NBO orbitals.

where N is the Avogadro number; α is the polarizability of the molecular system.

This equation is used for both solid and liquid states of the system under study. It is related to the volume of the molecules as well as to the London dispersive forces that act in the drug-receptor interaction. The calculated values of MR for the studied three conformers I, II, and III are 41.50, 42.02, and 41.37 e.s.u., respectively. Therefore, all three conformers have an adequate range of MR to be acceptable as a drug. The RBZ has molecular weight 281.33 g/mol and number of atoms 34. Therefore, RBZ satisfies all the Lipinski's criteria for being a good drug candidate.

4.6. HOMO-LUMO energy gap

The principal orbitals take part in the chemical reaction for the stability of the system is the highest occupied molecular orbital (HOMO) and lowest unoccupied molecular orbital (LUMO). The energies of HOMO (E_H) and LUMO (E_L) and their difference ($E_L - E_H$) determine the biological symptom of the molecule. The HOMO acts as a donor orbital which tends to donate electron and LUMO behaves as an acceptor orbital having tendency to capture electron for the stability of the molecule [62]. The molecular electronic transport property that measures electron conductivity is responsible for the chemical properties of a molecule was determined by HOMO and LUMO energy gap [63-65]. To understand the electronic transitions of RBZ, time-dependent DFT calculations have been conducted using (TD)-B3LYP/6–311++*G*(d,p) level for all the three conformers. The calculated HOMO-LUMO gap for the conformers I, II, and III are 4.9601, 4.9514, and 4.9476 eV, respectively. A small value of energy gap (4.9476 eV) between HOMO and LUMO for conformer III implies its high chemical reactivity whereas a large energy gap (4.9601 eV) for conformer I exhibit high chemical stability (or low chemical reactivity) than the remaining conformers. The HOMO and LUMO plots of all the conformers are shown in Fig. 6. In all the conformers, the charge is mostly confined over the sulfinyl group in HOMO whereas in LUMO charge diverges to aliphatic nitrogen (N7) and rings present in the molecule. This is also verified by MEP surface as interpreted in Section 4.7.1.

4.7. Chemical reactivity

The chemical reactivity of any chemical system can be investigated using the following tools: (i) MEP map, (ii) global reactivity descriptors, and (iii) local electronic reactivity descriptors.

4.7.1. Molecular electrostatic potential (MEP)

The MEP is used to explore the distribution of charge around the molecule in space which predicts the nucleophilic and electrophilic regions where the chemical reactions are probably taking place. It is a visual method to understand the relative polarity of the molecule [66, 67]. The 3D MEP of the three conformers of the title molecule is presented in Fig. 7. The electrostatic potential is illustrated based on distinct colors at the MEP surface. The color-coding is as follows: red represents most electronegative regions which show electrophilic reactivity, blue represents most electropositive regions which show nucleophilic reactivity, and green represents zero electrostatic potential [68]. In the MEP map of RBZ molecule, sulfinyl group (S1O2) is a most electronegative region which shows strong electrophilic reactivity and acts as a nucleophile for the environmental site. Whereas, hydrogen atoms in the imidazole ring, as well as N7H31, are most electropositive and show nucleophilic reactivity and, behave as an electrophile for the surrounding molecule in all the conformers. These sites are also justified as active binding sites in molecular docking as explored in Section 4.9.

4.7.2. Global reactivity descriptors

Koopman's theorem [69,70] explains the diverse global reactivity descriptors such as electronegativity (χ), chemical poten-

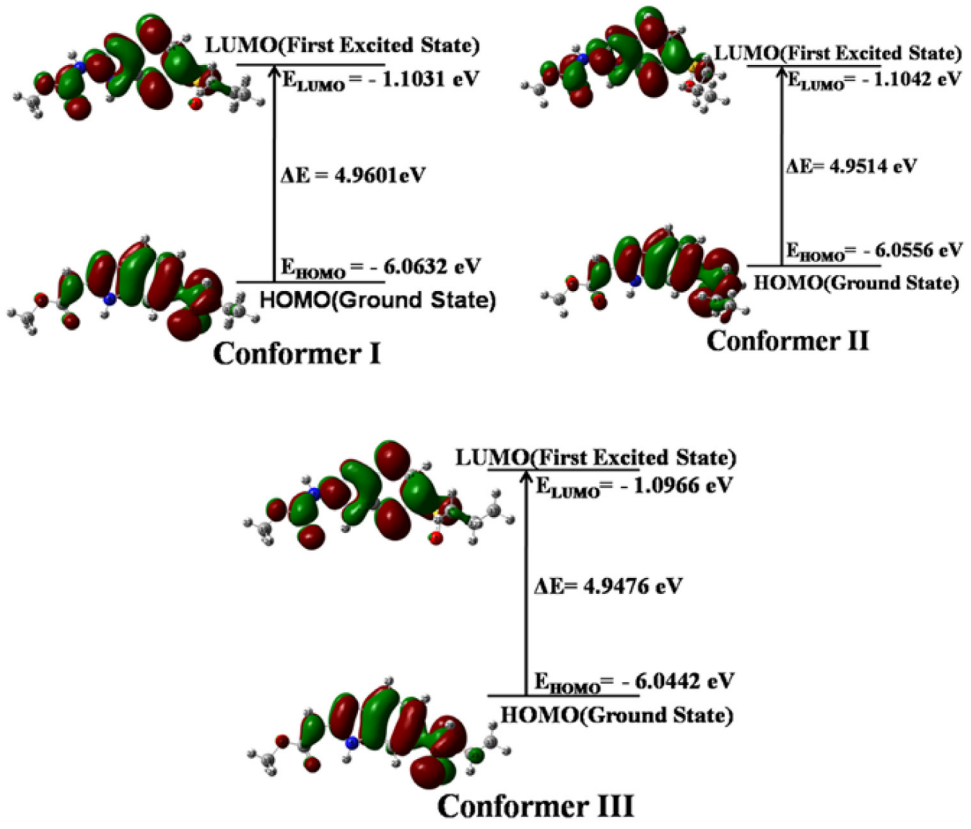

Fig. 6. Frontier molecular orbital's plot (HOMO-LUMO) for conformers (I-III) of RBZ.

tial (μ), global hardness (η), global electrophilicity index (ω), and global softness (S) and these descriptors are enumerated from the energies of frontier molecular orbitals E_{HOMO}, E_{LUMO} and are given by [71-76];

$$\chi = -\frac{1}{2}(E_{HOMO} + E_{LUMO})$$

$$\mu = -\chi = \frac{1}{2}(E_{HOMO} + E_{LUMO})$$

$$\eta = \frac{1}{2}(E_{LUMO} - E_{HOMO})$$

$$S = \frac{1}{2\eta}$$

$$\omega = \frac{\mu^2}{2\eta}$$

$$\Delta N_{max} = -\frac{\mu}{\eta}$$

According to Parr et al. [69], ω is a global reactivity index analogous to the chemical potential and chemical hardness. When the system gains an additional electronic charge (ΔN) from the surroundings, the stabilization energy is measured in terms of the global reactivity index (ω). The electronic chemical potential of the molecule exclusively determines the path of the charge transfer, whereas electrophile is a type of chemical category which can accept the electrons from the surroundings. So, its energy must decrease while accepting the electronic charge and its electronic chemical potential must be negative. Theoretical values of energies E_{HOMO}, E_{LUMO}, energy gap (E_L– E_H), χ, μ, η, S, and ω for all the three conformers are listed in Table 2. The calculated higher values of ω and energy gap (E_L–E_H) reveal that the conformer I behave as a strong electrophile, chemically less reactive, most stable, and hardest among all the three conformers.

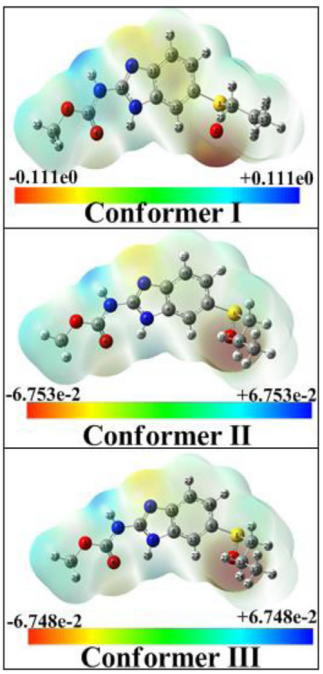

Fig. 7. Molecular electrostatic potential (MEP) surface formed by mapping of total density over electrostatic potential in the gaseous state for conformers (I-III) of RBZ.

Table 2
Calculated E_{HOMO}, E_{LUMO}, energy gap (E_L–E_H), chemical potential (μ), electronegativity (χ), global hardness (η), global softness (S), and global electrophilicity index (ω) for conformers (I-III) of RBZ.

Molecule	E_H (eV)	E_L (eV)	(E_L– E_H) (eV)	χ (eV)	μ (eV)	η (eV)	S $(eV)^{-1}$	ω (eV)	ΔN_{max}
Conformer I	−6.0633	−1.1032	4.9601	3.5832	−3.5832	2.4801	0.2016	2.5885	1.4448
Conformer II	−6.0557	−1.1042	4.9514	3.5800	−3.5800	2.4757	0.2020	2.5884	1.4460
Conformer III	−6.0442	−1.0966	4.9476	3.5704	−3.5704	2.4738	0.2021	2.5766	1.4433

Table 3
Calculated local reactivity properties of the selected atoms using Hirshfeld [B3LYP/6–311++*G*(d,p)] derived charges for conformers (I-III) of RBZ.

Atom	f_k^+	Atom	f_k^-	Atom	f_k^o
Conformer I					
O2	0.17229	C12	0.06433	S1	1.21969
S1	0.08739	C15	0.05609	C18	0.91565
C9	0.06941	C16	0.03264	C16	0.59882
N6	0.06642	C9	0.02996	C8	0.16906
C11	0.06077	S1	0.02748	C11	0.14272
C16	0.05877	C19	0.02713	C15	−0.20397
Conformer II					
O2	0.16948	C12	0.07097	S1	1.22877
S1	0.09063	C15	0.05663	C18	0.91549
C9	0.06938	C16	0.03389	C16	0.59788
N6	0.06500	C9	0.02784	C8	0.16443
C11	0.06094	C19	0.02755	C11	0.14392
C16	0.05864	C10	0.02519	C15	−0.20480
Conformer III					
O2	0.17316	C12	0.06534	S1	1.22151
S1	0.08916	C15	0.05508	C18	0.91645
C9	0.06707	C16	0.03018	C16	0.59980
N6	0.06547	C19	0.02959	C8	0.16398
C11	0.06069	C9	0.02677	C11	0.14493
C16	0.05847	O4	0.02233	C15	−0.20361

4.7.3. Local reactivity descriptors

Fukui function (FF) has been employed to calculate the reactivity of each atom in all the conformers of RBZ for the further chemical reaction. The atom with high-value FF is prominent to take part in the reaction in comparison to the other atoms in the molecule [77]. The Fukui functions (FF) (f_k^+,f_k^-,f_k^0), local softness (S_k^+,S_k^-,S_k^0) and local electrophilicity indices (ω_k^+,ω_k^-,ω_k^0) are the parameters which explain the reactivity of each atom in the anion, cation, and neutral states. To know these parameters, partial charges on each atom by Hirshfeld population analysis and Fukui functions were calculated through the equations [78].

$$f_k^+ = [q_k(N+1) - q_k(N)]\,\text{fornucleophilicattack}$$

$$f_k^- = [q_k(N) - q_k(N-1)]\,\text{forelectrophilicattack}$$

$$f_k^0 = [q_k(N+1) - q_k(N-1)]\,\text{forradicalattack}$$

where q_k is the atomic charge at the k^{th} atomic site in the neutral (N), anionic ($N + 1$) or cationic (N-1) state of the molecule. The numerical values of the FF for the nucleophilic and electrophilic attack of selected atoms of the sample molecule are presented in Table 3. The calculated Fukui functions for conformers (I-III) have been compared and presented in Figs. S4 and S5 (Supplementary Material) and their values are listed in Tables (S6-S8) (Supplementary Material). Our results showed that the most suitable reactive sites for electrophilic/nucleophilic/radical attack are O2/C12/S1 atoms respectively in all the conformers.

4.8. Atoms in molecule (AIM) calculation

AIM is based on the electron density used to investigate the intramolecular hydrogen bonding in the molecular systems. The strength and nature of hydrogen bonds are characterized by geometrical and topological parameters in terms of the charge density (ρ_{BCP}) and its Laplacian $\nabla^2(\rho)$ at the bond critical point (BCP). The molecular graph of RBZ using the AIM program is presented in Fig. 8. The intramolecular hydrogen bond energy for all the conformers is listed in Tables 4 and 5.

Table 4
Geometrical parameters for intramolecular hydrogen bonds in conformers (I-III) of RBZ: bond length (Å), bond angle (°), and the sum of Van der Waal radii of interacting atoms ($r_H + r_A$) in Å.

D-H...A	D-H (Å)	H...A (Å)	D-H...A (°)	(r_H+ r_A) (Å)
Conformer I				
C12-H22...O2	1.08446	2.41052	106.15647	2.72
N5-H26...O4	1.01129	2.12395	118.29519	2.72
Conformer II				
C12-H22...O2	1.08434	2.39753	106.37893	2.72
N5-H26...O4	1.01133	2.12673	118.20813	2.72
Conformer III				
C12-H22...O2	1.08449	2.41032	106.25647	2.72
N5-H26...O4	1.01131	2.12586	118.23876	2.72

For the existence of H-bond, Koch and Popelier [79] has proposed a set of criteria in which the electron density (ρ) between proton (H) and acceptor (A) lie in the range 0.002−0.040 a.u. and the Laplacian ($\nabla^2\rho_{BCP}$) of electron density should be in the order 0.024−0.139 a.u. Two intramolecular hydrogen bonds C12-H22...O2 and N5-H26...O4 were found in the RBZ in all the conformers and they are in good agreement with Koch and Popelier criteria. Moreover, the strength of H-bond has been explained by Rozas et al. [80] in terms of ($\nabla^2\rho_{BCP}$) and total electron energy density (H_{BCP}). For weak H-bond the criteria should be ($\nabla^2\rho_{BCP}$) > 0 and (H_{BCP}) > 0. For partially covalent in nature, it should be ($\nabla^2\rho_{BCP}$) > 0 and (H_{BCP}) < 0. But for strong and covalent, it should be ($\nabla^2\rho_{BCP}$) < 0 and (H_{BCP}) < 0. In RBZ both the bonds are partially covalent and medium in nature. Furthermore, the bond O4...H26 is stronger in comparison to O2...H22 as it has a high value of interaction energy (E_{int}) in all three conformers.

4.9. Molecular docking

Molecular docking is the fundamental tool that insight the binding site of the ligand with the predicted target protein. Docking calculation of RBZ has been carried out by using Autodock software [37]. For protein-ligand interaction, the targets are predicted from online Swiss Target Prediction [81] as presented in Fig. S6 (Supplementary Material). Three proteins have been chosen and their PDB code were downloaded from RCSB PDB [82]: Poly [ADP-ribose] polymerase-1(PARP) (PDB code: 1UK1, 2PAW, 6I8M); MAP kinase p38 alpha (MAPK) (PDB Code: 3BX5, 3LFA, 3LFB) and Adenosine A2a receptor (PDB Code: 3PWH, 3QAK) to explore the binding site and strength of RBZ.

The PARP protein is used to repair DNA, programmed cell death, and genomic stability [83] whereas the MAPK protein is used to recover osmotic stress, heat shock, metogens [84] but Adenosine A2a receptor is responsible to controls the planning and initiation of voluntary movement [85].

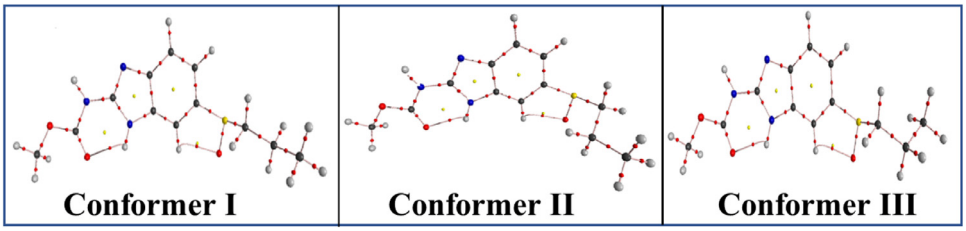

Fig. 8. Molecular graph for conformers (I-III) of RBZ: bond critical points (small red spheres), bond path (pink lines), ring critical points (small yellow spheres).

Table 5
Geometrical parameter (bond length) and topological parameters for bonds of interacting atoms for conformers (I-III) of RBZ: electron density (ρ_{BCP}), Laplacian of electron density ($\nabla^2\rho_{BCP}$), electron kinetic energy density (G_{BCP}), electron potential energy density (V_{BCP}), total electron energy density (H_{BCP}) at the bond critical point (BCP) and estimated interaction energy (E_{int}).

Interactions	Bond Length (Å)	ρ_{BCP} (a.u)	$\nabla^2\rho_{BCP}$ (a.u)	G_{BCP} (a.u)	V_{BCP} (a.u)	H_{BCP} (a.u)	E_{int} (kcal/mol)
Conformer I							
O2...H22	2.41052	0.01392	0.05399	−0.00173	−0.01003	−0.01176	−3.14671
O4...H26	2.12395	0.01989	0.07628	−0.00256	−0.01396	−0.01651	−4.37854
Conformer II							
O2...H22	2.39753	0.01421	0.05462	−0.00174	−0.01017	−0.01191	−3.19007
O4...H26	2.12673	0.01978	0.07584	−0.00255	−0.01387	−0.01641	−4.35157
Conformer III							
O2...H22	2.41032	0.01392	0.05396	−0.00173	−0.01003	−0.01176	−3.14624
O4...H26	2.12586	0.01981	0.07597	−0.00255	−0.01389	−0.01644	−4.35927

Table 6
Bond length, Binding energy, and Ligand efficiency of RBZ against different protein targets.

Protein	PDB code	Bond length(Å)	Amino acid	Binding energy (kcal/mol)	Ligand efficiency
Poly [ADP-ribose] polymerase-1	1UK1	2.32	ASP:726	−7.60	−0.40
		2.01	ASP:726		
	2PAW	1.87	ASP:770	−7.15	−0.38
		2.11	ASP:770		
		3.17	ARG:878		
		3.18	ASN:767		
	6I8M	2.09	ASP:766	−7.16	−0.38
		2.11	ASN:767		
MAP kinase p38 alpha	3BX5	2.13	GLU:215	−5.52	−0.29
		1.85	GLU:215		
		2.66	TYR:188		
		3.38	THR:221		
	3LFA	2.06	MET:109	−5.78	−0.30
	3LFB	2.11	GLU:71	−8.07	−0.42
		1.80	GLU:71		
Adenosine A2a receptor	3PWH	2.80	LEU:194	−5.81	−0.31
	3QAK	3.04	ARG:111	−6.39	−0.34
		2.23	ARG:1008		

The active site of protein has been confined within the grid size 60 *Å* × 60 *Å* × 60 Å to investigate the residues of the active sites. Proteins were prepared by removing co-crystallized ligands and water molecules using Discovery Studio Visualizer 4.5 software [38]. Out of many docked conformations, one which well-bounded the active sites were taken into consideration is visualized in Fig. 9. The binding energy of ligand with the target and the bond length of the H-bond formed between them are presented in Table 6. The interaction of 1UK1 shows two hydrogen bonds H31/H26 (2.32/2.01 Å) with residue ASP: 726 with binding energy −7.60 kcal/mol and similar type of interactions are found in 6I8M with H31/H26 (2.09 Å, ASP:766/2.11 Å, ASN:767) with binding energy −7.16 kcal/mol. But 2PAW gives four conventional H-bonds, two with H31/H26 (2.11/1.87 Å, ASP: 770) another with a carbonyl group (3.17 Å, ARG: 878), and sulfinyl group (3.18 Å, ASN: 767) with binding energy −7.15 kcal/mol. Besides these interactions, 3BX5 exhibits four conventional H-bonds. H26 binds with two residue GLU: 215/TYR: 188 with bond length 1.85/2.66 Å. H31 again binds with GLU: 215 with bond length 2.13 Å and O3 interact with THR: 221 having bond length of 3.88 Å with a binding energy of −5.52 kcal/mol. Moreover, 3LFA shows the interaction with H31 (2.06 Å, MET:109) with binding energy −5.78 kcal/mol and 3LFB interact with H31/H26 (2.11/1.80 Å, GLU:71) with binding energy −8.07 kcal/mol. 3QAK/3PWH of Adenosine A2a receptor shows the binding with H31/H26 (2.23 Å, ARG:1008/2.80 Å, LEU:194) with binding energy −6.39/−5.81 kcal/mol respectively. Thus, molecular docking of RBZ reveals that H31 and H26 are the active sites for interactions. The favorable active binding sites are also justified in

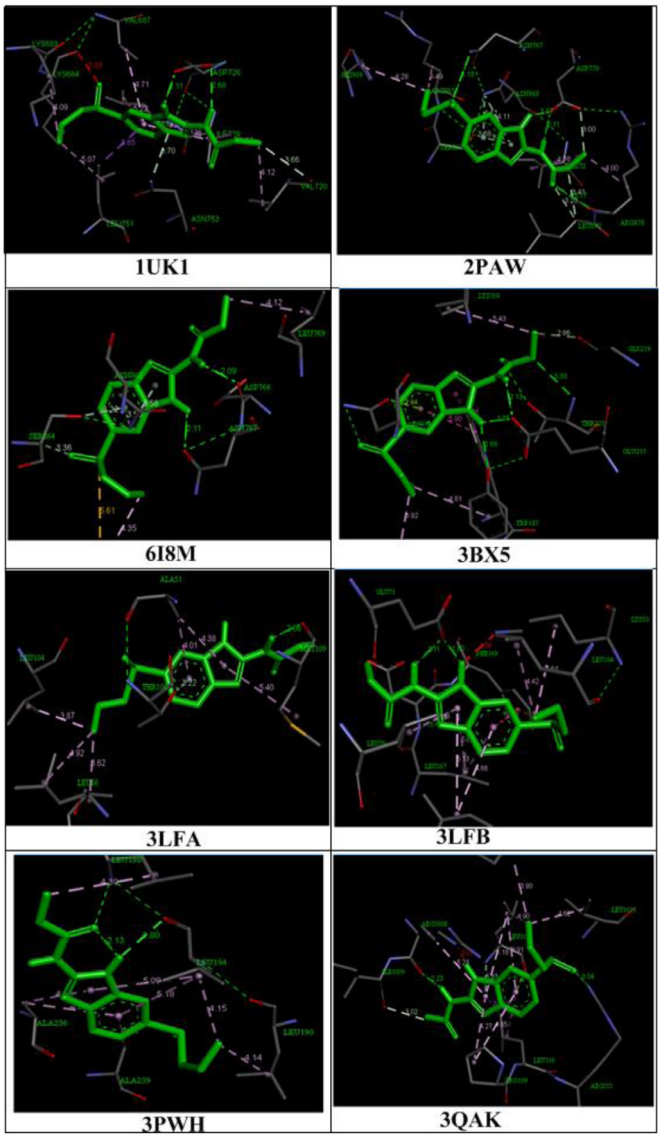

Fig. 9. Molecular Docking of RBZ with different protein targets.

MEP surface analysis as explained in Section 4.7.1. However, further *in vitro* and *in vivo* studies have to be performed to confirm its activities.

5. Conclusion

Conformational, vibrational spectroscopic, and quantum chemical calculation of RBZ were performed. The conformational analysis revealed the three most stable conformers (I–III) at room temperature by using DFT/B3LYP/6–311++*G*(d,p) level having minimum energy –787,322.8843 kcal/mol for the most stable conformer I. A comparative study of the calculated IR and Raman with experimental data exhibits the significant resonance between them. The potential energy distribution (PED) for each mode of vibration was presented in which the calculated $\nu(C=O)$ and ν(SO) identical with the experimental values. The NBO analysis demonstrates that the transition LP(1)N7 $\rightarrow \pi^*$(O4-C18) stabilizes the molecular system with the highest stabilization energy 61.96 kcal/mol. The frontier molecular orbital (HOMO-LUMO) analysis and their energy gap showed that the conformer I is most stable, and conformer III having least electrophilic index (ω) is the most chemically reactive among the three. Fukui function analysis focussed that the atom O2 is more electrophilic whereas the atom C12 and S1 are more suitable for neuclophilic and radical attack respectively for further reaction. The QTAIM study administered that there were two intramolecular hydrogen bonding interactions (medium in nature) C12-H22**...**O2 and N5-H26**...**O4 with energies –3.14671 and –4.37854 kcal/mol at BCP respectively. This is also justified by vibrational spectra as explained in Section 4.3. Molecular docking confirmed that in most cases the active sites in RBZ are H26, H31, O2, O3, and S1 which is also satisfied by the Fukui function calculation. Hence, the title molecule is a good inhibitor for the predicted target proteins.

Credit author statement

Manoj Kumar Chaudhary: Writing-original draft, Formal analysis & Data simulation
Preeti Prajapati: Editing & Reviewing
Karnica Srivastava: Conceptualization, Methodology & Simulation
Keilla Façanha Silva: Data record & Analysis of spectroscopy
Bhawani Datt Joshi: Supervision, reviewing & editing
Poonam Tandon: Supervision, Editing & Software
Alejandro Pedro Ayala: Supervision

Declaration of Competing Interest

The authors declare that they have no known competing financial interests or personal relationships that could have appeared to influence the work reported in this paper.

Acknowledgement

M.K. Chaudhary is grateful to centre for Co-Operation in Science and Technology among Developing Societies (CCSTDS), India for providing partial financial support under the Indian Science and Research Fellowship (ISRF-2019), with award ID (DO/CCSTDS/204/2019). We are thankful to Dr. T. Karthick, Dr, Rajesh Kumar and Mr. Keshav Kumar Singh for their coperation and remarkable sugession during manuscript preperation.

Supplementary materials

Supplementary material associated with this article can be found, in the online version, at doi:10.1016/j.molstruc.2021.129889.

References

[1] H.D. Brown, A.R. Matzuk, I. Ilves, L.H. Peterson, S.A. Harris, L.H. Sarett, J.R. Egerton, J.J. Yakstis, W.C. Campbell, A.C. Cuckler, J. Am. Chem. Soc. 83 (7) (1961) 1764–1765.
[2] C.E. Lanusse, G.L. Virkel, S.F. Sanchez, L.I. Alvarez, A.L. Lifschitz, F. Imperiale, A. Monfrinotti, Res. Vet. Sci. 65 (1) (1998) 5–10.
[3] C.E. Lanusse, R.K. Prichard, Drug Metab. Rev. 25 (3) (1993) 235–279.
[4] W.J. Foreyt, Vet. Parasitol. 26 (3–4) (1988) 261–264.
[5] A. Dib, S. Palma, G. Suárez, C. Farias, P. Cabrera, S. Castro, D. Allemandi, L. Moreno, C. Lanusse, S. Sanchez Bruni, J. Vet. Pharmacol. Ther. 34 (2) (2011) 136–141.
[6] Z. Wu, M. Razzak, I.G. Tucker, N.J. Medlicott, J. Pharm. Sci. 94 (5) (2005) 983–993.
[7] Q.A. McKellar, E.W. Scott, J. Vet. Pharmacol. Ther. 13 (3) (1990) 223–247.
[8] A. Bongioanni, B.S. Araujo, Y.S. de Oliveira, M.R. Longhi, A. Ayala, C. Garnero, AAPS Pharm Sci Tech 19 (3) (2018) 1468–1476.
[9] E.A. Formentini, O.N. Mestorino, E.L. Marino, J.O. Errecalde, J. Vet. Pharmacol. Ther. 24 (3) (2001) 199–202.
[10] J.E. Riviere, M.G. Papich, Veterinary Pharmacology and Therapeutics, Wiley, Hoboken, 2009.
[11] A. García, M.G. Barrera, G. Piccirilli, M.D. Vasconi, R.J. Di Masso, D. Leonardi, Parasitol. Int. 62 (6) (2013) 568–570.
[12] H.S. Walter, S. Ahmed, Targeted therapies in cancer, Surgery (Oxford) 36 (3) (2018) 122–127.
[13] R.G. Woodgate, A.J. Cornell, N.C. Sangster, in: Antimicrobial Drug Resistance, Springer, Cham, 2017, pp. 1305–1326.

[14] J. Priotti, M.V. Baglioni, A. García, M.J. Rico, D. Leonardi, M.C. Lamas, M.M. Márquez, AAPS Pharm Sci Tech 19 (8) (2018) 3734–3741.
[15] L.R. Stuchlíková, P. Matoušková, I. Vokřál, J. Lamka, B. Szotáková, A. Sečkařová, D. Dimunová, L.T. Nguyen, M. Várady, L. Skálová, Int. J. Parasitol-Drug. 8 (1) (2018) 50–58.
[16] A. Dib, A.J. Paredes, N. Eliópulos, C.E. Farias, G. Suárez, A. Aldrovandi, S.D. Palma, D.A. Allemandi, C.E. Lanusse, S.F. Sanchez Bruni, Pharmacokinetic Assessment of Novel Controlled Release Formulations of Ricobendazole Intended for Oral Administration in Dogs, 2015.
[17] J. Priotti, D. Leonardi, G. Pico, M.C. Lamas, AAPS Pharm Sci Tech 9 (3) (2018) 1152–1159.
[18] Y. Kawabata, K. Wada, M. Nakatani, S. Yamada, S. Onoue, Int. J. Pharm. 420 (1) (2011) 1–10.
[19] C.Y. Wu, L.Z. Benet, Pharm. Res. 22 (1) (2005) 11–23.
[20] G.L. Amidon, H. Lennernäs, V.P. Shah, J.R. Crison, Pharm. Res. 12 (3) (1995) 413–420.
[21] P. Prajapati, J. Pandey, M.R. Shimpi, A. Srivastava, P. Tandon, S.P. Velaga, K. Sinha, J. Mol. Struct. 1125 (2016) 193–203.
[22] National Center for Biotechnology Information. PubChem Compound Summary for CID 83969, Albendazole oxide. https://pubchem.ncbi.nlm.nih.gov/compound/Albendazole-oxide. Accessed Sep. 14, 2019.
[23] T.H. Dunning Jr., J. Chem. Phys. 90 (2) (1989) 1007–1023.
[24] D.E. Woon, T.H. Dunning Jr., J. Chem. Phys. 103 (1995) 4572–4585.
[25] A.D. Becke, J. Chem. Phys. 98 (1993) 5648–5652.
[26] M.J. Frisch, G.W. Trucks, H.B. Schlegel, G.E. Scuseria, J.R. Cheeseman, M.A. Robb, G. Scalmani, V. Barone, B. Mennucci, G.A. Petersson, H. Nakatsuji, M. Caricato, X. Li, H.P. Hratchian, A.F. Izmzylov, J. Bloino, G. Zheng, J.L. Sonnenberg, M. Hada, M. Ehara, K. Toyota, R. Fukuda, J. Ishida, M. Hasegawa, T. Nakajima, Y. Honda, O. Kitao, H. Nakai, T. Vreven, J.A. Montgomery Jr., J.E. Peralta, F. Ogliaro, M. Bearpark, J.J. Heyd, E. Brothers, K.N. Kudin, V.N. Staroverov, R. Kobayashi, J. Normand, A. Raghavachari, A. Rendell, J.C. Burant, S.S. Iyengar, J. Tomasi, M. Cossi, N. Rega, J.M. Millan, M. Klene, J.E. Knox, J.B. Cross, V. Bakken, C. Adamo, J. Jaramillo, R. Gomperts, R.E. Stratmann, O. Yazyev, A.J. Austin, R. Cammi, C. Pomelli, J.W. Ochterski, R.L. Martin, K. Morokuma, V.G. Zakrzewski, G.A. Voth, P. Salvador, J.J. Dannerberg, S. Dapprich, A.D. Daniels, J. Farkas, B. Foresman, J.V. Ortiz, J. Cioslowski, D.J. Fox, GAUSSIAN 09, Revision, Gaussian, Inc., Wallingford CT, 2009.
[27] C. Lee, W. Yang, R.G. Parr, *Phys. Rev*. B 37 (1988) 785–789.
[28] R.G. Parr, W. Yang, Density Functional Theory of Atoms and Molecules, Oxford, New York, 1989.
[29] A. Frisch, A.B. Nielson, A.J. Holder, GaussView User Manual, Gaussian Inc, Pittsburgh, PA, 2005.
[30] E.D. Glendening, A.E. Reed, J.E. Carpenter, F. Weinhold, NBO 3.0 Program Manual, Theoretical Chemistry Institute, University of Wisconsin, Madison, WI, 1996.
[31] J.M.L. Martin, C. VanAlsenoy, Gar2ped, University of Antwerp, Antwerp, 1995.
[32] P. Pulay, G. Fogarasi, F. Pang, J.E. Boggs, J. Am. Chem. Soc. 101 (1979) 2550–2560.
[33] R.F.W. Bader, S.G. Anderson, A.J. Duke, J. Am. Chem. Soc. 101 (6) (1979) 1389–1395.
[34] R.F.W. Bader, T.S. Slee, D. Cremer, E. Kraka, J. Am. Chem. Soc. 105 (15) (1983) 5061–5068.
[35] R.F.W. Bader, P.J. MacDougall, J. Am. Chem. Soc. 107 (24) (1985) 6788–6795.
[36] T.A. Keith, AIMALL Version 090201 TK Gristmill Software Overland Park, KS, USA, 2009.
[37] O. Trott, A.J. Olson, J. Comput. Chem. 31 (2010) 455–461.
[38] Discovery Studio 4.5 Guide, Accelrys Inc., San Diego, 2009 http://www.accelrys.com.
[39] P.L. Polavarapu, J. Phys. Chem. 94 (21) (1990) 8106–8112.
[40] G.A. Guirgis, P. Klaboe, S. Shen, D.L. Powell, A. Gruodis, V. Aleksa, C.J. Nielsen, J. Tao, C. Zheng, J.R. Durig, J. Raman Spectrosc. 34 (4) (2003) 322–336.
[41] M.P. Andersson, P. Uvdal, J. Phys. Chem. A 109 (2005) 2937–2941.
[42] G. Varsányi, M.A. Kovner, L. Láng, Assignments For Vibrational Spectra of Seven Hundred Benzene Derivatives, Academiai Kiado, 1973.
[43] R.M. Silverstein, G.C. Bassler, J. Chem. Educ. 39 (11) (1962) 546.
[44] K. Nakanishi, J. Chem. Educ. 40 (1963) 616.
[45] S.C. Myneni, S.J. Traina, G.A. Waychunas, T.J. Logan, Geochim. Cosmochim. Acta 62 (21–22) (1998) 3499–3514.
[46] M. Arivazhagan, R. Kavitha, J. Mol. Struct. 1011 (2012) 111–120.
[47] L.J. Bellamy, The IR Spectra of Complex Molecules, John Wiley and Sons, New York, 1975.
[48] M. Karabacak, E. Sahin, M. Cinar, I. Erol, M. Kurt, J. Mol. Struct. 886 (2008) 148–157.
[49] N. Sundaraganesan, S. Ilakiamani, P. Subramani, B.D. Joshua, Spectrochim. Acta A Mol. Biomol. Spectrosc. 67 (3–4) (2007) 628–635.
[50] F. Weinhold, C.R. Landis, Chemistry Education: Research and Practice (2001) 2291.
[51] E. Khan, P. Prajapati, P. Tandon, P. Bhart, P. Kumar, R. Maurya, J. Mol. Struct. 1175 (2019) 28–38.
[52] J.P. Foster, F. Weinhold, J. Am. Chem. Soc. 102 (1980) 7211–7218.
[53] E.D. Glendening, J.K. Badenhoop, F. Weinhold, J. Comput. Chem. 19 (6) (1998) 628–646.
[54] N. Gonohe, H. Abe, N. Mikami, M. Ito, J. Phys. Chem. 89 (1985) 3642–3648.
[55] M. Gutowski, G. Chalasinski, J. Chem. Phys. 98 (1993) 4540–4554.
[56] B.D. Joshi, A. Srivastava, P. Tandon, S. Jain, Spectrochim. Acta A Mol. Biomol. Spectrosc. 82 (1) (2011) 270–278.
[57] K. Srivastava, A. Srivastava, P. Tandon, K. Sinha, J. Wang, J. Mol. Struct. 1125 (2016) 751–762.
[58] C.A. Lipinski, F. Lombardo, B.W. Donimy, P.J. Feeny, Adv. Drug Delivery Rev. 23 (1997) 3–25.
[59] J.A. Padron, R. Carrasco, R.F. Pellon, J. Pharm. Pharmaceut. Sci. 5 (3) (2002) 258–266.
[60] R.P. Verma, C. Hansch, Bioorg. Med. Chem. 13 (7) (2005) 2355–2372.
[61] R.P. Verma, A. Kurup, C. Hansch, Bioorg. Med. Chem. 13 (2005) 237–255.
[62] P.W. Atkins, Physical Chemistry (2001).
[63] K. Fukui, T. Yonezawa, H. Shingu, J. Chem. Phys. 20 (1952) 722–725.
[64] D.F.V. Lewis, C. Ioannides, D.V. Parke, Xenobiotica 24 (1994) 401–408.
[65] D.C. Ghosh, J. Jana, Curr. Sci. (1999) 570–573.
[66] P.K. Weiner, R. Langridge, J.M. Blaney, R. Schaefer, P.A. Kollman, Proc. Natl. Acad. Sci. USA 79 (1982) 3754–3758.
[67] S. Chidangil, M.K. Shukla, P.C. Mishra, J. Mol. Model. 4 (1998) 250–258.
[68] M. Kumru, V. Kucuk, M. Kocademir, H.M. Alfanda, A. Altun, L. Sarı, Spectrochim. Acta A Mol. Biomol. Spectrosc. 134 (2015) 81–89.
[69] R.G. Parr, R.G. Pearson, Absolute hardness: companion parameter to absolute electronegativity, J. Am. Chem. Soc. 105 (26) (1983) 7512–7516.
[70] N.P.G. Roeges, A Guide to the Complete Interpretation of Infrared Spectra of Organic Structures, Wiley, New York, 1994.
[71] R.G. Pearson, J. Org. Chem. 54 (1989) 1423–1430.
[72] R. Kumar, T. Karthick, V. Parol, P. Rawat, P. Tandon, A. Gupta, A.N. Prabhu, V. Upadhyaya, J. Mol. Struct. (2020) 129144.
[73] P. Geerlings, F. De Proft, W. Langenaeker, Chem. Rev. 103 (2003) 1793–1874.
[74] R.G. Parr, L. Szentpaly, S. Liu, J. Am. Chem. Soc. 121 (1999) 1922–1924.
[75] P.K. Chattaraj, U. Sarkar, D.R. Roy, Chem. Rev. 106 (2006) 2065–2091.
[76] J. Padmanabhan, R. Parthasarathi, V. Subramaniaanand, P.K. Chattaraj, J. Phys. Chem. 111 (2007) 1358–1361.
[77] R.G. Parr, W. Yang, J. Am. Chem. Soc. 106 (1984) 4049–4050.
[78] K. Fukui, Science 218 (1987) 747–754.
[79] U. Koch, P.L.A. Popelier, J. Phys. Chem. 99 (1995) 9747–9754.
[80] I. Rozas, I. Alkorta, J. Elguero, J. Am. Chem. Soc. 122 (2000) 11154–11161.
[81] A. Daina, O. Michielin, V. Zoete, Nucleic Acids Res 47 (W1) (2019) W357–W364.
[82] P.W. Rose, B. Beran, C. Bi, W.F. Bluhm, D. Dimitropoulos, D.S. Goodsell, A. Prlić, M. Quesada, G.B. Quinn, J.D. Westbrook, J. Young, Nucleic Acids Res 39 (2010) D3.
[83] Z. Herceg, Z.Q. Wang, MUTAT RES-FUNDMOL M 477 (1–2) (2001) 97–110.
[84] J. Segalés, E. Perdiguero, P. Muñoz-Cánoves, Front. Cell Dev. Biol. 4 (2016) 91.
[85] A. Pinna, J. Wardas, M.R. Domenici, P. Popoli, G. Cossu, M. Morelli, Adenosine Receptors in Neurodegenerative Disease (187–213), Academic Press, 2017.

Spectrochimica Acta Part A: Molecular and Biomolecular Spectroscopy 246 (2021) 118976

Contents lists available at ScienceDirect

Spectrochimica Acta Part A: Molecular and Biomolecular Spectroscopy

journal homepage: www.elsevier.com/locate/saa

Molecular structure and quantum descriptors of cefradine by using vibrational spectroscopy (IR and Raman), NBO, AIM, chemical reactivity and molecular docking

Manoj Kumar Chaudhary [a,b], T. Karthick [c], Bhawani Datt Joshi [d,*], Preeti Prajapati [b], Maria Silmara Alves de Santana [e], Alejandro Pedro Ayala [e], V.S. Jeba Reeda [f], Poonam Tandon [b,*]

[a] Central Department of Physics, Tribhuvan University, Kirtipur, Kathmandu, Nepal
[b] Department of Physics, University of Lucknow, Lucknow 226 007, India
[c] Department of Physics, School of Electrical and Electronics Engineering, SASTRA Deemed University, Thanjavur 613 401, Tamil Nadu, India
[d] Department of Physics, Siddhanath Science Campus, Tribhuvan University, Mahendranagar 10406, Nepal
[e] Depertmento de Fisica, Universidade Federal do Ceará, C.P. 6030,60.455-900, Fortaleza, CE, Brazil
[f] Department of Physics and Research Center, Women's Christian College, Nagercoil 629001, Tamil Nadu, India

ARTICLE INFO

Article history:
Received 28 June 2020
Received in revised form 21 August 2020
Accepted 18 September 2020
Available online 24 September 2020

Keywords:
Cefradine
Vibrational spectroscopy
Natural bond orbitals
Chemical reactivity
Molecular docking

ABSTRACT

This study aims to investigate the structural and vibrational features of cefradine (the first-generation cephalosporin antibiotic) based on spectroscopic experiments and theoretical quantum chemical approach. The fundamental structural aspects of cefradine have been examined based on optimized geometry, spectroscopic behavior, intermolecular interaction, chemical reactivity, intramolecular hydrogen bonding, and molecular docking analysis. The most stable minimum energy conformer of the title molecule was identified by performing a one-dimensional potential energy surface scan along the rotational bonds at B3LYP/6-311++G (d,p) level of theory. The vibrational features of the molecule and information about the coupled modes were predicted. The chemical reactivity and stability of all the possible conformers of cefradine were estimated based on the HOMO-LUMO energy gap and NBO approach. The overall picture of accumulation of charges on individual atoms of the molecule was predicted by molecular electrostatic potential (MEP) surface map which in turn identifies the nucleophilic and electrophilic region or sites. The quantitative analysis of electrophilicity and nucleophilicity indices was done by Hirshfeld charge analysis and it was found that N8 atom is the most prominent site for nucleophilic attack while C14 atom is feasible for electrophilic attack. QTAIM study has also been performed to investigate the nature and strength of hydrogen bonding interactions. Besides, molecular docking studies were performed to examine the active binding residues of the target.

1. Introduction

Cefradine, (6*R*,7*R*)-7-[[(2*R*)-2-amino-2-cyclohexa-1,4-dien-1-ylacetyl]amino]-3-methyl-8-oxo-5-thia-1-azabicyclo[4.2.0]oct-2-ene-2-carboxylic acid, $C_{16}H_{19}N_3O_4S$, is the first generation, β-Lactam, cephalosporin antibiotic. It is often used to treat the bacterial infections of respiratory tract (for example tonsillitis, laryngotracheobronchitis, labor, and bronchopneumonia, etc) infections, urinary tract (cystitis, pyelonephritis, etc) infection as well as skin and soft tissue (such as impetigo, furunculosis, etc) infections. Cefradine is active against gram-positive and gram-negative bacteria as well as active against most strains of penicillinase-producing Staphylococci [1].

DFT study on the cefradine derivatives such as cefadroxil and cefalexin have been studied in the literature [2,3]. The antibacterial activity of cefradine is almost identical to cefalexin [4]. Being a drug molecule, the clinical and pharmaceutical properties of cefradine has been investigated by different research groups [5–10]. The anti-tumor activity of cefradine-metal complexes was studied through spectroscopic and physicochemical methods by Al-Khodira and Refat [5]. Due to its diverse applications as a copper corrosion inhibitor, mild steel inhibitor, combined electrochemical and quantum chemical studies were performed earlier [6,7]. Moreover, due to its overwhelming clinical response, it is greatly employed in the treatment of acute infective diseases [8,9]. The molecular structure of cefradine dihydrate was studied by dispersion corrected DFT functional by Van de Streek et al. [10].

* Corresponding authors.
E-mail addresses: bhawani.joshi@snsc.tu.edu.np (B.D. Joshi), tandon_poonam@lkouniv.ac.in (P. Tandon).

https://doi.org/10.1016/j.saa.2020.118976
1386-1425/

The conformational analysis along the rotational bonds has not been performed yet.

In our present study, the possible conformers of the title molecule at the room temperature, corresponding to the local minima by the possible rotations along the flexible bonds, were predicted and analyzed. Their geometrical parameters were compared with that of Van de Streek et al. [10]. Vibrational spectroscopic (FT-IR and FT-Raman) studies were performed to study molecule characteristics at the atomic level. The natural bond orbital (NBO) analysis was done to identify the hyper conjugative interactions and lone-pair to anti-bonding orbital interactions. Chemically reactive behavior of cefradine was evaluated by predicting the quantum chemical parameters such as the HOMO-LUMO energy gap, its associated descriptors (both global and local reactivity), and molecular electrostatic potential (MEP) surface. Further, a molecular docking study was performed to find the active binding sites of cefradine against the selected target. A literature survey reveals that the above-mentioned spectroscopic characterization, conformational analysis, and quantum chemical computational studies on the cefradine molecule were not reported so far. Hence, this study aims to work on the cefradine molecule to explore these molecular properties at the atomic (or microscopic) level.

2. Experimental details

The compound, cefradine, in solid form of purity level greater than 98% was purchased from the ABL Brasil (Antibioticos do Brasil Ltd). Without making any further purification process, the spectra (Infrared and Raman) has been recorded as it was obtained with analytical standard. The white crystalline powder of the sample, which is soluble in water, was used for spectral measurements. Bruker Vertex 70 FT-IR spectrometer was used to record the FT-IR spectrum of cefradine at room temperature. The spectrum of cefradine (in the pellet form) was recorded in the range of 400–4000 cm^{-1} with a resolution of 4 cm^{-1}. During the pellet formation, the proportion KBr:Sample was mixed in the ratio of 200:1 respectively to reduce the signal to noise ratio. Raman spectrum of the sample was recorded in the range 100–3500 cm^{-1} by implementing RAM II module in which diode-pumped Nd: YAG laser was employed. The laser source is capable of emitting the radiation of 1064 nm wavelength at low power (100 mW).

3. Computational details

To predict the lowest energy structure (local minima) of cefradine, the DFT calculations were carried out [11] using B3LYP [12,13] functional with 6-311++G(d,p) basis set [14–16] in the Gaussian 09 program package [17]. Relaxed z-matrix scans were performed on the selected rotational bonds and local minima structures upon each rotation of the bonds were obtained to identify the most stable conformer. Further, the calculations of the vibrational harmonic frequencies of the most stable conformer along with the conformers having closely related energies using B3LYP/6-311++G(d,p) approximation level were performed. The spectral peaks for the normal modes of vibrations were identified by following the normal coordinate analysis procedure suggested by Fogarasi et al. [18]. The potential energy distribution (PED) corresponding to the normal modes were calculated using Gar2Ped program [19]. The simulated IR and Raman spectra of cefradine were compared with the experimental spectra. Certain quantum chemical parameters that associated with chemical reactivity of the molecule such as natural bond orbitals (NBO), molecular electrostatic potential (MEP), global and local reactivity descriptors of the molecule were performed at B3LYP/6-311++G(d,p) approximation level. The electron density surface mapping of HOMO, LUMO orbitals and MEP surfaces were generated with the help of GaussView 05 [20]. The Quantum topological Atoms in Molecule (QTAIM) theory was employed to identify the strong and weak molecular interactions using AIM all software package and AIM 2000 visualization program [21–24]. To identify the inhibition capability of cefradine against certain targets that were not examined so far, molecular docking simulations were performed and the parameters of the docked complexes such as binding energy, ligand efficiency, and inhibition constant were predicted using Auto Dock 4.2 [25]. A grid size of 60 Å × 60 Å × 60 Å was chosen and tolerance value of 2.0 Å was fixed while clustering the conformers. The proteins were prepared by removing co-crystallized ligands and water molecules in the PDB file and then hydrogen atoms and Gasteiger charges were assigned to the protein residues using UCSF Chimera program [26]. Afterwards, the cefradine molecule was docked with the prepared protein targets. The Lamarckian Genetic Algorithm (LGA) [27] included in AutoDock 4.2 program was implemented for docking. For the visualization of interactions between cefradine and the protein structures, the LIGPLOT is drawn from Discovery Studio software [28].

4. Results and discussion

4.1. Conformational studies

The 2D-chemical structure and 3D-electronic geometry of cefradine with the atom labeling scheme are shown in Fig. 1(a,b). Initially, the ground state optimized structure was obtained by employing B3LYP/6-311++G(d,p) level of approximation. To obtain the lowest energy structure of cefradine at room temperature, the one-dimensional potential energy surface (PES) scan has been performed on the eight flexible bonds such as C19-C16, C16-N8, C16-C15, C15-N7, C12-C18, C18-O4, C17-C14, and N7-C10. The dihedral angles corresponding to these bonds are ϕ1(C21-C19-C16-N8), ϕ2(C19-C16-N8-H38), ϕ3(C19-C16-C15-O3), ϕ4(C16-C15-N7-C10), ϕ5(N6-C12-C18-O4), ϕ6(C12-C18-O4-H43), ϕ7(H33-C17-C14-C13) and ϕ8(C15-N7-C10-C9) as in Fig. 1 (b). The structure obtained from each point on the PES scan was optimized. The global and local minima of altogether twelve conformers were obtained and their energies were summarized in Table 1 to obtain the minimum energy conformer. The PES curves for all the rotational bonds are presented in Fig. S1 (Supplementary Material) and the self-consistent field energies of the optimized structures of twelve conformers along with relative energies are given in Fig. S2 (Supplementary Material).

During the PES scan, the torsional angle at each step was varied by 10° in the range 0–360° along the selected bond axis. The conformers whose relative energy is less than 0.56 kcal/mol (equivalent to the value of kT) with respect to the lowest energy conformer are considered as they are likely to exist at room temperature. The lowest energy of the conformer I was obtained from rotation along ϕ3 and is calculated to be – 931,719.0299 kcal/mol. The conformational analysis is provided that only four conformers (hereafter named as conformer I, conformer II, conformer III, and conformer IV according to their SCF energies) with relative energy less than the value of kT are likely to exist at room temperature.

4.2. Optimized structural parameters and AIM study

These four conformers are further optimized with WB97XD/6-311++G(d,p) [29]. The energy of all the four conformers obtained from WB97XD is more than the functional B3LYP as presented in Table S1 (Supplementary Material). Moreover, the benchmarking report explores that the result of functional B3LYP is closer to experimental than the functional WB97XD [30]. So, all the further calculations were carried out with the functional B3LYP. The structural overlapping of conformers (I-IV) with the structure given by Van de Streek et al. [10] has been done by using a least-squares algorithm which reduces the distances of the corresponding non-hydrogen atoms and is presented in Fig. S3 (Supplementary Material). From this figure, it is clear that conformer II is closer to the literature [10] and its relative energy with conformer I is nearly 0.0020 kcal/mol, which is not so large. That's why in this study we mainly focus on conformer II.

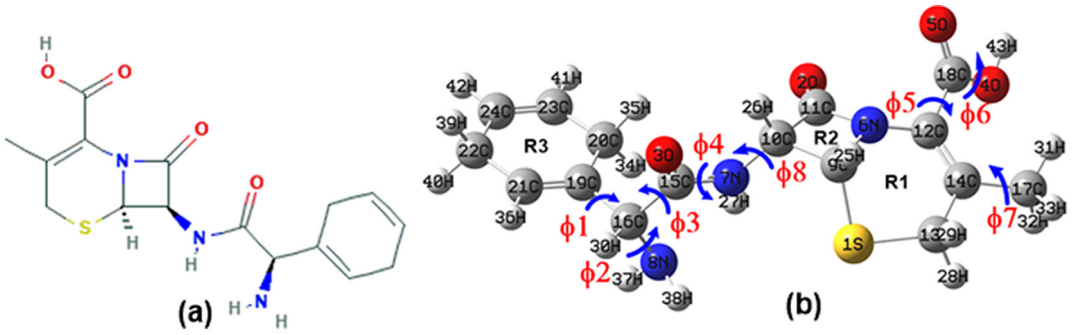

Fig. 1. (a) Chemical and (b) electronic structure of cefradine with atom numbering schemes. Rotational bonds are indicated with arrow marks.

Table 1
Ground-state optimized energy and energy difference of all the possible conformers of cefradine predicted at B3LYP/6-311++G(d,p) level.

Dihedral angles (°)	Conformers	Energy (Hartree)	Energy (kcal/mol)	Energy diffrence[a] (kcal/mol)
ϕ3(C19-C16-C15-O3)	I	−1484.788724	−931,719.0299	0.0000
ϕ5(N6-C12-C18-O4)	II	−1484.788721	−931,719.0279	0.0020
ϕ3(C19-C16-C15-O3)	III	−1484.788672	−931,718.9974	0.0325
ϕ2 (C19-C16-N8-H38)	IV	−1484.788397	−931,718.8243	0.2056
ϕ8(C15-N7-C10-C9)	V	−1484.786072	−931,717.3658	1.6641
ϕ1 (C21-C19-C16-N8)	VI	−1484.786072	−931,717.3657	1.6642
ϕ4(C16-C15-N7-C10)	VII	−1484.785941	−931,717.2835	1.7464
ϕ1 (C21-C19-C16-N8)	VIII	−1484.783035	−931,715.4597	3.5702
ϕ1 (C21-C19-C16-N8)	IX	−1484.782200	−931,714.9362	4.0937
ϕ4(C16-C15-N7-C10)	X	−1484.779738	−931,713.3909	5.6390
ϕ6(C12-C18-O4-H43)	XI	−1484.778566	−931,712.6558	6.3741
ϕ8(C15-N7-C10-C9)	XII	−1484.777751	−931,712.1443	6.8856

[a] Relative energies of the other eleven conformers with respect to the lowest energy conformer I.

The optimized geometry parameters: bond length, bond angle, and dihedral angle of all the conformers (I-IV) are tabulated in Table S2 (Supplementary Material). The bond length between four conformers has been compared which shows that the difference of 0.018 Å across the bond N8-C16 in conformer II and IV with respect to conformer I and III may be due to elongation of the bond while forming intramolecular H-bonding (H27…N8). However, in conformer II and IV, the bond length of N8-C16 appears to be shorter (~1.459 Å). The geometrical parameters of four conformers with the structure of literature [10] have been compared. The significant change in bond length of C—C, C—O, C—N, C—S, N—H, C—H groups, was not observed, however, the maximum difference is found to be 0.083 Å across O4-C18 group in all the conformers and this is due to presence of intramolecular H-bond interaction across O4…H31. Similarly, the maximum difference in bond angle 7.89/9.83/7.92/7.88° in conformer I/II/III/IV respectively was observed across O5-C18-C12 which is due to intra-molecular interaction with O5…H33. Another significant difference of 6.50° was observed in conformer I across N8-C16-H30. The prominent difference in angle was observed as 5.86/3.27/5.56/3.93° across C15-N7-H27 in conformer I/II/III/IV respectively.

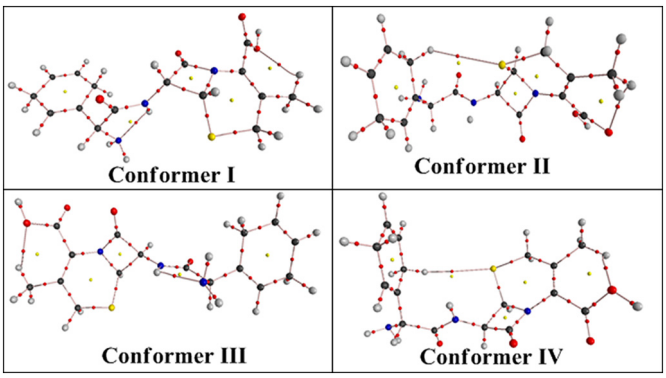

Fig. 2. Molecular graph of conformers (I-IV) of cefradine at bond critical points (small red spheres), ring critical points(small yellow sphere) and bond paths (pink lines).

Hence, to understand the structural changes between the conformers upon intramolecular hydrogen bonding interactions, QTAIM topology of all the conformers was generated as shown in Fig. 2. The geometrical and topological parameters of non-bonded intramolecular interactions of all the conformers of cefradine are presented in Tables 2 and 3. The interaction of H31…O4 in conformers I, III, and IV; the interaction of H27…N8 in conformers I and III and the interaction of H33…O5 in conformer II follow the geometrical criteria proposed by Koch and Popilier [31]. The interaction H35…S1 in conformer II and IV follow the criteria $\nabla^2\rho_{BCP} > 0$, $H_{BCP} < 0$, and bond length acceptor(A)-proton(H) > $(r_A + r_H)$ so from Rozas et al. [32] there is the formation of weak H-bond. Bader's [33] theory is used to estimate hydrogen bond energy (E). Espinosa [34] proposed proportionality between hydrogen bond energy (E) and potential energy density (V_{BCP}) at H…O contact:$E = \frac{1}{2}V_{BCP}$. The calculated interaction energy at BCP reveals that in the interactions H31…O4 in conformers I, III, and IV and H33…O5 in conformer II; the interaction H31…O4 is the strongest interaction. But the interaction H27…N8 in conformer III has the least bond length and the highest value of interaction energy so it is the strongest interaction.

4.3. Vibrational spectra

The cefradine molecule has 43 atoms and hence give rise 123 (3 N-6) normal modes of vibration. Table S3 (Supplementary Material) shows the assignments of normal modes with their potential energy distributions (PED). The comparison of experimental vibrational spectra (IR and Raman) and the simulated IR and Raman spectrum of conformers

Table 2
Topological parameters for intramolecular interaction in conformers (I-IV) of cefradine: ED (ρ_{BCP}), Laplacian of ED ($\nabla^2\rho_{BCP}$), electron kinetic energy density (G_{BCP}), electron potential energy density (V_{BCP}), total electron energy density (H_{BCP}), interaction energy (E_{int}) at BCP.

Interactions	Bond length (Å)	ρ_{BCP} (a.u)	$\nabla^2\rho_{BCP}$ (a.u)	G_{BCP} (a.u)	V_{BCP} (a.u)	H_{BCP} (a.u)	E_{int} (kcal/mol)
Conformer I							
H31…O4	2.3326	0.0143	0.0529	−0.0019	−0.0094	−0.0113	−2.9442
H27…N8	2.1652	0.0218	0.0845	−0.0029	−0.0153	−0.0182	−4.7949
Conformer II							
H33…O5	2.2908	0.0154	0.0564	−0.0021	−0.0099	−0.0120	−3.1142
H35…S1	3.7090	0.0014	0.0050	−0.0004	−0.0005	−0.0009	−0.1655
Conformer III							
H31…O4	1.0861	0.0143	0.0529	−0.0019	−0.0094	−0.0113	−2.9446
H27…N8	1.0140	0.0228	0.0874	−0.0029	−0.0161	−0.0189	−5.0368
Conformer IV							
H35…S1	3.4829	0.0021	0.0074	−0.0005	−0.0009	−0.0014	−0.2342
H31…O4	2.3305	0.0144	0.0534	−0.0019	−0.0095	−0.0114	−2.4945

Table 3
Geometrical parameters for intramolecular hydrogen bonds in conformers (I-IV) of cefradine: bond length (Å), bond angle (°) and the sum of Van der Waal radii of interacting atoms ($r_H + r_A$) in Å.

D-H···A	D-H (Å)	H···A (Å)	D-H···A (°)	($r_H + r_A$) (Å)
Conformer I				
C17-H31…O4	1.0861	2.3326	113.3850	2.72
N7-H27…N8	1.0140	2.1652	108.9447	2.75
Conformer II				
C17-H33…O5	1.0861	2.2908	116.6291	2.72
C20-H35…S1	1.0999	3.7090	130.4821	3.00
Conformer III				
C17-H31…O4	1.0861	2.3329	113.3072	2.72
N7-H27…N8	1.0140	2.1432	109.8265	2.75
Conformer IV				
C20-H35…S1	1.1000	3.4829	140.4263	3.00
C17-H31…O4	1.0860	2.3305	112.9911	2.72

(I-IV) are presented in Figs. 3 and 4. Quantum chemical calculation produces Raman amplitude, not Raman intensities, so Raman intensities were determined for each normal mode of vibration in terms of Raman scattering cross-section [35,36].

4.3.1. Scaling of Vibrational wavenumbers

In the vibrational spectral simulations, we may expect the overestimated harmonic frequencies which are due to the negligence of anharmonic frequencies. The overestimated frequencies were scaled down by a WLS scaling factor [37] and comparison was made with the observed spectra (IR and Raman). It is found that observed and simulated spectra from the scaled frequencies are matching well. Hence, only scaled calculated wavenumbers were compared with the experimental wavenumber for the modes in the following sections.

Almost all the calculated spectral values showed a good agreement with the experimentally observed values. However, the spectroscopic signatures of the conformer II are well-matched with the experimental one. This may be due to the overlapping of conformer II with the structure of literature [10] as explained in Section 4.2. Hence, the scaled wavenumbers of conformer II have been compared with the experimental IR and Raman spectra and depicted, wavenumbers of all the conformers (I-IV) are presented in Table S3 (Supplementary Material).

4.3.2. O—H vibrations

Cefradine has a single hydroxyl (O—H) group. In general, the free O—H stretching mode appears in the range 3640–3610 cm^{-1} while hydrogen-bonded O—H stretching appears in the range 3500–3200 cm^{-1} [38]. A sharp peak observed at 3557 cm^{-1} in both IR and Raman spectra and calculated at 3570 cm^{-1} are described to free O—H stretching. The O—H bending was calculated at 1149 cm^{-1} and observed at 1154/1155 cm^{-1} in IR/Raman spectrum. The torsion of the O—H group was observed at 643/642 cm^{-1} in IR/Raman spectrum but its simulation spectra were seen at 631 cm^{-1}.

4.3.3. N—H vibrations

The N—H asymmetric stretching mode of amine group (NH_2) was observed at 3435/3433 cm^{-1} in both IR/Raman spectra. It was calculated at 3434 cm^{-1} which matched well with the experimental one. The N—H stretching in simulated spectra was calculated at

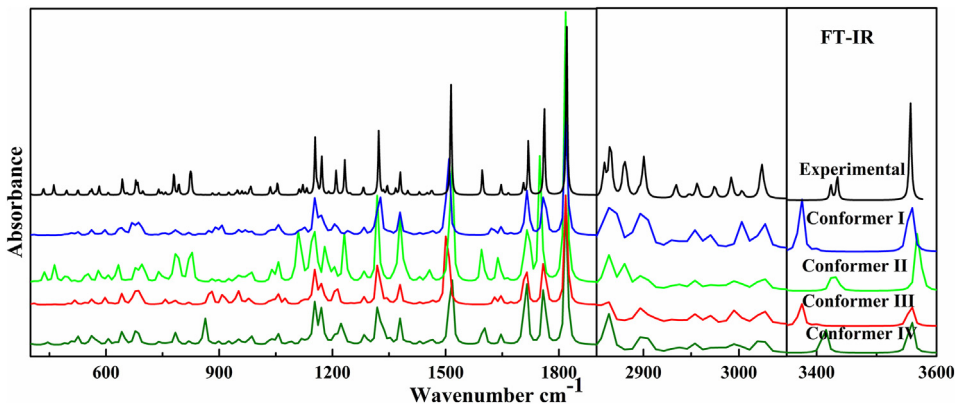

Fig. 3. Observed and calculated infrared spectra of cefradine in the region 400–1900 cm^{-1}, 2850–3050 cm^{-1} and 3350–3600 cm^{-1}.

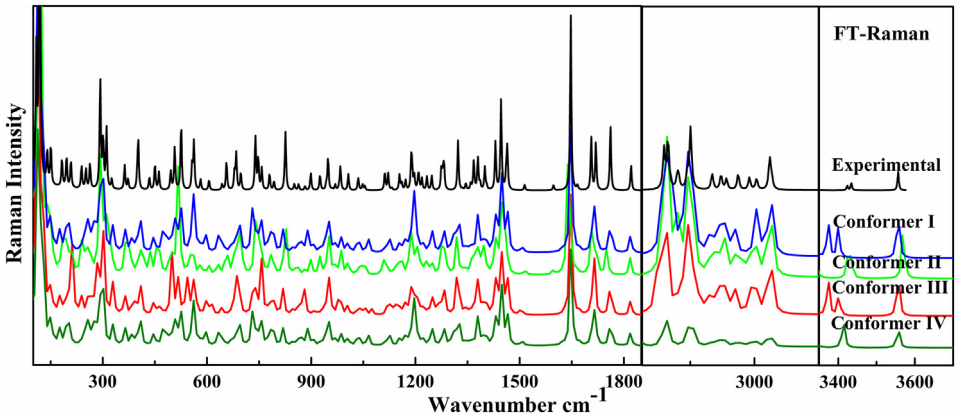

Fig. 4. Observed and calculated Raman spectra of cefradine in the region 100–1850 cm^{-1}, 2825–3100 cm^{-1} and 3350–3650 cm^{-1}.

3424 cm^{-1} but not observed in the experimental spectra. The N—H in-plane bending vibration (scissoring) of $N8H_2$ was calculated at 1597 cm^{-1} and observed at 1597 cm^{-1} in both IR and Raman spectra infer that the experimental and theoretical spectra are in good agreement. The rocking vibration of this group was observed in both IR and Raman spectrum at 1113 cm^{-1} and was calculated at 1116 cm^{-1}. The wagging of amine group calculated at 899 cm^{-1} match exactly with experimental spectra in the IR and Raman spectrum at 899 cm^{-1}. Another wagging vibration was calculated at 863 cm^{-1} and observed at 881/883 cm^{-1} in IR/Raman spectrum respectively.

4.3.4. C—H vibrations

The C—H stretching vibrations are generally observed in the range of 3000–3100 cm^{-1} [39,40]. The C—H stretching was observed in the higher wavenumber region with many distinct peaks in both IR and Raman spectra. The prominent peak was observed at 3024 cm^{-1} in both IR and Raman spectra corresponding to R3[ν_a(CH)] asymmetric stretching mode and was calculated at 3026 cm^{-1}. Another prominent peak corresponds to asymmetric C—H stretching was observed at 2865 cm^{-1} in both IR and Raman spectra and was calculated at 2865 cm^{-1}. The CH_2 out of plane bending, in the ring R1, was calculated at 1429 cm^{-1} and observed at 1430 cm^{-1} in both IR and Raman spectra. The symmetric deformation of $C17H_3$ was calculated at 1397 cm^{-1} and observed at 1399/1400 cm^{-1} in IR and Raman spectra.

4.3.5. C═O and C═C vibration

The strong stretching vibration absorption band of the carbonyl group (C═O) lies in the range 1670–1820 cm^{-1} [41,42]. Three distinct peaks observed at 1821, 1762, and1719 cm^{-1} in both IR and Raman spectra have good agreements with the calculated values at 1818, 1751, and 1719 cm^{-1} corresponding to stretching of carbonyl groups (C11═O2, C18═O5, C15═O3) respectively. The bond length of C18═O5 is increased by 0.067 Å in comparison to that of Van de Streek structure and its stretching wavenumber is lowered down by 11 cm^{-1}. This is due to intermolecular H-bonding with the neighboring molecule in the crystal structure. But we have studied for single-molecule in the gaseous state. This is also explored in Section 4.2 and due to the high value of the Fukui functions (f_k^-) as explained in Section 4.7.2. The C═C stretching of ring R3 was calculated at 1706 cm^{-1} and observed at 1706 cm^{-1} in both IR and Raman spectrum. Another C═C stretching peak of the ring R1 is seen at 1641 cm^{-1} but observed at 1647 cm^{-1} in both IR and Raman spectra.

4.4. Natural bond orbital analysis

By analyzing the natural bond orbitals, the various interactions between the electron lone pair orbitals and electron-deficient orbitals (antibonding orbitals) have been investigated. This study also includes the interactions between the bonding to antibonding orbitals. The second-order perturbation analysis of donor and acceptor NBO orbitals were done and the second-order perturbation energies E(2) [43–46] or stabilization energies of the prominent donor→acceptor species of conformer II are reported in Table S4 (Supplementary Material). The stabilization energies corresponding to the delocalization of $\sigma \rightarrow \sigma^*$ type such as σ(N6-C9) → σ*(O2-C11)/σ*(O2-C11), σ(C9-C10) → σ*(N6-C12), σ(C10-C11) → σ*(N6-C12), σ(C23-H41) → σ*(C22-C24), σ(C24-H42) → σ*(C20-C23) are predicted to be 6.22/6.38, 6.17, 7.21, 5.91 and 6.02 kcal/mol, respectively. The delocalization between the π orbitals π(C12-C14) → π*(O5-C18) stabilizes the molecule by 12.73 kcal/mol. The prominent lone pair to antibonding interactions (LP → σ*/π*) such as LP (2)O2 → σ*(N6-C11)/σ*(C10-C11), LP(2)O3 → σ*(N7-C15)/σ*(C15-C16), LP(2)O5 → σ*(O4-C18)/σ*(C12-C18) play an important role in the molecular stabilization and they stabilize the molecule by 30.52/24.10, 25.05/20.15 and 33.28/18.93 kcal/mol, respectively. The main interaction which gives the highest value of E(2) is LP(1) N7 → π*(O3-C15) with stabilization energy of about 61.87 kcal/mol.

4.5. Drug-likeliness

In addition to the spectroscopic characteristics, the drug-likeliness of the molecule was evaluated theoretically. For orally active drugs in humans, the value of molar refractivity (MR) should lie between 40 and 130. The MR value was measured in terms of polarizability and is given by Lorenz-Lorentz formula [47].

$$MR = \left[\frac{n^2-1}{n^2+2}\right]\left[\frac{MW}{\rho}\right] = 1.333\pi N\alpha$$

where n is the refractive index and its value depends on the wavelength of light, ρ is the density, MW is the molecular weight, and N is the Avogadro's number and α is the polarizability. Further, the drug-likeness of the molecule can be identified from Lipinski's five-rule [48,49]. According to Lipinski's five-rule, the number of atoms in the molecule should have a range from 20 to 70 and the molecular weight must lie between180 to 500.

In the title molecule, the number of atoms is 43, the molecular weight is 349.40 g/mol and the calculated molar refractivity is 57.8479, 57.9478, 53.9818 and 56.2732 e.s.u for conformers (I-IV) respectively. Thus, all the above-mentioned properties for the title molecule lie within the range of orally accepted drugs.

4.6. HOMO-LUMO energy gap ($\Delta E_{L\text{-}H}$)

The molecular orbitals, which participate in the chemical reactivity and stability of a system, are the highest occupied molecular orbital (HOMO) and lowest unoccupied molecular orbital (LUMO). The energies of HOMO (E_H) and LUMO (E_L) orbitals and their energy difference ($\Delta E_{L\text{-}H}$) determine the reactive behavior of the molecule [50,51]. In the molecular vicinity, HOMO and LUMO orbitals respectively donate and accept the electrons. The delocalization of electrons between these orbitals constitutes molecular stability.

A smaller value of this energy gap ($\Delta E_{L\text{-}H}$) implies less chemical stability and vice-versa [52]. To understand the electronic transitions of cefradine, time-dependent DFT (TD-DFT) calculations were performed at B3LYP/6-311++G(d,p) for all the four conformers. The HOMO and LUMO surface maps of the conformers (I-IV) are presented in Fig. 5. The calculated values ($\Delta E_{L\text{-}H}$) of conformers (I-IV) are 4.7454, 4.6978, 4.7731 and 4.7661 eV, respectively. From the calculations, it is noticeable that the conformer III is less reactive than the others. Furthermore, the conformer II is more chemically reactive whose IR and Raman spectra match well with the experimental spectra, as explored in Section 4.3. In HOMO surface maps of all the conformers, it was found that the orbital lobes are confined in the ring R3, C15═O3 and N7 whereas in LUMO surface maps, the orbital lobes spreaded over the ring R1, R2, carbonyl group (C18 = O5), hydroxyl group and $C17H_3$ regions.

4.7. Chemical reactivity

To obtain the local and global reactivity of the molecule and to determine the feasible sites for the electrophilic and nucleophilic attack, certain reactivity based DFT calculations were performed and the results are summarized in the following section:

4.7.1. Global reactivity descriptors

Global reactivity descriptors, such as electronegativity (χ), chemical potential (μ), global hardness (η), global softness (S), electrophilicity index (ω) have been determined on the basis of frontier molecular orbital energies as suggested in Koopman's theorem [53,54]. The stabilization energy, when the molecular system gains additional electronic charge from the surrounding, is measured in terms of electrophilicity index (ω) [55]. Electrophilicity encircles the strength of an electrophile to achieve additional electronic charge (ΔN) and the resistance of the system to exchange electronic charge with the surrounding. Besides that, the electrophilicity gives information about electron transfer (chemical potential) and stability (hardness). The energies of HOMO and LUMO, energy gap ($\Delta E_{L\text{-}H}$), χ, μ, η, S and ω for conformers (I-IV) of cefradine are presented in Table S5 (Supplementary Material). The chemical stability of a molecular system is recognized in terms of global hardness (η) and softness (S). The molecule with a large energy gap ($\Delta E_{L\text{-}H}$) is harder whereas the molecule with a small energy gap ($\Delta E_{L\text{-}H}$) is a softer one. The hard molecule is stable but the soft molecule is more polarizable and reactive. The value of $\Delta E_{L\text{-}H}$ (~4.6978 eV) is least for conformer II so it is more reactive with the highest electrophilicity index ω (3.8841) which can gain more additional charge ΔN (1.8186) from the surrounding in comparison to conformer I, III and IV of cefradine. The conformer III is more stable with the highest value of the energy gap $\Delta E_{L\text{-}H}$ (~4.7731 eV) with the least value of electrophilicity index ω (3.5689). Thus conformer II is more reactive in comparison to conformers I, III, and IV but conformer III is harder in comparison to conformers I, II, and IV of cefradine.

4.7.2. Local reactivity descriptors

Local reactivity descriptors describe which particular site in the molecular system is more chemically reactive. Fukui function f(r) has been used to identify the chemical reactivity and site selectivity of the molecule. The electrophilic and nucleophilic centers in the title molecule has also been predicted in terms of distribution of charge around the molecule from MEP surface analysis [56–58]. The red cloud across O2, O3, and O5 signifies the electrophilic region whereas the blue color region across H43 shows less electron density and is a nucleophilic region. For more precise measure of electrophilic and nucleophilic sites, Fukui function analysis was performed in this study. The sites having higher values of Fukui functions (FF) are more reactive points in the molecular system [59,60]. The Fukui functions were predicted corresponding to the cations, anions, and neutral radicals. Furthermore, local softness (s_k^+, s_k^-, s_k^0) and local electrophilicity indices (ω_k^+, ω_k^-, ω_k^0) are also used to illustrate the reactivity of atoms in the molecule and is given by relations:

$$s_k{}^+ = Sf_k{}^+, s_k{}^- = Sf_k{}^-, s_k{}^0 = Sf_k{}^0 \text{ for local softness}$$

$$\omega_k{}^+ = \omega f_k{}^+, \omega_k{}^- = \omega f_k{}^-, \omega_k{}^0 = \omega f_k{}^0 \text{ for local electrophilicity indices}$$

where +, − and 0 sign represents for nucleophilic, electrophilic and radical attack respectively. The maximum value of (f_k^+, s_k^+, ω_k^+) and (f_k^-, s_k^-, ω_k^-) infer the most nucleophilic and electrophilic site in the molecule respectively.

Fukui functions (f_k^+, f_k^-, f_k^0), local softness (s_k^+, s_k^-, s_k^0) and local electrophilicity indices (ω_k^+, ω_k^-, ω_k^0) for selected atomic sites of all the conformers (I-IV) of cefradine is reported in Table S6 (Supplementary Material). The significant sites for the nucleophilic attack are S1 and N8 whereas the significant sites for the electrophilic and radical attack are C14 and C18 respectively. The partial charge distribution for the nucleophilic and electrophilic attack in various atoms of cefradine are shown in Figs. S4 and S5 (Supplementary Materials), respectively.

4.8. Molecular docking

To explore the drug properties, the evaluation of ligand-protein interaction is essential to be investigated to get more insights into the active binding sites. To analyze the curative properties of cefradine, molecular docking simulation has been carried out by using AutoDock 4.2 software [25]. Based on the Swiss target prediction [61] search, three classes of target proteins were selected namely Dipeptidyl peptidase IV (DPP4), Protein farnesyltransferase (FTase) and Human Cyclooxygenase-2 and predicted targets are shown in Fig. S6 (Supplementary Material). The crystal structures of these proteins were collected from the RCSB data bank [62]. The parameters of the docked-complex with a large number of conformer clusters were collected in Table 4 and the LIGPLOT consisting of all possible interactions between the ligand and the protein structures were presented in Fig. 6. The ligand efficiency index of cefradine against the selected targets was provided since the predicted binding affinity is often closely proportional to the number of atoms in the ligand. The ligand efficiency is calculated dividing the score obtained in the docking simulation by the total number of non-hydrogen atoms of the ligand.

4.8.1. Docked complex of cefradine and Dipeptidyl peptidase IV (DPP4)

DPP4 is an enzyme that is used in immune regulation and it plays a significant role in glucose metabolism for the degradation of incretins (GLP-1) and the development of some tumors [63]. The inhibitors of DPP4 are a class of oral hypoglycemics that blocks the enzyme DPP4 and used in the treatment of type 2 diabetes. To explore the inhibition activity of cefradine against DPP4, the three PDB structures 1NU6, 1N1M, and 1J2E, with a resolution of 2.10 Å, 2.50 Å, 2.60 Å, were chosen from the RCSB data bank. The root mean square deviation (RMSD) values of the superimposition structures of 1NU6, 1N1M were predicted to be 0.586 and 0.577 with respect to the high resolution structure 1J2E and are given in Table 4.

Among the selected DPP4 structures, the amino acid residues of the target 1N1M bound to the cefradine molecule with higher binding energy (−6.01 kcal/mol). On the other hand, the value of inhibition constant of cefradine against 1N1M is predicted comparably lower than

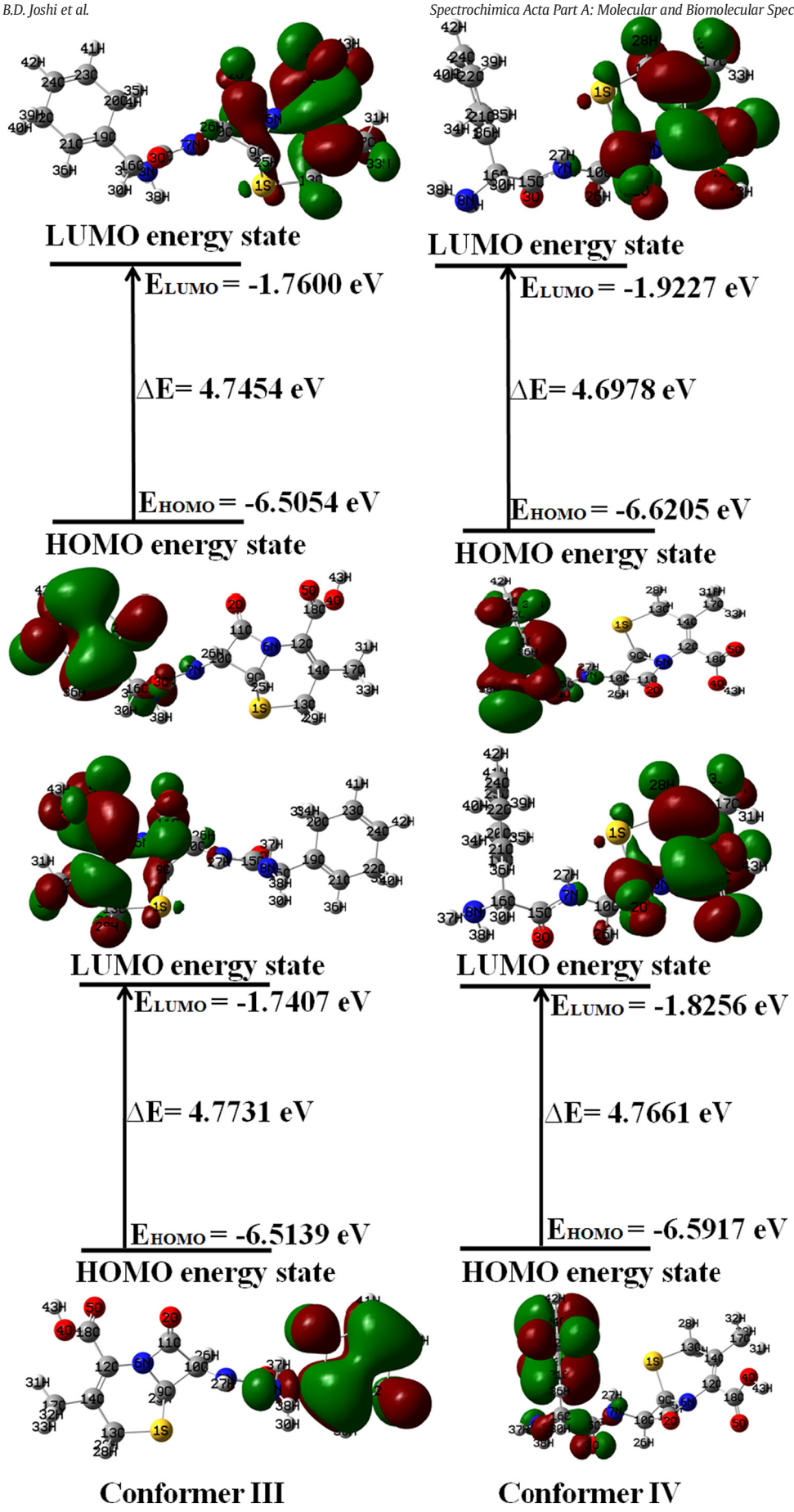

Fig. 5. HOMO-LUMO plot of conformers (I-IV) of cefradine.

Table 4
Bond length, binding energy and ligand efficiency of cefradine against different protein targets.

Target Proteins	Selected PDB structures with their resolutions	♀Hydrogen Bonding residues	Ligand efficiency	Inhibition constant (μM)	Binding energy (kcal/mol)	♀RMSD
Dipeptidyl peptidase IV (DPP4)	1NU6 (2.10 Å)	TYR70, LYS71, ARG61	−0.22	163.53	−5.17	–
	1N1M (2.50 Å)	PHE516, ASP515, LYS513, LYS536	−0.25	39.25	−6.01	0.586
	1J2E (2.60 Å)	THR251, ARG253, ASP192	−0.22	111.68	−5.39	0.577
Protein Farnesyltransferase	1MZC (2.00 Å)	GLU723, LHE762 LYS763	−0.24	69.28	−5.67	
	3E34 (2.05 Å)	LYS50, GLU41, ASP37	−0.2	310.15	−4.79	0.253
	1O1R (2.30 Å)	ASP297, ARG291, HIS248, TYR300	−0.22	111.28	−5.39	0.342
Human Cyclooxygenase-2 (COX-2)	5IKT (2.45 Å)	GLU346, ASP347, LYS358	−0.19	387.03	−4.66	
	5IKV (2.51 Å)	ALA239, ARG240, LYS243, GLU272, GLU290	−0.23	90.95	−5.51	0.137
	5KIR (2.70 Å)	ASP157, ASP133, GLN457	−0.24	64.53	−5.72	0.266

♀ The distance between the ligand and the binding residues is given in Angstrom units in the parenthesis.
♀ RMSD value of the superimposition of proteins with respect to the high resolution PDB structure is provided.

the other two PDB structures. The higher ligand efficacy (−0.25) and lower inhibition constant (39.25 μM) values indicate that cefradine can probably be a good candidate to block the enzymatic activity of DPP4.

4.8.2. Docked complex of cefradine and Protein farnesyltransferase (FTase)

FTase is a heterodimeric complex consisting of a regulatory alpha subunit shared with geranylgeranyltransferase I (also a CaaX prenyltransferase) and a unique catalytic beta subunit [64]. FTase enzyme is responsible for the posttranslational modification (farnesylation) of proteins carrying a carboxy-terminal CaaX motif, including Ras, Ras homologues, and other small G proteins. Hence, certain FTase inhibitors are used as anti-parasitic and anti-cancer agents.

In the present study, to investigate the binding affinity and inhibition capability of cefradine against FTase enzyme, three protein structures viz. 1MZC, 3E34, and 1O1R with the resolution of 2.0, 2.05, and 2.30 Å were chosen and found to have potential inhibition activity against FTase enzyme. Out of the selected targets, the protein structures with the PDB codes 3E34 and 1O1R superimpose with respect to the higher resolution structure 1MZC and the RMSD value of these superposition structures were predicted to be 0.253, and 0.342 respectively. The binding energy of the docked complex of 1MZC and cefradine was predicted as higher as −5.67 kcal/mol and being bind with the residues GLU723, LHE762, LYS763 through strong hydrogen bonds. The predicted inhibition constant is 69.28 μM. On the other hand, the other two PDB structures (3E34, 1O1R) of FTase is found to be comparatively loosely binding with the active residues.

4.8.3. Docked complex of cefradine and Human Cyclooxygenase-2 (COX-2)

The COX-2 is an enzyme in human encoded by Prostaglandin-endoperoxide synthase 2 (PTGS2) gene. The inhibitors of COX can provide relief from the symptoms of inflammation and pain [65]. To illustrate the active binding sites and inhibition capability of cefradine against COX-2, three COX-2 structures viz. 5IKT, 5IKV, and 5KIR were chosen and docked with cefradine by default docking protocol and parameters in Auto Dock 4.2 program. The results indicate that the COX-2 target (5KIR) residues such as ASP157, ASP133, GLN457 bind with the cefradine through strong hydrogen bonds. The ligand efficiency of cefradine as COX-2 inhibitor is predicted to be −0.24 and it is predicted to have lower inhibition constant (64.53 μM). The predicted lower RMSD values of the superposition structures of 5IKV and 5KIR with respect to the higher resolution structure indicate the amino acids of this protein are aligned with small deviations in their orientation.

The docking study implies that cefradine seems to be useful merit as the inhibitors of Dipeptidyl peptidase IV (DPP4), Protein farnesyltransferase (FTase), and Human Cyclooxygenase-2. However,

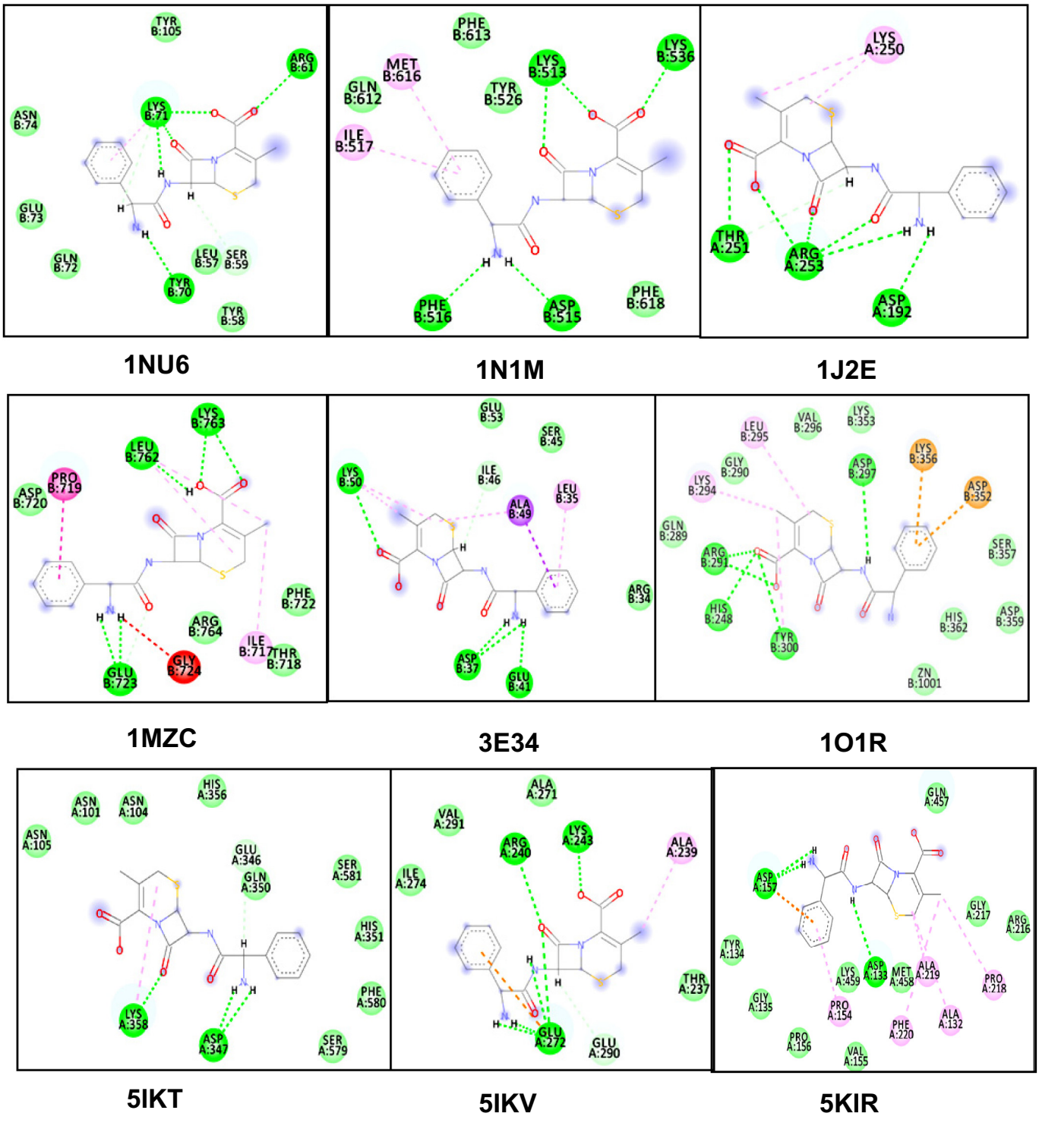

Fig. 6. Docking of cefradine with different protein targets.

further in vitro and in vivo studies have to be performed to confirm its activities.

5. Conclusion

The least energetic structure, chemical reactivity, drug-likeness, and binding sites of ligand (cefradine) has been studied on the spectroscopic and atomic level approach. The four possible conformers; conformer (I-IV) of cefradine having energies −931,719.0299, −931,719.0278, −931,718.9974 and −931,718.8243 kcal/mol respectively have been obtained at room temperature by using DFT and quantum chemical calculation method. QTAIM study infer that the interactions H31···O4, H27···N8, H33···O5 shows partial covalent bond with medium in nature as $\nabla^2\rho_{BCP} > 0$, $H_{BPC} < 0$ and bond length acceptor (A) - proton (H) $< (r_A + r_H)$. The interaction H35···S1 shows weak H-bond as $\nabla^2\rho_{BCP} > 0$, $H_{BPC} < 0$ and bond length acceptor (A) – proton (H) $> (r_A + r_H)$. The comparative study of the experimental and calculated vibrational spectra of the title molecule has been illustrated about the functional groups present in the molecule. The experimental values of the wavenumbers are in agreement with the calculated scaled wavenumbers of conformer II. NBO calculation shows that the charge transfer from LP(1)N7 → π*(O3–C15) plays a vital role in the stability of the molecule with stabilization energy 61.87 kcal/mol. From the HOMO–LUMO energy gap it is clear that conformer III is more stable as it has the largest energy gap (4.7731 e*V*) and conformer II is more chemically reactive as it has the highest value of softness (0.2129) than the others three conformers. In HOMO charge is concentrated in-ring R3, C15═O3, and N7 whereas it is scattered on ring R1, R2, carbonyl group (C18 = O5), hydroxyl group and C17H3 in LUMO. The carbonyl group (C=O) is the electrophilic region whereas the hydroxyl group (OH) is the nucleophilic region in all the four conformers and these are the favorite sites in molecular docking. Fukui calculation shows that N8 and C14 site is more nucleophilic and electrophilic region respectively. Docking studies demonstrate that the cefradine molecule binds with the selected targets with higher binding energy and predicted to have lower inhibition constant. The binding site of cefradine is found to be amine (NH_2) group which is also supported by the highest value of Fukui functions (FF) of N8 atom.

CRediT authorship contribution statement

Manoj Kumar Chaudhary: Drafting, Analysis, Simulation.
T. Karthick: Supervision, drafting, proofreading.
Bhawani Datt Joshi: Supervision, drafting, proofreading.
Preeti Prajapati: Analysis of spectroscopic data.
Maria Silmara Alves de Santana: Spectral measurement, analysis.
Alejandro Pedro Ayala: Conceptulation, Proof reading.
V.S. Reeda: Docking simulation, visualization of results.
Poonam Tandon: Supervision, proofreading.

Declaration of competing interest

The authors declare that they have no known competing financial interests or personal relationships that could have appeared to influence the work reported in this paper.

Acknowledgment

M.K. Chaudhary is grateful to Centre for Co-Operation in Science and Technology among Developing Societies (CCSTDS), India for providing partial financial support under the Indian Science and Research Fellowship (ISRF-2019), with award ID (DO/CCSTDS/204/2019).

Appendix A. Supplementary data

Supplementary data to this article can be found online at https://doi.org/10.1016/j.saa.2020.118976.

References

[1] L. Du, W. Luo, Crystallization optimizing of cefradine, The Open Catalysis Journal 3 (1) (2010) 19–23, https://doi.org/10.2174/1876214X01003010019.
[2] K. Muthu, K. Gunasekaran, A. Kala, P. Govindasamy, P. Rajesh, P.P. Moorthi, Spectroscopic (FT-IR, FT-Raman & UV-Vis) and density functional theory studies of Cefadroxil, Int.J.Curr.Microbiol.App.Sci. 4 (11) (2015) 211–225http://www.ijcmas.com.
[3] P.S. Ganeshvar, S. Gunasekaran, T. Gnanasambandan, K. Viswanathan, Cefalexin: molecular structure, vibrational spectroscopy, natural bond orbital analysis and HOMO, LUMO studies, Int. J. Sci. Res. 4 (10) (2015) 182–189, https://doi.org/10.36106/ijsr.
[4] E. Finkelstein, R. Quintiliani, R. Lee, A. Bracci, C.H. Nightingale, Pharmacokinetics of oral cephalosporins: cephradine and cephalexin, J. Pharm. Sci. 67 (1978) 1447–1450, https://doi.org/10.1002/jps.2600671033.
[5] F.A.I. Al-Khodir, M.S. Refat, Physicochemical, spectroscopic, and anti-tumor studies of cefradine complexes with Ca (II), Zn (II), Fe (III), Au (III), and Pd (II) ions, Russ. J. Gen. Chem. 87 (2017) 1087–1092, https://doi.org/10.1134/S1070363217050322.
[6] Ž.Z. TasićMarija, B. Petrović, M. Milan, B. RadovanovićAna, T. SimonovićMilan, M. Antonijević, Cephradine as corrosion inhibitor for copper in 0.9% NaCl solution, J. Mol.Struct. 1159 (2018) 46–54, https://doi.org/10.1016/j.molstruc.2018.01.031.
[7] A.K. Singh, A.K. Singh, E.E. Ebenso, Inhibition effect of cefradine on corrosion of mild steel in HCl solution, Int. J. Electrochem. Sci. 9 (2014) 352–364http://www.electrochemsci.org.
[8] I. Weliky, H.H. Gadebusch, K. Kripalani, P. Arnow, E.C. Schreiber, Cephradine: absorption, excretion, and tissue distribution in animals of a new cephalosporin antibiotic, Antimicrob. Agents Chemother. 5 (1974) 49–54, https://doi.org/10.1128/AAC.5.1.49.
[9] M.G. Sayed, M. Aboubakr, S. Rabea, Pharmacokinetics and tissue residues of cephradine in healthy and experimentally Salmonella Entretidis infected broiler chickens, World J. Pharm. Pharm. Sci. 6 (2016) 61–74.
[10] J. Van de Streek, J. Rantanen, A.D. Bond, Structures of cefradine dihydrate and cefaclor dihydrate from DFT-D calculations, Acta Crystallogr. C Struct. Chem. 69 (2013) 1229–1233, https://doi.org/10.1107/S0108270113026863.
[11] P. Hohenberg, W. Kohn, Inhomogeneous electron gas, Phys. Rev. B 136 (1964) 864–871, https://doi.org/10.1103/PhysRev.136.B864.
[12] C.T. Lee, W.T. Yang, R.G. Parr, Development of the Colle-Salvetti correlation-energy formula into a functional of the electron density, Phys. Rev. 37B (1988) 785–789, https://doi.org/10.1103/PhysRevB.37.785.
[13] R.G. Parr, W. Yang, Density Functional Theory of Atoms and Molecules, New York, Oxford, 1989.
[14] T.H. Dunning Jr., Gaussian basis sets for use in correlated molecular calculations. I. The atoms boron through neon and hydrogen, J. Chem. Phys. 90 (1989) 1007–1023, https://doi.org/10.1063/1.456153.
[15] D.E. Woon, T.H. Dunning Jr., Gaussian basis sets for use in correlated molecular calculations. V. Core-valence basis sets for boron through neon, J. Chem. Phys. 103 (1995) 4572–4585, https://doi.org/10.1063/1.470645.
[16] A.D. Becke, Density-functional thermochemistry. III. The role of exact exchange, J. Chem. Phys. 98 (1993) 5648–5652, https://doi.org/10.1063/1.464913.
[17] M.J. Frisch, G.W. Trucks, H.B. Schlegel, G.E. Scuseria, J.R. Cheeseman, M.A. Robb, G. Scalmani, V. Barone, B. Mennucci, G.A. Petersson, H. Nakatsuji, M. Caricato, X. Li, H.P. Hratchian, A.F. Izmzylov, J. Bloino, G. Zheng, J.L. Sonnenberg, M. Hada, M. Ehara, K. Toyota, R. Fukuda, J. Ishida, M. Hasegawa, T. Nakajima, Y. Honda, O. Kitao, H. Nakai, T. Vreven, J.A. Montgomery Jr., J.E. Peralta, F. Ogliaro, M. Bearpark, J.J. Heyd, E. Brothers, K.N. Kudin, V.N. Staroverov, R. Kobayashi, J. Normand, A. Raghavachari, A. Rendell, J.C. Burant, S.S. Iyengar, J. Tomasi, M. Cossi, N. Rega, J.M. Millan, M. Klene, J.E. Knox, J.B. Cross, V. Bakken, C. Adamo, J. Jaramillo, R. Gomperts, R.E. Stratmann, O. Yazyev, A.J. Austin, R. Cammi, C. Pomelli, J.W. Ochterski, R.L. Martin, K. Morokuma, V.G. Zakrzewski, G.A. Voth, P. Salvador, J.J. Dannerberg, S. Dapprich, A.D. Daniels, J. Farkas, B. Foresman, J.V. Ortiz, J. Cioslowski, D.J. Fox, GAUSSIAN 09, Revision, Gaussian, Inc., Wallingford CT, 2009.
[18] P. Pulay, G. Fogarasi, F. Pang, J.E. Boggs, Systematic ab initio gradient calculation of molecular geometries, force constants, and dipole moment derivatives, J. Am. Chem. Soc. 101 (1979) 2550–2560, https://doi.org/10.1021/ja00504a009.
[19] J.M.L. Martin, C. VanAlsenoy, Gar2ped, University of Antwerp, Antwerp, 1995.
[20] A. Frisch, A.B. Nielson, A.J. Holder, GaussView User Manual, Gaussian Inc, Pittsburgh, PA, 2005.
[21] T.A. Keith, AIMALL Version 090201 TK Gristmill Software Overland Park, KS.USA, 2009.
[22] R.F.W. Bader, S.G. Anderson, A.J. Duke, Quantum topology of molecular charge distributions.1, J. Am. Chem. Soc. 101 (1979) 1389–1395, https://doi.org/10.1021/ja00500a006.
[23] R.F.W. Bader, T.S. Slee, D. Cremer, E. Kraka, Description of conjugation and hyperconjugation in terms of electron distributions, J. Am. Chem. Soc. 105 (1983) 5061–5068, https://doi.org/10.1021/ja00353a035.
[24] R.F.W. Bader, P.J. MacDougall, Toward a theory of chemical reactivity based on the charge density, J. Am. Chem. Soc. 107 (1985) 6788–6795, https://doi.org/10.1021/ja00310a007.

[25] G.M. Morris, R. Huey, W. Lindstrom, M.F. Sanner, R.K. Belew, D.S. Goodsell, A.J. Olson, AutoDock4 and AutoDockTools4: automated docking with selective receptor flexibility, J. Comput. Chem. 30 (16) (2009) 2785–2791, https://doi.org/10.1002/jcc.21256.
[26] E.F. Pettersen, T.D. Goddard, C.C. Huang, G.S. Couch, D.M. Greenblatt, E.C. Meng, T.E. Ferrin, UCSF chimera–a visualization system for exploratory research and analysis, J. Comput. Chem. 25 (2004) 1605–1612.
[27] G.M. Morris, D.S. Goodsell, R.S. Halliday, R. Huey, W.E. Hart, R.K. Belew, A.J. Olson, Automated docking using a Lamarckian genetic algorithm and an empirical binding free energy function, J. Comput. Chem. 19 (1998) 1639–1662, https://doi.org/10.1002/(SICI)1096-987X(19981115)19:14%3C1639::AID-JCC10%3E3.0.CO;2-B.
[28] Discovery Studio 4.5 Guide, Accelrys Inc., San Diego, http://www. accelrys.com (2009).
[29] J.D. Chai, M. Head-Gordon, Long-range corrected hybrid density functionals with damped atom–atom dispersion corrections, Phys. Chem. Chem. Phys. 10 (44) (2008) 6615–6620, https://doi.org/10.1039/B810189B.
[30] S. Tortorella, M.M. Talamo, A. Cardone, M. Pastore, F. De Angelis, Benchmarking DFT and semi-empirical methods for a reliable and cost-efficient computational screening of benzofulvene derivatives as donor materials for small-molecule organic solar cells, J. Phys. Condens. Matter 28 (7) (2016), 074005, https://doi.org/10.1088/0953-8984/28/7/074005.
[31] U. Koch, P. Popelier, Characterization of CHO hydrogen bonds on the basis of the charge density, J. Phys. Chem. A 99 (24) (1995) 9747–9754, https://doi.org/10.1021/j100024a016.
[32] I. Rozas, I. Alkorta, J. Elguero, Behavior of ylides containing N, O, and C atoms as hydrogen bond acceptors, J. Am. Chem. Soc. 122 (45) (2000) 11154–11161, https://doi.org/10.1021/ja0017864.
[33] R.F.W. Bader, Atoms in Molecules a Quantum Theory, Oxford University Press, Oxford, 1990.
[34] E. Espinosa, E. Molins, C. Lecomte, Hydrogen bond strengths revealed by topological analyses of experimentally observed electron densities, Chem. Phys. Lett. 285 (3–4) (1998) 170–173, https://doi.org/10.1016/S0009-2614(98)00036-0.
[35] G.A. Guirgis, P. Klaboe, S. Shen, D.L. Powell, A. Gruodis, V. Aleksa, C.J. Nielsen, J. Tao, C. Zheng, J.R. Durig, Spectra and structure of silicon-containing compounds. XXXVI—Raman and infrared spectra, conformational stability, ab initio calculations and vibrational assignment of ethyldibromosilane, J. Raman Spectrosc. 34 (4) (2003) 322–336, https://doi.org/10.1002/jrs.989.
[36] P.L. Polavarapu, Ab initio vibrational Raman and Raman optical activity spectra, J. Phys. Chem. 94 (21) (1990) 8106–8112, https://doi.org/10.1021/j100384a024.
[37] M.P. Andersson, P. Uvdal, New scale factors for harmonic vibrational frequencies using the B3LYP density functional method with the triple-ζ basis set 6-311+ G (d, p), J. Phys. Chem. A 109 (12) (2005) 2937–2941, https://doi.org/10.1021/jp045733a.
[38] N.B. Colthup, L.H. Daly, S.E. Wiberley, Introduction to Infrared and Raman Spectroscopy, Academic Press, New York, 1990.
[39] G. Varsanyi, Assignments for Vibrational Spectra of Seven Hundred Benzene Derivatives, vol. 1 and 2, Academia Kiado, Budapest, 1973.
[40] A. Thamarai, R. Vadamalar, M. Raja, S. Muthu, B. Narayana, P. Ramesh, R.R. Muhamed, S. Sevvanthi, S. Aayisha, Molecular structure interpretation, spectroscopic (FT-IR, FT-Raman), electronic solvation (UV–Vis, HOMO-LUMO and NLO) properties and biological evaluation of (2E)-3-(biphenyl-4-yl)-1-(4-bromophenyl) prop-2-en-1-one: experimental and computational modeling approach, Spectrochim. Acta A Mol. Biomol. Spectrosc. 226 (2020) 117609, https://doi.org/10.1016/j.saa.2019.117609.
[41] R.M. Silverstein, G.C. Bassler, T.C. Morrill, Spectrometric Identification of Organic Compounds, 4th ed. John Wiley and Sons, New York, 1981.
[42] J. Mohan, Organic Spectroscopy, Principles and Applications, 2nd edition Narosa Publishing House, New Delhi, 2009.
[43] A.E. Reed, L.A. Curtiss, F. Weinhold, Intermolecular interactions from a natural bond orbital, donor-acceptor viewpoint, Chem. Rev. 88 (6) (1988) 899–926, https://doi.org/10.1021/cr00088a005.
[44] C.S. Abraham, S. Muthu, J.C. Prasana, S. Armaković, S.J. Armaković, B. Geoffrey, Computational evaluation of the reactivity and pharmaceutical potential of an organic amine: a DFT, molecular dynamics simulations and molecular docking approach, Spectrochim. Acta A Mol. Biomol. Spectrosc. 222 (2019) 117188, https://doi.org/10.1016/j.saa.2019.117188.
[45] E.D. Glendening, C.R. Landis, F. Weinhold, Wiley Interdiscip, Rev. Comput. Mol.Sci 2 (2012) 1–42.
[46] R. Mishra, B.D. Joshi, A. Srivastava, P. Tandon, S. Jain, Quantum chemical and experimental studies on the structure and vibrational spectra of an alkaloid–Corlumine, Spectrochim. Acta A Mol. Biomol. Spectrosc. 118 (2014) 470–480, https://doi.org/10.1016/j.saa.2013.09.015.
[47] R.P. Verma, A. Kurup, C. Hansch, On the role of polarizability in QSAR, Bioorg. Med. Chem. 13 (1) (2005) 237–255, https://doi.org/10.1016/j.bmc.2004.09.039.
[48] C.A. Lipinski, L. Franco, W.D. Beryl, J.F. Paul, Experimental and computational approaches to estimate solubility and permeability in drug discovery and development settings, Adv. Drug Deliv. Rev. 23 (1–3) (1997) 3–25, https://doi.org/10.1016/S0169-409X(96)00423-1.
[49] H. Chow, H. Chen, T. Ng, P. Myrdal, S.H. Yalkowsky, Using backpropagation networks for the estimation of aqueous activity coefficients of aromatic organic compounds, J. Chem. Inf. Comput. Sci. 35 (4) (1995) 723–728, https://doi.org/10.1021/ci00026a009.
[50] R.M. Issa, M.K. Awad, F.M. Atlam, Quantum chemical studies on the inhibition of corrosion of copper surface by substituted uracils, Appl. Surf. Sci. 255 (5) (2008) 2433–2441, https://doi.org/10.1016/j.apsusc.2008.07.155.
[51] P. Prajapati, J. Pandey, P. Tandon, K. Sinha, Combined spectroscopic and quantum chemical approach to study the effect of hydrogen bonding interactions in ezetimibe, Spectrochim. Acta A Mol. Biomol. Spectrosc. 206 (2019) 246–253, https://doi.org/10.1016/j.saa.2018.08.023.
[52] K. Fukui, Role of frontier orbitals in chemical reactions, Science 218 (4574) (1982) 747–754https://www.jstor.org/stable/1689733.
[53] P. Ramesh, M.L. Caroline, S. Muthu, B. Narayana, M. Raja, A.B. Geoffrey, Spectroscopic, chemical reactivity, molecular docking investigation and QSAR analyses of (2E)-1-(3-bromo-2-thienyl)-3-(2, 5-dimethoxyphenyl) prop-2-en-1-one, Spectrochim. Acta A Mol. Biomol. Spectrosc. 222 (2019) 117190, https://doi.org/10.1016/j.saa.2019.117190.
[54] R.G. Parr, R.G. Pearson, Absolute hardness: companion parameter to absolute electronegativity, J. Am. Chem. Soc. 105 (26) (1983) 7512–7516, https://doi.org/10.1021/ja00364a005.
[55] R.G. Parr, L. Szentpály, S. Liu, Electrophilicity index, J. Am. Chem. Soc. 121 (9) (1999) 1922–1924, https://doi.org/10.1021/ja983494x.
[56] J.S. Murray, J.M. Seminario, M.C. Concha, P. Politzer, An analysis of molecular electrostatic potentials obtained by a local density functional approach, Int. J. Quantum Chem. 44 (2) (1992) 113–122, https://doi.org/10.1002/qua.560440204.
[57] J. Pandey, P. Prajapati, A. Srivastava, P. Tandon, K. Sinha, A.P. Ayala, A.K. Bansal, Spectroscopic and molecular structure (monomeric and dimeric model) investigation of Febuxostat: a combined experimental and theoretical study, Spectrochim. Acta A Mol. Biomol. Spectrosc. 203 (2018) 1–12, https://doi.org/10.1016/j.saa.2018.05.074.
[58] T. Brinck, J.S. Murray, P. Politzer, Molecular surface electrostatic potentials and local ionization energies of group V–VII hydrides and their anions: relationships for aqueous and gas-phase acidities, Int. J. Quantum Chem. 48 (2) (1993) 73–88, https://doi.org/10.1002/qua.560480202.
[59] R.G. Parr, W. Yang, Density functional approach to the frontier-electron theory of chemical reactivity, J. Am. Chem. Soc. 106 (14) (1984) 4049–4050, https://doi.org/10.1021/ja00326a036.
[60] K. Srivastava, A. Srivastava, P. Tandon, K. Sinha, J. Wang, Spectroscopic, quantum chemical calculation and molecular docking of dipfluzine, J. Mol. Struct. 1125 (2016) 751–762, https://doi.org/10.1016/j.molstruc.2016.07.078.
[61] A. Daina, O. Michielin, V. Zoete, SwissTargetPrediction: updated data and new features for efficient prediction of protein targets of small molecules, Nucleic Acids Res. 47 (W1) (2019) W357–W364, https://doi.org/10.1093/nar/gkz382.
[62] P.W. Rose, B. Beran, C. Bi, W.F. Bluhm, D. Dimitropoulos, D.S. Goodsell, A. Prlić, M. Quesada, G.B. Quinn, J.D. Westbrook, J. Young, The RCSB protein data Bank: redesigned web site and web services, Nucleic Acids Res. 39 (2010) D392–D401, https://doi.org/10.1093/nar/gkq1021.
[63] U.V. Wesley, M. McGroarty, A. Homoyouni, Dipeptidyl peptidase inhibits malignant phenotype of prostate cancer cells by blocking basic fibroblast growth factor signaling pathway, Cancer Res. 65 (4) (2005) 1325–1334, https://doi.org/10.1158/0008-5472.CAN-04-1852.
[64] S. Maurer-Stroh, S. Washietl, F. Eisenhaber, Protein prenyltransferases, Genome Biol. 4 (2003) 212, https://doi.org/10.1186/gb-2003-4-4-212.
[65] R.G. Kurumbail, A.M. Stevens, J.K. Gierse, J.J. McDonald, R.A. Stegeman, J.Y. Pak, D. Gildehaus, J.M. Iyashiro, T.D. Penning, K. Seibert, P.C. Isakson, W.C. Stallings, Structural basis for selective inhibition of cyclooxygenase-2 by anti-inflammatory agents, Nature 384 (1998) 644–648, https://doi.org/10.1038/384644a0.

Computational and Theoretical Chemistry 1191 (2020) 113031

Contents lists available at ScienceDirect

Computational and Theoretical Chemistry

journal homepage: www.elsevier.com/locate/comptc

Computational evaluation on molecular stability, reactivity, and drug potential of frovatriptan from DFT and molecular docking approach

Manoj Kumar Chaudhary[a,b], Anubha Srivastava[b], Keshav Kumar Singh[b], Poonam Tandon[b,*], Bhawani Datt Joshi[c,*]

[a] Central Department of Physics, Tribhuvan University, Kirtipur, Kathmandu, Nepal
[b] Department of Physics, University of Lucknow, Lucknow 226007, India
[c] Department of Physics, Siddhanath Science Campus, Tribhuvan University, Mahendranagar, 10406, Nepal

ARTICLE INFO

Keywords:
Frovatriptan
Natural bond orbital (NBO)
NLO
Chemical reactivity
Molecular docking

ABSTRACT

Molecular stability, fundamental chemical reactive sites, global reactivity descriptors in frovatriptan molecule have been investigated by using computational evaluation and molecular docking approach. The density functional theory has been employed with standard functional B3LYP/6–311 + + G(d,p). The possible minimum energy structure has been predicted by implementing one-dimensional potential energy surface (PES) scan. The charge delocalization for stability of the molecule with natural bond orbital (NBO) analysis and molecular electrostatic potential (MEP) surface analysis to observe the active region for further chemical reaction with surrounding species have been performed. The chemical reactivity and hardness of the molecule in terms of HOMO-LUMO energy gap ($\Delta E_{L\text{-}H}$) have been implemented in terms of reactivity parameters. The potential use of frovatriptan as non-linear optical (NLO) material and its thermodynamical studies have also been performed. Moreover, the molecular docking with a predicted target has been performed to check the binding interaction as well as sites of the molecule.

1. Introduction

Frovatriptan, (6*R*)-6-(methylamino)-6,7,8,9-tetrahydro-5*H*-carbazole-3-carboxamide, a member of carbazoles having molecular formula $C_{14}H_{17}N_3O$, is a triptan drug initiated by Vernalis. The pharmacological activity of triptan group drugs found great attention towards the acute migraine pain [1]. There are seven triptan group drugs for the treatment of migraine pain but the effectiveness of frovatriptan is most as studied by Carlo *et al.* [2]. Frovatriptan lies in the serotonin 5-HT_{1B} agonists group of receptors which has the therapeutic use to treat the migraine and vascular headaches, especially in women at the time of menstruation [1,3]. Frovatriptan dilates the arteries and veins so that blood can easily reach to the brain.

Many experimental and theoretical work of frovatriptan has been performed by the different research groups to enhance the potential of drugs [4–7]. This study figure out to obtain the stable structure of the title molecule at room temperature by employing the DFT [8,9] calculation under the B3LYP/6–311 + + G(d,p) level of theory by using one-dimensional potential energy surface (PES) scan. Natural bond orbital (NBO) analysis has been performed, in which we have discussed the interaction of electrons between filled and vacant orbitals. The distribution of charge around the molecule in space which predicts its reactive sites has been discussed by using molecular electrostatic potential (MEP) surface. The electron transport properties of the molecule have been analyzed in terms of global reactivity descriptors. The specific atom in the molecule active for further reaction with neighboring species has been figured out by using local reactivity descriptor with Hirshfeld charge analysis. The theoretical prediction of drug candidate of frovatriptan has also been examined. The non-linear optical (NLO) properties and temperature-dependent parameters have been studied. Furthermore, the molecular docking of the title molecule which theoretically confirms the active binding sites and binding strength with predicted target has been carried out. The above-mentioned atomic calculation of frovatriptan has not been discussed in the literature survey. Therefore, this study aims to work on the title compound to explore the molecular properties at the microscopic level.

2. Computational details

Computational evaluation of the title compound has been carried out by using the Gaussian 09 software package [10]. The optimization has been performed by employing the default settings in the Gaussian

* Corresponding authors.
E-mail addresses: poonam_tandon@yahoo.co.uk (P. Tandon), pbdjoshi@gmail.com (B.D. Joshi).

https://doi.org/10.1016/j.comptc.2020.113031
Received 26 June 2020; Received in revised form 24 August 2020; Accepted 14 September 2020
Available online 19 September 2020
2210-271X/

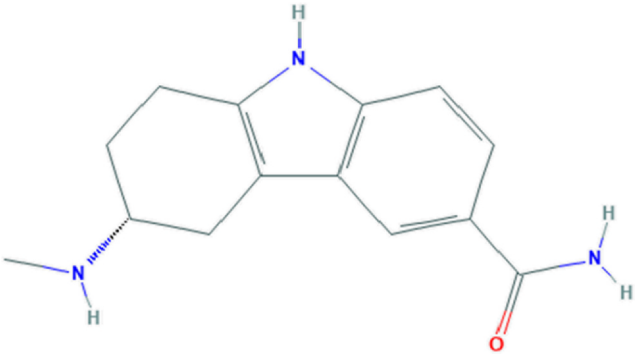

Fig. 1. Chemical structure of frovatriptan.

09 program package. Potential energy surface (PES) scan of the title compound and its optimization has been performed by using density functional theory (DFT) [11] with functional B3LYP [12,13] and 6–311 + + G(d,p) basis set [14–16]. Moreover, the NBO, NLO, thermodynamic parameters, MEP, HOMO-LUMO, and Hirshfeld charges have been calculated at the same level of theory as optimization. The visualization of charge distribution in the molecule (MEP, HOMO-LUMO) has been performed with GaussView 05 software [17]. Molecular simulation for docking of the molecule has been carried out with Auto Dock Tools (ADT) version 1.5.4 [18]. The binding sites of frovatriptan with amino acids of protein have been visualized using Discovery Studio Visualizer 4.5 [19].

3. Results and discussion

3.1. Conformational analysis

The chemical structure of frovatriptan from PubChem CID 77,992 [20] is shown in Fig. 1 and the optimized one with atom numbering is shown in Fig. 2. To reveal the possible conformers of frovatriptan at room temperature, PES scan was carried out across the flexible bonds N4-C18, C18-C15, C5-N3 and N3-C16 with corresponding dihedral angles ϕ1(H35-N4-C18-C15), ϕ2(N4-C18-C15-C17), ϕ3(C7-C5-N3-C16) and ϕ4(H31-C16-N3-C5). The dihedral angle is varied as 10° in each step from 0 to 360° along the bond axis. The variation of relative energy with the dihedral angle is shown in Fig. 3. From the PES graph all together six conformers are obtained and their relative energy with the most stable conformer is presented in Table S1 (Supplementary Material). The optimized structures of all (six) conformers with their relative energies are shown in Fig. S1 (Supplementary Material). Five conformers of energy less than 0.56 kcal/mol (equivalent to kT) are obtained at room temperature. Thereafter, these conformers are called conformer I, conformer II, conformer III, conformer IV, and conformer V, according to their SCF energies respectively. These minimum value energy structures of frovatriptan were also optimized with WB97XD [21] functional which measures the dispersion correction. However, their obtained energy is more than the functional B3LYP as presented in Table S2 (Supplementary Material). Also, the benchmarking report [22] suggested that the functional B3LYP gives better electronic and spectroscopic results with experimental than WB97XD. So, further electronic calculation has been carried out with the functional B3LYP which gives results closer to experimental values [23,24].

3.2. Optimized structure parameters

The selected optimized structural parameters: bond distance, bond angle and dihedral angle of conformers (I-V) of frovatriptan with B3LYP/6–311 + + G(d,p) functional are tabulated in Table 1, according to atom numbering scheme given in Fig. 2. The optimized structural parameters in detail are presented in Table S3 (Supplementary Material). The overlapping of conformer I with (II to V) of frovatriptan by using a least-squares algorithm that minimizes the distances of the corresponding non-hydrogen atoms are presented in Fig. S2 (Supplementary Material) which reveals that the rings R1, R2, and R3 are in the same plane. The side-chain containing an amine group (-N4H_2) also likely to overlap, however, the other one containing methyl group (-C16H_3) is slightly in a different plane. While comparing the bond lengths between conformers I and (II to V), the significant change has been found approx 0.011 Å across C5-C6 bond. This significant increase in bond length occurs due to N3 atom attached at ring R3 that takes part in intermolecular hydrogen bonding in solid form. However, this study is focused on a single molecule in the gaseous state. On comparing the bond angle in conformer I & II it is found to be approximately similar. However, the difference in angle in conformer I with respect to III, IV & V are found to be 4.36/4.34/4.34° and 5.53/4.34/5.54° across (N3-C5-H19) and (N3-C5-C16), respectively. Furthermore, in conformers, I & III and I & IV the difference in angle is found to be 5.51° and 5.94° across C13-C15-C18 and N3-C16-H31, respectively. The above differences are due to intermolecular interaction in compact (solid) form with N3 and N4 atoms. After comparing the

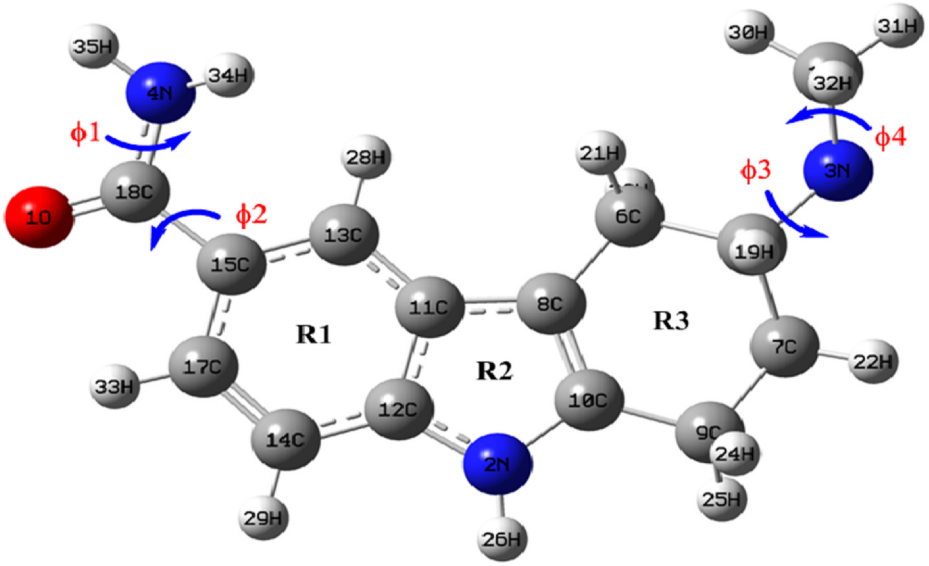

Fig. 2. Minimum energy level structure of frovatriptan with atom numbering scheme.

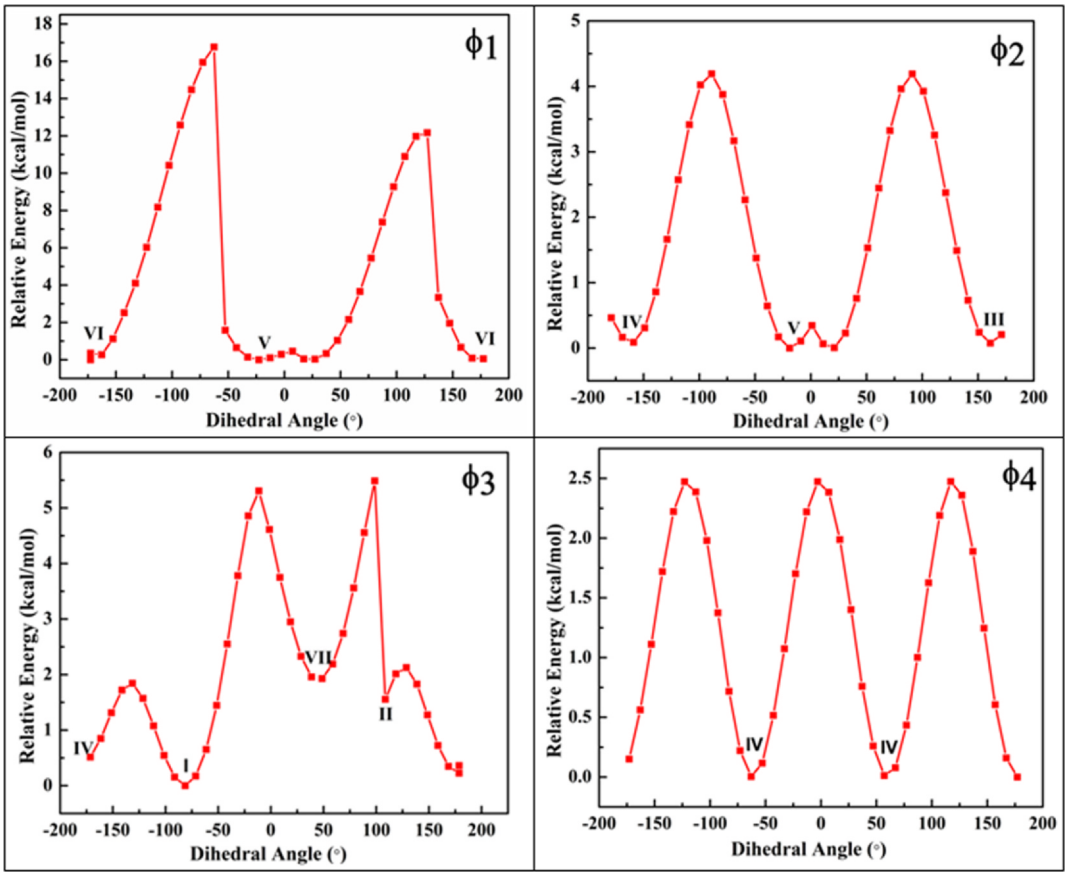

Fig. 3. Potential energy surface scan with varying dihedral angles ϕ1, ϕ2, ϕ3, ϕ4.

dihedral angles of conformer I with (II to V) the significant difference is observed only in those cases that involve the atoms O1, N3, and N4 which also infer that these atoms participate in intermolecular interaction in the solid form, however, work has been performed on a single molecule in the gaseous state.

3.3. Natural bond orbital (NBO) analysis

The stability of the molecular system has been analyzed based on natural bond orbital (NBO) analysis in terms of delocalization of charge from donor to acceptor level. The molecular system stabilizes due to the interaction of lone pair (donor) with electron defecate (acceptor) orbital which is popularly known as bonding-antibonding interaction [25]. The stability of the molecule is determined by stabilization energy E(2) between the donor (i) and acceptor (j) orbitals. The value of E(2) of frovatriptan between prominent bonding and antibonding orbitals based on the diagonal element of the Fock matrix from second-order perturbation theory [26–29] are tabulated in Table 2 which is calculated from the equation

$$E(2) = E(i,j) = -q_i\left[\frac{F_{i,j}^2}{E_i - E_j}\right]$$

where $F_{i,j}$ is the off-diagonal element of the Fock matrix, q_i is the occupancy of natural bond orbitals, E_i is the energy of donor orbital and E_j is the energy of acceptor orbital.

The delocalization of electrons from σ → σ* transitions plays a vital role in the stability of frovatriptan. The interaction of σ electrons from σ(O1-C18)/σ(N4-C18)/σ(N4-H34)/σ(N4-H35) → σ*(C13-C15) stabilizes the molecule with respective stabilizations energy 12.73/13.89/8.68/11.32 kcal/mol. Similarly, the interactions σ(N2-C10)/σ(C5-C6)/σ(C8-C11)/σ(C13-C15)/σ(C13-H28)/σ(C15-C17)/σ(C15-C18) → σ*(C12-C14) stabilizes the molecule with interaction energy 8.28/35.46/7.04/16.49/16.47/9.68/77.48 kcal/mol, respectively. Moreover, the transitions LP(1)N4 → π*(O1-C18) and LP(1)N2 → π*(C11-C12) also stabilizes the molecule with E(2): 37.82 and 35.19 kcal/mol, respectively.

3.4. Molecular electrostatic potential (MEP) surface

The reactive sites of active pharmaceutical ingredient can be predicted by MEP analysis [30]. MEP is the pictorial method to understand the distribution of electron density in space around the molecule and formation of dipole moment across it [31,32]. The molecular electrostatic potential V(r) produced across the molecule due to the combined effect of negative and positive charges corresponding to electrons and nuclei is given by the expression

$$V(r) = \sum_A \frac{Z_A}{|\vec{R_A} - \vec{r}|} - \int \frac{\rho(\vec{r})}{|\vec{r} - \vec{r}|}$$

where Z_A is the charge on nucleus A, present at R_A, and ρ(r′) is the electronic density function of the molecule.

The color code determines the electrostatic potential in which red gives the most negative, blue predicts the most positive, and green color shows the zero-potential region. The potential distribution in the MEP map increase in the order red < yellow < green < blue. MEP map of possible conformers (I-V) of frovatriptan with color code is given in Fig. 4. Hydrogen atoms H26 and H27 across amine group ($N4H_2$) show the intense blue regions and have the highest positive potential, and are responsible for nucleophilic attack for surrounding species. Whereas, oxygen atom across the carbonyl group (C18 = O) has a red region showing the highest negative potential, and is responsible for the electrophilic attack in all the conformers (I-V) of frovatriptan.

Table 1
Selected optimized parameters (bond distance, bond angle, and torsion angle) of frovatriptan by using the functional B3LYP/6–311 + +G(d,p).

	B3LYP				
Parameters	Conformer I	Conformer II	Conformer III	Conformer IV	Conformer V
Bond Distance(Å)					
R(O1-C18)	1.222	1.222	1.222	1.222	1.222
R(N2-C10)	1.388	1.388	1.389	1.388	1.388
R(N2-C12)	1.378	1.378	1.378	1.378	1.378
R(N2-H26)	1.007	1.007	1.007	1.007	1.007
R(N3-C5)	1.465	1.465	1.464	1.464	1.464
R(N3-C16)	1.460	1.461	1.461	1.460	1.460
R(N3-H27)	1.014	1.014	1.016	1.016	1.016
R(N4-C18)	1.378	1.377	1.377	1.378	1.378
R(N4-H34)	1.007	1.007	1.007	1.007	1.007
R(N4-H35)	1.009	1.009	1.009	1.009	1.009
R(C5-C6)	1.540	1.543	1.551	1.551	1.551
R(C5-C7)	1.540	1.537	1.539	1.538	1.538
R(C15-C18)	1.498	1.498	1.498	1.498	1.498
R(C16-H30)	1.104	1.093	1.101	1.094	1.101
R(C16-H31)	1.092	1.092	1.093	1.101	1.093
R(C16-H32)	1.093	1.104	1.094	1.093	1.094
Bond Angle(°)					
A(C10- N2-C12)	109.28	109.23	109.23	109.28	109.29
A(C10- N2-H26)	125.26	125.32	125.24	125.27	125.29
A(C12- N2-H26)	125.41	125.41	125.52	125.41	125.42
A(C5- N3-C16)	115.19	115.17	115.79	115.90	115.89
A(C5- N3-H27)	109.22	108.96	109.80	109.90	109.90
A(C16- N3-H27)	109.30	109.20	110.15	110.25	110.26
A(C18- N4-H34)	120.45	120.48	120.65	120.39	120.45
A(C18- N4-H35)	115.60	115.62	115.63	115.56	115.58
A(34- N4-H35)	117.01	117.03	117.05	116.97	116.99
A(N3– C5-C6)	109.38	110.90	114.91	114.93	114.92
A(N3– C5-C7)	110.87	109.16	109.08	109.11	109.09
A(N3– C5-H19)	110.69	110.91	106.33	106.35	106.35
A(C6- C5-C7)	110.56	110.58	110.69	110.65	110.67
A(C6- C5-H19)	107.66	107.36	107.75	107.72	107.70
A(C7- C5-H19)	107.62	107.88	107.77	107.77	107.79
A(C13-C15-C17)	120.23	120.23	120.15	120.24	120.23
A(C13-C15-C18)	122.70	122.72	117.20	122.70	122.70
A(C17-C15-C18)	117.05	117.04	122.65	117.06	117.06
A(N3-C16-H30)	113.67	110.44	115.14	109.18	115.16
A(N3-C16-H31)	109.23	109.12	109.09	115.16	109.11
A(N3-C16-H32)	110.43	113.68	109.16	109.11	109.18
A(H30-C16-H31)	108.36	107.21	107.94	107.78	107.92
A(H30-C16-H32)	107.77	107.86	107.80	107.44	107.76
A(H31-C16-H32)	107.16	108.30	107.45	107.90	107.45
A(O1-C18-N4)	121.08	121.08	121.01	121.10	121.08
A(O1-C18-C15)	122.42	122.42	122.45	122.43	122.42
A(N4-C18-C15)	116.48	116.49	116.53	116.47	116.48
Dihedral Angle(°)					
D(C16- N3– C5-C6)	160.49	68.32	63.56	63.40	63.46
D(C16- N3– C5-C7)	–77.34	–169.60	–171.50	–171.67	–171.60
D(C16- N3– C5-H19)	42.02	–50.88	–55.54	–55.69	–55.60
D(H27- N3– C5-C6)	37.07	–168.60	–61.94	–62.40	–62.34
D(H27- N3– C5-C7)	159.24	–46.53	63.00	62.53	62.59
D(H27- N3– C5-H19)	–81.40	72.20	178.96	178.51	178.60
D(C5- N3-C16-H30)	–52.36	–71.11	–61.32	59.93	–61.46
D(C5- N3-C16-H31)	–173.49	171.28	177.19	–61.44	177.05
D(C5- N3-C16-H32)	68.90	50.28	60.05	177.08	59.89
D(H27-N3-C16-H30)	71.02	165.94	64.01	–174.45	64.17
(H27- N3-C16-H31)	–50.12	48.33	–57.48	64.18	–57.33
D(H27-N3-C16-H32)	–167.72	–72.67	–174.63	–57.30	–174.49
D(H34- N4-C18-O1)	158.24	158.36	–158.95	158.07	–158.22
D(H34-N4-C18-C15)	–22.84	–22.70	22.03	–23.02	22.87
D(H35- N4-C18-O1)	8.28	8.24	–8.42	8.38	–8.33
D(H35-N4-C18-C15)	–172.80	–172.82	172.55	–172.71	172.76
D(N3– C5- C7-C9)	175.54	174.97	171.03	170.93	170.99
D(N3– C5- C7-H22)	53.51	53.08	48.49	48.41	48.44
D(N3– C5- C7-H23)	–63.16	–63.42	–67.81	–67.89	–67.84
D(C13-C15-C18-O1)	158.87	159.02	18.71	158.71	–158.83
D(C13-C15-C18-N4)	–20.03	–19.91	–162.28	–20.19	20.06
D(C17-C15-C18-O1)	–19.93	–19.81	–160.54	–20.12	20.07
D(C17-C15-C18-N4)	161.17	161.26	18.47	160.99	–161.04

Table 2
Second-order perturbation theory analysis of Fock matrix in NBO basis of frovatriptan (conformer I).

Donor NBO(i)	ED (i) /e	Acceptor NBO(j)	ED(j)/e	E(2)[a] kcal/mol	E(j)-E(i)[b] a.u.	F(i,j)[c] a.u.
σ(O1-C18)	1.99369	σ*(C13-C15)	0.02154	12.73	1.53	0.125
σ(N2-C10)	1.98370	σ*(C12-C14)	0.02175	8.28	0.86	0.075
σ(N4-C18)	1.99388	σ*(C13-C15)	0.02154	13.89	1.35	0.123
σ(N4-H34)	1.98736	σ*(C13-C15)	0.02154	8.68	1.19	0.091
σ(N4-H35)	1.98972	σ*(C13-C15)	0.02154	11.32	1.10	0.100
σ(C5-C6)	1.97281	σ*(C12-C14)	0.02175	35.46	0.70	0.141
σ(C5-C6)	1.97281	σ*(C16-H32)	0.01408	8.27	3.52	0.153
π(C8-C10)	1.82776	π*(C11-C12)	0.49429	16.50	0.29	0.067
σ(C8-C11)	1.96457	σ*(C9-C10)	0.02228	5.35	1.07	0.068
σ(C8-C11)	1.96457	σ*(C12-C14)	0.02175	7.04	0.71	0.063
σ(C11-C12)	1.95698	σ*(C6-C8)	0.02037	5.10	1.09	0.067
π(C11-C12)	1.56649	π*(C8-C10)	0.29730	17.19	0.29	0.065
π(C11-C12)	1.56649	π*(C14-C17)	0.30370	16.81	0.29	0.064
σ(C13-C15)	1.97223	σ*(C12-C14)	0.02175	16.49	0.75	0.100
π(C13-C15)	1.70662	π*(O1-C18)	0.27417	18.17	0.30	0.067
π(C13-C15)	1.70662	π*(C11-C12)	0.49429	16.77	0.28	0.064
π(C13-C15)	1.70662	π*(C14-C17)	0.30370	18.99	0.30	0.067
σ(C13-H28)	1.97797	σ*(C12-C14)	0.02175	16.47	0.58	0.088
σ(C14-C17)	1.97515	σ*(N2-C12)	0.02452	6.02	1.15	0.074
π(C14-C17)	1.72166	π*(C11-C12)	0.49429	20.25	0.28	0.071
σ(C15-C17)	1.97122	σ*(C12-C14)	0.02175	9.68	0.74	0.076
σ(C15-C18)	1.97384	σ*(C12-C14)	0.02175	77.48	0.72	0.211
LP(2)O1	1.87062	σ*(N4-C18)	0.06824	24.67	0.68	0.118
LP(1)N2	1.64263	π*(C8-C10)	0.29730	34.34	0.32	0.094
LP(1)N2	1.64263	π*(C11-C12)	0.49429	35.19	0.30	0.094
LP(1)N4	1.78111	π*(O1-C18)	0.27417	37.82	0.34	0.102
LP(1)N4	1.78111	σ*(C17-H33)	0.01295	8.42	2.43	0.135

[a] E(2) means the energy of hyper conjugative interaction (stabilization energy).
[b] Energy difference between donor (i) and acceptor (j) NBO orbitals.
[c] F(i,j) is the Fock matrix element between i and j NBO orbitals.

3.5. HOMO–LUMO energy gap (ΔE_{L-H})

The highest occupied molecular orbital (HOMO) tends to donate electrons and the lowest unoccupied molecular orbital (LUMO) accept them. The energy of HOMO orbital (E_H) and the energy of LUMO orbital (E_L) and their energy gap ($\Delta E_{L\text{-}H}$) measures the stability and chemical reactivity of the molecule. The highest value of $\Delta E_{L\text{-}H}$ infers that the molecule is more stable and less chemically reactive and vice versa [33–37]. $\Delta E_{L\text{-}H}$ of the title compound of all the conformers (I-V) of frovatriptan is calculated with B3LYP/6–311 + + G(d,p) level of theory and their values are 4.7345, 4.7476, 4.8268, 4.7544, and 4.7536 eV for conformers I, II, III, IV, and V, respectively. The highest and least value of $\Delta E_{L\text{-}H}$ for conformer III and I infer that the former one is more stable, however, the later one is more chemically reactive. The HOMO-LUMO plot of conformers (I-V) of frovatriptan is shown in Fig. 5. From Fig. 5, it is clear that charge in HOMO is localized across rings, whereas, the orbital lobs in LUMO diverge to amine group and rings also.

3.6. Global reactivity descriptor

Electronegativity (χ), chemical potential (μ), hardness (η), electrophilicity index (ω), and softness (S) are the global reactivity parameters suggested by Koopman's theorem [38]. These values are calculated in terms of the frontier's molecular orbital energies (E_H and E_L) and are given by the relations [38–40]:

$$\chi = -\frac{1}{2}(E_H + E_L)$$

$$\mu = -\chi = \frac{1}{2}(E_H + E_L)$$

$$\eta = \frac{1}{2}(E_L - E_H)$$

$$S = \frac{1}{2\eta}$$

$$\omega = \frac{\mu^2}{2\eta}$$

As suggested by Parr *et al.* [41], ω is measured in terms of μ and η which is always positive and measures the stabilization in energy when the system gains the extra charge (ΔN) from surrounding molecule [42]. The high/low value of μ and ω indicates the good electrophilic/nucleophilic behavior of molecules, respectively [43]. The calculated values of E_H, E_L, $\Delta E_{L\text{-}H}$, χ, μ, η, ω, and S of conformers (I-V) of frovatriptan is tabulated in Table 3. The high value of $\Delta E_{L\text{-}H}$ and η for conformer III interprets that it is more stable and less polarizable [44].

3.7. Local reactivity descriptors

The keen local reactivity parameter which is widely used to study the specific site for chemical reactivity and site selectivity is Fukui function, f(r) [45]. The reactive center in the active pharmaceutical ingredients is determined by the highest value of the Fukui function as suggested by Parr and Yang [38]. The Fukui functions for the nucleophilic, electrophilic and radical attack are f_k^+, f_k^- and f_k^0, respectively. They are measured on the basis of following equations [45]:

$f_k^+ = [q_k(N + 1)\text{-}q_k(N)]$ for nucleophilic attack

$f_k^- = [q_k(N)\text{-}q_k(N\text{-}1)]$ for electrophilic attack

$f_k^0 = [q_k(N + 1) - q_k(N\text{-}1)]$ for radical attackwhere N, N-1, N + 1 are total electrons present in neutral, cation and anion state of molecule respectively. +, – and 0 represents for nucleophilic, electrophilic, and radical attack respectively. Similarly, the local softness (s_k^+, s_k^-, s_k^0) and electrophilicity indices (ω_k^+, ω_k^-, ω_k^0) are also used to show the reactivity of atoms in molecule and is given by the equations

$s_k^+ = Sf_k^+$, $s_k^- = Sf_k^-$, $s_k^0 = Sf_k^0$

$\omega_k^+ = \omega f_k^+$, $\omega_k^- = \omega f_k^-$, $\omega_k^0 = \omega f_k^0$

The local reactivity descriptor of frovatriptan for selected atoms of conformers (I-V) is presented in Table 4, which inferred that the sites C8, C10, and N3 are close to the nucleophilic center, whereas, the atoms C13, O1, and C9 are prone to electrophilic center. The local

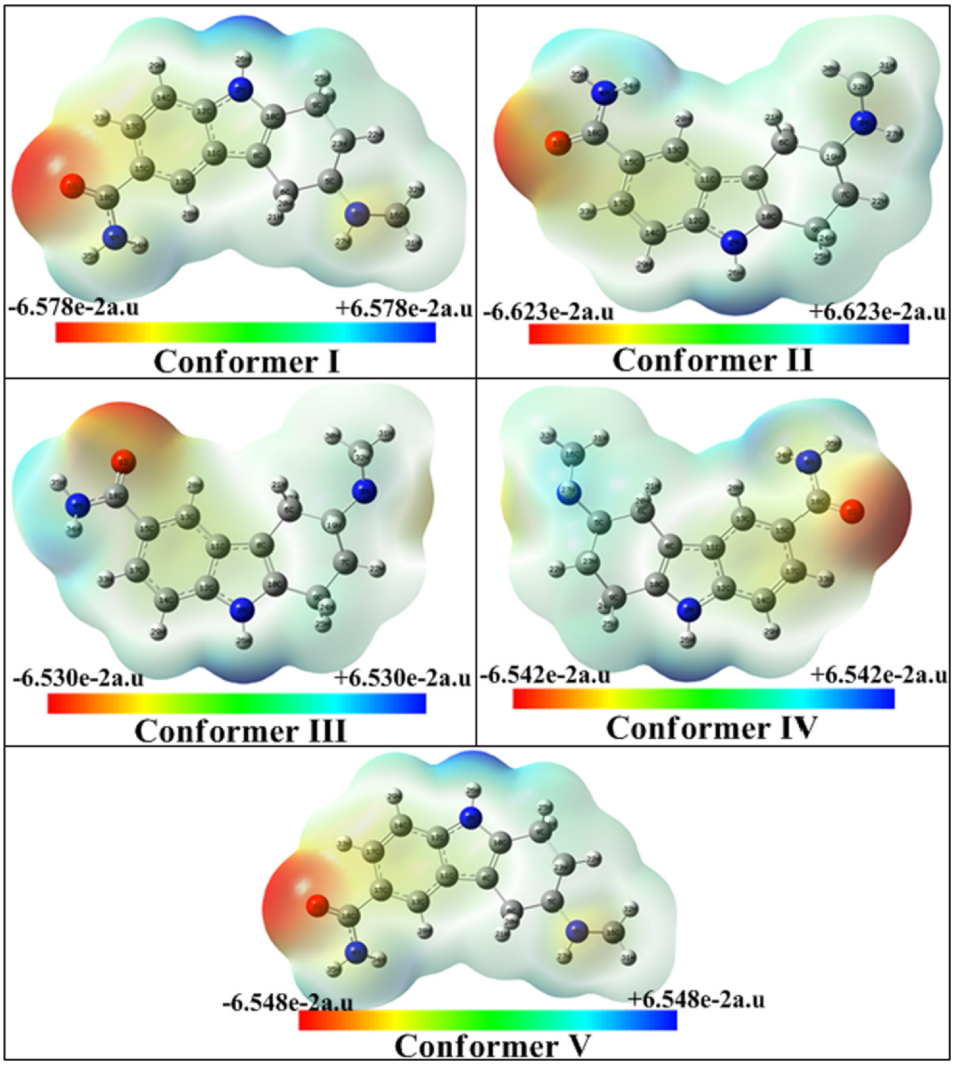

Fig. 4. Molecular electrostatic potential (MEP) formed by mapping of total density over the electrostatic potential of conformers (I- V) of frovatriptan.

reactivity descriptors for all the atoms of conformers (I-V) are tabulated in Tables (S4-S8) (Supplementary Material).

3.8. Thermodynamic properties

The temperature has a main role in the chemical reactivity as well as in pharmacodynamics [46,47]. The important thermodynamic functions like total energy, zero-point energy, and rotational constant of all the conformers (I-V) of frovatriptan were calculated at room temperature 298.15 K and the values obtained are presented in Table 5. Rest, the heat capacity ($C^{\circ}_{p,m}$), entropy (S°_{m}) and enthalpy (H°_{m}) of conformer I of frovatriptan obtained from output file in the temperature range 50 K to 300 K are listed in Table S9 (Supplementary Material) and their correlation is shown in Fig. 6. The correlation equations for conformer I are as follows

$C^{\circ}_{p,m} = 4.7627 + 0.2946\ T\ (R^2 = 0.9981)$

$S^{\circ}_{m} = 52.7758 + 0.2946\ T\ (R^2 = 0.9998)$

$H^{\circ}_{m} = 184.3200 + 0.0043\ T\ (R^2 = 0.9999)$

These equations are useful for further studies of thermodynamic energies and estimate the direction of chemical reactions of frovatriptan according to the second law of thermodynamics [48]. Fig. 6 inferred that the influence of temperature increases the thermodynamic properties.

3.9. Nonlinear optical (NLO) properties

Non-linear optical (NLO) properties of the material have potent use in optical communication, sensing, data storage, computing, and many more [49]. Total static dipole moment (μ_0), the first hyperpolarizability (β_0), mean polarizability ($\Delta\alpha_0$) and anisotropy of polarizability $|\alpha_0|$ of the molecular system have been calculated by using DFT at B3LYP/6–311 + + G(d,p) level of theory from the equations [50]

$$\mu_0 = (\mu_x^2 + \mu_y^2 + \mu_z^2)^{1/2}$$

$$|\alpha_0| = \frac{1}{3}(\alpha_{xx} + \alpha_{yy} + \alpha_{zz})$$

$$\Delta\alpha = 2^{-1/2}[(\alpha_{xx} - \alpha_{yy})^2 + (\alpha_{yy} - \alpha_{zz})^2 + (\alpha_{zz} - \alpha_{xx})^2 + 6\alpha_{xx}^2]^{1/2}$$

$$\beta_0 = [(\beta_{xxx} + \beta_{xyy} + \beta_{xzz})^2 + (\beta_{yyy} + \beta_{xxy} + \beta_{yzz})^2 + (\beta_{zzz} + \beta_{xxz} + \beta_{yyz})^2]^{1/2}$$

The significant delocalization of charge in a particular axis is determined by the component of polarizability in that direction. The components of μ_0, β_0, $\Delta\alpha_0$ and $|\alpha_0|$ of frovatriptan are presented in Table 6. The values of μ_0, $\Delta\alpha_0$, and β_0 of frovatriptan are 3.4, 7.5 and 7 times greater than that of experimental values of urea [51], respectively which motivate that the title compound can be treated as a good NLO material.

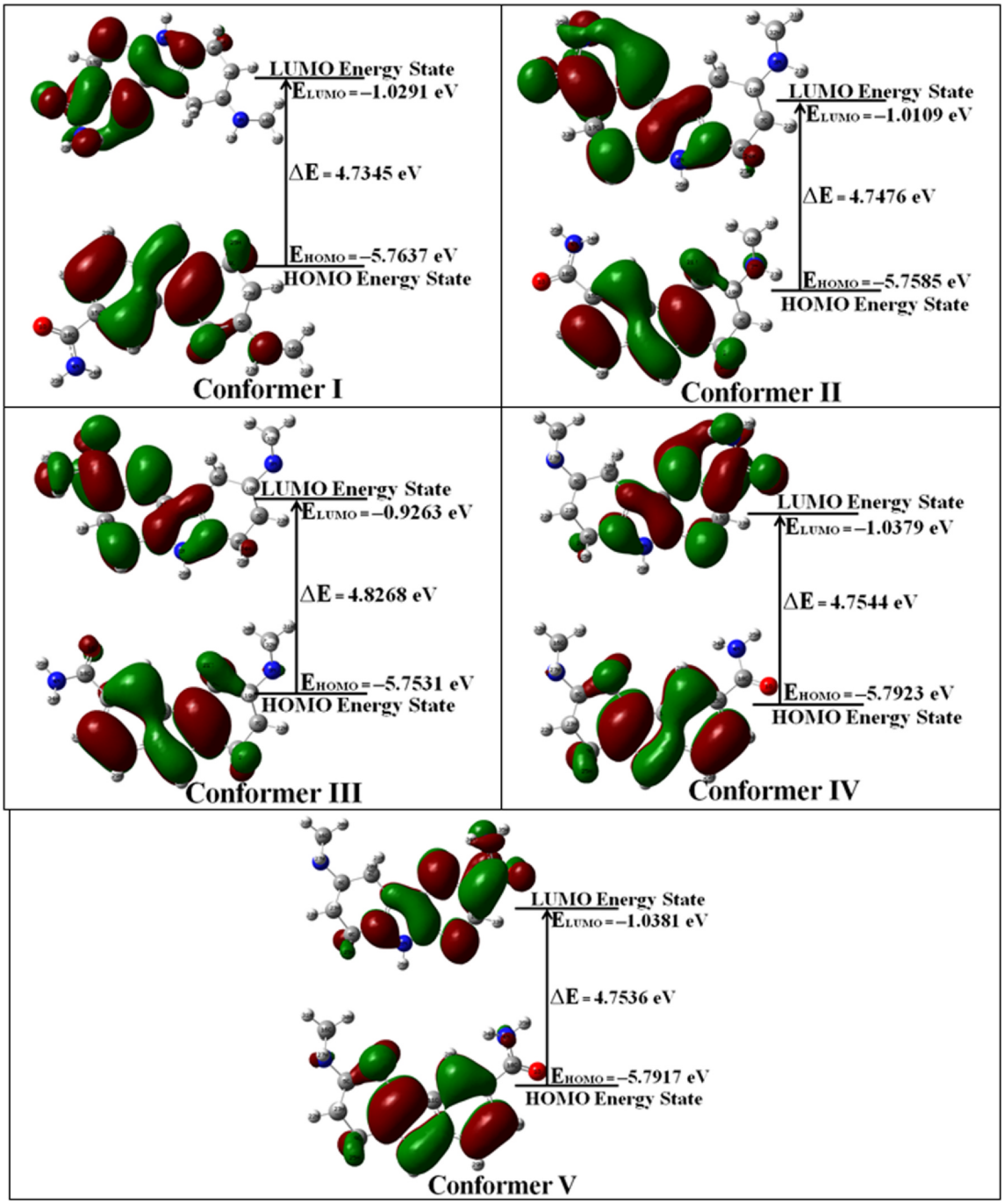

Fig. 5. HOMO-LUMO plot of conformers (I-V) of frovatriptan.

Table 3
Calculated E_{HOMO}, E_{LUMO}, energy gap (E_L–E_H), chemical potential (μ), electronegativity (χ), global hardness (η), softness (S) and electrophilicity index (ω) for all the conformers of frovatriptan.

Molecule	E_H(eV)	E_L(eV)	(E_L– E_H) (eV)	χ(eV)	μ(eV)	η(eV)	$S(eV)^{-1}$	ω(eV)	ΔN_{max}
Conformer I	–5.7637	–1.0291	4.7345	3.3964	–3.3964	2.3673	0.2112	2.4365	1.4347
Conformer II	–5.7585	–1.0109	4.7476	3.3847	–3.3847	2.3738	0.2106	2.4131	1.4259
Conformer III	–5.7531	–0.9263	4.8268	3.3397	–3.3397	2.4134	0.2072	2.3107	1.3838
Conformer IV	–5.7923	–1.0379	4.7544	3.4151	–3.4151	2.3772	0.2103	2.4530	1.4366
Conformer V	–5.7917	–1.0381	4.7536	3.4149	–3.4149	2.3768	0.2104	2.4532	1.4368

Table 4
Calculated local reactivity properties of frovatriptan of the selected atoms using Hirshfeld charges at B3LYP/6–311 + +G(d,p) level.

Site	f_k^+	s_k^+	ω_k^+	Site	f_k^-	s_k^-	ω_k^-	Site	f_k^0	s_k^0	ω_k^0
Conformer I											
C8	0.1523	0.0322	0.3711	C13	0.0375	0.0079	0.0914	C18	0.6476	0.1368	1.5780
C10	0.1171	0.0247	0.2853	O1	0.0332	0.0070	0.0809	C10	0.2425	0.0512	0.5908
N3	0.0924	0.0195	0.2251	C9	0.0266	0.0056	0.0648	C12	0.1801	0.0380	0.4389
Conformer II											
C8	0.1602	0.0337	0.3865	C13	0.0479	0.0101	0.1155	C18	0.6480	0.1365	1.5636
C10	0.1207	0.0254	0.2914	O1	0.0351	0.0074	0.0846	C10	0.2448	0.0515	0.5906
C17	0.1032	0.0217	0.2491	C15	0.0268	0.0057	0.0648	C12	0.1769	0.0372	0.4268
Conformer III											
C8	0.1563	0.0324	0.3612	C9	0.0203	0.0042	0.0470	C18	0.6556	0.1358	1.5148
N3	0.1015	0.0210	0.2346	O1	0.0186	0.0039	0.0430	C10	0.2386	0.0494	0.5513
C10	0.0998	0.0207	0.2306	C13	0.0173	0.0036	0.0400	C12	0.1771	0.0367	0.4092
Conformer IV											
C8	0.1547	0.0325	0.3794	C11	0.0418	0.0088	0.1025	C18	0.6487	0.1364	1.5914
C10	0.1157	0.0243	0.2838	C10	0.0378	0.0079	0.0927	C10	0.2263	0.0476	0.5552
C17	0.1016	0.0214	0.2492	C13	0.0353	0.0074	0.0867	C12	0.1762	0.0371	0.4323
Conformer V											
C8	0.1533	0.0322	0.3760	C13	0.0455	0.0096	0.1116	C18	0.6478	0.1363	1.5891
C10	0.1157	0.0243	0.2838	O1	0.0348	0.0073	0.0853	C10	0.2409	0.0507	0.5910
C17	0.1016	0.0214	0.2492	C14	0.0262	0.0055	0.0642	C12	0.1773	0.0373	0.4350

3.10. Drug likeness

In addition to the experimentally biological (or clinical) activities, the drug-likeliness of the molecule are evaluated theoretically [52]. Lipinski's rule of 5 [53,54] is famous for the initial classification of drug candidates. According to Lipinski's the number of atoms in the molecule should be from 20 to70 and the molecular weight must lies between180 and 500 g/mol. Moreover, the molar refractivity (MR) of the molecule should be in the range of 40 to 130 e.s.u. [55]. The value of MR is measured in terms of polarizability (α) and is given by the Lorenz-Lorentz formula [56]

$$MR = 1.333\pi N\alpha$$

where N is the Avogadro's number.

The number of atoms of frovatriptan is 35 and the molecular weight is 243.3 g/mol which is in the range given by Lipinski's rule. The MR value of the title compound is found to be 76.80/76.66/76.66/76.40/76.40 e.s.u. for conformers (I-V), respectively, which lies in the range mentioned above. Thus, frovatriptan can be taken as a drug candidate.

3.11. Molecular docking

Molecular docking is used to show the binding activities of drug molecules with protein [57]. The pharmacological action of frovatriptan is to treat anti migraine behavior which binds with the serotonin 1b (5-HT_{1B}) receptor for the medicinal activities [7,58] and its docking with this receptor has not been conducted so far. The receptor, 5-HT_{1B}, is predicted from online Swiss target prediction [59] as shown in Fig. S3 (Supplementary Material) and its three PDB codes: 4IAQ, 5 V54, 6G79 has been downloaded from the protein data bank [59]. Protein has been cleaned by removing the water molecules and its active site has been confined in the grid box of size 60Åx60Åx60Å.

Out of many docked conformations, which shows good interaction with ligand has been taken into consideration. The binding energy, the bond length of conventional H-bond with residues, and binding efficiency for all the docked conformations have been tabulated in Table 7. The pictorial presentation of binding sites of the ligand with protein is presented in Fig. 7. The binding sites in most of the cases are found to be amine group $N4H_2$ and N3H27. It means these atoms will participate in the intermolecular hydrogen bonding with the neighboring molecules as suggested in section 3.2 also. The coordinates of binding sites of frovatriptan are tabulated in Table S10 (Supplementary Material) according to atom numbering presented in Fig. S4 (Supplementary material). Out of three PDB codes, 5 V54 shows stable binding energy of − 9.16 kcal/mol with four conventional H-bonds (2.10 Å/SER:212, 2.62 Å /THR:209, 1.90 Å/ASP:129, 2.70 Å /TYR:359). Similarly, the docked conformation 4IAQ has two conventional H-bonds (1.94 Å/SER:66, 2.80 Å/PRO:366) and 6G79 showed four conventional H-bonds (2.23, 2.46 Å/GLY:27, 2.03 Å/SER:98, 2.12 Å/CYS:215) with stabilization energies − 6.44 kcal/mol and − 6.71 kcal/mol, respectively. Thus, theoretically, it can be predicted that frovatriptan has potent curative behavior as antimigraine. Moreover, among the three docked conformation the binding stability of the ligand is obtained in the order 5 V54 > 6G79 > 4IAQ.

4. Conclusion

The geometry optimization and conformational analysis of frovatriptan were carried out by using the important DFT functional B3LYP/6–311 + +G(d,p) which gives the result closer to experimental values. The five conformers of frovatriptan were obtained with energy −491616.9411 kcal/mol of the most stable one. Geometry optimization inferred that the atoms O1, N3, and N4 may participate in the intermolecular interaction in compact form (solid) that can help in the

Table 5
Total energy, zero-point energy, enthalpy, specific heat, entropy and rotational constant at 298.15 K calculated at B3LYP/6–311 + +G(d,p) level of theory for all the conformers (I-V) of frovatriptan.

Parameters	Conformer I	Conformer II	Conformer III	Conformer IV	Conformer V
Total energy (eV)	–21317.76	–21317.76	–21317.75	–21317.75	–21317.75
Zero-point energy (J/mol)	771168.2	771162.2	771035.3	770974.1	771076.5
Enthalpy (kcal/mol)	194.458	194.457	194.452	194.439	194.454
Specific heat (cal/mol-K)	63.982	63.973	64.102	64.090	64.065
Entropy (cal/mol-K)	127.547	127.637	127.820	127.858	127.794
Rotational constant GHz)	0.8818	0.7689	0.7681	0.7687	0.7672

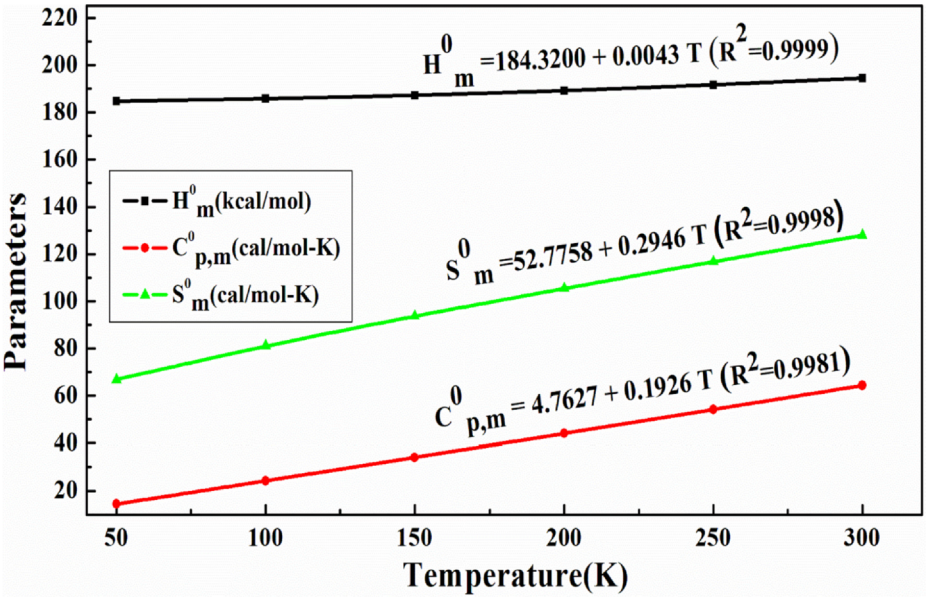

Fig. 6. Correlation graph of enthalpy (H°_{m}), specific heat ($C^{\circ}_{m,p}$) and entropy (S°_{m}) of frovatriptan with temperature.

prediction of the crystal structure of frovatriptan. The hyper conjugative interaction study indicates that the transition σ(C15-C18) → σ*(C12-C14) stabilizes the molecule with the highest interaction energy 77.48 kcal/mol. From the MEP surface graph, it has been inferred that the electrophilic and nucleophilic centers are carbonyl group and amine group, respectively. The highest value of $\Delta E_{L\text{-}H}$ (4.8268) and η (2.4134) indicates that the conformer III is more stable, whereas, the greater value of S (0.2112) and least value of $\Delta E_{L\text{-}H}$ (4.7345) of conformer I resulted that it is more polarizable (or more chemical reactive). From the local reactivity descriptor, it has been concluded that the atoms C8, C10, and N3 are prone to nucleophilic center, as well as the atoms C13, O1, and C9 are close to electrophilic centers, respectively, due to high-value Fukai function. The correlation graph of thermodynamical parameters predicts that their values increase with the rise in temperature. The significant high value of β_0 of frovatriptan motivates that it can be treated as a good NLO material. Molecular docking simulation of title compound motivates that it has remarkable curative behavior as anti-migraine and the binding site for that is predicted as $N4H_2$ and N3H27. The determination of the Fukui function also prone to the same sites for reactivity. Moreover, the molecular docking simulation of frovatriptan with predicted target protein reveals the pharmaceutical activity of the title compound.

Financial and ethical disclosures

No funding from any other company or research sections has been received for this study. The authors have contributed equally from their sides on collecting data and preparing the manuscript. All the computational works have been performed at the Macromolecular Lab,
University of Lucknow, India.

CRediT authorship contribution statement

Manoj Kumar Chaudhary: . **Anubha Srivastava:** . **Keshav Kumar Singh:** Methodology, Conceptualization. **Poonam Tandon:** Supervision. **Bhawani Datt Joshi:** Supervision.

Declaration of Competing Interest

The authors declare that they have no known competing financial interests or personal relationships that could have appeared to influence the work reported in this paper.

Acknowledgment

M.K.Chaudhary is grateful to Centre for Co-Operation in Science and Technology among Developing Societies (CCSTDS), India for providing partial financial support under the Indian Science and Research

Table 6
The calculated dipole moment (μ_0), mean polarizability|α_0|, anisotropy of polarizability ($\Delta\alpha$) and first hyperpolarizability (β_0) of frovatriptan at B3LYP/6–311 + + G(d,p) level.

Dipole moment (Debye)		Polarizability (*10^{-24} esu)		Hyperpolarizability (*10^{-30} esu)	
μ_x	–5.4122	α_{xx}	40.9096	β_{xxx}	4.4414
μ_y	–0.5549	α_{xy}	1.4574	β_{xxy}	2.6325
μ_z	–2.4254	α_{yy}	29.6220	β_{xyy}	1.3251
μ_0	5.9568	α_{xz}	0.3010	β_{yyy}	0.5426
μ_0 (Urea)	1.7410	α_{yz}	0.2886	β_{xxz}	–0.9551
		α_{zz}	17.8294	β_{xyz}	0.1358
		|α_0|	29.4537	β_{yyz}	–0.0564
		$\Delta\alpha$	73.7370	β_{xzz}	–0.4309
		$\Delta\alpha$(Urea)	9.7710	β_{yzz}	0.0294
				β_{zzz}	–1.1238
				β_0	6.5775
				β_0 (Urea)	0.9279

Table 7
Hydrogen bonding, binding energy and ligand efficiency of targets.

Ligand	Protein	PDB code	Bond length (Å)	Amino acid	Binding energy (kcal/mol)	Ligand efficiency
Frovatriptan	serotonin 1b (5-HT1b) receptor	4IAQ	1.94	SER:66	− 6.44	−0.36
			2.80	PRO:366		
		5 V54	2.10	SER:212	−9.16	−0.51
			2.62	THR:209		
			1.90	ASP:129		
			2.70	TYR:359		
		6G79	2.23	GLY:27	−6.71	−0.37
			2.46	GLY:27		
			2.03	SER:98		
			2.12	CYS:215		

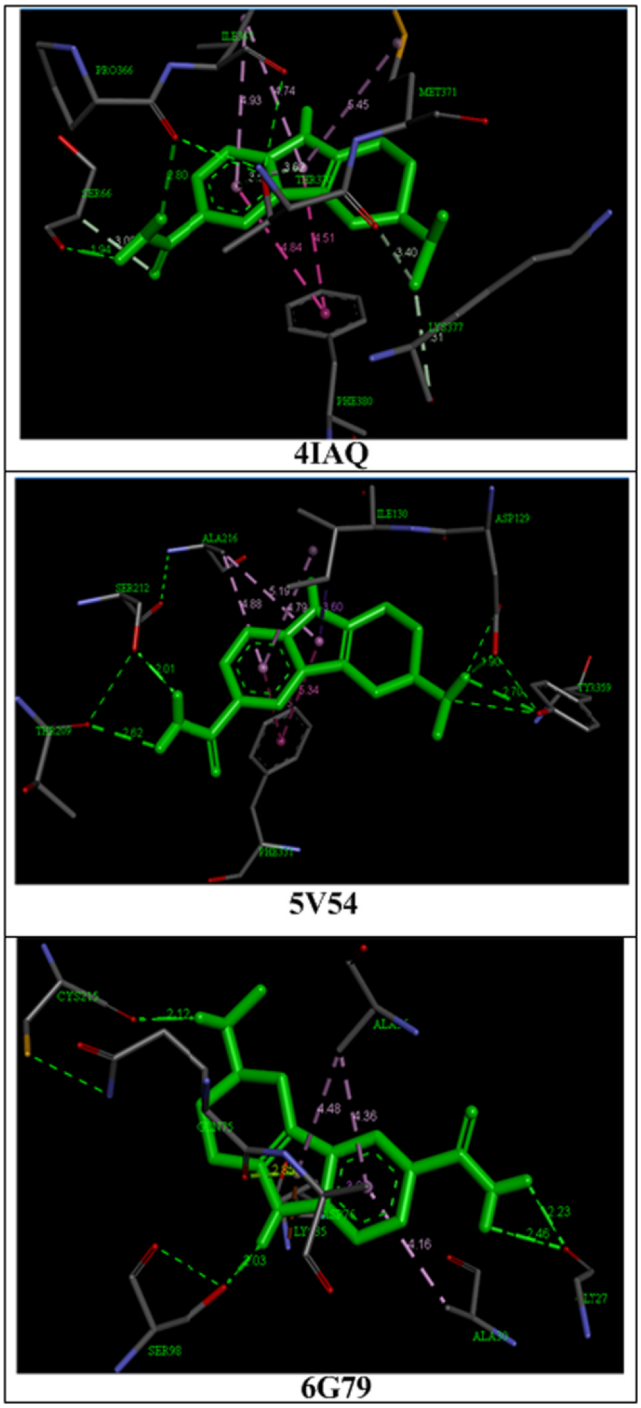

Fig. 7. Molecular docking of frovatriptan.

Fellowship (ISRF-2019), with award ID (DO/CCSTDS/204/2019).

Appendix A. Supplementary data

Supplementary data to this article can be found online at https://doi.org/10.1016/j.comptc.2020.113031.

References

[1] F. Markus, K. Mikko, Frovatriptan review, Expert Opin. Pharmacother. 8 (17) (2007) 3029–3033 https://di.org/10.1517/14656566.8.17.3029.
[2] C. Lisotto, M. Guidotti, D. Zava, L. Savi, Frovatriptan and rizatriptan economic EVAluation: the FREEVA study, Headache 14 (1) (2013) 96, https://doi.org/10.1186/1129-2377-14-96.
[3] M.D. Ferrari, K.I. Roon, R.B. Lipton, P.J. Goadsby, Oral triptans (serotonin 5-HT1B/1D agonists) in acute migraine treatment: a meta-analysis of 53 trials, Lancet 358 (9294) (2001) 1668–1675, https://doi.org/10.1016/S0140-6736(01)06711-3.
[4] U.C. Galgatte, P.D. Chaudhari, Development of frovatriptan succinate microemulsion for nasal delivery: Optimization, in vitro and in vivo evaluation, Asian J. Pharm. Clin. Res. 12 (4) (2019) 292–300.
[5] N. Mennini, S. Orlandini, S. Furlanetto, B. Pasquini, P. Mura, Development and Optimization by Quality by Design Strategies of Frovatriptan Orally Disintegrating Tablets for Migraine Management, Curr Drug Deliv 15 (3) (2018) 436–445, https://doi.org/10.2174/1567201814666170606100536.
[6] P. Buchan, C. Keywood, A. Wade, C. Ward, Clinical pharmacokinetics of frovatriptan, Headache 42 (2002) 54–62, https://doi.org/10.1046/j.1526-4610.42.s2.3.x.
[7] R. Ryan, G. Geraud, J. Goldstein, R. Cady, C. Keywood, Clinical efficacy of frovatriptan: placebo-controlled studies, Headache 42 (2002) 84–92, https://doi.org/10.1046/j.1526-4610.42.s2.6.x.
[8] W. Rohn, L.J. Sham, Self-Consistent Equations Including Exchange and Correlation Effects, Phys. Rev. A 140 (1965) 1133, https://doi.org/10.1103/Phys.
[9] B.G. Johnson, P.M. Gill, J.A. Pople, Preliminary results on the performance of a family of density functional methods, J. Chem. Phys. 97 (10) (1992) 7846–7848, https://doi.org/10.1063/1.463975.
[10] M.J. Frisch, G.W. Trucks, H.B. Schlegel. G.E. Scuseria, J.R. Cheeseman, M.A. Robb, G. Scalmani, V. Barone, B. Mennucci, G.A. Petersson, H. Nakatsuji, M. Caricato, X. Li, H.P. Hratchian, A.F. Izmzylov, J. Bloino, G. Zheng, J.L. Sonnenberg, M. Hada, M. Ehara, K. Toyota, R. Fukuda, J. Ishida, M. Hasegawa, T. Nakajima, Y. Honda, O. Kitao, H. Nakai, T. Vreven, J.A. Montgomery Jr., J.E. Peralta, F. Ogliaro, M. Bearpark, J.J. Heyd, E. Brothers, K.N. Kudin, V.N. Staroverov, R. Kobayashi, J. Normand, A. Raghavachari, A. Rendell, J.C. Burant, S.S. Iyengar, J. Tomasi, M. Cossi, N. Rega, J.M. Millan, M. Klene, J.E. Knox, J.B. Cross, V. Bakken, C. Adamo, J. Jaramillo, R. Gomperts, R.E. Stratmann, O. Yazyev, A.J. Austin, R. Cammi, C. Pomelli, J.W. Ochterski, R.L. Martin, K. Morokuma, V.G. Zakrzewski, G.A. Voth, P. Salvador, J.J. Dannerberg, S. Dapprich, A.D. Daniels, J. Farkas, B. Foresman, J.V. Ortiz, J. Cioslowski, D.J. Fox, GAUSSIAN 09, Revision, Gaussian, Inc., Wallingford CT, (2009).
[11] P. Hohenberg, W. Kohn, Inhomogeneous Electron Gas, Phys. Rev. B 136 (1964) 864–871, https://doi.org/10.1103/PhysRev.136.B864.
[12] C.T. Lee, W.T. Yang, R.G. Parr, Development of the Colle-Salvetti correlation-energy formula into a functional of the electron density, Phys. Rev. B Condens. Matter 37 (1988) 785–789, https://doi.org/10.1103/PhysRevB.37.785.
[13] A.D. Becke, Density-functional thermochemistry. III. The role of exact exchange, J. Chem. Phys. 98 (1993) 5648–5652, https://doi.org/10.1063/1.464913.
[14] T.H. Dunning Jr., Gaussian basis sets for use in correlated molecular calculations. I. The atoms boron through neon and hydrogen, J. Chem. Phys. 90 (1989) 1007–1023, https://doi.org/10.1063/1.456153.
[15] D.E. Woon, T.H. Dunning Jr., Gaussian basis sets for use in correlated molecular calculations. V. Core-valence basis sets for boron through neon, J. Chem. Phys. 103 (1995) 4572–4585, https://doi.org/10.1063/1.470645.
[16] A. Petersson, A. Bennett, T.G. Tensfeldt, M.A. Al-Laham, W.A. Shirley, J. Mantzaris, A complete basis set model chemistry. I. The total energies of closed-shell atoms and hydrides of the first-row elements, J. Chem. Phys. 89 (1988) 2193–2218, https://doi.org/10.1063/1.455064.

[17] A. Frisch, A.B. Nielson, A.J. Holder, GaussView User Manual, Gaussian Inc, Pittsburgh, PA, 2005.
[18] O. Trott, A.J. Olson, AutoDock Vina: improving the speed and accuracy of docking with a new scoring function, efficient optimization, and multithreading, J. Comput. Chem. 31 (2010) 455–461, https://doi.org/10.1002/jcc.21334.
[19] Discovery Studio 4.5 Guide, Accelrys Inc., San Diego, http://www.accelrys.com, (2009). https://pubchem.ncbi.nlm.nih.gov/search/search.cgi.
[20] J.D. Chai, M. Head-Gordon, Long-range corrected hybrid density functionals with damped atom–atom dispersion corrections, Phys. Chem. Chem. Phys. 10 (44) (2008) 6615–6620, https://doi.org/10.1039/B810189B.
[21] S. Tortorella, M.M. Talamo, A. Cardone, M. Pastore, F. De Angelis, Benchmarking DFT and semi-empirical methods for a reliable and cost-efficient computational screening of benzofulvene derivatives as donor materials for small-molecule organic solar cells, J. Phys. Condens. Matter 28 (7) (2016) 074005.
[22] K. Srivastava, A. Srivastava, P. Tandon, K. Sinha, J. Wang, Spectroscopic, quantum chemical calculation and molecular docking of dipfluzine, J. Mol. Struct. 1125 (2016) 751–762, https://doi.org/10.1016/j.molstruc.2016.07.078.
[23] B.D. Joshi, A. Srivastava, P. Tandon, S. Jain, A.P. Ayala, A combined experimental (IR, Raman and UV–Vis) and quantum chemical study of canadine, Spectrochim. Acta A: Mol. Biomol. Spectrosc. 191 (2018) 249–258, https://doi.org/10.1016/j.saa.2017.10.008.
[24] R. Singh, P. Kaur, R. Sachdeva, J.S. Grewal, V. Sathe, G.S.S. Saini, Computational study of effect of solvents on vibrational spectra of coumarin 500, Comput. Theor. Chem. 1130 (2018) 46–57, https://doi.org/10.1016/j.comptc.2018.03.008.
[25] A.E. Reed, F. Weinhold, Natural bond orbital analysis of near-Hartree–Fock water dimer, J. Chem. Phys. 78 (1983) 4066–4073, https://doi.org/10.1063/1.445134.
[26] F. Weinhold, C.R. Landis, Valency and Bonding: A Natural Bond Orbital Donor–Acceptor Perspective, Cambridge University Press, Cambridge, 2005.
[27] A.E. Reed, L.A. Curtis, F.A. Weinhold, Intermolecular interactions from a natural bond orbital, donor-acceptor viewpoint, Chem. Rev. 88 (1988) 899–926, https://doi.org/10.1021/cr00088a005.
[28] G. Varsanyi, Vibrational Spectra of Benzene Derivatives, Academic Press, New York, NY, USA, 1969.
[29] M. Kumru, V. Kucuk, M. Kocademir, H.M. Alfanda, A. Altun, L. Sarı, Experimental and theoretical studies on IR, Raman, and UV–Vis spectra of quinoline-7-carboxaldehyde, Spectrochim. Acta A Mol. Biomol. Spectrosc. 134 (2015) 81–89, https://doi.org/10.1016/j.saa.2014.06.094.
[30] P. Sjoberg, J.S. Murray, T. Brinck, P. Politzer, Average local ionization energies on the molecular surfaces of aromatic systems as guides to chemical reactivity, Can. J. Chem. 68 (8) (1990) 1440–1443, https://doi.org/10.1139/v90-220.
[31] P.K. Weiner, R. Langridge, J.M. Blaney, R. Schaefer, P.A. Kollman, Electrostatic potential molecular surfaces, Proc. Natl. Acad. Sci. U.S.A.79 (1982) 3754–3758, https://doi.org/10.1073/pnas.79.12.3754.
[32] R.C. Haddon, T. Fukunaga, Unified theory of the thermodynamic and kinetic criteria of aromatic character in the [4n+ 2] annulenes, Tetrahedron Lett 21 (1980) 1191–1192, https://doi.org/10.1016/S0040-4039(00)71367-0.
[33] T.G. Schmalz, W.A. Seitz, D.J. Klein, G.E. Hite, Elemental carbon cages, J Am Chem Soc. 110 (1988) 1113–1127, https://doi.org/10.1021/ja00212a020.
[34] D.S. Bethune, G. Meijer, W.C. Tang, H.J. Rosen, The vibrational Raman spectra of purified solid films of C60 and C70, Chem Phys Lett. 174 (1990) 219–222, https://doi.org/10.1016/0009-2614(90)85335-A.
[35] S. Radhakrishnan, R. Parthsarathi, V. Subramanian, N. Somnathan, Structure and properties of polythiophene containing hetero aromatic side chains, Comput. Mater. Sci. 37 (2006) 318–322, https://doi.org/10.1016/j.commatsci.2005.08.009.
[36] X. Liu, T.G. Schmalz, D.J. Klein, Favorable structures for higher fullerenes, Chem Phys Lett. 188 (1992) 550–554, https://doi.org/10.1016/0009-2614(92)80864-8.
[37] R.G. Parr, W. Yang, Density Functional Theory of Atoms and Molecules, Oxford University Press, New York, 1989.
[38] J. L. Gazquez, Perspectives on the density functional theory of chemical reactivity, J. Mex. Chem. Soc. 52 (2008) 3 − 10. ISSN 1870-249X.
[39] P. Geerlings, F.D. Proft, W. Langenaeker, Conceptual density functional theory, Chem. Rev. 103 (2003) 1793–1874, https://doi.org/10.1021/cr990029p.
[40] R.G. Parr, L. Szentpaly, S. Liu, Electrophilicity index, J. Am. Chem. Soc. 121 (1999) 1922–1924, https://doi.org/10.1021/ja983494x.
[41] E. Shweta, P. Khan, P. Tandon, P. Bharti, R. Kumar, Maurya, Experimental and quantum chemical studies on the structure and vibrational spectra of cearoin (a neoflavonoid), Can. J. Phys. 95 (10) (2017) 905–915, https://doi.org/10.1139/cjp-2016-0847.
[42] A. Srivastava, P. Rawat, P. Tandon, R.N. Singh, A computational study on conformational geometries, chemical reactivity and inhibitor property of an alkaloid bicuculline with γ-aminobutyric acid (GABA) by DFT, Comput. Theor. Chem. 993 (2012) 80–89, https://doi.org/10.1016/j.comptc.2012.05.025.
[43] P. Prajapati, J. Pandey, M.R. Shimpi, A. Srivastava, P. Tandon, S.P. Velaga, K. Sinha, J. Mol. Struct. 1125 (2016) 193–203, https://doi.org/10.1016/j.molstruc.2016.06.070.
[44] P.W. Ayres, R.G. Parr, Variational principles for describing chemical reactions: the Fukui function and chemical hardness revisited, J. Am. Chem. Soc. 122 (2000) 2010–2018, https://doi.org/10.1021/ja9924039.
[45] J. Bevan Ott, J. Boerio-Goates, Chemical thermodynamics: principles and applications, Academic Press, San Diego (CA), 2000.
[46] S.J. Basha, S.V. Chamundeeswari, S. Muthu, B.R. Raajaraman, J. Mol. Liq. 296 (2019) 111787, , https://doi.org/10.1021/ja9924039.
[47] N. Choudhary, P. Agarwal, A. Gupta, P. Tandon, Quantum chemical calculations of conformation, vibrational spectroscopic, electronic, NBO and thermodynamic properties of 2, 2-dichloro-N-(2, 3-dichlorophenyl) acetamide and 2, 2-dichloro-N-(2, 3-dichlorophenyl) acetamide, Comput. Theor. Chem. 1032 (2014) 27–41, https://doi.org/10.1016/j.comptc.2014.01.011.
[48] D.J. Williams, Angew. Chem. Int. Ed. Engl. 23 (9) (1984) 690–703, https://doi.org/10.1016/j.comptc.2014.01.011.
[49] S. Vidya, C. Ravikumar, I. Hubert Joe, P. Kumaradhas, B. Devipriya, K. Raju, Vibrational spectra and structural studies of nonlinear optical crystal ammonium D, L-tartrate: a density functional theoretical approach, J. Raman Spectrosc 42 (2011) 676–684, https://doi.org/10.1002/jrs.2743.
[50] C. Cassidy, J.M. Halbout, W. Donaldson, C.L. Tang, Nonlinear optical properties of urea, Opt. Commun. 29 (2) (1979) 243–246, https://doi.org/10.1016/0030-4018(79)90027-0.
[51] E. Khan, A. Shukla, A. Srivastava, P. Tandon, Molecular structure, spectral analysis and hydrogen bonding analysis of ampicillin trihydrate: a combined DFT and AIM approach, New J. Chem. 39 (12) (2015) 9800–9812, https://doi.org/10.1039/C5NJ01779C.
[52] C.A. Lipinski, F. Lombardo, B.W. Dominy, P.J. Feeney, Experimental and computational approaches to estimate solubility and permeability in drug discovery and development settings, Adv. Drug Deliv. Rev. 23 (1–3) (1997) 3–25, https://doi.org/10.1016/S0169-409X(96)00423-1.
[53] C.A. Lipinski, Lead-and drug-like compounds: the rule-of-five revolution, Drug Discov. Today Technol. 1 (4) (2004) 337–341, https://doi.org/10.1016/j.ddtec.2004.11.007.
[54] A.K. Ghose, V.N. Viswanadhan, J.J. Wendoloski, A knowledge-based approach in designing combinatorial or medicinal chemistry libraries for drug discovery. 1. A qualitative and quantitative characterization of known drug databases, J. Comb. Chem. 1 (1) (1999) 55–68, https://doi.org/10.1021/cc9800071.
[55] R.P. Verma, A. Kurup, C. Hansch, On the Role of Polarizability in QSAR, Bioorg. Med. Chem. 13 (1) (2005) 237–255, https://doi.org/10.1016/j.bmc.2004.09.039.
[56] Y.S. Mary, C.Y. Panicker, T. Thiemann, M. Al-Azani, A.A. Al-Saadi, C. Van Alsenoy, S.K. Srivastava, Molecular conformational analysis, vibrational spectra, NBO, NLO analysis and molecular docking study of bis [(E)-anthranyl-9-acrylic] anhydride based on density functional theory calculations, Spectrochim. Acta A Mol. Biomol. Spectrosc. 151 (2015) 350–359, https://doi.org/10.1016/j.saa.2015.06.075.
[57] M.B. Comer, Pharmacology of the selective 5-HT1B/1D agonist frovatriptan, Headache 42 (2002) 47–53, https://doi.org/10.1046/j.1526-4610.42.s2.2.x.
[58] A. Daina, O. Michielin, V. Zoete, SwissTargetPrediction: updated data and new features for efficient prediction of protein targets of small molecules, Nucleic Acids Res. 47 (W1) (2019) W357–W364, https://doi.org/10.1093/nar/gkz382.
[59] P.W. Rose, B. Beran, C. Bi, W.F. Bluhm, D. Dimitropoulos, D.S. Goodsell, A. Prlić, M. Quesada, G.B. Quinn, J.D. Westbrook, J. Young, The RCSB Protein Data Bank:redesigned web site and web services, Nucleic Acids Res. 39 (2010) D392–D401, https://doi.org/10.1093/nar/gkq1021.

JNPS **6** *(1), 73-83 (2020)* ***Research Article*** *© Nepal Physical Society*
ISSN: 2392-473X (Print), 2738-9537 (Online) *DOI: http://doi.org/10.3126/jnphyssoc.v6i1.30553*

Quantum Chemical Calculation and DFT Study of Sitagliptin: Insight from Computational Evaluation and Docking Approach

M. K. Chaudhary[1, 2], P. Prajapati[2] and B. D. Joshi[3, *]
[1]Central Department of Physics, Tribhuvan University, Kirtipur, Nepal
[2]Department of Physics, University of Lucknow, Lucknow-226007, India
[3]Department of Physics, Siddhanath Science Campus, Mahendranagar, Tribhuvan University, Nepal
[*]Corresponding Email: pbdjoshi@gmail.com

Received: *22 Apr., 2020;* ***Revised:*** *10 May, 2020;* ***Accepted:*** *29 Jun., 2020*

Abstract

This study aims to explore the structural and chemical behavior of sitagliptin using density functional theory (DFT). The chemical reactivity has been studied in terms of MEP, HOMO-LUMO energy gap, Hirshfeld charge, and global and local reactivity descriptors. Thermodynamic parameters like entropy, enthalpy and specific heat capacity and, nonlinear optical (NLO) properties have been analysed. Higher value of the first hyperpolarizability than that of urea show its potential use as NLO material. Intra-molecular Hydrogen bonding and topological parameters at the bond critical point (BCP) of title molecule have been studied by using the quantum theory of atoms in molecules (QTAIM) approach. The bond of 2.3777 Å between H42…N11 is noticed to be strongest one. The pharmacological behavior and protein-ligand interaction of the title molecule have been investigated in terms of drug-likeness and molecular docking which motivates that the amine and carbonyl group bind with the amino acid of the protein.

Keywords: Sitagliptin, Chemical reactivity, DFT, Hydrogen bonding, Molecular docking, NLO.

1. INTRODUCTION

Sitagliptin, (3*R*)-3-amino-1-[3-(trifluoromethyl)-6,8-dihydro-5*H*-1,2,4]triazolo[4, 3-a]pyrazin-7-yl]-4-(2,4,5-trifluorophenyl)butan-1-one, chemically named as Xelevia (or trade name Januvia) is an orally active member of the new dipeptidyl peptidase-4 (DPP-4) inhibitor class of drugs. It is used against type-2 diabetes and has low side effects in hypoglycemia to control the blood glucose level in humans by increasing insulin secretion [1], lowering HbA1c and fasting as well as postprandial glucose in monotherapy and insulin secretion [2]. Zerilli and Pyon [3] studied its pharmacology and clinical efficacy. Desai [4] analyzed its manufacturing evolution through three generations of process research and development. Similarly, Stofella *et al*. [5] carried out the solid-state characterization of its different crystalline forms.

Rajesh *et al*. [6] performed the DFT study of sitagliptin by using the Gaussian 03 package program incorporating B3LYP functional with the implementation of 6-31G(d,p) basis set. However, the properties regarding chemical reactivity, drug-likeness, nonlinear optical (NLO) properties, thermodynamic properties, atoms in the molecule (AIM), and molecular docking have not been performed by any research group so far. In this continuation, we have focused on these properties. DFT has broad spectrum to study hydrogen bonding, chemical reactivity, and electronic properties of pharmaceutical compounds [7-9]. AIM study reveals hydrogen bonding (H-bonding) whereas molecular docking explains the binding of drugs molecule with the target protein. NLO study tells whether the title molecule can be used further as NLO material and, the local reactivity descriptor justifies which particular site is active for further reaction with surrounding sites.

2. MATERIALS AND METHOD

2.1 Computational Details

Quantum chemical calculation and geometry optimization of the title molecule have been performed by using density functional theory (DFT) [10] with the support of Gaussian 09 package [11] at B3LYP/6-311++G(d, p) [12-14]

level of theory. Output files obtained from Gaussian 09 program are visualized with Gauss View 05 [15]. The formation of intramolecular hydrogen bonding in the molecule has been studied with AIMALL software [16] by implementing the quantum theory of atoms in the molecule (QTAIM) [17-20]. The molecular docking (ligand-protein) simulation of the investigated molecule has been performed to check its biological activity by using AutoDock 1.5.4 software [21]. Discovery Studio Visualizer 4.5 software [22] was used to analyze the active site in the molecule. The initial structure of sitagliptin was obtained from PubChem [23].

2.2 Theoretical Details

The global reactivity descriptors: electronegativity (χ), chemical potential (μ), global hardness (η), global electrophilicity index (ω) and global softness (S) are calculated from the energies of frontier molecular orbitals E_{HOMO} and E_{LUMO} and, are given by [24, 25];

$$\chi = -\frac{1}{2}(E_{HOMO} + E_{LUMO})$$

$$\mu = -\chi = \frac{1}{2}(E_{HOMO} + E_{LUMO})$$

$$\eta = \frac{1}{2}(E_{LUMO} - E_{HOMO})$$

$$S = \frac{1}{2\eta}$$

$$\omega = \frac{\mu^2}{2\eta}$$

The local reactivity descriptor reveals that which particular site in the molecular system is capable of further chemical reaction with surrounding molecules. This is studied by using Fukui function (FF) [26-29] calculation and is given by the equations:

$f_k^+ = [q_k(N+1)-q_k(N)]$ *for nucleophilic attack*

$f_k^- = [q_k(N)-q_k(N-1)]$ *for electrophilic attack*

$f_k^0 = [q_k(N+1) - q_k(N-1)]$ *for radical attack*

Where N, N-1, N+1 are total electrons present in neutral, cation and anion state of molecule respectively. +, – and 0 represents for nucleophilic, electrophilic, and radical attack respectively. Besides FF, Local softness (s_k^+, s_k-, s_k^0) and local electrophilicity indices (ω_k^+, ω_k-, ω_k^0) is also used to check the local reactivity behavior and is given by the equations:

$s_k^+ = Sf_k^+$, $s_k- = Sf_k-$, $s_k^0 = Sf_k^0$

for local softness

$\omega_k^+ = \omega f_k^+$, $\omega_k- = \omega f_k-$, $\omega_k^0 = \omega f_k^0$

for local electrophilicity indices

The first hyperpolarizability (β_o) is a third-ranked tensor which can be explained by a 3X3X3 matrix. The 27 components of the 3D-matrix can be reduced to 10 components from the Kleinman symmetry [30]. The lower part of the 3X3X3 matrix is tetrahedral. The components of (β_o) can be defined as the coefficients in the Taylor series expansion of the energy in the external electric field. For weak and homogenous electric field this expansion becomes:

$$E = E^0 - \mu_i F_i - \frac{1}{2}\alpha_{ij}F_iF_j - \frac{1}{6}\beta_{ijk}F_iF_jF_k$$

Where E^0 is the energy of the unperturbed molecules, F_i is the field at the origin and μ_i, α_{ij} and β_{ijk} are the components of dipole moment, polarizability and first hyperpolarizability respectively.

Total static dipole moment (μ_0), the first hyperpolarizability (β_0), mean polarizability ($\Delta\alpha_0$) and anisotropy of polarizability $|\alpha_0|$of the molecular system have been calculated by using DFT at B3LYP/6-311++G(d, p) level of theory and are given by the equations [31].

$$\mu_0 = (\mu_x^2 + \mu_y^2 + \mu_z^2)^{1/2}$$

$$|\alpha_0| = \frac{1}{3}(\alpha_{xx} + \alpha_{yy} + \alpha_{zz})$$

$$\Delta\alpha = 2^{-1/2}\left[(\alpha_{xx} - \alpha_{yy})^2 + (\alpha_{yy} - \alpha_{zz})^2 + (\alpha_{zz} - \alpha_{xx})^2 + 6\alpha_{xx}^2\right]^{1/2}$$

$$\beta_0 = \left[(\beta_{xxx} + \beta_{xyy} + \beta_{xzz})^2 + (\beta_{yyy} + \beta_{xxy} + \beta_{yzz})^2 + (\beta_{zzz} + \beta_{xxz} + \beta_{yyz})^2\right]^{1/2}$$

3. RESULTS AND DISCUSSION

3.1 Geometry Optimization

The optimized structure of sitagliptin with the numbering scheme used in this study is presented in Fig. 1. The calculated bond length, bond angle, and dihedral angles are found similar to the rsults by Rajesh *et al*. [6]. The ground state optimized energy obtained is -1567.1989 Hartree.

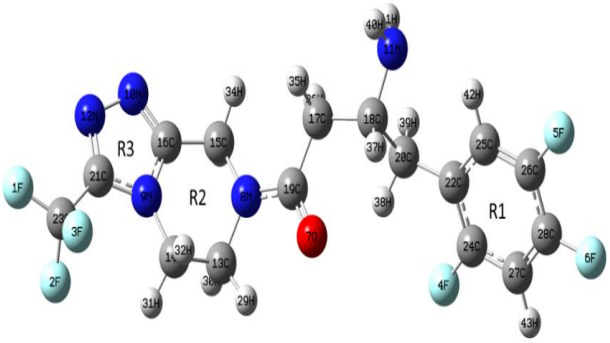

Fig. 1: *Optimized structure of sitagliptin and the atom numbering scheme adopted in this study.*

3.2 Molecular Electrostatic Potential (MEP)

The distribution of partial charges in space around the molecule, which infer about the reactive site of the molecule, is examined, and explained in terms of MEP [32-34]. The values of electrostatic potential are given in terms of distinct colors: red region identified the negative electrostatic potential; blue region recognized the positive electrostatic potential and green region represents the zero potential. Potential increases in the order red<orange<yellow<green<blue. The color code of MEP for title molecule is in the range - 4.986e-2 a.u to + 4.986e-2 a.u. The MEP mapped structure is presented in Fig. 2.

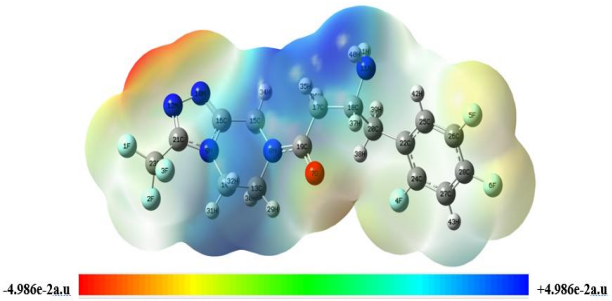

Fig. 2: *Molecular electrostatic potential (MEP) formed by mapping of total density over the electrostatic potential of sitagliptin.*

The negative charge is mostly concentrated across N10 and N12 of ring R3 and behaves as an electrophilic center but the partial negative charge is localized across carbonyl group (C19=O7) whereas the positive charge is concentrated across $N11H_2$, $C17H_2$ and the ring R2 which are the major nucleophilic centers.

3.3 Frontier Orbital Analysis

The highest molecular orbital (HOMO) and lowest molecular orbital (LUMO) are the main frontier orbitals which take part in chemical reaction for the chemical stability of the molecule [35]. The energy of HOMO (E_{HOMO}) is related to ionization potential whereas the energy of LUMO (E_{LUMO}) is related to electron affinity. Their gap energy ($\Delta E = E_{LUMO} - E_{HOMO}$) is the stability index that determines the electron transport properties [36]. This energy gap for sitagliptin is found to be 5.6714 eV. The HOMO-LUMO orbitals and their energies are presented in Fig. 3.

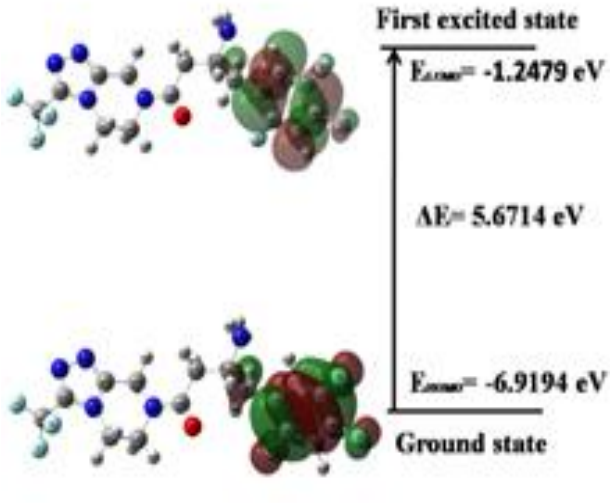

Fig. 3: *HOMO-LUMO plot of sitagliptin.*

3.4 Global Reactivity Descriptors

The calculated E_{HOMO}, E_{LUMO} and their energy gap (ΔE) and χ, μ, η, S, and ω values for sitagliptin are listed in Table 1. The HOMO–LUMO energy gap of the examined molecule is obtained as 5.6714 eV but the global softness is found to be 4.0836 eV. Small value of the energy gap represents the more chemically reactive molecule and softer whereas the high value of the energy gap stands for a harder molecule with more stable.

Table 1: Calculated E_{HOMO}, E_{LUMO}, energy ban gap (E_L–E_H), chemical potential (μ), electronegativity (χ), global hardness (η), global softness (S) and global electrophilicity index (ω) for sitagliptin.

E_H (eV)	E_L(eV)	$E_L - E_H$ (eV)	χ (eV)	μ (eV)	η (eV)	S $(eV)^{-1}$	ω (eV)
-6.9194	- 1.2479	5.6714	4.0836	- 4.0836	2.8357	0.1763	2.9404

3.4 Drug-Likeness

When a chemical compound has definite biological/pharmacological activity, for the orally active drug in humans, Lipinski's 'rule of five' evaluates drug-likeness. In an experiment for a better forecast of drug-likeness, the rules have generated many developments. Out of these developed rules, three of them state that the compound should have (i) a molar refractivity (MR) from 40 to 130 (ii) a molecular weight from 180 to 500 and (iii) its number of atoms from 20 to 70.

The value of molar refractivity (MR) is responsible for the binding property and lipophilicity of the studied system which is calculated from the Lorenz-Lorentz formula [37-39]. The values of MR, molecular weight, and the number of atoms for sitagliptin are 80 esu, 407.32 g/mol, and 43 respectively. All the above-mentioned values lie within the normal range. So, sitagliptin can be orally used for humans.

3.5 Local Reactivity Descriptors

The highest value of (f_k^+, s_k^+, ω_k^+) gives the idea of the most nucleophilic site whereas the peak value of (f_k-, s_k-, ω_k-) infer about the electrophilic region in the molecule respectively. The local reactivity properties of sitagliptin are calculated by using Hirshfeld derived charges at B3LYP/6-311++G(d,p) level and their values are presented in Table 2 and, the atoms N11 and H33 are the most responsible for the nucleophilic and electrophilic attack respectively.

Table 2: Calculated local reactivity properties of Sitagliptin using Hirshfeld [B3LYP/6-311++G(d,p)] derived charges.

Site	f_k^+	s_k^+	ω_k^+	f_k-	s_k-	ω_k-	f_k^0	s_k^0	ω_k^0
F1	0.0092	0.0016	0.0271	0.0101	0.0018	0.0298	−0.3195	−0.0563	−0.9394
F2	0.0079	0.0014	0.0232	0.0091	0.0016	0.0268	−0.3569	−0.0629	−1.0493
F3	0.0069	0.0012	0.0204	0.0084	0.0015	0.0248	−0.3550	−0.0626	−1.0437
F4	0.0495	0.0087	0.1456	0.0023	0.0004	0.0067	−0.3322	−0.0586	−0.9768
F5	0.0537	0.0095	0.1580	0.0096	0.0017	0.0283	−0.3168	−0.0559	−0.9316
F6	0.0538	0.0095	0.1582	0.0144	0.0025	0.0424	−0.3150	−0.0555	−0.9263
O7	0.0377	0.0066	0.1107	0.0188	0.0033	0.0553	−0.6190	−0.1091	−1.8202
N8	0.0328	0.0058	0.0964	0.0020	0.0004	0.0059	−0.5045	−0.0889	−1.4833
N9	0.0067	0.0012	0.0196	0.0077	0.0014	0.0226	−0.4128	−0.0728	−1.2137
N10	0.0517	0.0091	0.1520	0.0185	0.0033	0.0545	−0.2888	−0.0509	−0.8491
N11	0.1036	0.0183	0.3046	0.0187	0.0033	0.0550	−0.8055	−0.1420	−2.3685
N12	0.0450	0.0079	0.1324	0.0307	0.0054	0.0904	−0.2426	−0.0428	−0.7134
C13	−0.0024	−0.0004	−0.0070	0.0099	0.0017	0.0291	−0.1967	−0.0347	−0.5783
C14	−0.0024	−0.0004	−0.0069	0.0032	0.0006	0.0093	−0.1790	−0.0316	−0.5262
C15	−0.0046	−0.0008	−0.0136	0.0224	0.0039	0.0658	−0.2194	−0.0387	−0.6451
C16	−0.0005	−0.0001	−0.0015	0.0127	0.0022	0.0373	0.3715	0.0655	1.0923
C17	0.0082	0.0014	0.0241	0.0298	0.0053	0.0877	−0.4933	−0.0870	−1.4506
C18	−0.0056	−0.0010	−0.0164	0.0060	0.0011	0.0177	−0.0275	−0.0048	−0.0808
C19	−0.0062	−0.0011	−0.0183	0.0016	0.0003	0.0048	0.6996	0.1233	2.0571

C20	−0.0175	−0.0031	−0.0514	0.0104	0.0018	0.0304	-0.4158	-0.0733	−1.2227
C21	0.0224	0.0039	0.0659	0.0375	0.0066	0.1102	0.2439	0.0430	0.7170
C22	0.0918	0.0162	0.2700	−0.0015	−0.0003	−0.0043	−0.0338	−0.0060	−0.0994
C23	−0.0005	−0.0001	−0.0014	0.0067	0.0012	0.0196	1.0379	0.1830	3.0520
C24	0.0761	0.0134	0.2237	0.0005	0.0001	0.0016	0.4523	0.0797	1.3299
C25	−0.0069	−0.0012	−0.0203	0.0291	0.0051	0.0855	−0.2586	−0.0456	−0.7602
C26	0.0825	0.0146	0.2427	0.0076	0.0013	0.0223	0.3824	0.0674	1.1245
C27	0.0068	0.0012	0.0199	0.0302	0.0053	0.0887	−0.3218	−0.0567	−0.9461
C28	0.0775	0.0137	0.2278	0.0218	0.0038	0.0641	0.3926	0.0692	1.1543
H29	0.0024	0.0004	0.0070	0.0206	0.0036	0.0606	0.2478	0.0437	0.7287
H30	0.0144	0.0025	0.0423	0.0515	0.0091	0.1513	0.1783	0.0314	0.5242
H31	0.0138	0.0024	0.0407	0.0198	0.0035	0.0581	0.2206	0.0389	0.6488
H32	0.0063	0.0011	0.0186	0.0463	0.0082	0.1363	0.1962	0.0346	0.5768
H33	0.0164	0.0029	0.0483	0.1047	0.0185	0.3079	0.1714	0.0302	0.5041
H34	−0.0003	0.0000	−0.0008	0.0434	0.0077	0.1276	0.2176	0.0384	0.6397
H35	0.0149	0.0026	0.0438	0.0764	0.0135	0.2245	0.1949	0.0344	0.5731
H36	0.0120	0.0021	0.0354	0.0900	0.0159	0.2647	0.1721	0.0303	0.5061
H37	0.0124	0.0022	0.0365	0.0119	0.0021	0.0349	0.2109	0.0372	0.6201
H38	0.0164	0.0029	0.0481	0.0066	0.0012	0.0195	0.2364	0.0417	0.6951
H39	0.0315	0.0056	0.0926	0.0353	0.0062	0.1037	0.2046	0.0361	0.6017
H40	0.0196	0.0035	0.0577	0.0408	0.0072	0.1198	0.3461	0.0610	1.0178
H41	0.0156	0.0028	0.0459	0.0631	0.0111	0.1854	0.3243	0.0572	0.9537
H42	0.0160	0.0028	0.0471	0.0002	0.0000	0.0005	0.2639	0.0465	0.7758
H43	0.0312	0.0055	0.0917	0.0114	0.0020	0.0334	0.2490	0.0439	0.7320

3.6 Nonlinear Optical (Nlo) Properties

NLO phenomena are used to investigate the interaction of the applied magnetic field with organic materials which generate the new magnetic field altered in frequency, amplitude, phase, and many more physical phenomena which has the practical applications in optical sensing, data storage, optical communication, *etc.* [40-42].

The calculated values of dipole moment (μ_0), the first hyperpolarizability (β_0), mean polarizability ($\Delta\alpha_0$) and anisotropy of polarizability $|\alpha_0|$ of the investigated molecule are listed in Table 3. The values of the dipole moment (μ_0) and the first hyperpolarizability (β_0) of title molecule are obtained as 2.03714 Debye and $2.7733X10^{-30}$ esu, respectively. The dipole moment and first hyperpolarizability of the investigated molecule are greater than that of urea, hence this molecule can be considered as NLO active material.

Table 3: The calculated dipole moment (μ_0), mean polarizability$|\alpha_0|$ anisotropy of polarizability ($\Delta\alpha$) and first hyperpolarizability (β_0) of Sitagliptin at B3LYP/6-311++G(d, p).

Dipole moment (Debye)		**Polarizability ($*10^{-24}$esu)**		**First Hyperpolarizability ($*10^{-30}$esu)**	
μ_x	−0.4527	α_{xx}	43.8660	β_{xxx}	−0.4350
μ_y	−0.4270	α_{xy}	−2.0511	β_{xxy}	0.0164
μ_z	−1.9397	α_{yy}	31.1093	β_{xyy}	−0.9051

μ_0	2.0371	α_{xz}	2.3298	β_{yyy}	0.5594
μ_0 (Urea)	1.7410	α_{yz}	0.0706	β_{xxz}	−0.1117
		α_{zz}	24.9932	β_{xyz}	0.2994
		$\lvert\alpha_0\rvert$	33.3228	β_{yyz}	−0.4786
		$\Delta\alpha$	77.9074	β_{xzz}	−0.5016
		$\Delta\alpha$ (Urea)	9.7710	β_{yzz}	0.4545
				β_{zzz}	−1.2093
				β_0	2.7733
				β_0 (Urea)	0.9279

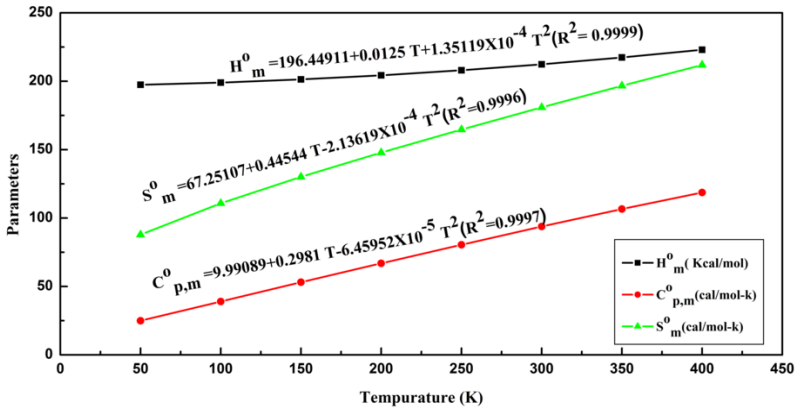

Fig. 4: *Correlation graph of enthalpy (H_m^o) (kcal/mol), specific heat ($C_{p,m}^o$) (cal/mol-K), entropy (S_m^o) (cal/mol-K) and temperature for sitagliptin. (Colour online).*

3.7 Thermodynamic Properties

Important thermodynamic properties of solids are entropy, enthalpy, heat capacity, specific heat capacity, and many more. Thermodynamics is used to analyze the effect of temperature on chemical reactions, the stability of the molecule, binding properties of biologically active molecules with protein, and physicochemical properties [43-45]. In this study, we have focused on the variation of thermodynamic parameters: heat capacity ($C_{p,m}^o$), entropy (S_m^o) and enthalpy (H_m^o) as a function of temperature in the range 50K to 400K. Total energy, zero-point vibrational energy, enthalpy, specific heat, entropy, and rotational constant of title molecule calculated at room temperature (298.15K) and normal pressure are listed in Table. 4. The graphic correlation of enthalpy (H_m^o), specific heat ($C_{p,m}^o$) and entropy (S_m^o) is presented in Fig. 4 and is given by the relations:

H_m^o = 196.44911+0.0125 T+1.35119X10^{-4} T^2 (R^2 = 0.9999)

$C_{p,m}^o$ = 9.99089+0.2981 T–6.45952X10^{-5} T^2 (R^2 = 0.9997)

S_m^o = 67.25107+0.44544 T–2.13619X10^{-4} T^2 (R^2 = 0.9996)

Fig. 4 reveals that the values of H_m^o, $C_{p,m}^o$ and S_m^o increase with the rise in temperature which is due to an increase in molecular vibrational intensities with an increase in temperature.

Table 4: Theoretically computed total energy (eV), zero-point energy (J/mol), enthalpy (kcal/mol), specific heat (cal/mol-K), entropy (cal/mol-K) and rotational constants(GHz) at 298.15 K at the B3LYP/6-311++G(d,p) level of sitagliptin.

Parameters	Values
Total energy (eV)	−42645.6718
Zero point energy (J/mol)	822583.6
Enthalpy (kcal/mol)	212.213
Specific heat (cal/mol-K)	93.322
Entropy (cal/mol-K)	180.323
Rotational constant (GHz)	0.51921

3.8 Atom In Molecule (Aim) Calculation

The Quantum theory of atoms in the molecule (QTAIM) explains the strength and nature of inter and intra-molecular hydrogen bonding [46]. The molecular graph of sitagliptin using the AIM program at B3LYP/6-311++G(d,p) level is presented in Fig. 5. The calculated topological and energy parameters for the intramolecular H-bonds of interacting atoms of sitagliptin is reported in Table 5. The geometrical parameters for the H-bonds of sitagliptin are given in Table 6. All the H-bonds have an electron density in the range 0.0020-0.0400 a.u., predicted by Koch and Popeliar [47] criteria. In this study, the bond H42…N11 has the smallest bond length, as given in Table 5, so it is a strong intra-molecular H-bond. However, the distance between the interacting atoms H31…F2 is greater than the sum of their Van der Waals radii, so this H-bond is week. The AIM result explores $\nabla^2\rho_{BCP} > 0$ and $H_{BCP} < 0$ so the nature of the bond is medium as suggested by Rozas *et al*. [48].

Table 5: Topological parameters for intramolecular interaction in sitagliptin: ED (ρ_{BCP}), Laplacian of ED ($\nabla^2\rho_{BCP}$), electron kinetic energy density (G_{BCP}), electron potential energy density (V_{BCP}), total electron energy density (H_{BCP}), interaction energy (E_{int}) at BCP.

Interactions	Bond Length (Å)	ρ_{BCP} (a.u)	$\nabla^2\rho_{BCP}$ (a.u)	G_{BCP} (a.u)	V_{BCP} (a.u)	H_{BCP} (a.u)	E_{int} (kcal/mol)
H31…F2	3.0634	0.0065	0.0268	−0.0010	−0.0046	−0.0057	−1.4482
H34…C17	2.4989	0.0130	0.0558	−0.0025	−0.0089	−0.0114	−2.7961
H42…N11	2.3777	0.0150	0.0468	−0.0017	−0.0084	−0.0100	−2.6290

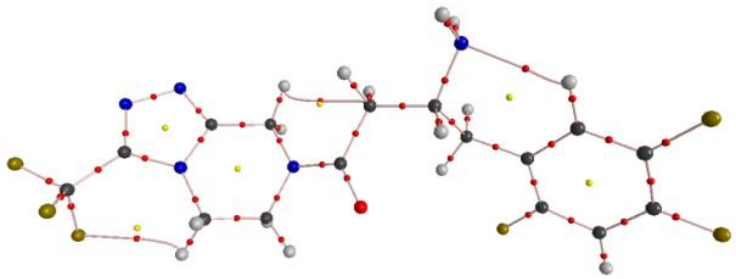

Fig. 5*: Molecular graph of sitagliptin: bond critical points (small red spheres), ring critical points (small yellow spheres), bond paths (pink lines).*

Table 6: Geometrical parameters for intramolecular hydrogen bonds in sitagliptin: bond length (Å), bond angle (°) and the sum of Van der Waals radii of interacting atoms ($r_H + r_A$) in Å.

D-H…A	D-H (Å)	H…A (Å)	D-H…A (°)	($r_H + r_A$) (Å)
C14-H31…F2	1.09055	3.0634	115.81191	2.67
C15-H34…C17	1.08699	2.4989	103.25822	2.60
C25-H42…N11	1.08261	2.3777	123.21447	2.75

3.9 Molecular Docking

Molecular docking has become an important tool in drug discovery with the study of the ligand-protein interaction mechanism. To examine the biological activity of sitagliptin, docking simulation has been performed using AutoDock software [22]. The active site of the enzyme was explained within the grid size 60ÅX60ÅX60Å to incorporate the residues of the active sites. Proteins were prepared by removing co-crystallized ligands and water molecules using Discovery Studio Visualizer 4.5 software [49]. It is a dipeptidyl peptidase-4 (DPP-4) inhibitor class of drugs and works by increasing the production of insulin and decreasing the production of glucagon by the pancreas. Therefore, DPP-4 was chosen as a target for sitagliptin which is predicted by Swiss Dock software and given in Fig. 6. The crystal structure of target protein DPP-4 (PDB

code: 1J2E and 1U8E) was downloaded from the RSCB PDB website [50]. The binding energy of ligand with the target and the bond length of the hydrogen bond formed between them are shown in Table 7. Out of many docked conformations, one which well-bounded the active sites was taken into consideration and is drawn in Fig. 7. 1J2E shows the formation of one hydrogen bond (2.49 Å, THR A: 251) with the carbonyl group, two hydrogen bonds (1.77 Å, GLU B: 237, 1.95 Å, PRO B: 249) with NH_2 group and one (2.21Å, ARG B:253) with the CF_3 group attached to the ring having binding energy −7.25 kcal/mol. Another interaction was also found with 1U8E in which two hydrogen bonds were observed with the NH_2 group having bond length and residues: 1.81 Å, ASP B:709, and 2.03 Å, ASP B:739 respectively. One hydrogen bond was also present with the C=O group (2.36 Å, LYS B: 122). The binding energy was −7.17 kcal/mol. The above discussed molecular docking study of sitagliptin explores its ligand-target interaction mechanism.

Table 7: Bond length, Binding energy and Ligand efficiency of sitagliptin against two protein targets.

Ligand	protein	PDB code	Bond length (Å)	Amino acid	Binding energy (kcal/mol)	Ligand efficiency
Sitagliptin	Dipeptidyl Peptidase-4 (DPP-4)	1J2E	1.77	GLU B:237	−7.25	−0.26
			1.95	PRO A:249		
			2.49	THR A:251		
			2.21	ARG A: 253		
		1U8E	1.81	ASP B:709	−7.17	−0.26
			2.03	ASP B:739		
			2.36	LYS B:122		

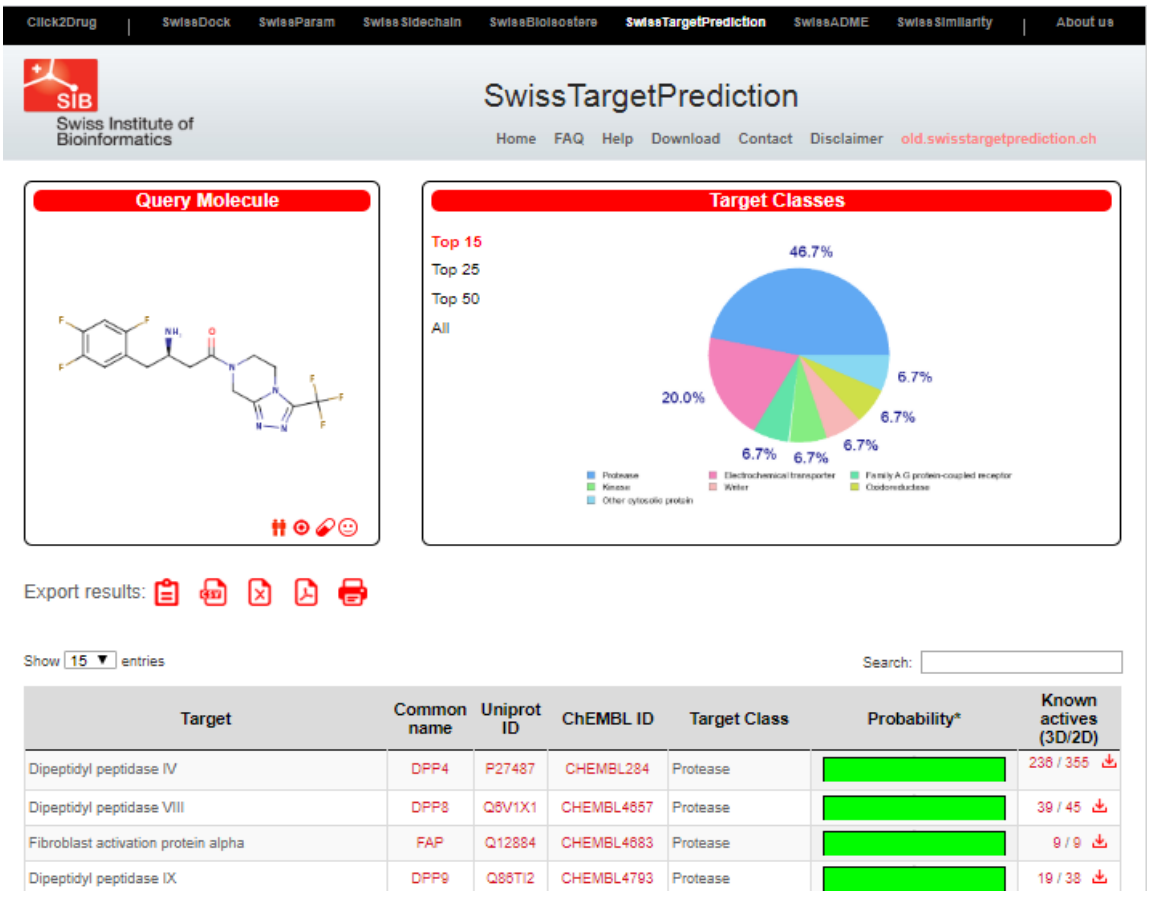

***Fig. 6**: Swiss Dock used to suggest different target proteins to perform the molecular docking simulation.*

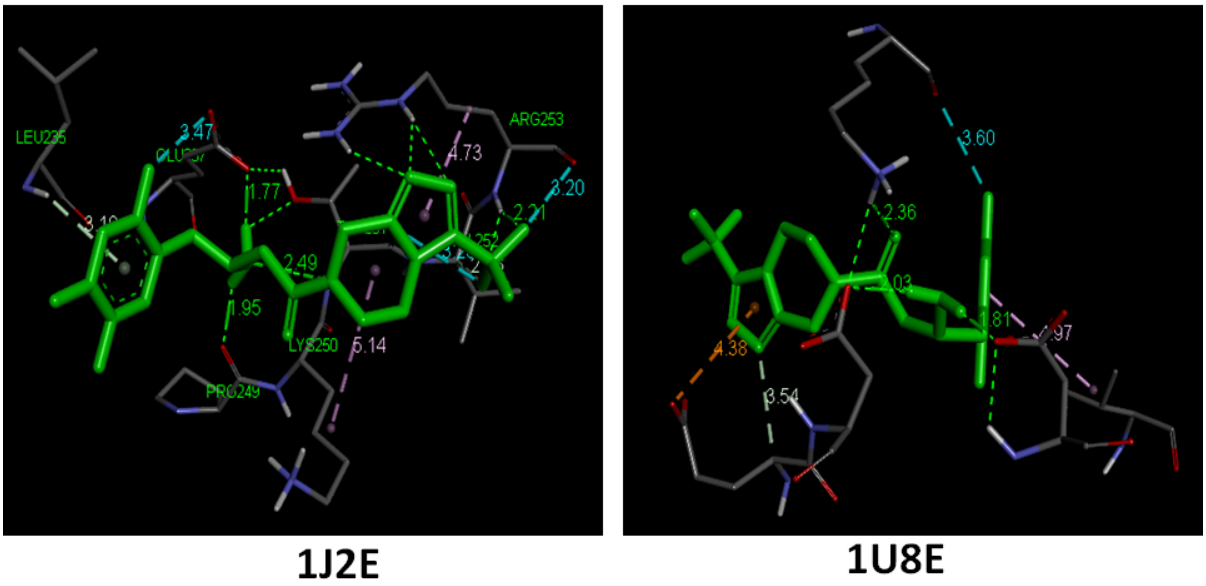

***Fig. 7**: Docking of sitagliptin with the molecular target.*

4. CONCLUSION

Theoretical investigations on sitagliptin molecule, a novel oral hypoglycemic drug of the dipeptidyl peptidase-4 inhibitor (DPP-4) class, have been done by DFT method. The optimized ground state energy is -1567.1989 Hartree. From the molecular electrostatic potential (MEP) map, it is found that the negative charge is concentrated across N10 and N12 of ring R3 while the positive charge is concentrated across $N11H_2$, $C17H_2$, and ring R2. The HOMO-LUMO energy gap is found to be 5.6714eV which explains that the title molecule is chemically more reactive. From local reactivity descriptor analysis N11 and H33 are the key atoms responsible for the nucleophilic and electrophilic attack, respectively.

The dipole moment (μ_0) and first hyperpolarizability (β_0) of title molecule are found to be and $2.7733X10^{-30}$ esu, respectively which are higher than the standard values of urea, its potential as NLO material. The enthalpy, specific heat, and entropy of title molecule at room temperature are found to be 212.213 kcal/mol, 93.322 cal/mol-K and 180.323 cal/mol-K respectively. The QTAIM infer that the title molecule has three intra-molecular hydrogen bonding with $\nabla^2\rho_{BCP} > 0$ and $H_{BCP} < 0$. So, there is medium H-bond with partially covalent bond H42…N11 and has the smallest bond length which is the strongest one in nature. Molecular docking has been explored that the investigated molecule can be used as against type-2 diabetes.

ACKNOWLEDGMENTS

Manoj Kumar Chaudhary is grateful to the Center for Co-Operation in Science and Technology among Developing Societies (CCSTDS) for financial support under the Indian Science and Research Fellowship (ISRF-2019) award. Our sincere thanks go to Prof. Poonam Tandon, Head of Physics Department and Macromolecular Laboratory, Lucknow University, Lucknow-226007, India for providing laboratory facilities.

REFERENCES

[1] Rosenstock, J., Brazg, R., Andryuk, P.J., Lu, K., Stein, P., and Study, S. Efficacy and safety of the dipeptidyl peptidase-4 inhibitor sitagliptin added to ongoing pioglitazone therapy in patients with type 2 diabetes: a 24-week, multicenter, randomized, double-blind, placebo-controlled, parallel-group study. *Clinical therapeutics*, **28(10)**, 1556-1568 (2006).

[2] Gallwitz, B. Review of sitagliptin phosphate: a novel treatment for type 2 diabetes. *Vascular health and risk management*, **3(2)**, 203 (2007).

[3] Zerilli, T., and Pyon, E.Y. Sitagliptin phosphate: a DPP-4 inhibitor for the treatment of type 2 diabetes mellitus. *Clinical therapeutics*, **29(12),** 2614-2634 (2007).

[4] Desai, A. A. Sitagliptin manufacture: a compelling tale of green chemistry, process intensification, and industrial asymmetric catalysis. *Angew*. Chem. *Int. Ed.,* **50(9)** 1974-1976 (2011).

[5] Stofella, N.C., Veiga, A., Oliveira, L.J., Montin, E.F., Andreazza, I.F., Carvalho Filho, M.A.,

Bernardi, L.S., Oliveira, P.R., and Murakami, F.S. Solid-state characterization of different crystalline forms of sitagliptin. *Materials*, **12(15)**, 2351 (2019).

[6] Rajesh, S., Gunasekaran, S., and Rajesh, P. HOMO-LUMO, NBO and Vibrational analysis of Sitagliptin by using DFT calculations and Experimental Study (FT-IR, FT-Raman and UV-Visible Spectroscopies). *Int.J. Chem Tech. Res.*, **11**, 107-122 (2018).

[7] Ulahannan, R.T., Panicker, C.Y., Varghese, H.T., Musiol, R., Jampilek, J., Van Alsenoy, C., War, J.A. and Srivastava, S.K. Molecular structure, FT-IR, FT-Raman, NBO, HOMO and LUMO, MEP, NLO and molecular docking study of 2-[(E)-2-(2-bromophenyl) ethenyl] quinoline-6-carboxylic acid. *Spectrochim. Acta A*, **151**, 184-197 (2015).

[8] Arjunan, V., Santhanam, R., Sakiladevi, S., Marchewka, M.K., and Mohan, S. Synthesis and characterization of an anticoagulant 4-hydroxy-1-thiocoumarin by FTIR, FT-Raman, NMR, DFT, NBO and HOMO–LUMO analysis. *J. Mol. Struct.*, **1037**, 305-316 (2013).

[9] Karaca, C., Atac, A., and Karabacak, M. Conformational analysis, spectroscopic study (FT-IR, FT-Raman, UV, 1H and 13C NMR), molecular orbital energy and NLO properties of 5-iodosalicylic acid. *Spectrochim. Acta A,* **136**, 295-305 (2015).

[10] Ferrari, V., Pruneda, J.M., and Artacho, E. Density functionals and half-metallicity in La2/3Sr1/3MnO3. *Phys. Stat. Sol. (A)*, **203(6)**, 1437-1441 (2006).

[11] Frisch, M.J., Trucks, G.W., Schlegel, H.B., Scuseria, G.E., Cheeseman, J.R., Robb, M.A., Scalmani, G., Barone, V., Mennucci, B., Petersson, G.A. and Nakatsuji, H., JM M illan, Klene, M., Knox, J.E., Cross, J.B., Bakken, V., Adamo, C., Jaramillo, J., Gomperts, R., Stratmann, R.E., Yazyev, O., Austin, A.J., Cammi, R., Pomelli, C., Ochterski, J.W., Martin, R.L., Morokuma, K., Zakrzewski, V.G., Voth, G.A., Salvador, P., Dannerberg, J.J., Dapprich, S., Daniels, A.D., Farkas, J., Foresman, B. Ortiz, J.V., Cioslowski, J. And Fox, D.J., GAUSSIAN 09, (2009).

[12] Becke, A. D. A new mixing of Hartree–Fock and local density-functional theories. *J. Chem. Phys.*, **98(2)**, 1372-1377 (1993).

[13] Parr, R.G., and Yang, W., Density Functional Theory of Atoms and Molecules, Oxford, New York, (1989).

[14] Pulay, P., Fogarasi, G., Pang, F., and Boggs, J.E. Systematic ab initio gradient calculation of molecular geometries, force constants, and dipole moment derivatives. *J. Am. Chem. Soc.*, **101(10)**, 2550-2560 (1979).

[15] Frisch, A., Nielson, A.B., and Holder, A.J., Gauss View User Manual, Gaussian Inc., Pittsburgh, PA, (2000).

[16] Keith, T.A., AIMALL Version 090201 TK Gristmill Software Overland Park, KS. USA; (2009).

[17] Bader, R.F.W., Atoms in Molecules, A Quantum Theory, Oxford University Press, Oxford,(1990).

[18] Bader, R.F.W., Anderson, S.G., and Duke, A.J. Quantum topology of molecular charge distributions. 1. *J. Am. Chem. Soc.*, **101(6)**, 1389-1395 (1979).

[19] Bader, R.F.W., Slee, T.S., Cremer, D., and Kraka, E. Description of conjugation and hyperconjugation in terms of electron distributions. *J. Am. Chem. Soc.*, **105(15)**, 5061-5068 (1983).

[20] Bader, R.F.W., and MacDougall, P.J. Toward a theory of chemical reactivity based on the charge density. *J. Am. Chem. Soc.*, **107(24)**, 6788-6795 (1985).

[21] Trott, O., and Olson, A.J. AutoDock Vina: improving the speed and accuracy of docking with a new scoring function, efficient optimization, and multithreading. *J. Comput. Chem.,* **31(2)**, 455-461 (2010).

[22] Studio, D. 2.5 Guide, Accelrys Inc., San Diego, (2009).

[23] https://pubchem.ncbi.nlm.nih.gov/search/search.cgi.

[24] Parr, R. G., Szentpaly, L. V., and Liu, S. Electrophilicity index. *J. Am. Chem. Soc*., **121(9)**, 1922-1924 (1999).

[25] Chattaraj, P. K., and Giri, S. Stability, reactivity, and aromaticity of compounds of a multivalent superatom. *J. Phys. Chem. A*, **111(43)**, 11116-11121 (2007).

[26] Parr, R.G., and Yang, W., Density functional Theory of Atoms and Molecules, Oxford University Press, Oxford, New York, 34 (1989).

[27] Pearson, R.G. Absolute electronegativity and hardness: applications to organic chemistry. *J. Org. Chem.*, **54(6)**, 1423-1430 (1989).

[28] Parr, R.G., and Pearson, R.G. Absolute hardness: companion parameter to absolute electronegativity. *J. Am. Chem. Soc.*, **105(26)**, 7512-7516 (1983).

[29] Geerlings, P., Proft, F.D., and Langenaeker, W. Conceptual density functional theory. *Chem. Rev.*, **103(5)**, 1793-1874 (2003).

[30] Wortmann, R., Krämer, P., Glania, C., Lebus, S. and Detzer, N.,. Deviations from Kleinman symmetry of the second-order polarizability tensor in molecules with low-lying perpendicular electronic bands. *Chemical physics*, ***173*(1)**, 99-108 (1993).

[31] Alyar, H., Kantarci, Z., Bahat, M., and Kasap, E. Investigation of torsional barriers and nonlinear

optical (NLO) properties of phenyltriazines. *J. Mol. Struct*., **834**, 516-520 (2007).

[32] Chidangil, S., Shukla, M. K., and Mishra, P. C. A molecular electrostatic potential mapping study of some fluoroquinolone anti-bacterial agents. *J. Mol. Model.*, **4(8)**, 250-258 (1998).

[33] Alkorta, I., and Perez, J. J. Molecular polarization potential maps of the nucleic acid bases. *Int. J. Quantum Chem.*, **57(1)**, 123-135 (1996).

[34] Murray, J. S., and Sen, K., Molecular Electrostatic Potentials: Concepts and Applications, Elsevier, Amsterdam, (1996).

[35] Gunasekaran, S., Balaji, R. A., Kumaresan, S., Anand, G., and Srinivasan, S. Experimental and theoretical investigations of spectroscopic properties of N-acetyl-5- methoxytryptamine. *Can. J. Anal. Sci. Spectrosc.*, **53(4)**, 149-162 (2008).

[36] Padmaja, L., Amalanathan, M., Ravikumar, C., and Hubert Joe, I. NBO analysis and vibrational spectra of 2, 6-bis (p-methyl benzylidene cyclohexanone) using density functional theory. *Spectrochim. Acta, Part A*, **74(2)**, 349-356 (2009).

[37] Padro_n, J.A., Carasco, R., and Pello_n, R.F. Molecular descriptor based on a molar refractivity partition using Randic-type graph-theoretical invariant. *J. Pharm. Pharm. Sci.*, **5(3)**, 258-266 (2002).

[38] Verma, R.P., and Hansch, C. A comparison between two polarizability parameters in chemical–biological interactions. *Bioorg. Med. Chem.*, **13(7)**, 2355-2372 (2005).

[39] Verma, R.P., Kurup, A., and Hansch, C. On the role of polarizability in QSAR. *Bioorg. Med. Chem.*, **13(1)**, 237-255 (2005).

[40] Williams, D.J. Organic polymeric and non-polymeric materials with large optical nonlinearities. *Angew. Chem. Ed. Engl.*, **23(9)**, 690-703 (1984).

[41] Lipscomb, G.F., Garrito, A.F., and Narang, R.S. An exceptionally large linear electro□optic effect in the organic solid MNA. *J. Chem. Phys.*, **75(3)**, 1509-1516 (1981).

[42] Dehu, C., Meyers, F., and Bredas, J.L. Donor-acceptor diphenylacetylenes: geometric structure, electronic structure, and second-order nonlinear optical properties. *J. Am. Chem. Soc.*, **115(14)**, 6198-6206 (1993).

[43] Joshi, B.D., and Chaudhary, M.K. NBO, nonlinear optical and thermodynamic properties of 10-Acetyl-10H-phenothiazine 5-oxide. *BIBECHANA*, **15**, 131-139 (2018).

[44] Joshi, B.D., Mishra, R., Tandon, P., Oliveira, A.C. and Ayala, A.P. Quantum chemical studies of structural, vibrational, NBO and hyperpolarizability of ondansetron hydrochloride. *J. Mol. Struct.*, **1058**, 31-40 (2014).

[45] Bevan Ott, J., Boerio-Goates, J., Chemical thermodynamics: principles and applications. San Diego (CA): Academic Press; (2000).

[46] Matta, I.F., and Boyd, R.J., An Introduction to the Quantum Theory of Atoms in Molecules, Wiley-VCH VerlagGmbh, (2007).

[47] Koch, U., and Popelier, P. Characterization of CHO hydrogen bonds based on the charge density. *J. Phys. Chem. A*, **99(24)**, 9747-9754 (1995).

[48] Rozas, I., Alkorta, I., and Elguero, J. Behavior of ylides containing N, O, and C atoms as hydrogen bond acceptors. *J. Am. Chem. Soc.*, **122(45)**, 11154-11161 (2000).

[49] Morris, G.M., Huey, R., Lindstrom, W., Sanner, M.F., Belew, R.K., Goodsell, D.S., and Olson, A.J. AutoDock4 and AutoDockTools4: Automated docking with selective receptor flexibility. *J. Comput. Chem.*, **30 (16)**, 2785-2791 (2009).

[50] Bourne, P. E., Addess, K.J., Bluhm, W.F., Chen, L., Deshpande, N., Feng, Z., Fleri, W., Green, R., Merino-Ott, J.C., Townsend-Merino, W. and Weissig, H. The distribution and query systems of the RCSB Protein Data Bank. *Nucleic acids research,* **32**(suppl_1), D223-D225 (2004).

BIBECHANA
ISSN 2091-0762 (Print), 2382-5340 (Online)
Journal homepage: http://nepjol.info/index.php/BIBECHANA
Publisher: Department of Physics, Mahendra Morang A.M. Campus, TU, Biratnagar, Nepal

Simulated spectra (IR and Raman), NLO, AIM and molecular docking of carisoprodol from DFT approach

Manoj Kumar Chaudhary[1,2], Tarun Chaudhary[1], Bhawani Datt Joshi[3*]
[1]Central Department of Physics, Tribhuvan University, Kirtipur, Kathmandu, Nepal
[2]Department of Physics, University of Lucknow, Lucknow-226007, India
[3]Department of Physics, Siddhanath Science Campus, Tribhuvan University, Mahendranagar, 10406, Nepal
[*] Email: pbdjoshi@gmail.com

Article Information:
Received: May 20, 2020
Accepted: June 20, 2020

Keywords:
Carisoprodol
Vibrational spectroscopy (IR and Raman)
Molecular docking

ABSTRACT
The aim of this study to explore the spectroscopic behavior of carisoprodol in terms of simulated spectra (IR and Raman). The intramolecular H-bond of the molecule has been inspected from the Atoms in Molecule (AIM) approach which infers that there exist partial covalent H-bond in nature. The protein-ligand binding activity of the drug molecule has been analyzed theoretically from the molecular docking approach with the predicted targets in terms of binding energy and conventional H-bond with residue. The molecular docking analysis of the title molecule explores that the binding energy with the protein acetylcholinesterase is more than the protein epoxide hydrolase1. The nonlinear optical (NLO) behavior of title molecule has been scrutinized which motivates that the potent use of the molecule as NLO material.

DOI: https://doi.org/10.3126/bibechana.v18i1.29036

1. Introduction

Carisoprodol, (RS)-2-{[(amino carbonyl) oxy] methyl}-2methyl pentyl isopropyl carbamate, with the molecular formula ($C_{12}H_{24}N_2O_4$) is a centrally acting skeletal muscle relaxant belonging to the BCS class II drug [1-3]. Carisoprodol is generally prescribed for the treatment of various muscular problems, mainly for lower back pain [2]. Further, it is used in the treatment of muscular spasm related to the craniomandibular disorder, lumbago, sciatica, and other lower back syndromes [4]. The anticholinergic, antipyretic, and analgesic property behavior of carisoprodol has been studied regarding the treatment of distress associated with painful musculoskeletal conditions in adults [4,5].

It is triclinic in the crystalline structure lies in P_1 space group with the cell dimensions a = 5.334(3), b = 10.831(5), c = 13.114(5)Å, α =92.66(4), β = 96.03(4), γ = 92.70 (4)º and it is fully in extended conformations due to intramolecular C-H···O hydrogen bonding [6]. To enhance the potential of drugs many pharmacological and drug behavior of

carisoprodol has been carried out [7-9]. The structural and spectroscopic properties of this molecule at the atomic level have not been conducted so far. Therefore, in present work, an endeavor has been made to investigate the employments of the quantum computational method (applying DFT) to explore the vibrational spectra (FT-IR and FT-Raman), nonlinear optical (NLO) properties and atoms in molecule (AIM) of the molecule. Furthermore, molecular docking is performed to study hydrogen bonding and the biological activity of carisoprodol with different proteins. Ultimately, the study of different molecular properties might have great importance in designing and developing new efficient drugs in the coming days on the basis of protine ligand binding interaction [10-12].

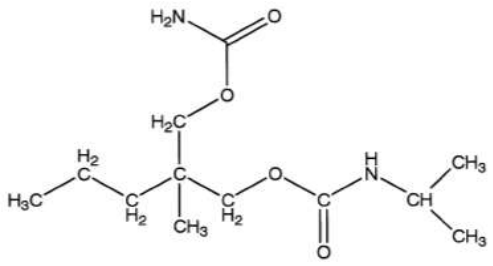

Fig. 1: Chemical structure of carisoprodol.

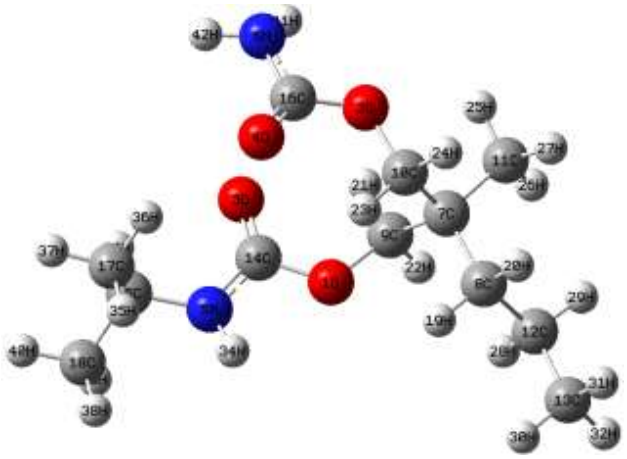

Fig. 2: Optimized structure atom numbering scheme of carisoprodol.

The chemical structure of carisoprodol is shown in Fig. 1. The optimized structure of the title molecule using functional B3LYP/6-31G(d,p) with the atom numbering system used in this study is shown in Fig. 2. The minimum energy position of the molecule has been predicted based on geometry optimization with DFT calculation by using the functional B3LYP/6-31G(d,p) which gives better agreement with the X-Ray crystal structure [13]. The optimization energy of the title compound was calculated at room temperature is - 553413.0830 kcal/mol which is less than the value of kT. This gives support towards the stability of the molecule at room temperature.

2. Computational and theoretical details

The geometry optimization of carisoprodol was performed with the Gaussian-09 software package [14]. The density functional theory (DFT) study has been performed by using the functional B3LYP/6-31G(d,p) basis set [15,16]. The hybrid exchange functional Becke's three parameters contain local, non-local, and HF (Hartree-Fock) with Lee-Yang-Par correlation functional. The literature survey reveals that the result of the functional B3LYP is closer to the experimental values [17,18]. So, we have considered the functional B3LYP for the calculation. It is one of the most frequently used functional for quantum computing procedure to investigate theoretical results as supporting tools to the experimental results. The output data of Gaussian-09 has been visualized with Gauss view 05 software. The Raman intensity, Infrared absorption, and first-order hyperpolarizability were calculated at the same level of theory as optimization. The atom in the molecule (AIM) of the title molecule has been studied with AIM 2000 and AIM all software, employing Quantum theory of atoms in molecule (QTAIM) [19,20]. The molecular docking of carisoprodol has been carried out with AutoDock software and ligand-protein interaction has been visualized with bio visualizer software [21,22].

The Raman intensity for vibration is obtained in terms of Raman scattering cross-section, $\frac{\partial\sigma_j}{\partial\Omega}$, which depend on Raman amplitude and is given by the expression [23,24]

$$\frac{\partial\sigma_j}{\partial\Omega} = \left(\frac{2^4\pi^4}{45}\right)\left(\frac{(\nu_0-\nu_j)^4}{1-exp\left[\frac{-hc\nu_j}{kT}\right]}\right)\left(\frac{h}{8\pi^2 c\nu_j}\right)S_j \quad (1)$$

where S_j= scattering activities, ν_j = predicted wavenumbers for j^{th} normal mode, ν_0 = wavenumber of Raman excited state and h, c and k are universal constants. The Lorentzian line shape (FWHM= 8 cm^{-1}) is used to produce simulated spectra from the calculated Raman and IR intensities to convolute each predicted vibrational mode.

Total static dipole moment (μ_0), the first hyperpolarizability (β_0), mean polarizability ($\Delta\alpha_0$) and anisotropy of polarizability $|\alpha_0|$ of the molecular system were calculated by using DFT at B3LYP/6-31G(d, p) level of theory and are given by the equations [25,26].

$$\mu_0 = \left(\mu_x^2 + \mu_y^2 + \mu_z^2\right)^{1/2} \quad (2)$$

$$|\alpha_0| = \frac{1}{3}\left(\alpha_{xx} + \alpha_{yy} + \alpha_{zz}\right) \quad (3)$$

$$\Delta\alpha = 2^{-1/2}\left[\left(\alpha_{xx}-\alpha_{yy}\right)^2 + \left(\alpha_{yy}-\alpha_{zz}\right)^2 + (\alpha_{zz}-\alpha_{xx})^2 + 6\alpha_{xx}^2\right]^{1/2} \quad (4)$$

$$\beta_0 = \left[\left(\beta_{xxx}+\beta_{xyy}+\beta_{xzz}\right)^2 + \left(\beta_{yyy}+\beta_{xxy}+\beta_{yzz}\right)^2 + \left(\beta_{zzz}+\beta_{xxz}+\beta_{yyz}\right)^2\right]^{1/2} \quad (5)$$

3. Results and Discussion

3.1 Vibrational spectra

The carisoprodol molecule has 42 atoms so it has 120 (3N-6) modes of vibration including stretching and bending. All the normal modes of vibration are both IR and Raman active. In the calculated spectra with B3LYP, the overestimated wavenumber is obtained due to anharmonicity present in a real system. So, the wavenumber is lowered down by wavenumber linear scaling (WLS) factor [27] which gives better resonance with experimental data. The graph of calculated IR absorbance and Raman intensity of the title molecule with scaled wavenumber is plotted as shown in Fig. 3.

3.1.1 Amine group (NH_2) vibration

From the literature survey, the stretching of an amine group (NH_2) lies in the range between 3200-3500 cm^{-1} [28]. In this study, the asymmetric stretching of NH_2 was calculated at 3534 cm^{-1} in both IR and Raman spectrum. And the symmetric stretching was calculated at 3420 cm^{-1} but the in-plane bending is calculated at 1603 cm^{-1}. The intense peak for N-H stretching was at 3441 cm^{-1} in both IR and Raman spectrum. The C-N stretching is seen in IR and Raman spectra at 1233 cm^{-1} in the scaled DFT. The increase in wave number of asymmetric stretching of the amine group infers that the amine group take part in intermolecular H-bonding with neighboring molecules in the crystalline structure. In this study, we have taken a single molecule in the gaseous state that shows some differences in the vibrational frequencies.

3.1.2 Carbonyl group (C=O) vibration

The stretching for carbonyl group was calculated at 1793 cm^{-1} in the IR and 1770 cm^{-1} in Raman band. From the literature, the range for stretching of the carbonyl group is 1670-1820 cm^{-1} [29]. The out of plane bending was calculated at 773 cm^{-1} and 757 cm^{-1} in IR and Raman spectra, respectively.

3.1.3 CH_2 and CH_3 vibration

A literature survey reveals that the range of symmetric stretching for CH_2 is 3000-3100 cm^{-1} [30]. In this study, the intense peaks for symmetric stretching are calculated at 2894 cm^{-1}, 2930 cm^{-1}, and 2944 cm^{-1} but another intense peak for asymmetric stretching for CH_2 is obtained in both IR and Raman spectra at 2981 cm^{-1}. The distinct peak for symmetric stretching of CH_3 in the title molecule is obtained at 2915 cm^{-1}.

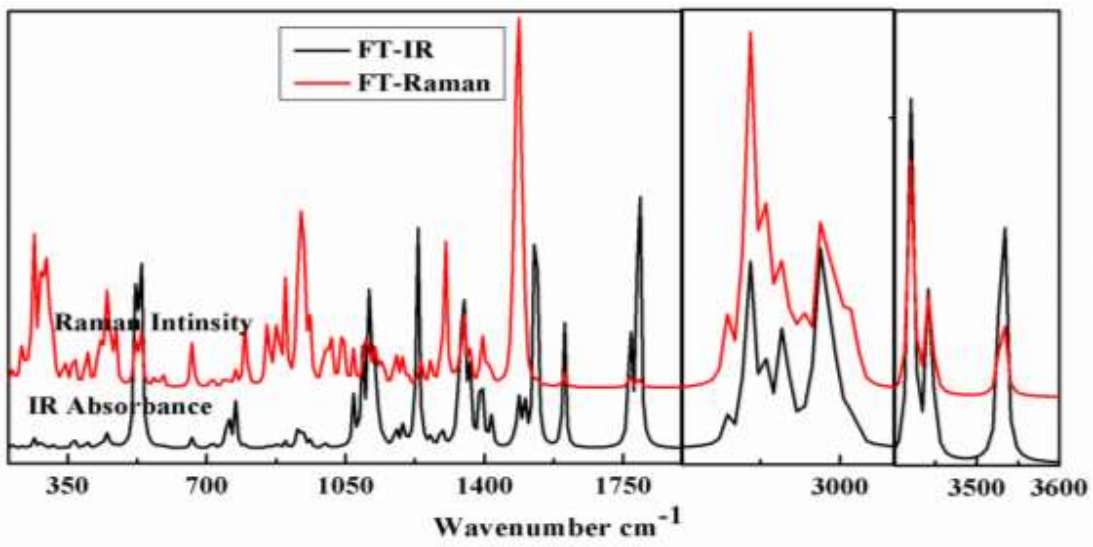

Fig. 3. Simulation of calculated IR and Raman spectra of carisoprodol.

3.2 Nonlinear optical (NLO) properties

The attractive potential application of NLO properties of the material is in optical communication, optical sensing, and data storage. The NLO properties of the material are explained in terms of static dipole moment (μ_0), the mean polarizability ($\Delta\alpha$), the first hyperpolarizability (β_0) and the anisotropy of polarizability ($|\alpha_0|$). These values of carisoprodol are calculated from B3LYP/6-31G(d,p) and their values are presented in Table 1.

Table 1: The calculated dipole moment (μ_0), mean polarizability$|\alpha_0|$, anisotropy of polarizability ($\Delta\alpha$) and first hyperpolarizability (β_0) of carisoprodol at B3LYP/6-31G(d,p).

Dipole moment (Debye)		Polarizability (*10^{-24}esu)		Hyperpolarizability (*10^{-30}esu)	
μ_x	−0.8384	α_{xx}	12.5980	β_{xxx}	0.9424
μ_y	−1.0866	α_{xy}	0.5476	β_{xxy}	0.3385
μ_z	0.6195	α_{yy}	21.9204	β_{xyy}	−0.5901
μ_0	1.5058	α_{xz}	−0.6665	β_{yyy}	−0.4011
μ_0(Urea)	1.3732	α_{yz}	1.6162	β_{xxz}	0.0089
		α_{zz}	19.0427	β_{xyz}	0.2270
		$\|\alpha_0\|$	17.8537	β_{yyz}	−0.0855
		$\Delta\alpha$	23.3704	β_{xzz}	−0.6754
		$\Delta\alpha$(Urea)	9.7710	β_{yzz}	−0.2433
				β_{zzz}	0.1166
				β_0	0.4467
				β_0(Urea)	0.3728

The significant delocalization of charge in a particular direction is mentioned by the component of polarizability in that direction. The dipole moment (μ_0), the anisotropy of polarizability ($\Delta\alpha$), and the first hyperpolarizability (β_0) of carisoprodol obtained as 1.5058 Debye, $23.3704X10^{-24}$esu, and $0.4467X10^{-30}$esu respectively. These values are more than the experimental values of urea, so carisoprodol can be used as NLO material.

3.3 Atoms in molecule (AIM)

Atoms in molecules' (AIM) is the proper way to evaluate the inter and intramolecular H-bonding. The quantum theory of atoms in molecules (QTAIM) has wide application for identification and classification of H-bonding in terms of electron density (ρ) and Laplacian of electron density ($\nabla^2\rho$) at the bond critical point (BCP). The molecular graph of carisoprodol by using the functional B3LYP/6-31G(d,p) with AIM 2000 and AIM All software is presented in Fig. 4. The topological parameters: ED (ρ_{BCP}), Laplacian of ED ($\nabla^2\rho_{BCP}$), electron kinetic energy density (G_{BCP}), electron potential energy density (V_{BCP}), total electron energy density (H_{BCP}), interaction energy (E_{int}) at BCP; in carisoprodol is presented in Table 2. The geometrical parameters, bond length, bond angle, and the sum of van der Waal radii of interacting atoms ($r_H + r_A$) is visualized in Table 3.

In the carisoprodol molecule, four intramolecular H-bond has been observed and they have the electron density (ρ) between proton (H) and acceptor (A) in the order 0.002−0.040 a.u. and the Laplacian ($\nabla^2\rho_{BCP}$) of electron density lies in the order 0.024−0.139 a.u. These values are in the range proposed by Koch and Popelier [31] for the existence of H-bond. For the investigated molecule it has been identified that ($\nabla^2\rho_{BCP}$) > 0 and (H_{BCP}) < 0, so the H-bond is partially covalent as given by Rosa et al. criteria [32]. But for strong H-bond and weak H-bond, the criteria given by Rosa et al. are ($\nabla^2\rho_{BCP}$) < 0 and (H_{BCP}) < 0, and ($\nabla^2\rho_{BCP}$) > 0 and (H_{BCP}) > 0 respectively. Out of the four H-bond, the interaction C9-H21…O3 has the highest values of electron density, Laplacian of electron density, and interaction energy as presented in Table 2,
So it is the strongest interaction. This interaction is similar as explained by Horio et al. [6].

Table 2: Topological parameters for intramolecular interaction in carisoprodol: ED (ρ_{BCP}), Laplacian of ED ($\nabla^2\rho_{BCP}$), electron kinetic energy density (G_{BCP}), electron potential energy density (V_{BCP}), total electron energy density (H_{BCP}), interaction energy (E_{int}) at BCP.

Interactions	Bond Length (Å)	ρ_{BCP} (a.u)	$\nabla^2\rho_{BCP}$ (a.u)	G_{BCP} (a.u)	V_{BCP} (a.u)	H_{BCP} (a.u)	E_{int} (kcal/mol)
H36…O4	2.5062	0.0085	0.0276	−0.0006	−0.0056	−0.0063	−1.4828
H21…O3	2.2215	0.0203	0.0850	−0.0024	−0.0164	−0.0189	−4.3367
C16…O3	3.1270	0.0059	0.0239	−0.0012	−0.0036	−0.0048	−0.9414
H28…H22	2.2443	0.0084	0.0347	−0.0021	−0.0044	−0.0066	−1.1719

Table 3: Geometrical parameters for intramolecular hydrogen bonds in carisoprodol: bond length(Å), bond angle (°), and the sum of van der Waal radii of interacting atoms ($r_H + r_A$) in Å.

D-H...A	D-H (Å)	H...A (Å)	D-H...A (°)	(r_H+ r_A) (Å)
C17-H36…O4	1.0931	2.5062	159.1608	2.72
C9-H21…O3	1.0905	2.2215	105.8896	2.72
N6-C16…O3	1.3684	3.1270	90.2495	3.22
C12-H28…H22	1.0971	2.2443	113.4188	2.40

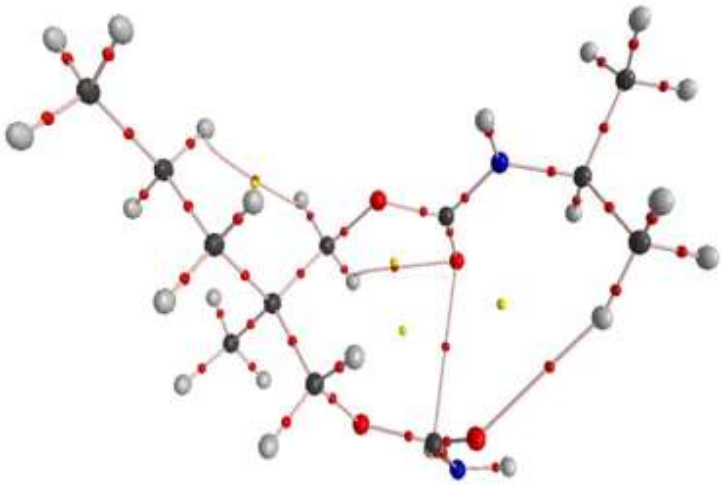

Fig. 4. Molecular graph of carisoprodol obtained by AIM.

3.4 Molecular docking

Molecular docking is a fundamental tool, which predicts the non-covalent binding of a receptor. It is used to study the protean-ligand binding affinity of bound conformations. To predict the active binding sites of carisoprodol, a docking study was performed using AutoDock-Vina software [21]. The proteins epoxide hydralase1 and acetylcholinesterase were predicted with online Swiss Target Prediction as shown in Fig. 5. The crystal structure of epoxide hydrolase with PDB code; 4XDV, 4XDW, and acetylcholinesterase with PDB code; 2ACE, 2V96 were downloaded from RSCB PDB website. Epoxide hydralase1 is an enzyme that is mainly found in the endoplasmic reticulum. It has curative behavior to metabolize reactive epoxide to less toxic water-soluble diols [33,34]. Protein acetylcholinesterase is mainly found in the central nervous system having curative behavior to terminate nerve impulse and prevents nerve firing at the nerve ending and assists in the normal functioning of the central and peripheral nervous system [35].

The protein was prepared by removing water molecules and crystallized ligand from it. Further, polar hydrogen and Kollman charges were added to the protein using AutoDock tools. The active site of protein was confined in the grid box of size 60Å×60Å×60Å with the spacing of 0.347 Å. Biovia Discovery studio 2020 was used for visualization of AutoDock-Vina result. The protein-ligand interaction of docked conformers is presented in Fig. 6. The calculated value of binding energy, the number of hydrogen bonds, and active binding residues are tabulated in Table 4. Out of four docked conformations, 2V96 showed the best binding energy −6.6 kcal/mol which binds with residue SER B:286 (2.77Å and 2.82 Å). Similarly, the conformer 2ACE of acetylcholinesterase bind with carisoprodol and gives three hydrogen bond (2.54 Å, ASP A:72, and 3.02/2.71 Å, TYRA:121) with the binding energy −6.5 kcal/mol. From this study, it is observed that the amine group and carbonyl group behave as active binding sites which is also explored in the section 3.1.1.

Table 4: Bond length, and binding energy of carisoprodol against two protein targets.

Ligand	**Protein**	**PDB code**	**Binding energy (kcal/mol)**	**Bond Length** (Å)	**Amino acid**	**No. of hydrogen bond**
Carisoprodol	Epoxide Hydrolase1	4XDV	− 6.1	3.08(O3) 3.09(O3) 2.09(H41) 2.74(H42) 2.37(H42)	ASN G:92 SER G:91 SER G:90 GLU G:25 SER H:91	5
		4XDW	−5.7	2.81(H42) 2.83(H41) 3.13(O4) 2.99(O3)	TYR B:53 PRO B:59 ASN B:55 THR B:70	4
	Acetylcholi-nesterase	2ACE	− 6.5	2.54(H42) 3.02(04) 2.71(O1)	ASP A:72 TYRA:121 TYRA:121	3
		2V96	−6.6	2.77(H42) 2.82(H34)	SERB:286 SERB:286	2

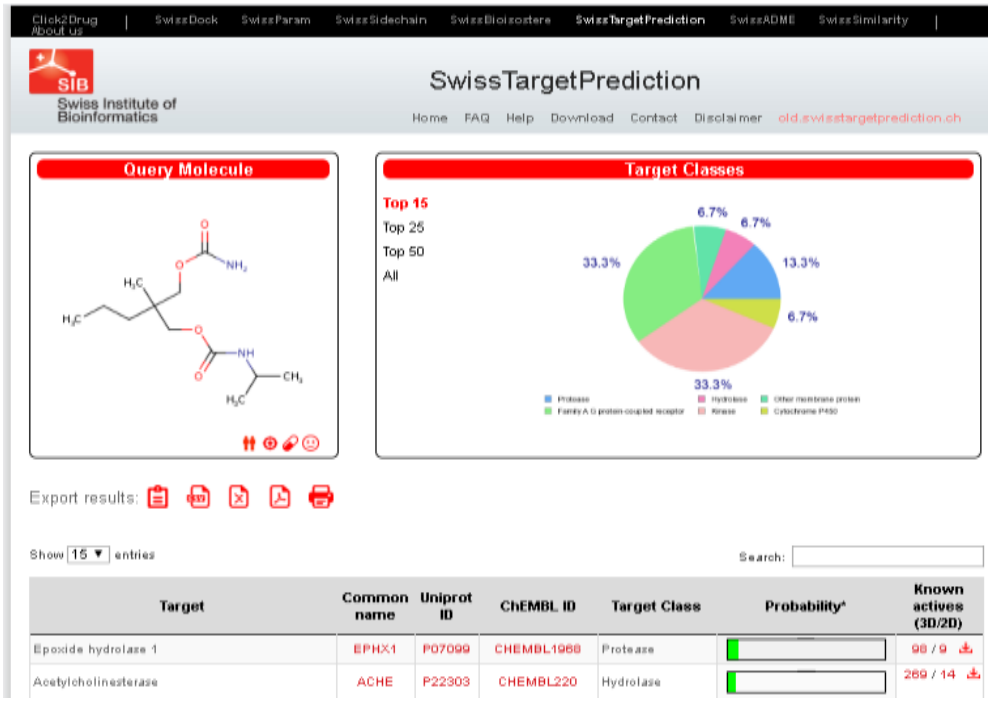

Fig. 5: Swiss Target Prediction of carisoprodol.

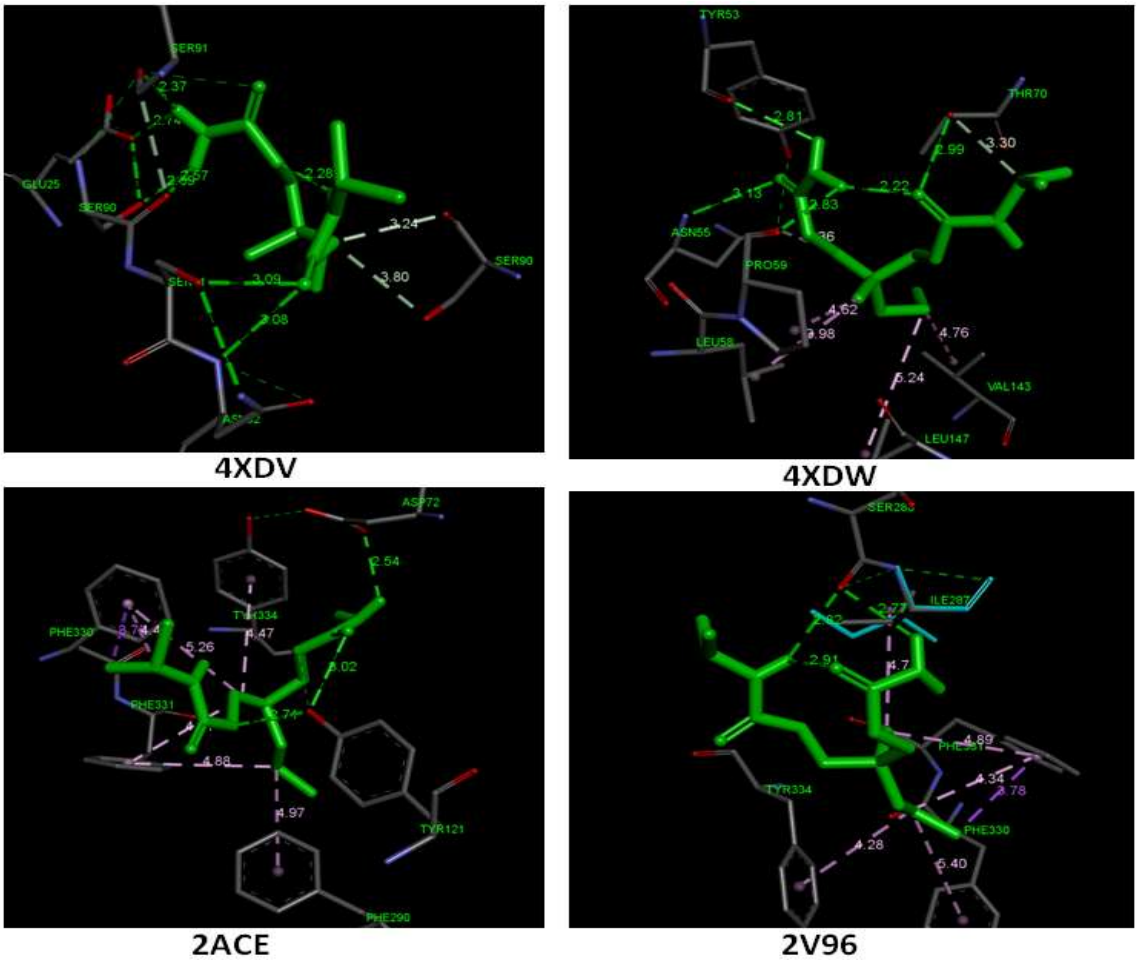

Fig. 6: Molecular docking of carisoprodol.

4. Conclusions

From the simulated IR and Raman spectra of the title molecule, it is observed that functional groups: carbonyl (C=O), amine (NH_2), CH_2, and CH_3 vibrations are in the range given by the literature survey. The dipole moment (μ_0), polarizability ($\Delta\alpha$), and first hyperpolarizability (β_0) of carisoprodol are 1.5058 D, 23.3704X10^{-24}esu, and 0.4467X10^{-30}esu, respectively. These values are more than the experimental values of urea (taken as a standard NLO material), so this material can be treated as NLO material besides the medicinal properties. The outcome of the AIM study of investigated molecule showed four intermolecular H-bonds which are partially covalent. Among them, the interaction C9-H21…O3 is the strongest due to the highest interaction energy (E_{int} = − 4.3367) at BCP. The molecular docking studies reveal good binding with acetylcholinesterase protein, PDB code: 2V96 with a binding energy of − 6.6 kcal/mol.

References

[1] R.R. Reeves, O.S. Carter, H.B. Pinkofsky, F.A. Struve, D.M. Bennett, Carisoprodol (Soma) Abuse Potential and Physician Unawareness, J. Addict. Dis. 18 (1999) 51-56. https://doi.org/10.1300/J069v18n02_05

[2] J.G. Bramness, S. Skurtveit, J. Mørland, Impairment due to intake of carisoprodol, Drug Alcohol Depend, 74 (2004) 311-318. https://doi.org/10.1016/j.drugalcdep.2004.01.007

[3] V.G. Rajurkar, S.K. Somware, A. Aher, V. Pansare, Tablet formulation and enhancement of aqueous solubility of carisoprodol by solvent evaporation co-crystal technique, Anal. Chem. Lett. 5 (2015) 364-376. https://doi.org/10.1080/22297928.2015.1129288

[4] K. A. Kumar, V.S. Lakshmipathi, S. Meenakshi, M.H. Balakrishnan, Synthesis and Characterization of Potential Impurity of Muscle Relaxant Drug Carisoprodol, J. Chem. Sci. 7 (4) (2017) 352-360. www.chemistry-journal.org

[5] M.B. Bolattin, S.T. Nandibewoor, S.D. Joshi, S.R. Dixit, S.A. Chimatadar, Interaction between carisoprodol and bovine serum albumin and effect of β-cyclodextrin on binding: insights from molecular docking and spectroscopic techniques, RSC Adv. 6 (2016) 63463-63471. https://doi.org/10.1039/C6RA08063D

[6] K. Horio, R. Tanaka, H. Akama, M. Haramura, A. Tanaka, T. Akimoto, N. Hirayama, Crystal Structure of Carisoprodol, Anal. Sci.: X-ray Structure Analysis Online, 20 (2004) x43-x44. https://doi.org/10.2116/analscix.20.x43

[7] S. Niemi, Muscle Relaxants and Antispasticity Drugs, In: Abd-Elsayed A. (eds) Pain, Springer, Cham. (2019) 279-283. https://doi.org/10.1007/978-3-319-99124-5_61

[8] Y. Li, C. Delcher, J. D. Brown, Y. J. Wei, G. M. Reisfield, A. G. Winterstein, Impact of Schedule IV controlled substance classification on carisoprodol utilization in the United States: An interrupted time series analysis, Drug Alcohol Depend. 202 (2019)172-177. https://doi.org/10.1016/j.drugalcdep.2019.05.025

[9] T. M. Carbonaro, V. Nguyen, M. J.Forster, M. B. Gatch, L. Prokai, Carisoprodol pharmacokinetics and distribution in the nucleus accumbens correlates with behavioral effects in rats independent from its metabolism to meprobamate, Neuropharmacol. (2020) 108152. https://doi.org/10.1016/j.neuropharm.2020.108152

[10] P. Taslimi, Y. Erden, S. Mamedov, L. Zeynalova, N. Ladokhina, R. Tas, B. Tuzun, A. Sujayev, N.Sadeghian, S.H. Alwasel, I. Gulcin, The Biological Activities, Molecular Docking Studies, and Anticancer Effects of 1-Arylsuphonylpyrazole Derivatives, J Bio. Mol. Struct. Dyn (2020) 1-20. https://doi.org/10.1080/07391102.2020.1763838

[11] S. Bal, R. Kaya, P. Taslimi, A. Aktaş, M. Karaman, İ. Gulçin, Novel 2-methylimidazolium salts: synthesis, characterization, molecular docking, and carbonic anhydrase and acetylcholinesterase inhibitory properties, Bioorg. Chem. 94 (2020) 103468. https://doi.org/10.1016/j.bioorg.2019.103468.

[12] J. C. Prasana, S. Muthu, C. S. Abraham, Molecular docking studies, charge transfer excitation and wave function analyses (ESP, ELF, LOL) on valacyclovir: a potential antiviral drug, Comput. Biol. Chem. 78 (2019) 9-17. https://doi.org/10.1016/j.compbiolchem.2018.11.014

[13] L. A. Anthony, D. Rajaraman, M. Shanmugam, K. Krishnasamy, Synthesis, Spectral techniques, X-ray Crystal structure, DFT method, Hirshfeld surface analysis and Molecular docking studies of 1-(furan-2-yl) methyl)-4, 5-diphenyl-2-(p-tolyl)-1H-imidazole, Chem. Data Collect. (2020) 100421. :https://doi.org/10.1016/j.cdc.2020.100421

[14] M.J. Frisch, G.W. Trucks, H.B. Schlegel, G.E. Scuseria, J.R. Cheeseman, M.A. Robb, G. Scalmani, V. Barone, B. Mennucci, G.A. Petersson, H. Nakatsuji, M. Caricato, X. Li, H.P. Hratchian, A.F. Izmzylov, J. Bloino, G. Zheng, J.L. Sonnenberg, M. Hada, M. Ehara, K. Toyota, R. Fukuda, J. Ishida, M. Hasegawa, T. Nakajima, Y. Honda, O. Kitao, H. Nakai, T. Vreven, J.A. Montgomery Jr., J.E. Peralta, F. Ogliaro, M. Bearpark, J.J. Heyd, E. Brothers, K.N. Kudin, V.N. Staroverov, R. Kobayashi, J. Normand, A. Raghavachari, A. Rendell, J.C. Burant, S.S. Iyengar, J. Tomasi, M. Cossi, N. Rega, J.M. Millan, M. Klene, J.E. Knox, J.B. Cross, V. Bakken, C. Adamo, J. Jaramillo, R. Gomperts, R.E. Stratmann, O. Yazyev, A.J. Austin, R. Cammi, C. Pomelli, J.W. Ochterski, R.L. Martin, K. Morokuma, V.G. Zakrzewski, G.A.Voth, P. Salvador, J.J. Dannerberg, S. Dapprich, A.D. Daniels, J. Farkas, B. Foresman, J.V. Ortiz, J. Cioslowski, D.J. Fox, GAUSSIAN 09, Revision, Gaussian, Inc., Wallingford CT, (2009).

[15] A. D. Becke, A new mixing of Hartree–Fock and local density-functional theories, J. Chem. Phys. 98 (2) (1993) 1372-1377. https://doi.org/10.1063/1.464304

[16] R.G. Parr, W. Yang, Density Functional Theory of Atoms and Molecules, Oxford, New York, (1989). https://doi.org/10.1002/qua.560470107

[17] P. Prajapati, J. Pandey, M.R. Shimpi, A. Srivastava, P. Tandon, S.P. Velaga, K. Sinha, J. Mol. Struct. 1125 (2016) 193-203. https://doi.org/10.1016/j.molstruc.2016.06.070

[18] J. Pandey, P. Prajapati, M. R.Shimpi, P.Tandon, S. P. Velaga, A. Srivastava, K. Sinha, Studies of

molecular structure, hydrogen bonding and chemical activity of a nitrofurantoin-L-proline cocrystal: a combined spectroscopic and quantum chemical approach, RSC Adv. 6(78) (2016) 74135-74154. doi:https://doi.org/10.1039/C6RA13035F

[19] T.A. Keith, AIMALL Version 090201 TK Gristmill Software Overland Park, KS. USA; (2009).

[20] R.F.W. Bader, Atoms in Molecules, A Quantum Theory, Oxford University Press, Oxford, (1990).

[21] O. Trott, A.J. Olson, AutoDock Vina: improving the speed and accuracy of docking with a new scoring function, efficient optimization, and multithreading, J. Comput. Chem. 31 (2010) 455-461. https:// doi.org/10.1002/jcc.21334

[22] Discovery Studio 4.5 Guide, Accelrys Inc., San Diego, http://www.accelrys.com, 2009.

[23] G.A. Guirgis, P. Klaboe, S. Shen, D.L. Powell, A. Gruodis, V. Aleksa, C.J. Nielsen, J.

[24] Tao, C. Zheng, J.R. Durig, Spectra and structure of silicon-containing compounds. XXXVI—Raman and infrared spectra, conformational stability, ab initio calculations and vibrational assignment of ethyldibromosilane, J. Raman Spectrosc. 34 (2003) 322-336. https://doi.org/10.1002/jrs.989

[25] P.L. Polavarapu, Ab initio vibrational Raman and Raman optical activity spectra, J. Phys. Chem. 94 (1990) 8106–8112. https://doi.org/10.1021/j100384a024

[26] B.D. Joshi, M.K. Chaudhary, NBO, nonlinear optical and thermodynamic properties Of10-Acetyl-10H-phenothiazine5-oxide, BIBECHANA 15 31-139 (2018). https://doi.org/10.3126/bibechana.v15i0.18385

[27] F. Weinhold, C.R. Landis, Valency and Bonding: A Natural Bond Orbital Donor– Acceptor Perspective, Cambridge University Press, Cambridge, 2005.

[28] H. Yoshida, K. Takeda, J. Okamura, A. Ehara, H. Matsurra, A new approach to vibrational analysis of large molecules by density functional theory: wavenumber-linear scaling method, J. Phys. Chem. 106 (2002) 3580–3586. https://doi.org/10.1021/jp013084m

[29] A. Prabakaran, S. Muthu, "Normal Coordinate Analysis and Vibrational Spectroscopy (FT-IR and FT-Raman) Studies of (2S)-2-Amino-3-(3,4-Dihydroxyphenyl)-2-ethylpropnoic Acid Using ab Initio HF and DFT Method," Spectrochim. Acta Part A. 99 (2012) 90–96. https://doi.org/10.1016/j.saa.2012.09.014

[30] R.M. Silverstein, G.C. Bassler, T.C. Morrill, Spectrometric identification of organic compounds. 4th ed. John Wiley and Sons, New York, 1981.

[31] H.S. Barbara, University of Technology, Sydney, Australia, Infrared Spectroscopy: Fundamentals and Applications. https://doi.org/10.1002/0471238961.0914061810151405.a01.pub2
U. Koch, P. Popelier, Characterization of CHO hydrogen bonds on the basis of the charge density, J. Phys. Chem. A 99 (24) (1995) 9747-9754. https://doi.org/10.1021/j100024a016

[32] I. Rozas, I. Alkorta, Elguero, Behavior of ylides containing N, O, and C atoms as hydrogen bond acceptors, J. Am. Chem. Soc. 122 (45) (2000) 11154-11161. https://doi.org/10.1021/ja0017864

[33] C. Hassett, L. Alcher, J.S. Sidhu, C.J. Omieclnskl, Human microsomal epoxide hydrolase: genetic polymorphism and functional expression in vitro of amino acid variants, Hum. Mol. Genet. 3 (1994) 421-428. https://doi.org/10.1093/hmg/3.3.421

[34] R. Vaclavíkova, D.J. Hughes, P. Soucek, Microsomal epoxide hydrolase 1 (EPHX1): Gene, structure, function, and role in human disease, Gene 571 (2015) 1-8. https://doi.org/10.1016/j.gene.2015.07.071

[35] M.G. Lionetto, R. Caricato, A. Calisi, M.E. Giordano, T. Schettino, Acetylcholinesterase as a biomarker in environmental and occupational medicine: new insights and future perspectives, BioMed Res. Int. (2013). http://dx.doi.org/10.1155/2013/321213